NTNU – Trondheim
Norwegian University of
Science and Technology

Experimental and Numerical Assessment og the Hydrogeological Behaviour of the Soil-Rock Interface

Hallvard H Nordbrøden

Geotechnology
Submission date: June 2014
Supervisor: Krishna Kanta Panthi, IGB
Co-supervisor: Thomas Pabst, Norges Geotekniske Institutt

Norwegian University of Science and Technology
Department of Geology and Mineral Resources Engineering

NTNU
Norwegian University of Science and Technology

Department of Geology and Mineral Resources Engineering

Your ref.: MS/N17T26/IGB/HHNKKP

Date: 08.01.2014

TGB4930 INGGEOL/BERGMEK - MSc thesis

for

Eng. geo. student Hallvard Haugen Nordbrøden

EXPERIMENTAL AND NUMERICAL ASSESSMENT OF THE HYDROGEOLOGICAL BEHAVIOUR OF THE SOIL – ROCK INTERFACE

Background

The construction of an underground excavation has generally an impact on the surrounding hydrogeological environment. The analysis of the hydrogeological conditions is therefore an important part of most of the tunnelling and underground excavation projects. Such analysis helps determine how much water may seep into the excavation (inflow), what may be the consequences of a tunnel on the topographic environment and how may the groundwater table be affected.

The candidate has carried out during the autumn 2013 a project work that included field and lab tests for three different locations in Oslo. The position of the groundwater table is continuously monitored in these locations. The MSc thesis is the continuation of the project work and will have two main goals. First, assess the internal lateral run-off at the soil-rock interface, thus improving the calculation of the water balance and assess the response of the water table to precipitation. Secondly, determine the infiltration rate from the top soil cover to the rock mass. This point is particularly critical to predict the consequences of the drawdown of the groundwater table due to the construction of a tunnel or any underground excavation.

MSc thesis task

Therefore, this MSc thesis shall analyse under which conditions the groundwater table in the overburden soil is affected and influenced if an underground excavation is made underneath. In this respect, the MSc thesis shall address the following issues:

- Theoretical literature review connected to the area of analysis with relevant case studies;
- Topographic and geological description of the studied localities.

- Carry out numerical simulations to evaluate the hydrogeological properties of the rock mass at three different locations (where field tests were carried out);
- Calibrate models based on both laboratory test results (infiltration through layered profiles) and in-situ monitoring data
- Assess 2D models covering various conditions such as large rain event, slope conditions, soil thickness and location of tunnel at depth;
- Correlate the results with project cases, assess groundwater flow through soil-rock interface for various soil category and rock mass conditions;
- Try to establish a link between groundwater movement, soil and rock mass conditions and weather conditions.

Relevant computer software packages

Seep/W 2012 (GeoSlope Int., 2012) and other relevant softwares.

Background information for the study

- The information provided by the supervisors.
- Information, field and laboratory test data collected by the candidate during autumn 2013.
- Scientific papers, reports and books related to hydrogeology, engineering geology and tunnelling

Cooperating partner

NGI Oslo is the cooperating partner. Candidate shall work very closely with **Dr. Thomas Pabst** who is a co-supervisor for this MSc thesis.

The project work is to start on January 13, 2014 and to be completed by June 10, 2014.

The Norwegian University of Science and Technology (NTNU)
Department of Geology and Mineral Resources Engineering

January 08, 2014

Krishna Panthi

Dr. Krishna K. Panthi
Associate Professor of geological engineering, main supervisor

NTNU
Det skapende universitet

Preface

"Experimental and Numerical Assessment of the Hydrogeological Behaviour of the Soil-Rock Interface" is a master's thesis work written at the Department of Geology and Mineral Resources Engineering at the Norwegian University of Science and Technology (NTNU) in Trondheim. It is written cooperation with Norway's Geotechnical Institute (NGI) in Oslo. The work has been carried out during the spring semester of 2014.

The aim of this master's thesis has been to greater the understanding of the behaviour of water over the soil-rock interface. A lot of the work has been done by processing and simulating laboratory and field data gathered in the autumn of 2013. This has been a tedious and long-lasting process in which the learning of the software Seep/W from the GeoStudio suite has been a major task. The simulation of the data has led to the construction of large scale models, which gives examples of case scenarios of infiltration over the soil-rock interface.

I would like to give both my supervisor Associate Professor Krishna Panthi (NTNU) and co-supervisor Mr. Thomas Pabst (NGI) my sincerest thanks. They have always answered my emails quickly and been encouraging all the way during the course of this thesis. Without their supervising I would not have been able to carry out this thesis.

Trondheim, June 10, 2014

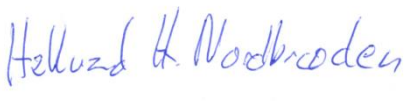

Hallvard H. Nordbrøden

Abstract

"Experimental and Numerical Assessment of the Hydrogeological Behaviour of the Soil-Rock Interface" is written by Hallvard Haugen Nordbrøden. It is a master's thesis written at the Department of Geology and Mineral Resources Engineering at the Norwegian university of Science and Technology (NTNU) in Trondheim, Norway. It is written in cooperation with Norwegian Geotechnical Institute (NGI) in Oslo. In total there are 116 pages excluding appendixes.

Constructing underground excavations may affect the groundwater balance in an area. The effects of this may influence on both tunnel stability and life time, and settlement on the surface.

In geotechnical engineering, knowledge about water transportation is good. The mechanisms for water transport in soils are throughout described in numerous publications. For rock masses behaviour of water is more unpredictable because it follows fractures and weakness zones. There is little knowledge about the behaviour of the water transport over the interface between the two matters. This thesis is addressing these topics with special regard on the infiltration over the soil-rock interface.

Slug tests in the field and a layered 1D model of soils in the laboratory are executed and simulated using the numerical software Seep/W from the GeoStudio suite. By the simulation of these cases, it is showed that continuous models can simulate water propagation between different materials.

Large scale models with and without excavations are created with emphasis on realistic cases, different rock mass and tunnel depths. These are simulated and evaluated throughout.

The findings are that this approach to estimate water flow over interfaces proves promising as the results from the large scale models are found realistic. By further evaluation of the found data and more investigations on the laboratory test, results the creation of new improved large scale models can be done. If based on and compared with results from previous real life cases it is thought that the models and methodology of this thesis is promising and a good approach.

Sammendrag

"Experimental and Numerical Assessment of the Hydrogeological Behaviour of the Soil-Rock Interface" er skrevet av Hallvard Haugen Nordbrøden. Det er en masteroppgave skrevet ved Institutt for geologi og bergteknikk ved Norges teknisk-naturvitenskapelige universitet (NTNU) i Trondheim, Norge. Oppgaven er skrevet i samarbeid med Norges geotekniske institutt (NGI) i Oslo. Det er totalt 116 sider uten vedlegg.

Utbygning av undergrunnsanlegg kan påvirke grunnvannsbalansen i et område. Effektene av dette kan påvirke både undergrunnanleggets stabilitet og levetid, samt lage setninger på overflaten.

Innenfor geoteknikk er kunnskapen om vanntransport god. Mekanismene for vanntransport i løsmasser er beskrevet utfyllende i en rekke artikler. For bergmasser er vanntransport mer uforutsigbar fordi den følger sprekkesett og svakhetssoner. Lite er kjent om bevegelsen mellom de to mediene. Denne masteroppgaven tar for seg disse temaene med spesielt hensyn på infiltrasjon over grenseflaten mellom løsmasser og bergmasser.

Slugtester i felten og en lagvis 1D-modell av løsmasser i laboratoriet blir utført og simulert ved hjelp av det numeriske modelleringsprogrammet Seep/W fra GeoStudio-pakken. Ved å simulere disse tilfellene blir det vist at kontinuerlige modeller kan simulere vanntransport mellom materialene.

Storskalamodeller med og uten tunneler blir lagd i programpakken med vekt på realistiske situasjoner, ulike bergmasseegenskaper og tunneldybder. Disse blir simulert og analysert grundig.

Resultatene fra oppgaven viser at denne fremgangsmåten er lovende da resultatene fra storskalamodellene synes å være realistiske. Ved videre analyse av de fremstilte dataene samt grundigere undersøkelser omkring laboratorietestens resultater bør forbedrede storskalamodeller kunne lages. Dersom de blir basert på og sammenliknet med innhentede data fra kjent litteratur antas det at modellene og fremgangsmetoden er en god metode å undersøke denne typen problemstillinger på.

Contents

Preface I

Abstract II

Sammendrag III

Figures IX

Tables XIII

1.0 Introduction 1

1.1 Background 1

1.2 Aims and limitations of the research 1

2.0 Literature review 3

2.1 Introduction to hydrology 3

2.1.1 The hydrologic cycle 3

2.1.2 The general water balance equation 3

2.1.3 The saturated and unsaturated zone 4

2.1.4 Aquifers 4

2.2 Basic geological parameters 6

2.1.1 Porosity 6

2.2.2 Bulk density 10

2.2.3 Moisture content 11

2.2.4 Saturation ratio 11

2.2.5 Capillarity 12

2.2.6 Darcy's law 14

2.2.7 Intrinsic Permeability 15

2.3 Water in the saturated zone 15

2.3.1 Hydraulic conductivity in fully saturated soils 15

2.3.2 Viscosity 16

2.3.3 Gravitational potential and hydraulic gradient 17
2.4.1 Water in the unsaturated zone 18
2.4.2 Moisture movement and hydraulic conductivity characteristics of the unsaturated zone 19
2.4.3 Water retention characteristics 20
2.4.4 Water movement in the unsaturated soil 21
2.4.5 Hydraulic conductivity of unsaturated soils 22
2.5.1 Hydrogeology of rocks 24
2.5.2 Fractures and discontinuities of rocks 24
2.5.2.1 Fault and shear zones 25
2.5.2.2 Foliation 26
2.5.2.3 Fractures 26
2.5.2.4 Bedding plane 26
2.5.3 Hydrology of fractures and discontinuities 26
2.5.4 Skin, filling and stress' effect on permeability 29
2.6 Introduction to water balance 30
2.6.1 Infiltration 30
2.6.2 Evapotranspiration 33
2.6.3 Runoff 33
2.7 Well tests 34
2.7.1 The pump test 34
2.7.2 The packer/Lugeon test 35
2.7.3 The slug test 35
2.8 The Q-method 37
3.0 Software 39
3.1.1 Seep/W 39
3.1.2 Van Genuchten input parameters 39
4.0 Field tests 40

4.1 Test sites 40
4.1.1 Vettakollen 40
4.1.1.1 The test site 40
4.1.1.2 Topography and geology 41
4.1.2 Bekkelaget 43
4.1.2.1 The test site 43
4.1.2.2 Geology and topography 43
4.1.2.3 Observations 45
4.1.3 Folkehelseinstituttet 45
4.1.3.1 Topography and geology 46
4.2 Methodology 49
4.2.1 Slug tests 49
4.2.1.1 Test equipment 49
4.2.1.2 Test procedure 50
4.2.2 Simulations 51
4.2.2.1 Objective 51
4.2.2.2 General assumptions 51
4.2.2.2.1 Geometry 51
4.2.2.2.2 Water flow and rock mass characteristics 52
4.2.2.2.3 Boundary conditions 53
4.2.2.2.4 Well diameters 53
4.2.2.2.5 Special cases 53
4.2.2.3 Procedure 53
4.3 Results 55
4.3.1 Overview 55
4.3.2 Vettakollen 56
4.3.3 Bekkelaget 56
4.3.4 Folkehelseinstituttet 57

4.4 Analysis 58
4.4.1 Low permeability well: KJ7 58
4.4.2 High permeability well: BL2 59
4.4.3 Sensitivity analysis 61
5.0 Laboratory tests 62
5.1 methodology 62
5.1.1 Test equipment and procedures 62
5.1.1.1 Material 62
5.1.1.2 Apparatus 64
5.1.1.3 Test 1: Coarse material over fine 65
5.1.1.4 Test 2: Fine material over coarse 69
5.1.2 Simulations 71
5.1.2.1 Objective 71
5.1.2.2 General assumptions 71
5.1.2.3 Geometry and boundary conditions 72
5.1.2.4 Test1: Coarse over fine 72
5.1.2.5 Test2: Fine over coarse 73
5.2 Results 74
5.2.1 Measured values 74
5.2.1.1 Test1: Coarse over fine 74
5.2.1.2 Test2: Fine over coarse 75
5.2.2 Simulated values 76
5.2.2.1 Test1: Coarse over fine 76
5.2.2.2 Test2: Fine over coarse 79
5.3 Analysis 82
5.3.1 Test1: Coarse over fine 82
5.3.2 Test2: Fine over coarse 83
5.3.3 Evaluation and improvement suggestions 83

6.0 Large scale models 84
6.1 Objective 84
6.1.1 General assumptions 84
6.1.2 Geometry and boundary conditions 85
6.1.3 Climatic functions 85
6.2 Case scenarios 86
6.2.1 Flat case 87
6.2.2 Slope case 89
6.2.3 Lake case 91
6.3 Results and evaluation of large scale models 94
6.3.1 Basic case 94
6.3.1.1 Results 94
6.3.1.2 Analysis 96
6.3.2 Climatic effects 96
6.3.2.1 Results 97
6.3.2.2 Analysis 99
6.3.3 Soil effects 100
6.3.3.1 Results 100
6.3.3.2 Analysis 105
6.3.4 Rock mass effects 106
6.3.4.1 Results 106
6.3.4.2 Analysis 108
6.3.5 Slope effects 109
6.3.5.1 Results 109
6.3.5.2 Analysis 111
6.3.6 Lake effects 111
6.3.6.1 Results 112
6.3.6.2 Analysis 114

6.3.7 General trends 115
7 Conclusion 116
8 Further work 116
Reference list 117
Apendix A 120
Appendix B: 126
Appendix C 131
Appendix D: Simulation data large scale: Flat case 142
Appendix E: Simulation data large scale: Lake case 148
Appendix F: Simulation data large scale: Slope case 156

Figures

Figure 1 – A principal sketch of both a) confined and b) unconfined aquifers from (Dellur 1999) 5
Figure 2 - Packing of two uniformely sorted materials; A the largest possible porosity and B the least possible porosity (Dellur 1999). 8
Figure 3 - Examples of different porosities for typical rock and soils by Dellur (1999). 9
Figure 4 – An illustration of capillarity by Dellur (1999) courtesy of Lohman (1972) 13
Figure 5 – An illustration of the soil-water characteristic curves from (Dellur 1999) 19
Figure 6 – Different types of fractures (left) and schematic illustration of a fault with dip and strike (right) (Dellur 1999) 25
Figure 7 – Fracture aperture versus hydraulic conductivity (Gupta&Singhal 2010). 28
Figure 8 – The Figure shows different hydraulic conductivities for different rock and soil types (Gupta&Singhal 2010). 29
Figure 9 - Hypothetical rainfall event and infiltration capacity from Dellur (1999) 31
Figure 10 – Cumulative infiltration I_c in the event of a hypothetical rainfall event (Dellur 1999). 32
Figure 11- A principal sketch of the effect of the slug on a well in a slug test from Gupta&Singhal (2010) 36
Figure 12 – From (NGI 2013), the classification of RQD values. 37
Figure 13 – From (NGI 2013) on the Q-values rock mass quality. 38
Figure 14 – Arial photograph of the Vettakollen area with the wells (marked as BH) and the tunnels to the overhead storage basin. 41
Figure 15 - Geological map with the wells marked in red with approximate well locations, courtesy of (NGU 2013). 42
Figure 16 - Q values from the Vettakollen site 43
Figure 17 - Geology of the Bekkelaget site with approximate well locations marked with red dots (NGU 2013). 44
Figure 18 – Topographic map of the Bekkelaget site. 44

Figure 19 – The wells in the area of Folkehelseinstituttet. 46
Figure 20 – The geology of the area courtesy of (NGU 2013) 47
Figure 21 – RQD, J_r and J_a for the bore holes in the Folkehelseinstituttet test site 48
Figure 22 – The setup during testing of well BH5 at Vettakollen. There can be seen water for injection, groundwater level measurement device with a measuring tape, fishing line and a watch in the picture. This well had an angle of 65˚ with the horizontal plane. 50
Figure 23 – Total head after pouring and drainage of KJ7 52
Figure 24 - Modelling of both pouring and drawdown steps of well BH3 from the Vettakollen area 56
Figure 25 Modelling of pouring steps of well BL2 from the Bekkelaget site 56
Figure 26 - Modelling of pouring steps of well KJ6 from the Folkehelseinstituttet site 57
Figure 27 - Modelling of drawdown steps of well KJ6 from the Folkehelseinstituttet site 57
Figure 28 - Modelling of pouring steps of well KJ7 58
Figure 29 - Modelling of drawdown of well KJ7 59
Figure 30 - Modelling of pouring and draining steps of well BL2 60
Figure 31 – sensitivity analysis of well BL2 based on different saturated(SWC) and residual water contents(RWC). The line "simulation" is the assumed water contents used for all the simulations at SWC=0,03 and RWC=0,01. The line "Sensitivity" is given a SWC=0,06 and a RWC=0,015. 61
Figure 32 – Grain size distribution of the fine material from NOAH&NGIs Langøya Deposit Project. 63
Figure 33 – The apparatus used at the laboratory testing at NGI. The apparatus is partially filled with material and has two sensors installed at this point. 65
Figure 34 - Installation of sensor 66
Figure 35 – The full setup after preparing both the fine and coarse material as well as the sensors within the cell. 67
Figure 36 - The cell in the middle of the test. If watched closely it is possible to see the water front approximately halfway down in the fine material. 68
Figure 37 – The cell ready during the second test after the first pouring. Note the small layer of water on top of the fine material. 69
Figure 38 - Water propagation and water head above the fine material. 70
Figure 39 – the setup of the model in Seep/W, axis values in centimetres. 72
Figure 40 – Volumetric water content for a random fine over coarse case. 73
Figure 41 – The short term test phase of test 1. Water content (%) versus time. 74
Figure 42 – The long term draining phase of test 1. Water content (%) versus time. 74
Figure 43 – The short term test phase of test 2. Water content (%) versus time. 75
Figure 44 – The long term draining phase of test 2. Water content (%) versus time. 75
Figure 45 – Simulated and measured values of lowest port in the coarse material. 77
Figure 46– Simulated and measured values of highest port in the coarse material. 77
Figure 47– Simulated and measured values of lowest port in the fine material. 78
Figure 48 – Simulated and measured values of highest port in the fine material. 78
Figure 49 – Simulated and measured values of highest port in the fine material. 79
Figure 50– Simulated and measured values of lowest port in the fine material. 80
Figure 51– Simulated and measured values of highest port in the coarse material. 80
Figure 52– Simulated and measured values of lowest port in the coarse material. 81
Figure 53 – Infiltration function of Lillehammer 86
Figure 54 – Infiltration function of Bergen 86
Figure 55 – Example of the flat area case. Soil thickness 10m, tunnel depth 10m beneath rock mass surface. 87

Figure 56 - Example of the slope case. Soil thickness 2m, tunnel depth 10m beneath rock mass surface. 89
Figure 57 - Example of the lake case. Soil thickness 12m, tunnel depth 20m beneath rock mass surface. 92
Figure 58 – Groundwater table from pressure head of the case Flat D5 S1. 94
Figure 59 – Groundwater table from pressure head for the case Flat S1 95
Figure 60 – Cases Flat S1 and Flat D5 S1. Effect of tunnel excavation on infiltration over soil-rock interface at soil thickness 1m with and without tunnel. 95
Figure 61 – Climatic effects on the lake scenario with Bergen and Lillehammer climatic conditions over the soil-rock interface. Cases with and without tunnels (20m depth). Rock mass material is the same (BH4). 97
Figure 62 - Climatic effects on the lake scenario with Bergen and Lillehammer climatic conditions over the tunnel interface. Cases with tunnels of 20m depth. Rock mass material is the same (BH4). 97
Figure 63- Case Lake Bergen D20 BH4. Groundwater level is shown as a result of tunnel construction and climatic effects of the Bergen location. 98
Figure 64 – Case Lillehammer D20 BH4. Groundwater level is shown as a result of tunnel construction and climatic effects of the Lillehammer location. 98
Figure 65 - Daily infiltration[m^3/s] versus time[days] of flat area cases over a tunnel interface at depth 10m and soil thicknesses 1m, 5m and 10m. 100
Figure 66 - Daily infiltration[m^3/s] versus time[days] of flat area cases on soil-rock interface without tunnel, soil thicknesses 1m, 5m and 10m. 101
Figure 67 – Case Flat D10 S1. Volumetric Water content 1 year after tunnel construction of a 10m deep tunnel with 1m soil thickness. 102
Figure 68 – Case Flat D10 S1. Groundwater table shown as pressure head 1 year after tunnel construction 102
Figure 69– Case Flat D10 S5. Volumetric Water content 1 year after tunnel construction of a 10m deep tunnel with 5m soil thickness. 103
Figure 70– Case Flat D10 S5. Groundwater table shown as pressure head 1 year after tunnel construction. 103
Figure 71 – Case Flat D10 S10. Volumetric Water content 1 year after tunnel construction of a 10m deep tunnel with 10m soil thickness. 104
Figure 72 – Case Flat D10 S10. Groundwater table shown as pressure head 1 year after tunnel construction. 104
Figure 73 – Figure show daily infiltration over a tunnel interface at 20m depth in a slope case. Cases are with two different rock types, BL2 and BL3, with Lillehammer and Bergen climatic conditions. 106
Figure 74 - Figure show daily infiltration over the soil-rock interface at 20m depth in a slope case. Cases are with two different rock types, BL2 and BL3, with Lillehammer and Bergen climatic conditions. 107
Figure 75 – case Lillehammer D20 BL2. Groundwater from pore pressure 1 year after tunnel construction. 108
Figure 76 Case Lillehammer D20 BL3. Groundwater from pore pressure 1 year after tunnel contruction. 108
Figure 77 – Cases Slope Bergen D10 BL2, Slope Bergen D20 BL2 and Slope Bergen BL2 compared with the corresponding properties in a flat case. The graph show effect of tunnel on infiltration [m^3/s] over soil-rock interface for a tunnel compared with no tunnel. 109
Figure 78 - Case Slope Bergen D10 BL2. Groundwater table from pressure head. 110
Figure 79 – Case Slope Bergen D20 BL2. Groundwater table from pressure head. 111

Figure 80 –Case Lake Lillehammer D20 BH3. XY velocity magnitude of lake case with a tunnel depth of 20m and rock material BH3. 112
Figure 81 – Lake Lillehammer D20 BH3. Groundwater table of lake case with material BH3. 112
Figure 82 - Cases Lake Bergen D10 BH3 and Lake Bergen BH3. Cases with and without tunnel, infiltration rate over lake-soil interface. 113
Figure 83 - Modelling of pouring steps of well KJ2 132
Figure 84 - Modelling of drawdown of well KJ2 133
Figure 85 - Modelling of pouring and draining steps of well KJ3 133
Figure 86 - Modelling of pouring steps of well KJ4 134
Figure 87 - Modelling of drawdown of well KJ4 134
Figure 88 - Modelling of pouring steps of well KJ5 134
Figure 89 - Modelling of drawdown of well KJ5 135
Figure 90 – modelling of pouring steps of well KJ6 135
Figure 91 - Modelling of drawdown steps of well KJ6 136
Figure 92 - Modelling of pouring steps of well KJ7 136
Figure 93 - Modelling of drawdown of well KJ7 136
Figure 94 - Modelling of pouring and draining steps of well BL1 137
Figure 95 - Modelling of pouring and draining steps of well BL2 137
Figure 96 - Modelling of pouring and draining steps of well BL2 138
Figure 97 - Modelling of pouring and draining steps of well BH2 138
Figure 98 - Modelling of pouring and draining steps of well BH3 139
Figure 99 – Modelling of pouring steps of well BH0034 139
Figure 100 – Modelling of drawdown of well BH4 140
Figure 101 - Modelling of pouring and draining steps of well BH5 140
Figure 102 – sensitivity analysis of well BL2 based on different saturated (SWC) and residual water contents(RWC). The line “simulation” is the assumed water contents used for all the simulations at SWC=0,03 and RWC=0,01. The line “Sensitivity” is given a SWC=0,06 and a RWC=0,015. 141
Figure 103 – Infiltration rates over tunnel interface 142
Figure 104 – Infiltration rates over tunnel interface 142
Figure 105 – Infiltration rates over tunnel interface 143
Figure 106 – Infiltration rates over soil-rock interface 143
Figure 107 – Infiltration rates over soil-rock interface 144
Figure 108 – Infiltration rates over soil-rock interface 144
Figure 109 - Flat S10 145
Figure 110 - Flat S1 145
Figure 111 - Flat D5 S10 145
Figure 112 - Flat D2 S1 146
Figure 113 - D5 S5 146
Figure 114 - Flat D20 S10 146
Figure 115 - Flat D20 S5 147
Figure 116 - Flat D20 S1 147
Figure 117 – Infiltration rate over tunnel interface 149
Figure 118 – Infiltration rate over tunnel interface 149
Figure 119 – Infiltration rate over tunnel interface 150
Figure 120 – Infiltration rates over soil-rock interface 150
Figure 121 – Infiltration rates over soil-rock interface 151
Figure 122 – Infiltration rates over soil-rock interface 151

Figure 123 – Lake Bergen BH3 152
Figure 124 - Lake Bergen BH4 152
Figure 125 - Lake Bergen D10 BH3 153
Figure 126 - Lake Bergen D20 BH3 153
Figure 127 - Lake Lillehammer BH3 154
Figure 128 – Lake Lillehammer BH4 154
Figure 129 - Lake Lillehammer D10 BH3 155
Figure 130 – Infiltration rates over soil-rock interface 157
Figure 131 – Infiltration rates over soil-rock interface 157
Figure 132 – Infiltration rates over tunnel interface 158
Figure 133 - Slope Bergen BL2 158
Figure 134 - Slope Bergen BL3 159
Figure 135 - Slope Bergen D20 BL3 159
Figure 136 - Slope Bergen D10 BL2 160
Figure 137 - Slope Lillehammer BL2 160
Figure 138 - Slope Lillehammer BL3 161

Tables

Table 1 – RQD values of bore hole logging from the Bekkelaget site 45
Table 2 – Simulated well data from slug tests 55
Table 3 – properties of simulated results of laboratory test coarse over fine. Est. means the hydraulic conductivity is estimated as a function of matric suction. 76
Table 4 – Coarse material properties 76
Table 5 – properties of simulated results of laboratory test fine over coarse. Est. means the hydraulic conductivity is estimated as a function of matric suction. 79
Table 6 – material properties of the silt material used in all large scale tests 84
Table 7 – Cumulative infiltration amount per unit length over the course of 1 year (2006). 85
Table 8 – Rock mass properties of rock surrounding well KJ3 at the Folkehelseinstituttet site 87
Table 9 – Test case specifications. 88
Table 10 – test case specifications 90
Table 11 - Rock mass properties of rock surrounding well BL2 and BL3 at the Bekkelaget site 90
Table 12 - test case specifications 93
Table 13 - Rock mass properties of rock surrounding well BH3 and BH4 at the Vettakollen site 92
Table 14 – Cumulative infiltration [m^3] values of cases Lake Bergen D20 BH4 and Lake Lillehammer D20 BH4 over the tunnel interface after 1 year. 98
Table 15 – Cumulative infiltration amounts over the tunnel interfaces 101
Table 16 – Cumulative infiltration 1 year after construction of tunnel over the tunnel interface. 107
Table 17 – Cumulative infiltration over soil-rock interface for slope and flat cases with same input parameters. 110

Table 18 – Cumulative infiltration amounts over the tunnel interface of tunnel depth 20m with different climatic and rock mass properties 113
Table 19 - Pouring amounts test1 125
Table 20 - Pouring amounts test2 130
Table 21 – Slug test measurements Bekkelaget 131
Table 22 – Slug test measurements Vettakollen 131
Table 23 – Initial infiltration rates over tunnel interface 148
Table 24 - Initial infiltration rates over soil-rock interface 148
Table 25 – Initial infiltration rates over tunnel interface 156
Table 26 - Initial infiltration rates over soil-rock interface 156

1.0 Introduction

1.1 Background

Constructing underground excavations has been done for several hundred years. It involves many factors affecting the stability of the excavation. One particularly important factor is the presence of water.

An underground excavation also affects the hydrogeological conditions in the area of construction. The understanding of this is both important for tunnel stability and the general water balance of the area. In such an event where the groundwater is significantly altered this could lead to settlements.

Water also affects the both the stability and the support structures within an excavation (Nilsen&Broch 2009). During the construction of an underground excavation the presence of water influences the speed of which an excavation can be constructed at. This can be by high water pressures hindering charging and blasting. During the life time of the excavation water can affect the long term stability by activating swell clay. Another threat is corrosion on construction support.

Because of these problems related to water in underground excavations the understanding of infiltration of water in to underground excavations is important. Especially understanding the water infiltration on the soil-rock interface is important to understand the effects in a underground excavation.

1.2 Aims and limitations of the research

The aim of this thesis is to process gathered data from field and laboratory work in to models which simulates the injection of water in to rock mass wells and the propagation of water over different material interfaces. By establishing that the tests carried out can be simulated with a desirable outcome it is thought that the results will show:

- Simulation of water injection to rock mass wells will prove that continuous models can simulate water propagation in to rock masses

- Simulation of water movement over an interface between two different materials will prove that the models can simulate the infiltration between the two matters with good retention parameters.

Finally the thesis will give examples large scale models of realistic scenarios. By the validation of the simulation of the field and laboratory tests the large scale models are thought to be valid.

Since this thesis is limited to a 20 week period the main limitation of this research will be time. A central part of the thesis is the learning of the numerical modelling software used in the thesis and this is thought to be time consuming. More field investigation and correlation of data processed would be interesting to obtain more detailed knowledge about the outcome but here the time frame of this thesis also comes in to play.

2.0 Literature review

In the following subchapters general literature review will be found. It focuses on giving a throughout introduction to hydrogeology and the parameters affecting water flow. Some emphasis has been put on the theoretical approach to the field tests carried out.

2.1 Introduction to hydrology

2.1.1 The hydrologic cycle

The hydrologic cycle is the name of the cycle which water moves through on Earth. It is a cycle which both transports and shifts water from phase to phase. The entire cycle is driven by energy from the sun (Brattli 2011). There are several means of transportation of water within the cycle of which the atmosphere is the necessary connecting link between the ocean and the land. Evaporation transports water from the oceans to the atmosphere which gets rid of it in the form of precipitation. Rivers and groundwater flow represent the main on-land forms of water transportation. These two transportation systems both eventually drain everything into the oceans which is the Earths large storage site for water.

To illustrate this 97% of Earths water is bound in the oceans as saltwater, while only 2,5% is fresh water (Brattli 2011). Much of this is not available as it is bound as ice and snow, non-drainable soil moisture or in biological marshes. The consequences of this is that groundwater represent 99% of the available fresh water on earth (Dellur 1999).

The hydrologic cycle has its name because it is thought to be an eternal process and therefore has the name cycle. This is of course not entirely true as it is highly dependent on the sun (Brattli 2011). In the human time perspective though, the sun's life time will be eternal. This means that the cycle has neither natural starting nor ending point which implies that all of the contributing factors to the cycle can happen at once or individually.

2.1.2 The general water balance equation

A very simplified water balance equation can be sketched by quantifying the individual parts of the hydrologic cycle:

$$P = E + Q \pm \Delta M \ [m^3]$$

Equation 1

where P is precipitation, E evapotranspiration, Q runoff and ΔM the change of the stored water amount (Brattli 2011). Solely practical this means that the changed amount of stored water in a ground water reservoir is the increased volume represented by precipitation minus the lost volume represented by runoff and evapotranspiration.

2.1.3 The saturated and unsaturated zone

Water in the subsurface can according to Gupta&Singhal (2010) broadly be defined as two zones; the saturated and the unsaturated zone. As the names indicate the two zones are distinguished from one another by the amount of water which is present in the ground. In the saturated zone all pores of the material are filled with water. In the unsaturated zone the degrees to which the pores are filled with water vary. The level of which separates the two zones is commonly known as the groundwater table or the depth of the groundwater (Brattli 2011). At the groundwater table the pressure is equal to the atmospheric pressure.

The different properties of the two zones will be presented and discussed thoroughly later on.

2.1.4 Aquifers

Aquifer is the common name of a storage medium for groundwater, also known as a groundwater reservoir. It commonly consists of both rocks and soils, and different geological properties give various aquifer properties. The nature of geological deposits is that there are large variations and the properties of the deposits are seldom equal. This means it is hard to distinguish different aquifer types and extensive data is often needed for exact characterization (Gupta&Singhal 2010). Gupta&Singhal (2010) present different aquifer types which are presented in the following together with a principal sketch of the two most common aquifers, confined and unconfined aquifers from Dellur (1999).

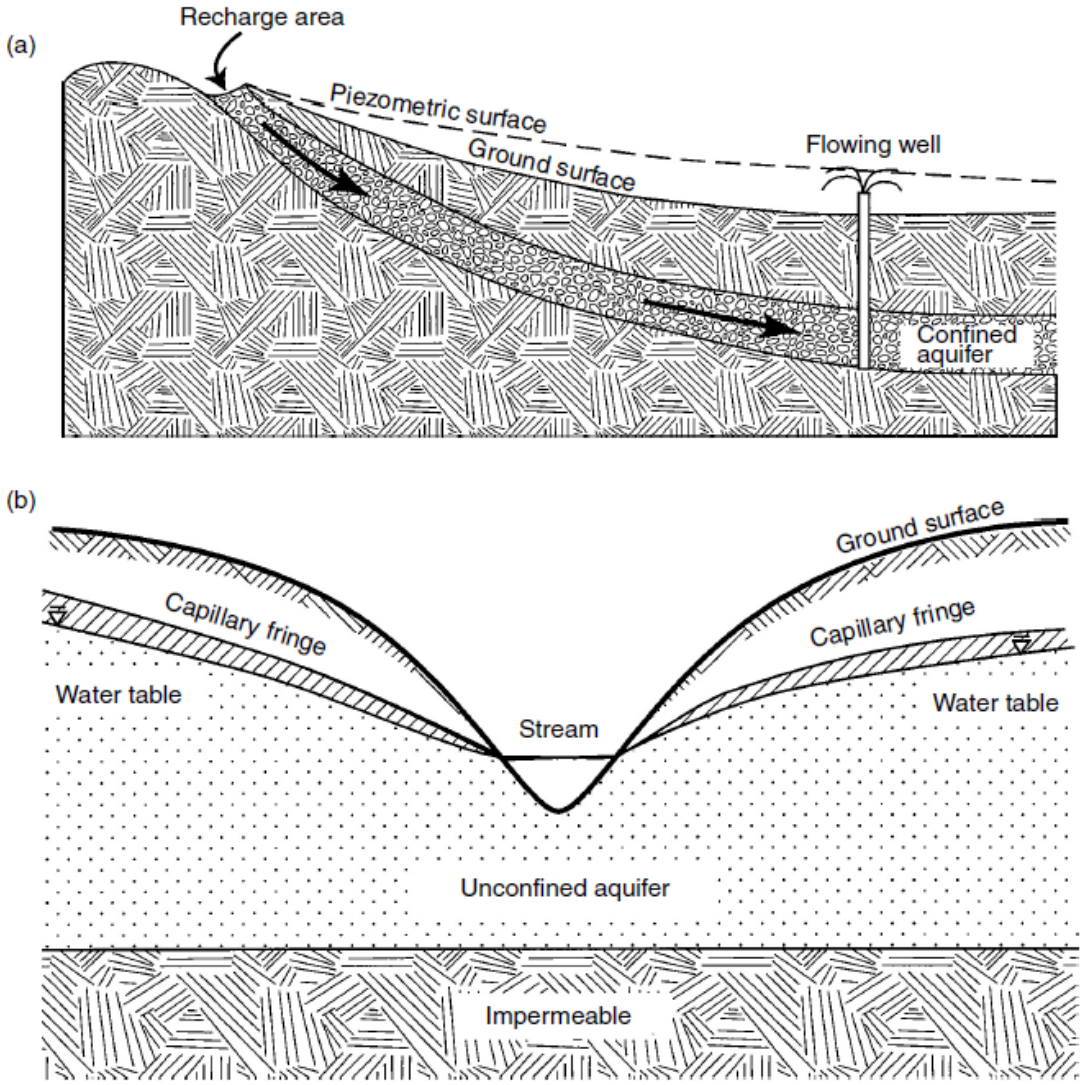

Kinds of aquifers. (a) Confined aquifer; (b) unconfined aquifer.

Figure 1 – A principal sketch of both a) confined and b) unconfined aquifers from (Dellur 1999)

Confined aquifers are just that, confined, and are also called artesian aquifers (Gupta&Singhal 2010). This means that it has impermeable layers hindering the flow of water both out from and in to the aquifer. The pressure of the aquifer is higher than the atmospheric pressure. This means that a confined aquifer with a pressure height reaching higher than the surface can act as an artesian well. The formations of confined aquifers are multilayered formations, fractures and joints and solution cavities.

Unconfined aquifers are aquifers with an open surface without any impermeable layer hindering the aquifer surface to be at atmospheric pressure. There is the need of a confining layer underneath which blocks the water from infiltrating further down in the soil, see Figure 1.

Leaky or semi-leaky aquifers are a combination of the aforementioned aquifers. This is often the state of which one will find a confined aquifer in nature as it is seldom that an aquifer is fully confined (Gupta&Singhal 2010). Normally an impermeable layer will, to some extent, be leaky or a water transporting fracture will intersect the impermeable layer.

Three more but also less usual are *perched*, *double* and *triple aquifers*. The first is an unconfined aquifer totally separated from a larger scale main aquifer. The two others are characterized by two and three transportation mediums for water such as fractures and karst formations.

2.2 Basic geological parameters

In the following chapters frequently used parameters will be described.

2.1.1 Porosity

The porosity of a geological material describes how much of the material which is occupied by voids. There is no unit for porosity which is a relation between sample volume and pore volume. When the entire volume of a rock mass is V_t and the volume of the pores in the material is V_p the porosity can be described as

$$n = \frac{V_p}{V_t}$$

Equation 2

(Dellur 1999). Determining the V_p and the V_t can be done by obtaining a soil sample of a known volume, and put in water whilst measuring the volume change (Dellur 1999). The samples volume minus the change of volume of the water will determine the V_p. This means that the porosity n equals the saturated water content θ_s:

$$n = \theta_s$$

Brattli (2011) presents another equation for determining the porosity without knowing the exact pore volume. This is based on the specific weight of a sample before and after the sample being dried.

$$n = \left(1 - \frac{\gamma_s}{\gamma_d}\right) = 1 - \left(\frac{\frac{W_s}{V_t}}{\frac{W_s}{V_s}}\right)$$

Equation 3

Here V_t is the total volume of the sample, V_s the volume of the solids and W_s is the weight of this.

Sometimes not all the pores in a material will be interconnected and therefore not open for water flow. This makes the aforementioned method not sufficient for determining the porosity. The porosity which water moves trough is called *effective porosity* (Dellur 1999). When finding the V_s it is important that there is no effective porosity, otherwise the V_s value will be wrong. The effective porosity is mainly associated with rocks.

As for soils, the sorting and grading of a material is important for the porosity. When a material has a god sorting it means that there is a uniformly distributed grain size. A well graded material will have a wide range of grain sizes. This affects the porosity because a well graded material will have many small grains that can fill the pore volumes between the larger grains. A well sorted material will have a larger porosity than a poorly sorted one because the grain size is uniform.

Another important property for porosity is packing. This is illustrated in Figure 2 where A shows the largest porosity obtained by a packed material with grains of equal size which is 47,65 % while B shows the smallest obtainable porosity at 25,95 % (Dellur 1999). Stating this however, it must be pointed out that both these scenarios are not very realistic as there to some extent will always be grains of a different size in the material and a packing as in case A will not occur naturally.

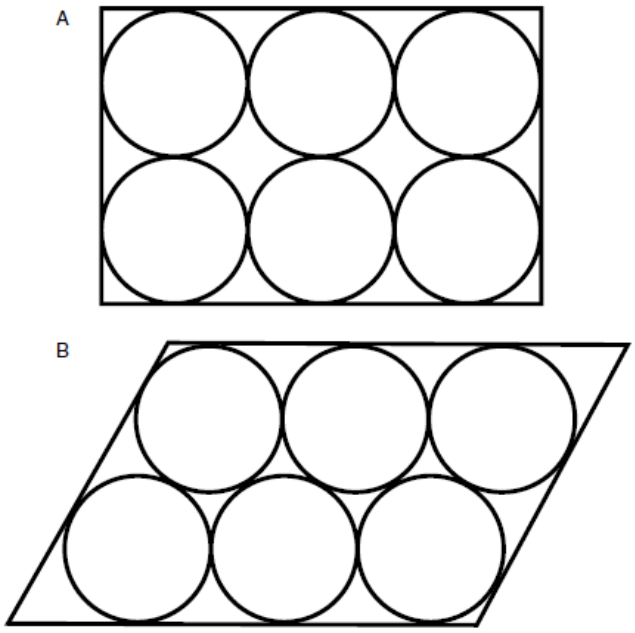

(A) Cubic packing; (B) Rhombohedral packing.

Figure 2 - Packing of two uniformely sorted materials; A the largest possible porosity and B the least possible porosity (Dellur 1999).

The porosity of a rock mass is much more complicated. The porosity will depend on different factors; fracture aperture and spacing, effective porosity and fracture fill material. A typical rock mass will also have a much smaller porosity than a soil. This lies in the nature of a rock mass being either a compacted, consolidated or melted state of an aggregate. This is illustrated in Figure 3 where the soils have a typical porosity of 30-50 % whereas a rock has a typical porosity of 5-30 % (Dellur 1999).

Important Physical Properties of Soil and Rock

Lithology	Porosity (percent)	Hydraulic conductivity (cm/sec)	Compressibility, α (m^2/N or Pa $^{-1}$)
Unconsolidated			
Gravel	25–40	10^{-2}–10^{2}	10^{-8}–10^{-10}
Sand	25–50	10^{-4}–1	10^{-7}–10^{-9}
Silt	35–50	10^{-7}–10^{-3}	no data
Glay	40–70	10^{-10}–10^{-7}	10^{-6}–10^{-8}
Glacial Till	10–20	10^{-10}–10^{-4}	10^{-6}–10^{-8}
Indurated			
Fractured Basalt	5–50	10^{-5}–1	10^{-8}–10^{-9}
Karst Limestone	5–50	10^{-4}–10	not applicaple
Sandstone	5–30	10^{-8}–10^{-4}	10^{-11}–10^{-10}
Limestone, Dolomite	0–20	10^{-7}–10^{-4}	$< 10^{-10}$
Shale	0–10	10^{-11}–10^{-7}	10^{-7}–10^{-8}
Fractured Crystalline Rock	0–10	10^{-7}–10^{-2}	—10^{-10}—
Dense Crystalline Rock	0–5	10^{-12}–10^{-8}	10^{-9}–10^{-11}

Source: Adapted from Domenico, P.A. and Schwartz, F.W 1990. *Physical and Chemical Hydrogeology*, John Wiley and Sons, Inc., New York; Freeze, R.A. and Cherry, J.A., 1979. *Groundwater*. Prentice-Hall, Inc., Englewood Cliffs, NJ; Fetter, C.W., 1994. *Applied Hydrogeology*, 3rd ed. Macmillan College Publishing Co. Inc., New York; Narashimhan, T.N., and Goyal, K.P., 1984. Subsidence due to geothermal fluid withdrawal, in Man-Induced Land Subsidence, *Reviews in Engineering Geology, v.* VI, 35–66, Geological Society of America, Boulder, Co.

Figure 3 - Examples of different porosities for typical rock and soils by Dellur (1999).

The uniformity coefficient C_u describes how well a soil material is graded. The C_u can be found by the formula

$$C_u = \frac{D_{60}}{D_{10}}$$

Equation 4

Where D_{10} and D_{60} is the diameter of which is found when 10 % and 60 % respectively of a sifted soil are finer. I.e. at the diameter one have when 40 % of a material has passed through sieves of different meshes will be D_{60}. A C_u of 4 or less will indicate a well sorting and a C_u of 6 or higher will indicate a poor sorting with the latter having the lowest porosity (Dellur 1999).

The porosity can also be described as

$$n = \frac{1}{1 + \frac{1}{e}} = \frac{e}{(1 + e)}$$

Equation 5

Where the e is called the void ratio and is determined by:

$$e = \frac{V_p}{V_s}$$

Equation 6

V_s is the volume of the solids of the rock mass and V_p the pores (Dellur 1999). Hillel (1998) states that engineering geologists normally prefer using the void ratio rather than the porosity because it relates the pore volume to the volume of the solids and not the total volume. This means that a change in the pore volume will only affect the numerator as the two values are independent of each other.

2.2.2 Bulk density

The Bulk density relates the mass of a solid to the total volume of a sample (Hillel 1998). There are two different types of bulk density; the dry and total, sometimes called dry, bulk density. The dry bulk density will always be less than the total bulk density. The dry bulk density is expressed as

$$\rho_b = \frac{M_s}{V_t} = \frac{M_s}{V_s + V_a + V_w} = \frac{M_s}{V_s + V_p} \left[{}^{g}/_{cm^3} \right]$$

Equation 7

Here the W_s is the weight of the solids, V_w denotes volume of water, V_t total volume of the sample, V_a the air volume, V_s the volume of the solids and V_p the pore volume (Hillel 1998).

The total bulk density is the ratio between a saturated samples weight and the volume of it, hence:

$$\rho_t = \frac{W_t}{V_t} = \frac{W_s + W_w}{V_s + V_p} \left[{}^{g}/_{cm^3} \right]$$

Equation 8

Where W_w is the weight of the water in the sample (Hillel 1998).

2.2.3 Moisture content

The moisture content of a rock or soil sample can be decided by two definitions, either gravimetrical or volumetric. The volumetric definition is mostly used albeit some applications require a gravimetrical definition. Moisture content is measured in percent (Hillel 1998, Dellur 1999).

Volumetric moisture content:

$$\theta = \frac{V_w}{V_t} = \frac{V_w}{V_s + V_w + V_a} = \frac{V_w}{V_s + V_p}$$

Equation 9

Gravimetrical moisture content:

$$w = \frac{W_w}{W_s}$$

Equation 10

By using the bulk and water densities the volumetric and gravitational moisture content can be related to each other (Hillel 1998):

$$\theta = w * \left(\frac{\rho_b}{\rho_w} \right)$$

Equation 11

Here ρ_w is the bulk density and ρ_w is the density of water.

2.2.4 Saturation ratio

Related to the parameters of moisture content is the saturation ratio which describes to what degree a pore volume is filled with water. It is denoted by S_r, and given by:

$$S_r = \frac{V_w}{V_p}$$

Equation 12

The degree of saturation is the saturation ratio expressed as a percentage (Hillel 1998, Dellur 1999).

If the degree of saturation and porosity is known it is possible to calculate the volumetric moisture content in percent by

$$\theta = S_r * n = \frac{V_w}{V_p} * \frac{V_p}{V_t} = \frac{V_w}{V_t}$$

Equation 13

(Dellur 1999).

2.2.5 Capillarity

Capillarity is the ability fluids have to rise along walls of materials due to intermolecular forces between the fluid and the solid known as adhesive forces (Dellur 1999). This forms a curved meniscus which is illustrated easily with water in a straw that rises higher along the walls than in the middle, see Figure 4 by Dellur (1999). The rise stems from the pressure at the bottom of the meniscus within the water is lower than the atmospheric pressure. The narrower the tube is the higher the raise in the cylinder will be.

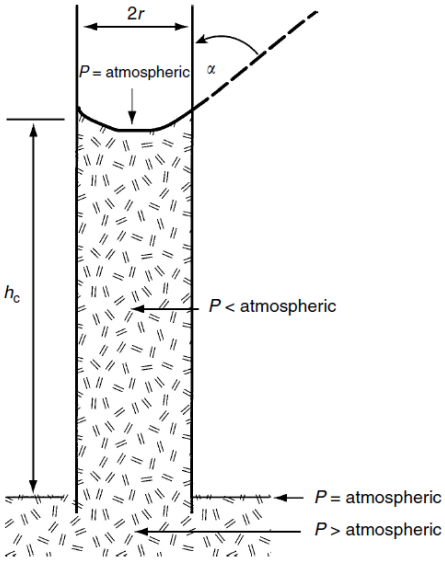

Capillary rise in a tube. (Adapted from Lohman, S.W. 1972. *Ground-Water Hydraulics.* U.S. Geological Survey Prof. Paper 708, U.S. Government Printing Office, Washington, DC.)

Figure 4 – An illustration of capillarity by Dellur (1999) courtesy of Lohman (1972)

In the example of the straw in Figure 4 the capillary rise will be determined from

$$h_c = \frac{2\sigma \cos \alpha}{\gamma_w r} [cm]$$

Equation 14

Where h_c is the capillary rise in centimetres, r the radius in centimetres, σ is the surface tension in N/m of water at 0˚C, γ_w the specific weight and α is the contact angle of the fluid. For water this is α = 0˚.

The height the fluid rises at 0˚C is described by Domenico&Schwartz (1990) as:

$$h_c = \frac{0{,}153}{r} [cm]$$

Equation 15

This means that a smaller diameter gives a higher capillary rise. This is derived from the previous equation by using the values of σ =0,0756 N/m γ_w=9,805 kN/m^3 and α = 0˚.

As for groundwater in soils the capillarity is high given a soil's large surface area albeit it will naturally change a lot with the actual soil at hand. Mavis&Tsui (1939) states that the capillary rise of a soil can be described as

$$h = \frac{2.2}{d_H} * \left(\frac{1-n}{n}\right)^{2/3} [mm]$$

Equation 16

Where n denotes the porosity and d_H [mm] the mean harmonic diameter of the grains. This indicates that a soil such as clay with a low d_H will give a high capillary rise. In opposition, a coarse material with high d_H will have a very capillary rise.

2.2.6 Darcy's law

Darcy's law describes the flow rate through a fully saturated porous media, and states that the flow rate is proportional to the loss of head. Given that one has a porous media over a cross section A [m^2] where K is the hydraulic conductivity of the material and a hydraulic gradient I = dh/dl, Darcy's law describes flow rate as:

$$Q = qA = -KA\frac{dh}{dl} = KAi$$

Equation 17

(Dellur 1999).

Because the movement follow a gravitational potential from the highest to lowest point there is a negative gradient. The q parameter introduced is the specific discharge or Darcy velocity. Dellur (1999) also describe the pore velocity ν as

$$\nu = \frac{q}{n_{eff}} [^m/_s]$$

Equation 18

and this gives the average velocity in the pores. The Darcy velocity q is a measurement of speed over a distance.

Important to note is that Darcy's equation is only applicable for fully saturated porous media. This means that the hydraulic conductivity is at its maximum and thus it is in an ideal flow state regarding the medium properties at hand (Hillel 1998, Dellur 1999). In groundwater the fluid properties will belong to water, which does not change too much with neither

temperature nor pressure. This means that the medium properties are the main contributor to the change of flowing properties within an aquifer which justifies the use of the hydraulic conductivity over the permeability.

2.2.7 Intrinsic Permeability

Permeability describes a fluid's ability to transmit water from one pore to another in a porous material. Dellur (1999) gives a simple equation based on the average pore diameter d and an empirical constant C which takes packing and sorting amongst other parameters into account. The equation for the permeability k is:

$$k = C * d^2[m^2]$$

Equation 19

It is important to note that the permeability is a constant relying on the medium of which a fluid is transported through and nothing else. This leaves out properties of the through passing fluid as well as temperature and pressure. The unit of the permeability is Darcy and is commonly given in millidarcy which is defined by centipose and atmospheric pressure. According to Dellur (1999);

$$1\ darcy = 9{,}87 * 10^{-9}[cm^2]$$

Equation 20

However, some authors use the unit cm^2 directly instead of millidarcy.

2.3 Water in the saturated zone

The saturated zone of a soil is the zone of where the degree of saturation is 100%. This means that all the pores are filled with water. The level where the degree of saturation goes from 100% to less is called the groundwater table and is the interface between the saturated and unsaturated zone. There is a distinction between the two zones because the properties that affect the groundwater movement are different.

2.3.1 Hydraulic conductivity in fully saturated soils

While the intrinsic permeability does not take fluid properties into account the hydraulic conductivity does that. This means the hydraulic conductivity takes the permeability a step

towards an estimation of a realistic water flow in a porous media. This is a simplified way of putting it, and the soil's ability to let water flow freely depends on many factors. Amongst them is the effective porosity, size of the pores and the fluid's viscosity properties. Both the effective porosity and the pore size depend solely on the geological material at hand. This includes how well graded and sorted the soil is, grain size distribution and grain geometry. E.g. clay will have a low hydraulic conductivity due to the small grain size and adhesion caused by the grains surface area, despite clay having a large porosity (Brattli 2011). Another example is moraine which has a well graded sorting and thus a low hydraulic conductivity due to low porosity.

It is important to note that the hydraulic conductivity differs from permeability by the consideration of the fluid's viscosity and temperature as well as medium properties (Dellur 1999). It is defined as

$$K = \frac{k\rho g}{\mu} [^{m}/_{s}]$$

Equation 21

where ρ is density of the fluid, μ dynamic viscosity and k the permeability.

A method of estimating the hydraulic conductivity was suggested by (Kozeny 1927) and later modified by (Carman 1937, Carman 1956) and is widely known as the Kozeny-Carman equation. It utilizes a grain distribution curve and material properties to estimate the hydraulic conductivity:

$$K = \left(\frac{\rho g}{\mu}\right) * \left[\frac{{n_{eff}}^3}{\left(1 - n_{eff}\right)^2}\right] * \left(\frac{{d_{10}}^2}{180}\right) [^{m}/_{s}]$$

2.3.2 Viscosity

Viscosity is a factor related to any fluid flow and is a measurement of the shear force the fluid generates with the solids it moves along. Viscosity is defined as the proportionality factor between the force required move a fluid with shear, and the velocity of the shear when a fluid is moved (Hillel 1998). It is given by the equation:

$$\tau = F_s * A = \mu * \frac{\mathrm{du}}{dx} \left[{}^{kN}/_{m^2} \right]$$

Equation 22

Further this gives the equation for the dynamic viscosity

$$\mu = \frac{\tau}{\frac{du}{dx}} \left[{}^{g}/_{cm * s} \right]$$

Equation 23

where τ is the shear stress calculated from the force F_s acting on the area A. The μ is the coefficient of dynamic viscosity which is multiplied with the velocity gradient perpendicular to the area A.(Hillel 1998).

Furthermore Brattli (2011) states that the kinematic viscosity is a constant that expresses how resistant a fluid is to shear ignoring the density of the fluid. The kinematic viscosity is expressed as

$$\nu = \frac{\mu}{\rho} \left[{}^{m^2}/_{s} \right]$$

Equation 24

2.3.3 Gravitational potential and hydraulic gradient

Because of gravity a energy potential will be present for any water flow. This means that there will be a potential ranging from nil to any positive number (Hillel 1998) called the gravitational potential and is expressed as

$$E_g = Mgz = \rho_w V g z \left[{}^{kgm}/_{s^2} \right]$$

Equation 25

Where E_g is the potential energy of the water mass M occupying the volume V on a level z above a reference point. ρ_w is the density of water and g the gravitational force (Hillel 1998).

(Brattli 2011) defines the total hydraulic pressure height with the equation:

$$h = z + h_p[m]$$

Equation 26

Here h is the hydraulic potential which is the sum of the pressure height h_p and height z above a reference level.

Furthermore whenever there is a groundwater flow in a soil this is related to the hydraulic potential. The relationship between those two parameters is the hydraulic gradient which determines the loss of head per unit length of flow and is expressed by:

$$I = \frac{dh}{dl}$$

Equation 27

This does not have a dimension (Dellur 1999). This is a significant part of groundwater flow and is present in e.g. Darcy's Law.

2.4.1 Water in the unsaturated zone

The unsaturated zone is the part of the soil which has a saturation ratio of $S_r > 1$. This means that it is not in the fully saturated area of the soil. Therefore a part of the unsaturated soil's pores are filled with air which leads to different water transportation properties than a fully saturated soil with $S_r = 1$. In addition, some of the main driving forces of saturated flow make a lesser impact on the flow.

The water amount in the unsaturated zone is dependent on infiltration of rainfall and surface water as well as evaporation, evapotranspiration and runoff. The moisture content in the unsaturated zone will also vary with the depth as can be seen in Figure 5 from Dellur (1999). It shows the moisture content and hydraulic conductivity as a function of pressure head varying with depth and saturation. Note that this is a principal sketch and not the exact curve that always will be present in an unsaturated soil. The space between the drying and wetting curve is caused by hysteresis. This is a complex phenomenon which Dellur (1999) briefly

describes as strong capillary and adhesive forces that draws the water to a soil with a low moisture content, and holds the water when the soil is being drained.

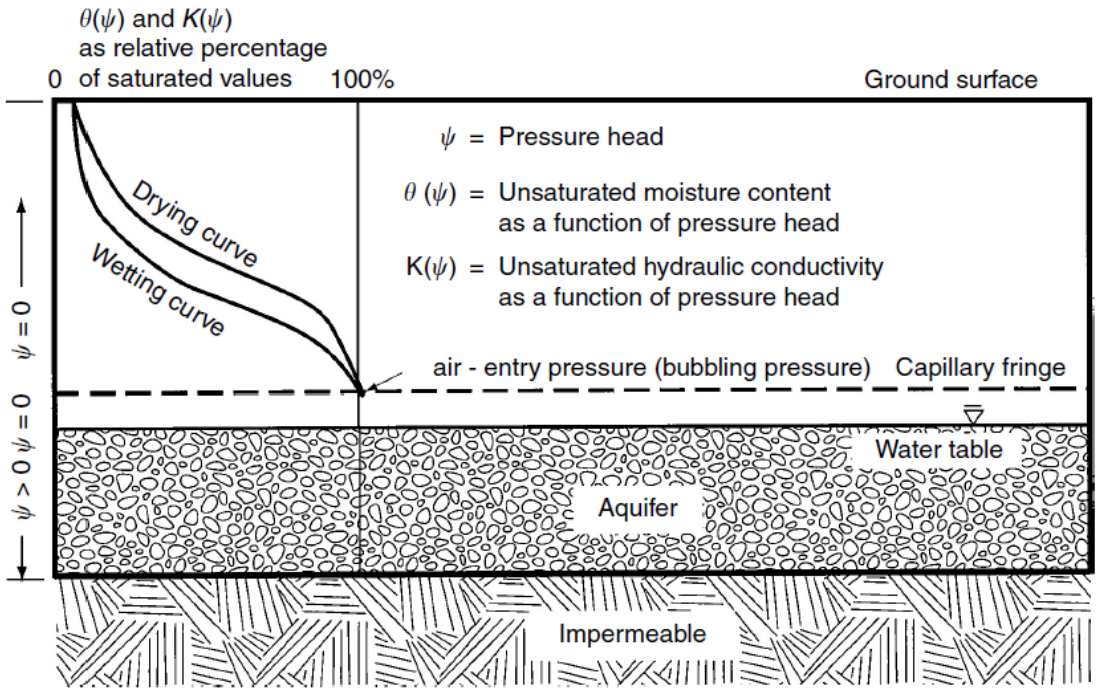

Figure 5 – An illustration of the soil-water characteristic curves from (Dellur 1999)

When the saturated zone is reached the hydraulic conductivity reaches its maximum and remains constant for the entire saturated zone. In addition Dellur (1999) describes the moisture content in the unsaturated zone as not evenly distributed, which means that there will be variations of moisture both horizontally and vertically. This is because a large variation of factors including soil types, anisotropy, infiltration rates and surface conditions apply. Furthermore this will make any estimation of flow properties in the unsaturated zone even more uncertain.

2.4.2 Moisture movement and hydraulic conductivity characteristics of the unsaturated zone

In an unsaturated soil the water movement is driven by the pore pressure, hydraulic height, the gravitational potential and a pressure potential known as the matrix potential. The latter is negative due to surface tensions and hence does a work opposite of the gravitational potential. Which of the matrix or gravitational potential are dominating depends on the moisture content (Brattli 2011).

Generally the rule of thumb is that high moisture content will give a higher flow rate, which is saying that the gravitational potential is the main driving force. This is because water will try to move where there is already water. Because of this, high moisture content reduces the matrix potentials role in the water transportation processes. If there moisture content is close to the soil's specific retention though, the matrix potential can be several orders larger than the gravitational potential (Brattli 2011). The specific retention is the non-drainable water within the pores of a material.

The volumetric water content is a function the matrix potential and can only be determined experimentally and presented graphically (Brattli 2011). The curve presented in Figure 5 represents this relationship and it illustrates a wetting and drying sequence at atmospheric pressure.

2.4.3 Water retention characteristics

The soil's water retention characteristics describe a soil's ability to store or release water (Dellur 1999). The equation for the capillary rise for water at 20˚C from the chapter on capillary rise will be:

$$h_c = \frac{0{,}149}{r}[cm]$$

Equation 28

It is noteworthy that the nominator value changes due to a temperature change of 20˚C. With regard to the water retention characteristics the h_c will here be the soil water suction (Dellur 1999). The value of h_c represents the value where the pores are still full until they exceed this value when a soil is in a drying state. However when the soil is wetting, the pores will start to fill when h drops below the h_c. The hysteresis is the difference between the increase and decrease of suction when the values of h rise or drop below h_c (Dellur 1999). According to Dellur (1999) problems arise when determining the hysteresis because of the generally poor knowledge of soil structures.

2.4.4 Water movement in the unsaturated soil

As for obtaining an estimate of the water movement in an unsaturated soil, Dellur (1999) gives a method which is described in the following:

Considering a one dimensional vertical flow with a positive z downwards, moisture content θ and soil water flux q the continuity equation is described as

$$\frac{\partial \theta}{\partial t} = -\frac{\partial q}{\partial z}$$

Equation 29

The soil water flux is given from the previously stated Darcy's law with the hydraulic conductivity K:

$$q = -K(\theta)\frac{\partial H}{\partial z}[^m/_s]$$

Equation 30

The equation of the soil water transfer can then be given as

$$\frac{\partial \theta}{\partial t} = -\frac{\partial}{\partial z}\left[K(\theta)\left(\frac{\partial h}{\partial z} - 1\right)\right]$$

Equation 31

Here h is the soil water pressure head relative to the atmospheric pressure, h≤0 because h=0 is the groundwater table, and H is the hydraulic head:

$$H = h(\theta) - z[m]$$

Equation 32

The soil water diffusivity is defined as:

$$D(\theta) = K(\theta)\frac{dh}{d\theta}\left[^{m^2}/_s\right]$$

Equation 33

From this it is possible to transform the soil water transfer equation to only being θ-dependent:

$$\frac{\partial \theta}{\partial t} = \frac{\partial}{\partial z}\left[D(\theta)\frac{d\theta}{\partial z} - K(\theta)\right]$$

Equation 34

This equation is known as the Fokker-Planck equation. Doing the same by expressing the soil water transfer equation to being only dependent on the soil water pressure head h whilst presenting the specific capacity C(θ)

$$C(\theta) = \frac{d\theta}{dh}$$

Equation 35

one get the equation known as Richard's equation:

$$C(\theta)\frac{\partial h}{\partial t} = \frac{\partial}{dz}\left[K(\theta)\left(\frac{\partial h}{\partial z} - 1\right)\right]\left[m^3/_s\right]$$

Equation 36

Note that this is a one dimensional equation (Dellur 1999, Todd&Mays 2005).

2.4.5 Hydraulic conductivity of unsaturated soils

It is hard to estimate the hydraulic conductivity of unsaturated soils. It is because it is difficult to quantify the driving forces of the hydraulic conductivity of the unsaturated soil. They are largely based on empirical approximations. The general approach would be as for saturated conductivity to combine viscosity properties, intrinsic permeability and specific densities as Dellur (1999) presents as:

$$K(\theta) = k\frac{\rho_w g}{\mu_w}k_{rw}(\theta)[^m/_s]$$

Equation 37

Here K(θ) is the hydraulic conductivity which is dependent on moisture content while k_{rw} is the relative water permeability which is a function of the saturation. Compared to the fully saturated hydraulic conductivity the only addition is the saturation ratios additional effect. The knowledge of soil structures are good but hard to describe in an exact fashion. There are generally three different approaches made by Brooks&Corey (1964), Campbell (1974) and

Van Genuchten (1980) which are commonly used for estimation of unsaturated hydraulic conductivity. The three approaches are presented in the following derived from both (Dellur 1999, Todd&Mays 2005):

Generally, K(θ) is the moisture content dependent hydraulic conductivity, K_s is the saturated hydraulic conductivity (i.e. the maximum value of K), n porosity, λ the pore-size index, θ_r the residual water content.

Brooks&Corey (1964):

$$\frac{K(\theta)}{K_s} = \left[\frac{\theta - \theta_r}{n - \theta_r}\right]^m = k_r$$

Equation 38

$$m = 3 + {}^{2}/_{\lambda}$$

Equation 39

Campbell (1974):

$$\frac{K(\theta)}{K_s} = \left(\frac{\theta}{n}\right)^m$$

Equation 40

$$m = 3 + {}^{2}/_{\lambda}$$

Equation 39

Van Genuchten (1980):

$$\frac{K(\theta)}{K_s} = \sqrt{\frac{\theta - \theta_r}{n - \theta_r}} * \left\{1 - \left[\left[\frac{\theta - \theta_r}{n - \theta_r}\right]^{1/m}\right]^m\right\}^2$$

Equation 41

$$m = \frac{\lambda}{(\lambda + 1)}$$

Equation 42

λ is a purely soil related hydraulic conductivity scaling factor.

2.5.1 Hydrogeology of rocks

The hydrogeology of rocks has many of the same characteristics as hydrogeology of soils with respect to parameters describing the hydrogeological processes. The main difference, though, is illustrated from the different characteristics of rocks and soils with regard to importance of groundwater flow. Brattli (2011) states that the water flow in rocks seldom follows Darcy's law as soils do, but a rather complex flow system that highly depends on fracture orientation, aperture, spacing and fill material. For a soil the only place water, or other fluids for that sake, can move is from pore to pore within the media. For a rock mass, however, the water can move from pore to pore as well, albeit with a much smaller conductivity than for a soil because of the natural low porosity of rocks. The main transportation system for water in rock though, is fractures and discontinuities. Stating this however, Gupta&Singhal (2010) describes porosity, permeability and groundwater flow characteristics as poorly understood, especially on a large scale. This is mainly because of the extremely large variations different rock types can have regarding to rock type, porosity and degree of fracturing.

Knowing that fractures and discontinuities is the most important water transporting character of rock masses, it is important to understand the physical characters of the fractures and discontinuities.

2.5.2 Fractures and discontinuities of rocks

Rocks are to a very varying degree fractured caused by many different factors. A fracture within a rock mass is called a discontinuity and can have various properties regarding water transportation and origin. There is a difference between primary discontinuities such as stratification, schistosity and karst cavities, and secondary discontinuities like fractures and faults (Scesi&Gattioni 2009). Moreover the discontinuities and water bearing zones in rocks differs from the rock type. E.g. Scesi&Gattioni (2009) describes fractures being mostly present in intrusive rocks, fractures and schistosity in metamorphic and for sedimentary rocks karst phenomenon, lack of cementation, fracturing and stratifications are the most common.

Furthermore Scesi&Gattioni (2009) describes two categories of "vacuums", i.e. open spaces, in rocks:

- Open spaces created by dishomogenous consolidation, dissolution, lack of cementation etc.

- Open spaces created by schistosity, fractures, faults, stratifications, karst phenomenon etc.

These two categories differs from each other by the first having small fragments that interconnect the spaces within the rock in a similar fashion as for soils. The second category has got larger and more continuous systems where water can flow. For the latter, the water flow is highly dependent on both the geometric and mechanical properties of the open spaces. This is also the most predominant water transporting system of the two.

When considering water flow of the second category the structure of the features water is allowed to flow along will be the actual direction of the water flow. Knowing this, the formation of such paths of water flow is important for understanding the motion of groundwater in rocks.

Gupta&Singhal (2010) describes faults and shear zones, foliation, fractures and bedding planes as different possible discontinuities.

2.5.2.1 Fault and shear zones

Faults and shear zones are made from rupture and shear of the stresses created from mountain building tectonic activity (Gupta&Singhal 2010). A shear zone is a strongly deformed area, typically created by a fault. A fault is a plane where two opposite walls has moved in opposite directions. These can be of large magnitudes, sometimes several hundred kilometres long. Both phenomenon are illustrated in Figure 6.

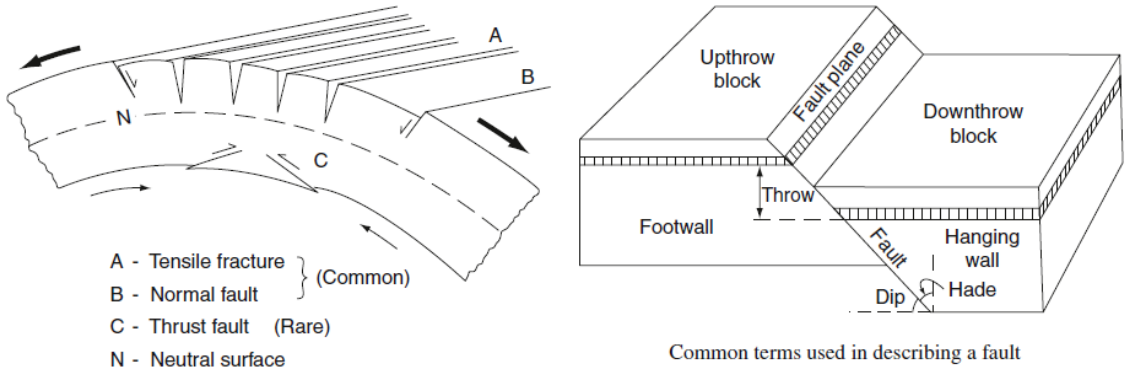

Figure 6 – Different types of fractures (left) and schematic illustration of a fault with dip and strike (right) (Dellur 1999)

2.5.2.2 Foliation

A foliation is a structure weakness planes within a metamorphic rock. The foliation planes are created parallel to the direction of shear forces and can be very small in thickness (Gupta&Singhal 2010). A rock can be fractured along the foliation planes and the degree of this varies a lot from rock type to rock type. A typical example of a foliation plane is a gneiss with lots of schist.

2.5.2.3 Fractures

Fractures, or joints, are planes within a rock mass which has lost some of its cohesion due to shear stresses. Normally the fractures are relative smooth and planar (Gupta&Singhal 2010). Important, though, is that there is little visible movement on the surface as it then will be classified as a fault. A single fracture is not the cause of extensive water transport itself, but when there is extensive cracking within a rock mass there will be significant water transportation. One can classify fractures of rocks in different ways, but a common way is by first- and second-order fractures as well as by genesis with shear, dilation and hybrid fractures. A first order fracture will cut through several layers of rocks, whereas a second-order will only be propagating within one rock layer. A *shear fracture* gives signs of being created by shear forces. *Dilation fractures* are created by tensile stresses and are typically perpendicular to bedding planes.

2.5.2.4 Bedding plane

A bedding plane is the plane of which sedimentary rocks is sedimentated on. It is normally the most significant discontinuity of sedimentary rocks. It can be completely horizontal, angled, planar or folded. These factors contribute largely to the effect on groundwater flow in sedimentary rocks (Gupta&Singhal 2010).

2.5.3 Hydrology of fractures and discontinuities

As Gupta&Singhal (2010) states fractures control the hydraulic characteristics in low permeable rocks as well as forming the main water movement ores in clastic sedimentary rocks. The porosity of rock types varies a lot from one rock type to another. The water movement within the porosity matrix is therefore varying a lot, too. Knowing that the various rock types will be affected differently with regard to water transportation systems it is natural

to divide them in two categories (Gupta&Singhal 2010, Brattli 2011). The hydraulic conductivity of rocks can therefore be expressed as

$$K_{tot} = K_m + K_f [^m/_s]$$

Equation 43

where K_m is the hydraulic conductivity of the matrix and K_f is the hydraulic conductivity of fractures. The conductivity of only one fracture is estimated from the formula

$$K_f = \frac{Q}{A * I} [^m/_s]$$

Equation 44

where Q is the total flux [m^3/s], A the area and I the hydraulic gradient (Brattli 2011). The total flux Q is in this equation expressed different from in a soil by substituting the porosity with aperture opening a;

$$Q = q * A = \frac{\rho * g * a^2}{12\mu} * A \left[m^3/_s \right]$$

Equation 45

(Gupta&Singhal 2010). Reorganizing and substituting gives

$$K_f = \frac{ga^2}{12\nu} * I [^m/_s]$$

Equation 46

where a is aperture opening, g gravity, ν kinematic viscosity and I the hydraulic gradient (Gupta&Singhal 2010). This, however, is only applicable for a single fracture. For a set of parallel fractures the conductivity can be described as

$$K_{f,tot} = \frac{a}{s} * K_f = \frac{ga^3}{12 * s * \nu} * I [^m/_s]$$

Equation 47

(Gupta&Singhal 2010, Brattli 2011).

As the equation indicates the aperture is very important for the conductivity of the material. This proves right as well if one compares a aperture of 0,1mm and 1mm which gives a hydraulic conductivity in the region 10^{-6} and 10^{-3} respectively (Gupta&Singhal 2010). From

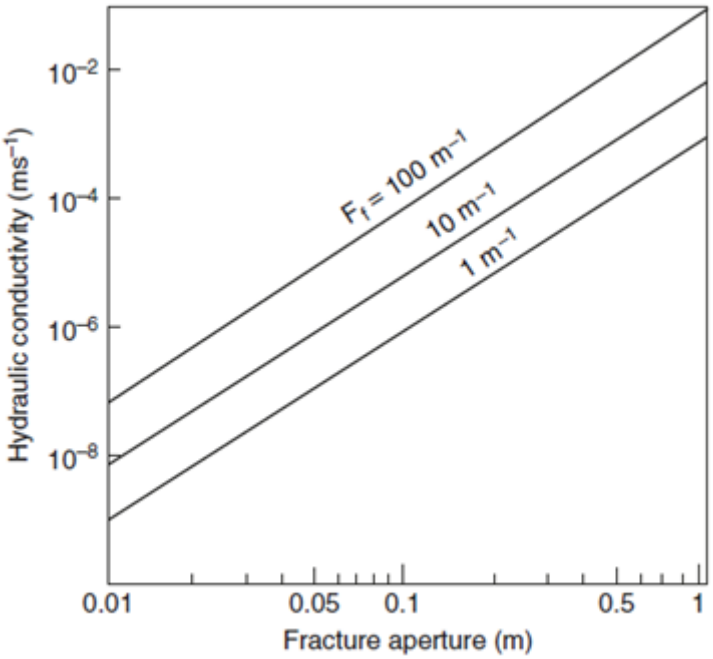

Figure 7 – Fracture aperture versus hydraulic conductivity (Gupta&Singhal 2010).

In Figure 8 one can see conductivities of different rock types and soils. Gravel and sands has the largest hydraulic conductivity whereas massive crystalline rocks represent the opposite end of the scale. One can see that silty sand is approximately the same as fractured shale, siltstone and basalt, as well as karst limestone and dolomite. What those rocks have in common, though, is that they at times are extensively fractured.

Table 8.2 Range of values of hydraulic conductivity and permeability for various types of geological materials

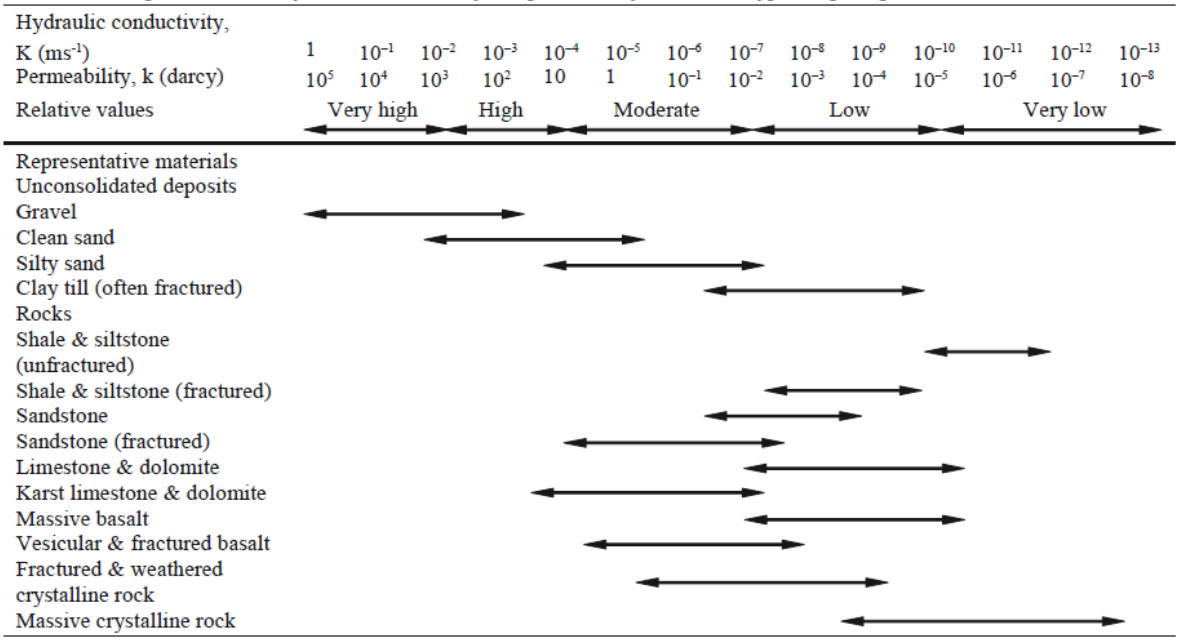

Figure 8 – The Figure shows different hydraulic conductivities for different rock and soil types (Gupta&Singhal 2010).

2.5.4 Skin, filling and stress' effect on permeability

Stress has got an effect on the permeability of fractures. As Gupta&Singhal (2010) states, stress perpendicular to the general fracture orientation reduces permeability of fractured rocks whereas fractures along the largest stress orientation tends to be open. This means that the directions of both fractures and stresses are important when estimating groundwater flow as a particular fracture sett might be almost closed and another very wide due to the stress directions. When there is water flowing in a fracture, the water forms a pressure outwards which works in the opposite direction of the normal stress that acts on a fracture. This leads to normal stress minus the fluid pressure being denoted the effective stress. In most cases the effective stress is positive, but in some cases it can be negative. Hydrofracturing is an example of this. In practise this means that fluid flow will increase along the positive effective stress direction in a rock with a notable degree of fracturing.

Another effect on the permeability of rocks is the presence of fracture skin and filling material along and inside fractures. This can be clay, iron or manganese oxides (Gupta&Singhal 2010) as well as clay, silt and other small fragmented soil deposits. The material can either be solutes or fine material which stems from the drilling of a well (Todd&Mays 2005). This will both reduce the permeability of the fractures and increase the transportation of fine material.

Scesi&Gattioni (2009) also stress that the influence skin has on the hydraulic conductivity increases with the thickness compared to the joint's aperture.

2.6 Introduction to water balance

The water balance describes the in- and output of water to a system and the most common mechanisms for the water balance are described further in this chapter.

2.6.1 Infiltration

Infiltration is the process of water being absorbed in to the soil or rock on the surface, originating from either rainfall or surface water. Water that enters the soil from infiltration is important because it describes the difference between runoff, evaporation and the water that percolates in to the ground. Predicting infiltration is challenging due to the infiltration being a time varying parameter that changes a lot both in the horizontal and vertical direction in a soil (Dellur 1999).

Obtaining an equation for the prediction of infiltration can be done by starting with Equation 48 where n is the porosity and θ the volumetric water content:

$$\theta = \frac{w * \rho_b}{\rho_w}$$

Equation 48

Here w is the mass of the water, ρ_b the dry bulk density and ρ_w, the water density. The degree of saturation can then be described as

$$S = \frac{\theta}{n}$$

Equation 49

(Dellur 1999). Furthermore the effective saturation is defined by Equation 50

$$S_e = \frac{\theta - \theta_r}{\theta_s}$$

Equation 50

where θ_r and θ_s are the residual water content and saturated water content respectively.

From the equation for Darcy velocity, q, shown in Equation 17 Dellur (1999) defines one dimensional infiltration on the surface as

$$i(t) = -K(\theta)\left(\frac{dh}{dz} + 1\right)_{surf}$$

Equation 51

where z is the vertical direction. By taking the area under Equation 51 one get the maximum amount of water a soil can hold at any time, $I_c(t)$ [m^3/m^2], where c denotes infiltration capacity. The unit of the infiltration capacity is unit volume infiltrated over a given surface area (Dellur 1999). This represents a fully saturated soil with a hydraulic conductivity not being dependent of θ anymore. If the precipitation exceed the I_c capacity the excess water will be runoff on the soil surface. The proceeding Figure from Dellur (1999) illustrates a rainfall event and the infiltration capacity over a time period. Note that this Figure 9 presents a precipitation example of a storm event whereas a normal rainfall event will be less prone to exceeding the infiltration capacity. An effect of exceeding the infiltration capacity is runoff on the surface as well as erosion of soils.

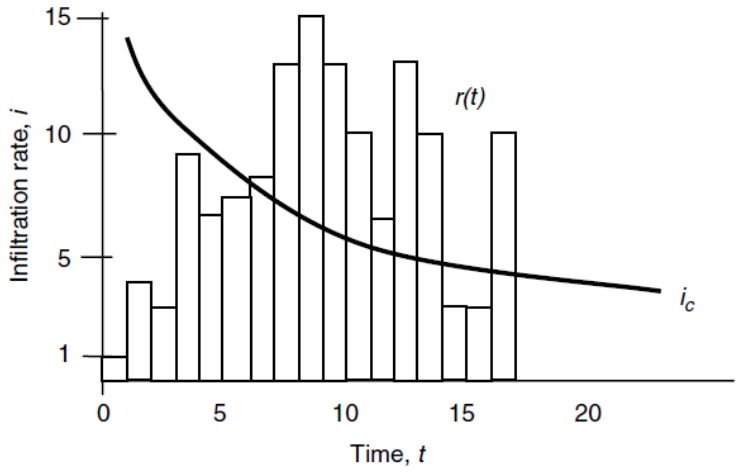

Hypothetical rainfall event, $r(t)$, and soil infiltration capacity, $i_c(t)$. The rainfall event starts at $t = 0$.

Figure 9 - Hypothetical rainfall event and infiltration capacity from Dellur (1999)

As Dellur (1999) points out the infiltration capacity is not exceeded at t = 7 where the rainfall exceed the infiltration capacity for the first time. Instead the total rainfall is plotted along side with the infiltration capacity over time in Figure 10. Here one can see that the intersection between the two curves for rainfall and infiltration capacity represents the time at which there will be an excess water amount compared to what the soil can handle. This point is reached at $t_p \approx 13$.

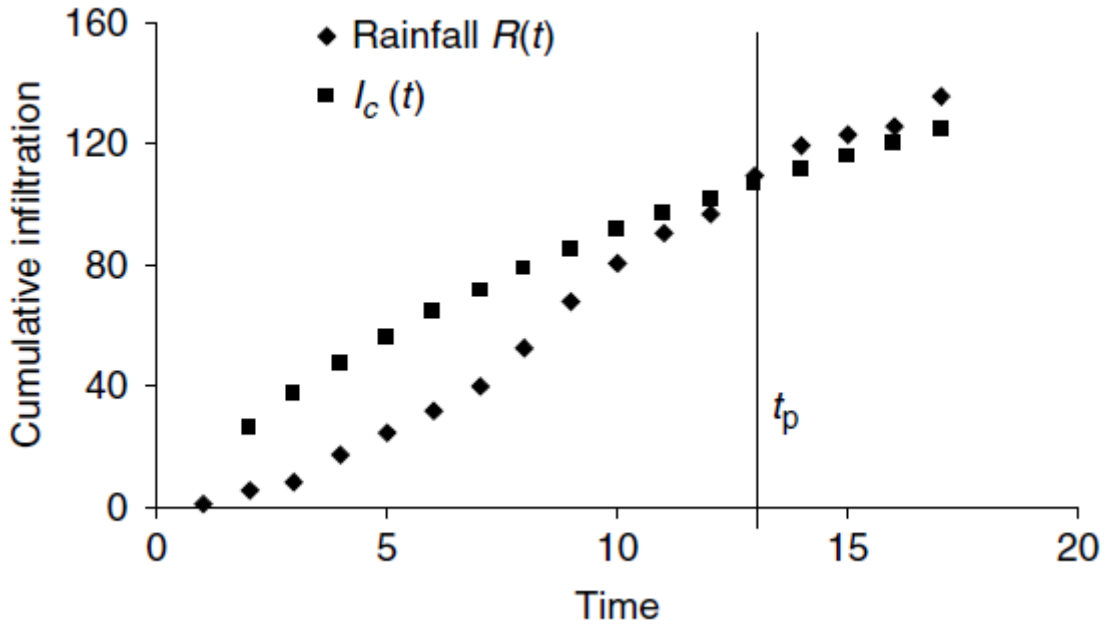

Figure 10 – Cumulative infiltration I_c in the event of a hypothetical rainfall event (Dellur 1999).

A commonly used solution to estimating values for i(t) and I(t) is the *Green and Ampt* approach (Green&Ampt 1911, Hillel 1998, Todd&Mays 2005). It was suggested in 1911 by Green&Ampt (1911) and is a simplified theoretical approach to infiltration processes. It is an approach that has turned out to work well for dry, coarse-textured soils with a well developed wetting front. Albeit giving estimation for the infiltration functions with time it does not reveal anything about wetting profile.

An initial assumption is that there is a distinct and precise wetting front with constant matrix suction during infiltration with a uniformly wet material behind the wetting front and a completely dry material ahead. This is, obviously, not a exactly realistic assumption, but it proves to work for estimations (Hillel 1998).

Hillel (1998) derives an expression of the cumulative infiltration from the Green and Ampt equations and gets

$$I \cong Kt + \delta[m^3]$$

Equation 52

And

$$L_f \cong \frac{Kt}{\Delta\theta} + \delta\ [m]$$

Equation 53

where I denotes the cumulative infiltration over a time t and with a hydraulic conductivity K. L_f is here the depth of the wetting front while the δ is a constant.

2.6.2 Evapotranspiration

As water reaches a soil surface there will be an amount of the water that will not be infiltrated in to the soil as it will disappear as both evapotranspiration and runoff. The quantification of evapotranspiration depend on numerous factors such as humidity, sun activity, wind speed and temperature (Brattli 2011). Evapotranspiration is the sum of evaporation and transpiration. Evaporation is loss of water to the air from the soil or a mass of water whereas transpiration is the loss of water from plants. Both water losses are in the form of vapour. The evaporation can be measured by using an evaporation pan. This is a pan filled with a known amount of water which is put at the site of investigation and the loss of water is measured after a given time period (Brattli 2011).

2.6.3 Runoff

Runoff is water that moves on the soil surface. The rate of runoff depends highly on the precipitations intensity, form and duration, topography, vegetation and the soil's infiltration capacity. Typically the denser the soil surface is the more prone it will be to runoff albeit (Brattli 2011). A frozen ground will also give a large runoff. The saturation ratio of a soil is also important for runoff as a wet soil will absorb less water than a dry soil.

Brattli (2011) present an equation for the infiltration capacity by Horton (1933), Horton (1940) which says

$$f_p = f_c + (f_o + f_c)e^{-kt} \left[{}^{m}/_{s}\right]$$

Equation 54

Where f_p is the total infiltration capacity [m/s] at a given time t, f_c the infiltration capacity at equilibrium, f_o starting infiltration capacity and k is a constant which describes the rate of which the infiltration capacity decreases.

The equation gives that if the precipitation is less than f_c everything that does not evaporate will infiltrate in to the soil. If the precipitation is greater than f_c but less than the starting infiltration capacity f_o all of the water will infiltrate from the start of the precipitation but not all the way through the rainfall event. During the rainfall event the total infiltration capacity will be less than the accumulated precipitation and some of the precipitation will have to be transported on the soil surface as runoff (Brattli 2011). Preferred properties for a high infiltration capacity are loose soils, coarse grain sizes, low saturation ratio and a porous top soil (Brattli 2011).

2.7 Well tests

There are a few different well tests that can be executed in the field. The choice of well test depends highly on the purpose of the test and the scale of investigation (Gupta&Singhal 2010). In addition there are other factors such as time, cost, contamination and expected conductivity.

The different well tests that are most common include the pump test, the Packer/Lugeon test and the slug test.

2.7.1 The pump test

The pump test is a test where a pump draws water out of an aquifer in order to lower the groundwater table. This enables the ability to know the drawdown of the water-table which can be measured either manually or automatically. When the pumping has continued long enough there is created equilibrium where the pump rate and inflow are equal which means that the drawdown is stabilized. The radius r from the well to a point where the water-table is at the initial level exists (Gupta&Singhal 2010). This method requires observation wells or piezometers in order to measure the drawdown. In addition the cross section area and the pumping rate must be known in order to calculate the hydraulic conductivity.

2.7.2 The packer/Lugeon test

The packer/Lugeon test is used mostly when the desired outcome is to understand the properties of a single layer or horizon of the rock mass. By isolating a part of a well with a packer one can put water under pressure at a constant head one can measure the flow rate of the steady state condition (Gupta&Singhal 2010). The limitation of the packer/Lugeon test is that it only reaches a small area around the well. Bliss&Rushton (1984) describes a test interval of 10 feet to being applicable for a 30 feet radius around the bore hole. This restricts the test to a small area around the well.

2.7.3 The slug test

The slug test is a test to perform than the previous tests and is common whenever there is need of a convenient and low cost test. It is especially applicable for aquifers where there is expected a low hydraulic conductivity. There is also a low fluctuation of water when the test is performed which is desirable in cases with pollution. The test is performed by injecting a slug in to a well whilst measuring the change of water height as well as restoring of water table to the normal state with time (Gupta&Singhal 2010). It is crucial that the volume of the slug is known, and the slug can be either a metal piece or a volume of water. The device one measure the change of water table in the well with is normally a pressure transducer which measures the water head in a column above with constant intervals. The volume of the slug and the time used can be adjusted during the test. This is favourable as a low permeability rock mass need a longer test time than a rock mass high permeability(Gupta&Singhal 2010).

In Figure 11 there is a sketch of the events that occur when a slug test is being performed. As seen the original piezometric surface is lifted up a height of h_0 at a time t_0. When time passes the height as a function of time, h_t, is measured. By knowing the height loss h_0-h_t and the well diameter over a given time it is possible to see what rate the aquifer receives water. Seeing the sketch of the slug test it becomes apparent that it is crucial knowing the volume of water of the slug as well as the diameter of the well. This is because when measuring the heights h_0 and h_t they are directly related to the radius of the well and the volume when calculating the out flow rate from the well. For an analytical interpretation of the test the head is the only really important parameter.

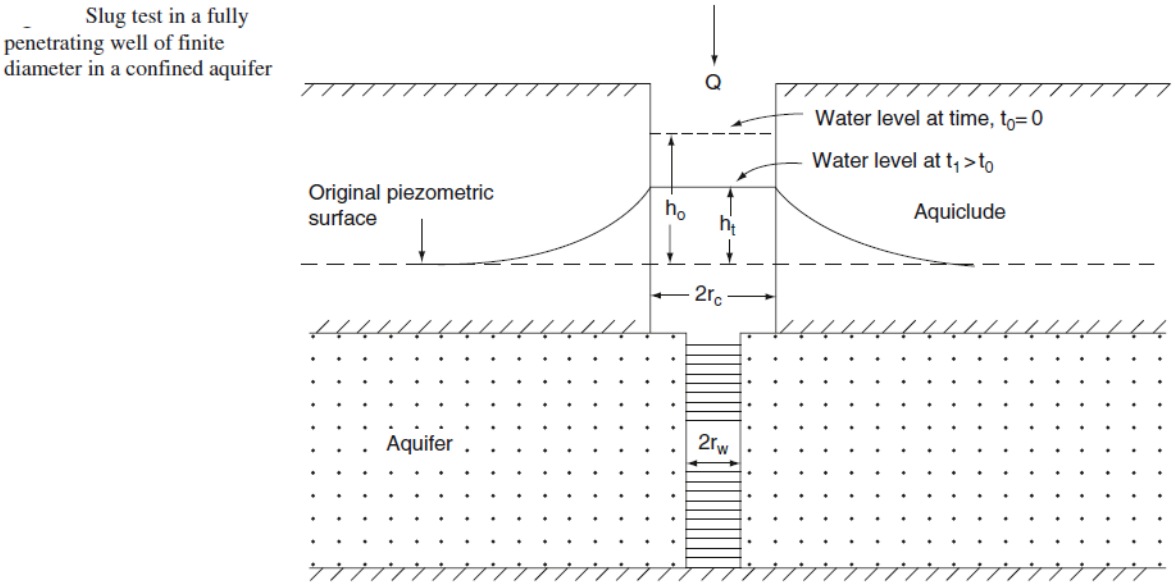

Figure 11- A principal sketch of the effect of the slug on a well in a slug test from Gupta&Singhal (2010)

Butler (1998) states that it is important to measure the heights h_0 and h_t very accurately and as fast as possible after the slug initiation. As an example a measurement error of 0,5 cm of a well with a diameter D=20 cm gives an error of 0,157 L. If the slug has got a volume of 1 L this equals up to 15,7%. This is, obviously, a rather extreme case, albeit it illustrates the fatalities a measurement error can make. In addition Butler (1998) also states that there need to be a sufficient time before a new slug test is performed in the same well. Injecting more than one time per slug test is common but for a new test of the well Butler (1998) states that the water table cannot be changed by more than 5% of the head change.

Furthermore it is apparent that there is a small portion of an aquifer that is being tested with the slug test since it has a relatively low volumetric displacement. The effect of this is that the test results are only applicable for a small portion of the aquifer. Knowing this, a factor such as skin effect is affecting the calculated hydraulic conductivity. Because of this, a well-developed well is preferable because it reduces the uncertainties skin effect can have (Gupta&Singhal 2010).

2.8 The Q-method

The Q-method is a rock mass quality classification method developed by Norwegian Geotechnical Institute (NGI) between 1971 and 1974 (Barton 1974). It is an empirical method for classification of tunnel support design. It is widely used in both Norwegian and international tunneling design. The equation for calculating the Q-value is:

$$Q = \frac{RQD}{J_n} * \frac{J_r}{J_a} * \frac{J_w}{SRF}$$

Where the parameters are **RQD**: Rock Quality Designation, $\mathbf{J_n}$: Joint set numbers, $\mathbf{J_r}$: Joint roughness number, $\mathbf{J_a}$**:** Joint alteration number, $\mathbf{J_w}$: Joint water reduction number.

The only parameter of the Q-method equation used in this paper is the RQD is a percentage of a sample which is longer than 10cm without cracks. It is considered a rock quality indication and the rock quality groups can be seen in Figure 12.

1 RQD (Rock Quality Designation)			RQD
A	Very poor	(> 27 joints per m³)	0-25
B	Poor	(20-27 joints per m³)	25-50
C	Fair	(13-19 joints per m³)	50-75
D	Good	(8-12 joints per m³)	75-90
E	Excellent	(0-7 joints per m³)	90-100
Note: i) Where RQD is reported or measured as ≤ 10 (including 0) the value 10 is used to evaluate the Q-value ii) RQD-intervals of 5, i.e. 100, 95, 90, etc., are sufficiently accurate			

Figure 12 – From (NGI 2013), the classification of RQD values.

The Q-system classification values can be seen in Figure 13. This included because some Q-values are presented in this paper and commented as part of a quality evaluation.

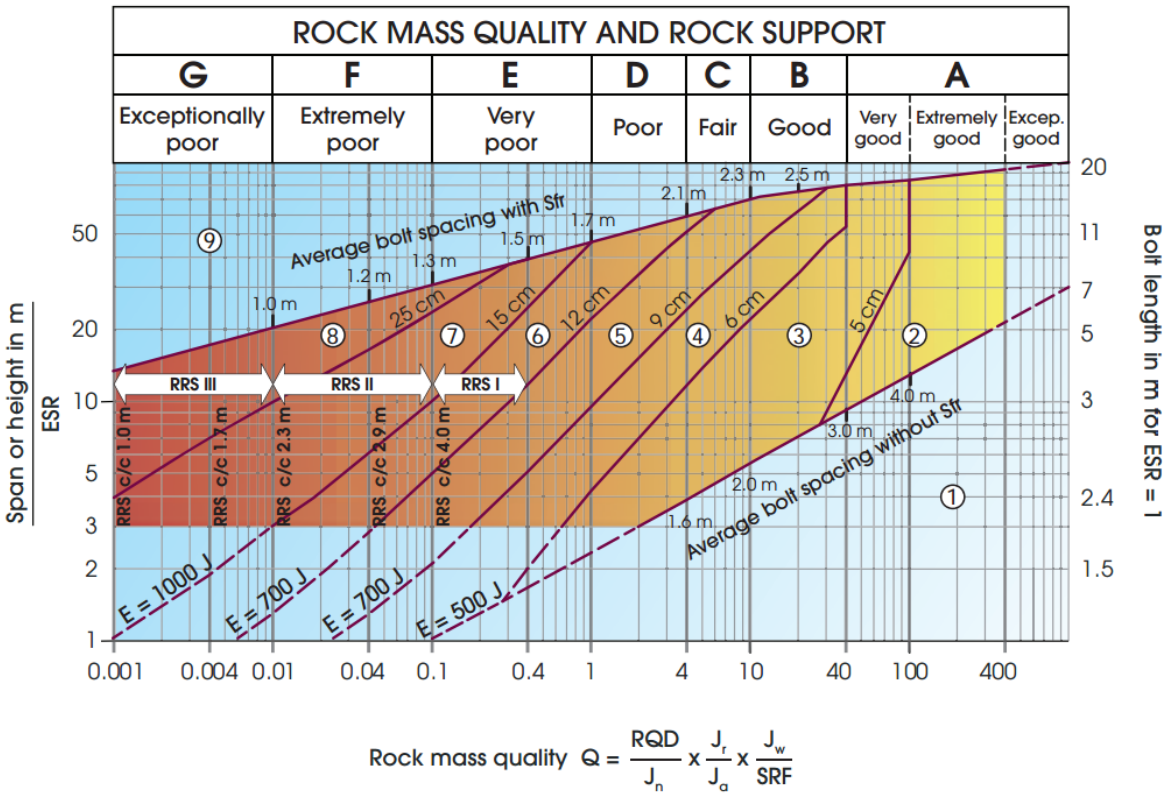

Figure 13 – From (NGI 2013) on the Q-values rock mass quality.

3.0 Software

In the following the software used and the most important input parameters will be presented.

3.1.1 Seep/W

The numerical software that has been used in this project is Seep/W from the GeoStudio suite by Geo-Slope International. Seep/W is a finite element CAD type software for modelling groundwater seepage and pore water pressure problems. The program can model both saturated and unsaturated flow in addition to steady state and transient state flow. The possibility of modelling an unsaturated/saturated flow enables time dependent precipitation simulations to be done. The numerical code seep/W has been validated as a suitable tool for this kind of research (Chapuis 2001). Because of these properties and the earlier proved applicability with the problem at hand Seep/W was considered suitable to the problems of this paper. Especially as modelling the long term effects of precipitation is one of the most important tasks.

A saturated/unsaturated state for the materials has been chosen with a Van Genuchten equation as a basis for the calculations. The program then assumes that a material can have both a saturated and unsaturated flow and use different calculation methods for the two flow types. Additionally, a Van Genuchten function has been used as the basis of calculating the volumetric water content functions.

3.1.2 Van Genuchten input parameters

The input for the material properties are split in two; volumetric water content function and hydraulic conductivity function.

The volumetric water content function there are two necessary parameters for the Van Genuchten equation that are input parameters in Seep/W. Those are the air entry value a, and the adjustment parameter to the model of Van Genuchten (1980), n.

The hydraulic conductivity function can be either constant or non-constant. A non-constant hydraulic conductivity function is for a unsaturated state. It is estimated on the basis of minimum and maximum suction, saturated hydraulic conductivity, residual water content and the volumetric water content function.

4.0 Field tests

The field tests were executed in order to get a basis to evaluate a set of slug tests on. With the simulation of the slug tests hydraulic parameters of different rock masses will be found. In addition the simulation of the slug tests will, if successful, show that a continuous model is appropriate for simulating water transport in rock masses.

4.1 Test sites

The field work that has been carried out lies within the Oslo Rift structure called the Oslo Graben which was formed during a geological rifting in Permian time. The graben consists of Permian igneous rocks such as basalt and rhomb porphyry which are extrusive rocks in addition to several kinds of intrusive rocks with granitic structures such as Larvikite (Neumann 1991). These structures are represented in the geology which was met in the field tests where both igneous and sedimentary rocks have been encountered.

The field work was done at two different sites; the Vettakollen and Bekkelaget sites. There will also be given a presentation of the site Folkehelseinstituttet. The tests for this area were carried out by Mr. Thomas Pabst at NGI and the results are made available for use in this project.

4.1.1 Vettakollen

The field work at the site Vettakollen was done over the course of three days from 25th of September to 27th of September 2013.

4.1.1.1 The test site

The area of Vettakollen is situated in the northern parts of Oslo in southern Norway. The area is forested and lies on the slopes of the peak Vettakollen. The wells stem from a project carried out by the consultant company Sweco as a part of pre-investigations of the construction of an extension of an underground overhead storage basin for water supply to the Oslo municipality. There are in total five wells in the area which can be seen in Figure 14 on an aerial photograph of the area with the tunnels drawn as well.

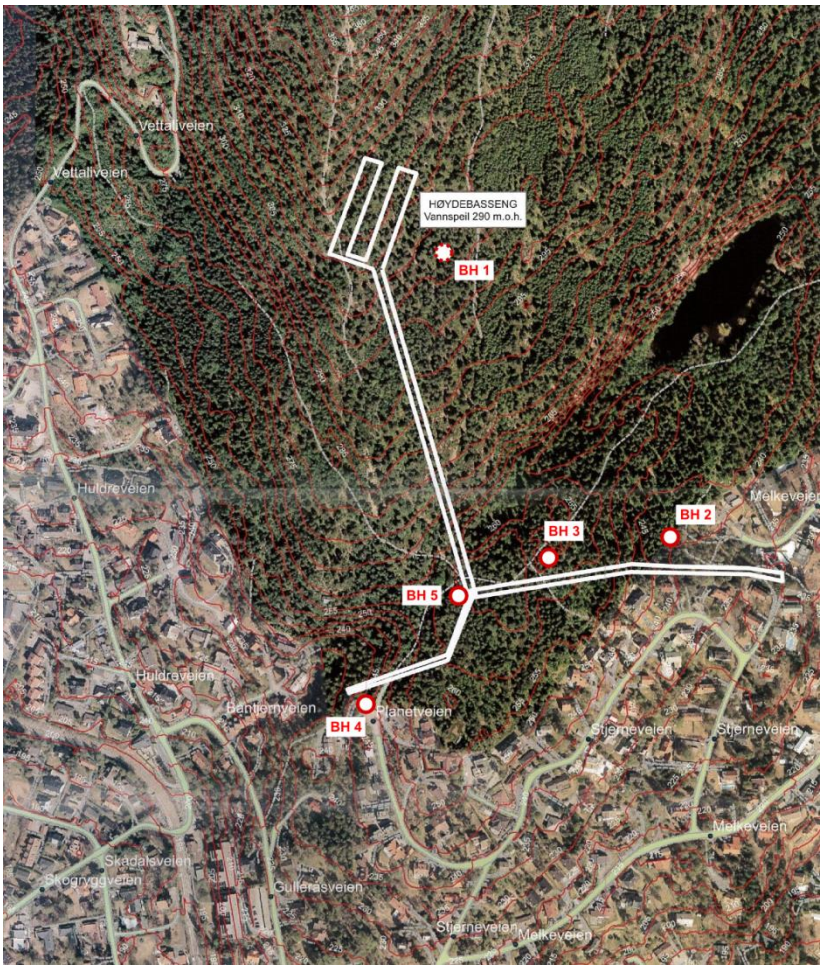

Figure 14 – Arial photograph of the Vettakollen area with the wells (marked as BH) and the tunnels to the overhead storage basin.

4.1.1.2 Topography and geology

Topography wise there is a relatively large potential weakness zone going from the lake Båntjern in a south-eastern direction. The wells BH4 and BH5 lies close to this while well BH2 lies within another smaller depression in the terrain which could be a weakness zone as well.

The geological map in Figure 15 (NGU 2013) show the area of the wells which are marked with red circles. As seen from the map the wells are located in transitioning zone between two main rock types where the purple represents an igneous rock by medium grained monzodiorite, according to the geological map. The light green is a sedimentary rock, slate with silt to sand fractions as well as some limestone inclusions. The white streak which crosses the light blue in the SW-NE direction is also a type of slate and limestone which is

shifting between those two rock types. Further north the pink represents a coarse syenite, nordmarkite, and the grey rhomb porphyry.

The consulting company SWECO has created a report from bore hole loggings in the area. Along the three wells which were drilled several different rock types were found; hornfels, breccia, rhombus porphyryr, marble, mozonite diorite, and syenite. These findings correspond well to the geological map and indicate a rather complex geological area.

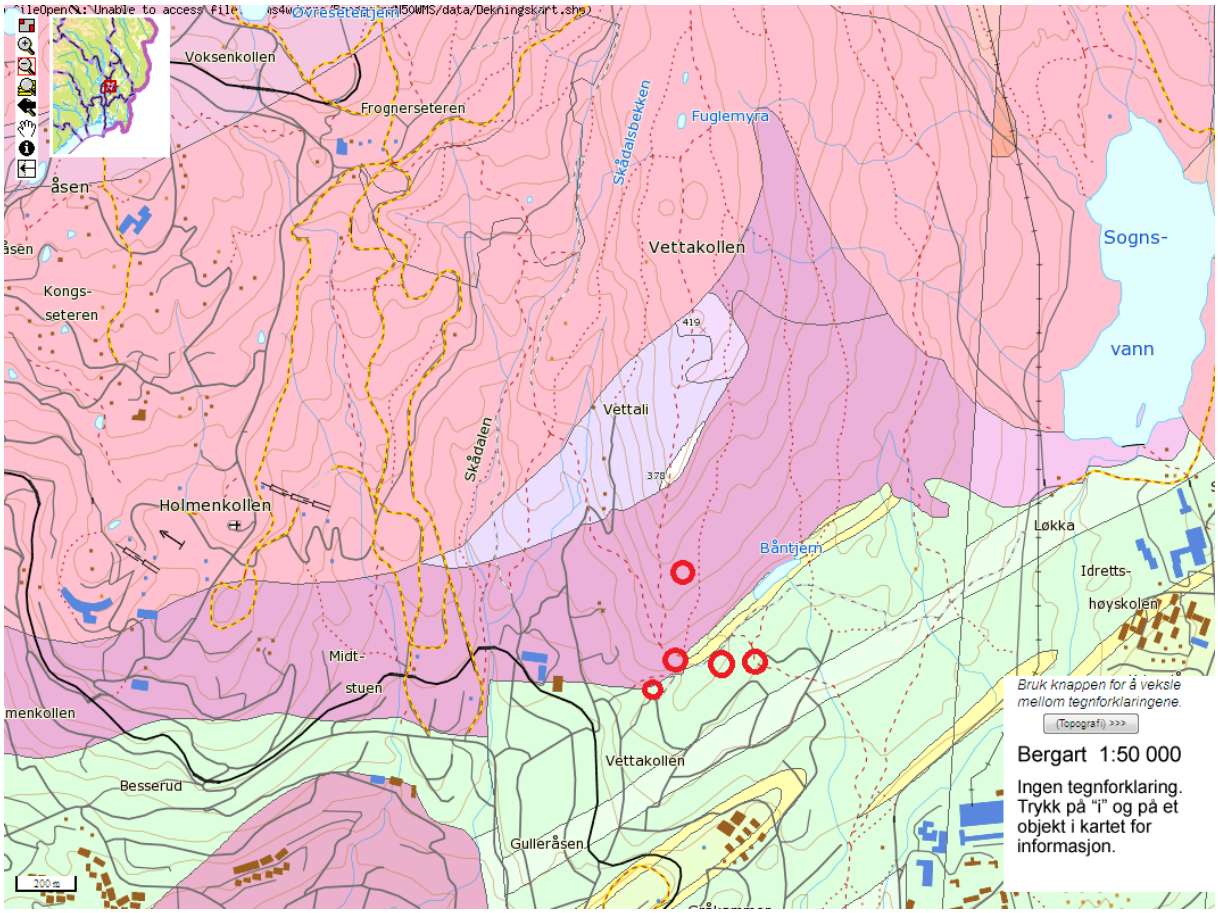

Figure 15 - Geological map with the wells marked in red with approximate well locations, courtesy of (NGU 2013).

The report from the bore hole loggings estimates the average Rock Quality Designation, RQD, to be RQD=72. This is a measurement of the percentage of cracks within the rock mass. The distribution of the Q values can be seen in Figure 16. Note that 84% of the values lie above Q=4 which is considered medium. Q=10-40 good and above Q=40 is very good quality as seen in Figure 13.

Q value	%
> 0,01 – 0,1	1
> 0,1 – 1	3
> 1 – 4	12
> 4 – 10	25
> 10 – 40	52
> 40 - 100	7

Figure 16 - Q values from the Vettakollen site

4.1.2 Bekkelaget

The field work at Bekkelaget in south-eastern Oslo in southern Norway was planned as slug tests in the same manner as the field work at the Vettakollen site. The field work at the site was done on the 8th of November 2013.

4.1.2.1 The test site

The area of Bekkelaget is an urbanized and has 5 wells installed as a pre-project to an underground sewage treatment plant which is planned to be built in the area. The wells are located both on top of the steep hillside towards the Oslofjorden in west.

The wells can be seen in the topographic map in Figure 18 denoted with numbers 1-5.

4.1.2.2 Geology and topography

The geology of the site can be seen in the geological map in Figure 17. As seen, there are relatively few rock types in the area. The main rock type with pink colours in the map is tonalitic granitic gneiss which has medium to coarse grains. All of the wells are situated in this rock type. A little way east the long, thin intrusion in purple is a rhomb porphyry and further east the dark pink is a granitic to granodioritic gneiss with lenses of alkali feldspar.

A report composed by NGI, Norwegian Geotechnical Institute, from bore hole loggings of support the geological map by identifying the rocks drilled for the wells as shifting layers of different gneiss types such as granitic, amphibolitic and pegmatitic gneiss as well as band of fault breccia.

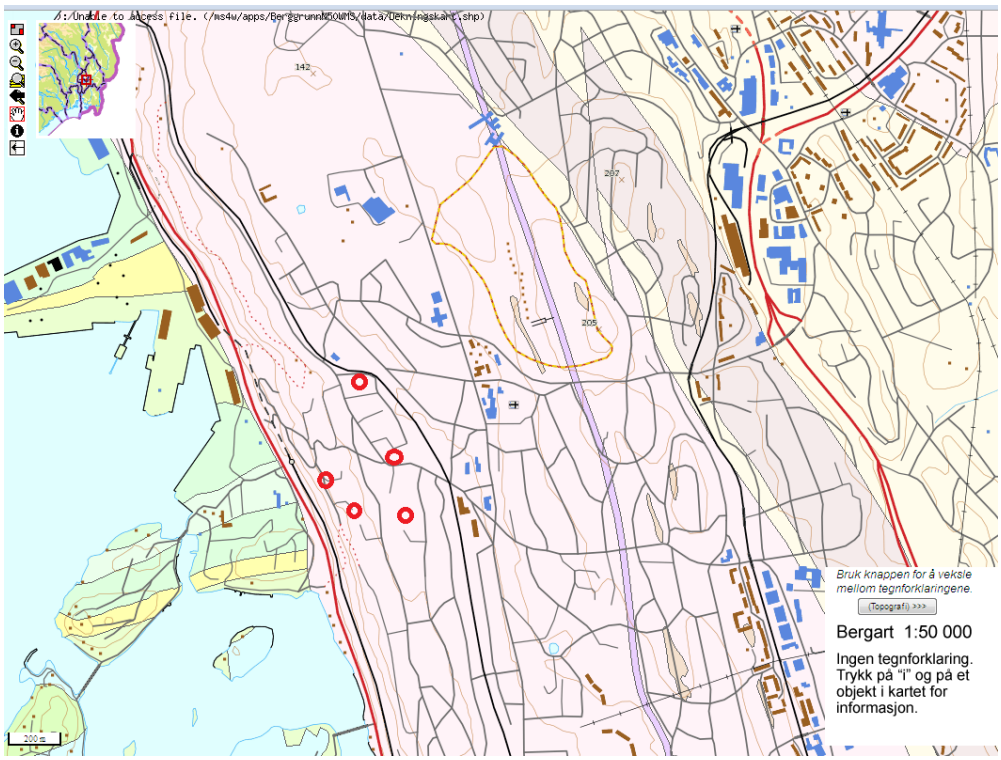

Figure 17 - Geology of the Bekkelaget site with approximate well locations marked with red dots (NGU 2013).

Topography wise none of the easternmost wells are situated at weakness zones as far as the map indicates. BL-4A/B and BL-5A/B are however situated on the western slopes of the hill down towards the Oslofjorden which is a large regional weakness zone.

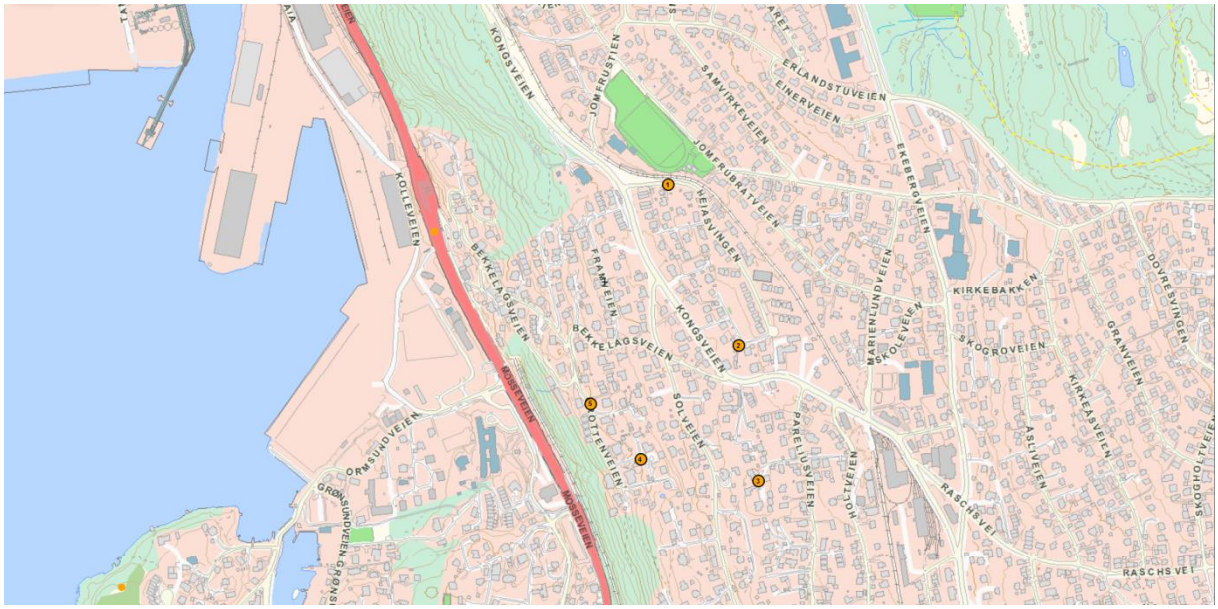

Figure 18 – Topographic map of the Bekkelaget site.

From the report from the core loggings the average RQD values can be seen in Table 1. Since it is not possible to determine the SRF and J_w from bore hole logging the Q values are not presented.

Table 1 – RQD values of bore hole logging from the Bekkelaget site

	RQD
Maximum	100
Minimum	40
Average	96
Variation of averages	89-99

4.1.2.3 Observations

The tests of the wells went smoothly except for the last well, BL-5A/B. The well had a groundwater table at 20,47m and a narrow part approximately 15m down the well. This made it hard to measure the groundwater table, and when the Micro-Diver data logger sensor got stuck the test had to be abandoned for this well. The sensor was lost and there therefore no results are available either.

4.1.3 Folkehelseinstituttet

The test site Folkehelseinstituttet is situated in downtown Oslo in southern Norway. It is the office of the National Healthcare Institute of Norway. In Figure 19 an overview of the wells in the area can be seen. In total there are five wells in the area.

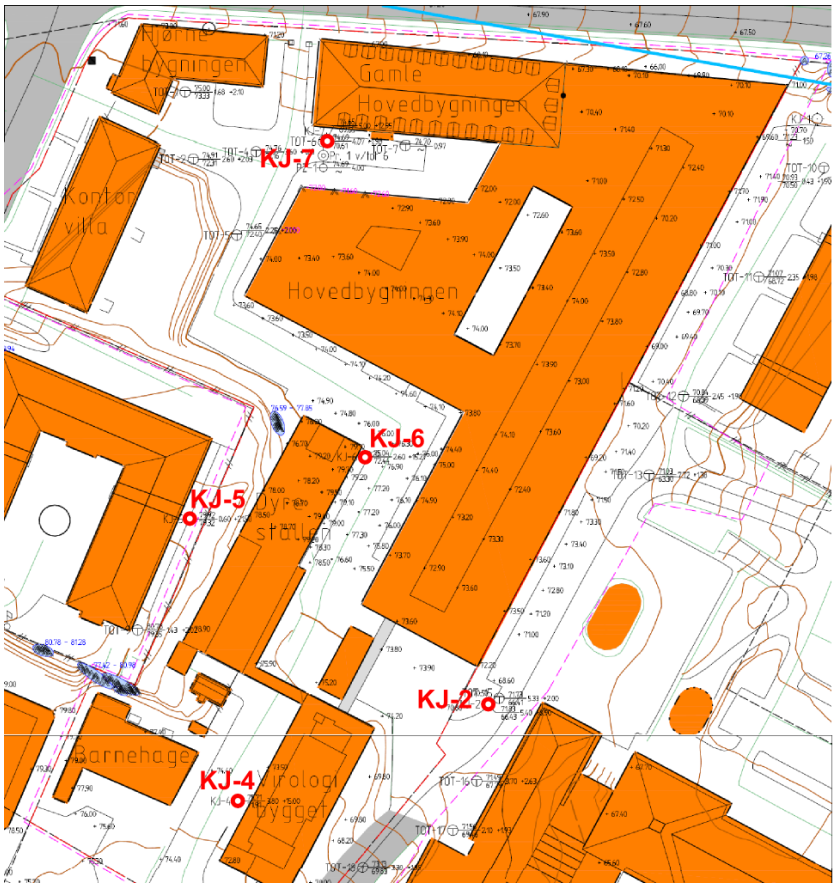

Figure 19 – The wells in the area of Folkehelseinstituttet.

4.1.3.1 Topography and geology

The site lies in a flat area which is urbanized and lies relatively close to the river Akerselva. There are no apparent potential weakness zones that are observable from aerial photos and topographical maps except for Akerselva which is 7-800 meters from the wells.

The geology of the site consists of slate with different origins. There are variations between silty and sandy slates and often with lenses of lime or layers of limestone. The rock masses of the area are fairly massive (NGU 2013).

The map in Figure 20 show the geology of the rock masses within the area from (NGU 2013). The two varieties of rocks which can be seen in the figure are a sandy and a silty slate. These two are of the same origin and thus the geology in the area is rather uniform.

A report about bore hole loggings in the area has been created by Norwegian Geotechnical Institute (NGI). This report states that all the wells used in this paper were drilled in a slate with spatial occurrence of limestone inclusions. This correlates well with the geological map.

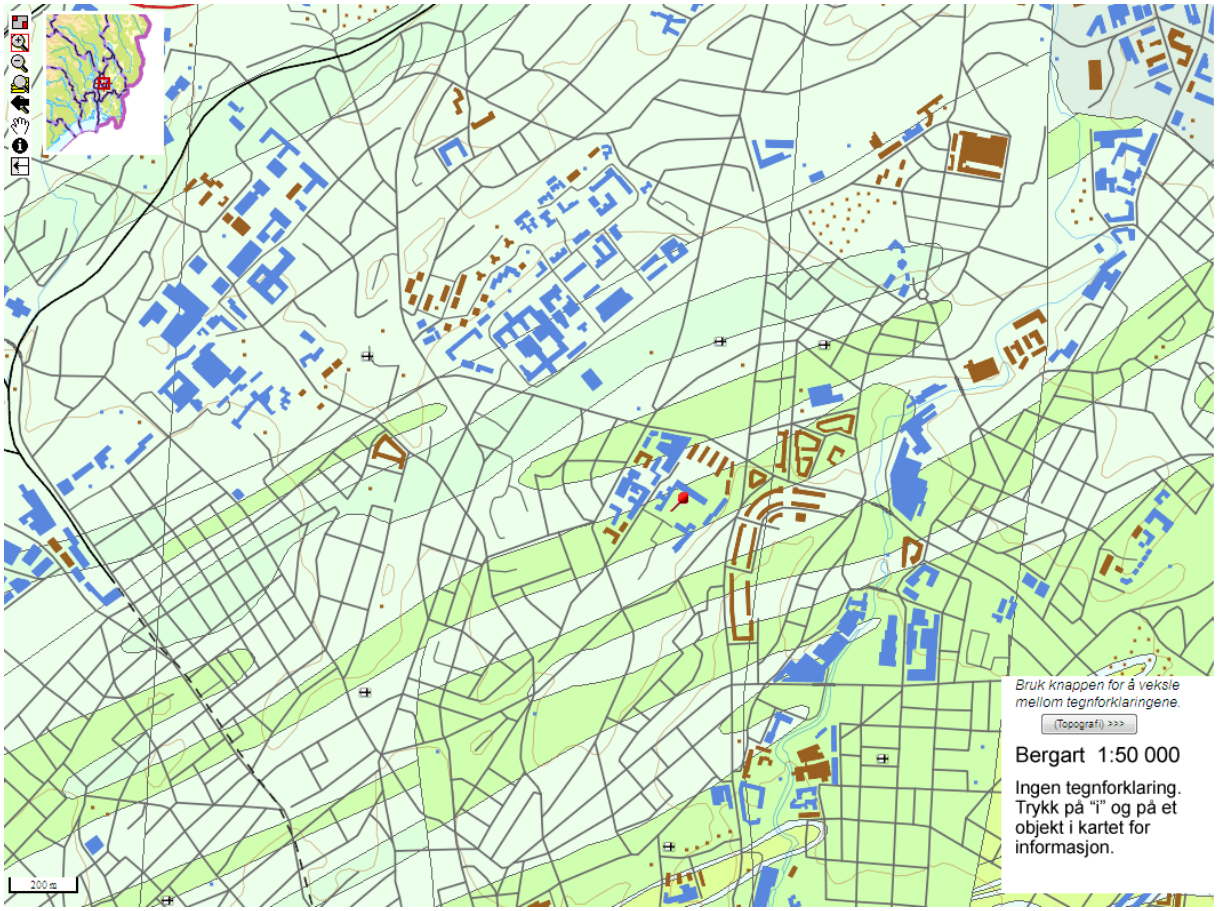

Figure 20 – The geology of the area courtesy of (NGU 2013)

In the bore hole report the average RQD values are presented as can be seen in

The report also says that there were little to no joint fillings. A comment is also made to point out that the RQD could be lower because it is though that some cracks are mechanically induced while drilling.

Borehole	*RQD*	*Jr*	*Ja*	Crack frequency [cracks/m]	Crushed core[cm]
KJ2	80	3,0	0,9	6	20
KJ3	87	2,6	0,9	5	12
KJ4	68	2,8	0,9	8	19
KJ5	77	2,9	1,0	7	60
KJ6	87	2,8	1,0	6	1
KJ7	85	2,5	1,0	6	11

Figure 21 – RQD, J_r and J_a for the bore holes in the Folkehelseinstituttet test site

4.2 Methodology

In the following the test procedures for both the field tests and the simulations will be explained throughout.

4.2.1 Slug tests

The slug test is described theoretically throughout in earlier chapters. Water was decided to be used as a slug medium for all the tests. This was because water gives flexibility with regard to changing the injection volume in cases where the permeability properties of the rock mass around a well are not known. It also makes simulations easier and is within the ASTM (ASTM 2008) requirements.

4.2.1.1 Test equipment

- Groundwater table logger
- Schlumberger Micro-Diver compact data logger
- Timer
- Measuring cup
- Fishing line
- Water

The Groundwater table logger was used to measure the initial and new groundwater tables. The data logger was installed below the groundwater table before the injections by the use of the fishing line.

Figure 22 – The setup during testing of well BH5 at Vettakollen. There can be seen water for injection, groundwater level measurement device with a measuring tape, fishing line and a watch in the picture. This well had an angle of 65° with the horizontal plane.

4.2.1.2 Test procedure

Some of the wells had non-vertical pipes and these angles and orientations were measured. The level of the groundwater was measured manually in order to have an initial water level as a reference for the tests. All the wells were tested with the same procedure albeit the amount of water and the number of water injections were varying based on the speed of well head recovery which was measured manually throughout the test.

The procedure of the tests was as following:

1. Check the level of the groundwater table
2. Install the Micro-Diver water head data logger below the groundwater table
3. Inject a known amount of water
4. Measure the new level of the groundwater table in the well manually
5. Repeat every 5 minutes.

The amount of water for every injection varied but the amounts used spanned between 1 L and 10 L. Whenever there was a large drop or small increase compared to the injected volume the amount of water would be either increased or kept at the same level for the next injection.

4.2.2 Simulations

All of the Slug tests have been simulated in the software Seep/W.

4.2.2.1 Objective

The objective of the simulation of the slug tests is to obtain data from different rock materials and test sites. Another important part of reason to simulate the slug tests is to verify that a continuous model can simulate water flow in rocks in a satisfactory manner.

4.2.2.2 General assumptions

Some general assumptions has been made during the simulations which are common for all of the wells simulated.

4.2.2.2.1 Geometry

The models were created axisymmetric around the center of the well. All slug tests were created with a 25m horizontal boundary. In the vertical direction the boundary varies depending on the depth to the groundwater level from the well surface. These boundaries have proven sufficient for all wells as exemplified by the well KJ7 in Figure 23. Here the effect of the slug is shown not to affect more than half to the horizontal boundary which is satisfactory as the end boundary of the model will not affect the results.

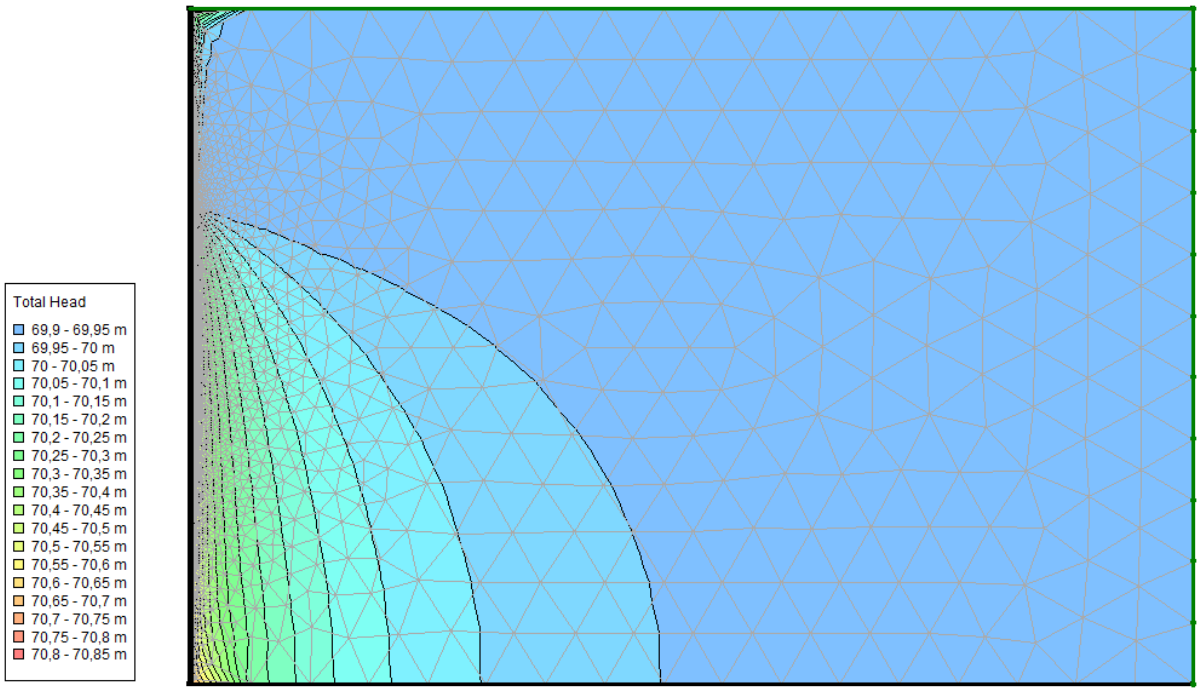

Figure 23 – Total head after pouring and drainage of KJ7

4.2.2.2.2 Water flow and rock mass characteristics

The saturated and residual water contents have been assumed to be 0,03[m^3/m^3] and 0,01[m^3/m^3] respectively. As seen in Figure 3 crystalline rocks vary from 0-10% in porosity with dense crystalline rocks at 0-5%. This is the total porosity while saturated water content will be the same as the effective porosity.

As an example Barton (2001) give a typical joint aperture of 600µm. Assuming a rock mass with 15-20 water bearing cracks has an average area of 1m^2 this give an effective porosity of 0,9-1,2%. Given mechanical fractures from drilling and the reports on the core loggings estimating RQD values from 65-95 it is thought that the effective porosity will be larger than the estimated 0,9-1,2%, thus the given values have been chosen. The values have for simplicities sake been kept the same for all of the rock masses based on the rocks being massive with assumed low permeabilities. A simple sensitivity analysis has been done by changing the saturated and residual water content to 0,06 [m^3/m^3] and 0,015 [m^3/m^3] respectively which does not show any significant differences, see Figure 31.

The hydraulic conductivity function has been kept constant for all the rock masses. The reason for this is by assuming that the rock mass is saturated testing is done more or less below the water table, thus the hydraulic conductivity is kept constant at K_{sat}.

4.2.2.2.3 Boundary conditions

The boundary conditions used in the models were a total flux for injecting water and initial water tables. Both the boundary conditions correspond to the measured values during the field work, i.e. the measured initial water table.

4.2.2.2.4 Well diameters

The well diameters were measured in the field. Since it is difficult to tell whether the well diameter is constant or not, an effective well diameter was calculated based on the volume of water injected and the measured heave in the well. Because the measured values can differ from the actual rise the effective well diameters were adjusted in the model to fit the measured values from the divers. Generally the effective well diameters have been small, ranging from approximately 5 cm to over 15 cm.

4.2.2.2.5 Special cases

A couple special cases in the Vettakollen area were the wells BH4 and BH5 which were not vertical. These have been simulated as vertical given that it is complicated to do a two dimensional analysis of the case in the software. The results are presented in the results chapter nonetheless.

4.2.2.3 Procedure

All of the slug tests were simulated in the same fashion. The models were created by defining a rock mass and an estimated well diameter. By selecting the used number of time steps, their duration and the correct amount of water for each step the simulations proceeded in a trial-and-error manner with regards to curve fitting.

Convergence problems were encountered during the process and proved to be problematic a lot of the time. This is probably because of relative low injection volume compared to the size of the models. It was partially solved by refining the mesh and time steps as well as choosing a total flux [m^3/s] over a unit flux [m/s].

In total 13 slug tests were performed and some of the output data can be seen below in the results chapter. The rest of the results can be found in Appendix C. Output data in this case are the properties necessary to describe the same material in a large scale model; adjustment parameter to the Van Genuchten equation, air entry value, saturated and residual water contents and the hydraulic conductivity.

4.3 Results

4.3.1 Overview

All of the output parameter results for the wells that were tested are presented in Table 2. Below one graphical result from each test site is presented to give an impression on the results whilst the rest of the results is enclosed in Appendix C.

Table 2 – Simulated well data from slug tests

Area	**Folkehelseinstituttet**						**Bækkelaget**			**Vettakollen**			
Well	**FHI KJ2**	**FHI KJ3**	**FHI KJ4**	**FHI KJ5**	**FHI KJ6**	**FHI KJ7**	**BL1**	**BL2**	**BL3**	**BH 2**	**BH 3**	**BH 4**	**BH 5**
Hydraulic conductivity [m/s]	5,00 E-09	8,50 E-07	1,50 E-08	9,00 E-10	1,2E-8	7,00 E-09	8,00 E-10	1,50 E-06	8,50 E-08	4,00 E-05	1,50 E-06	9,80 E-08	1,50 E-06
Air entry value, a [kPa]	0,1	0,1	0,1	0,1	1	0,1	0,1	0,1	0,1	0,1	0,1	0,1	0,1
Van Genuchten parameter, n	2	2	3	1,1	1,000 00000 1	1,5	1	1,1	1,00 000 5	6	2,2	1,5	1,5
Residual Water content [%]	0,01	0,01	0,01	0,01	0,01	0,01	0,01	0,01	0,01	0,01	0,01	0,01	0,01
Saturatued Water content [%]	0,03	0,03	0,03	0,03	0,03	0,03	0,03	0,03	0,03	0,03	0,03	0,03	0,03

4.3.2 Vettakollen

Example of a graph of well BH4 from the Vettakollen area.

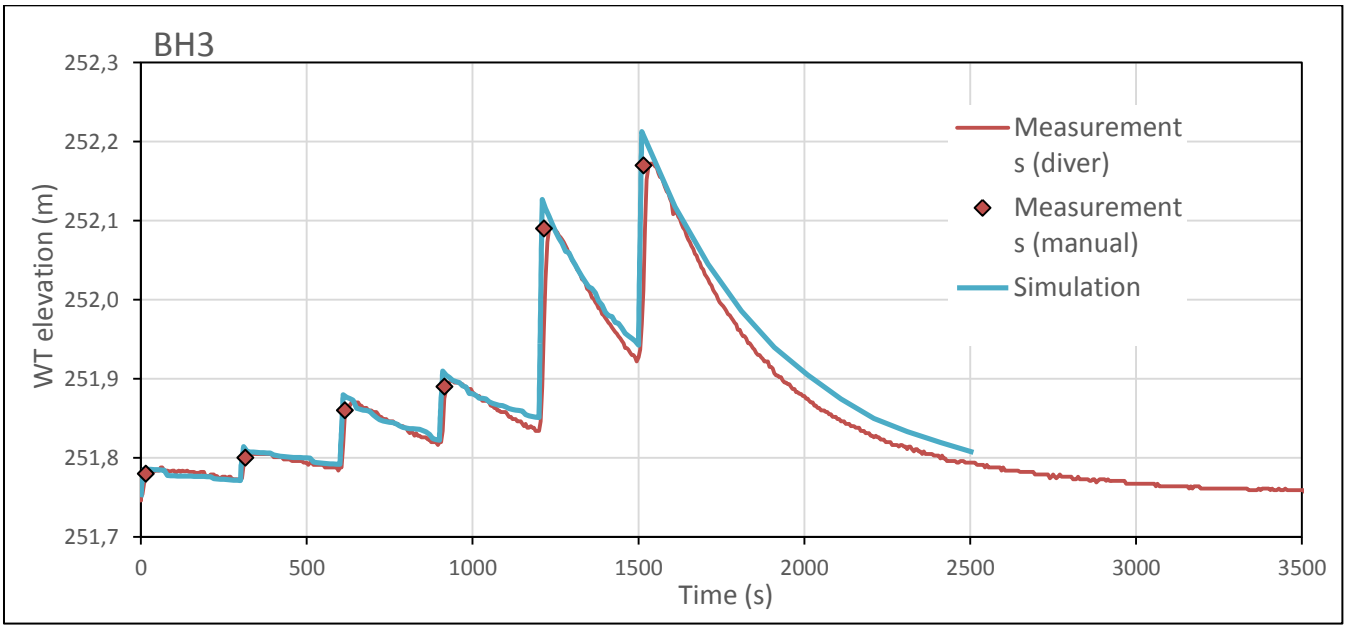

Figure 24 - Modelling of both pouring and drawdown steps of well BH3 from the Vettakollen area

4.3.3 Bekkelaget

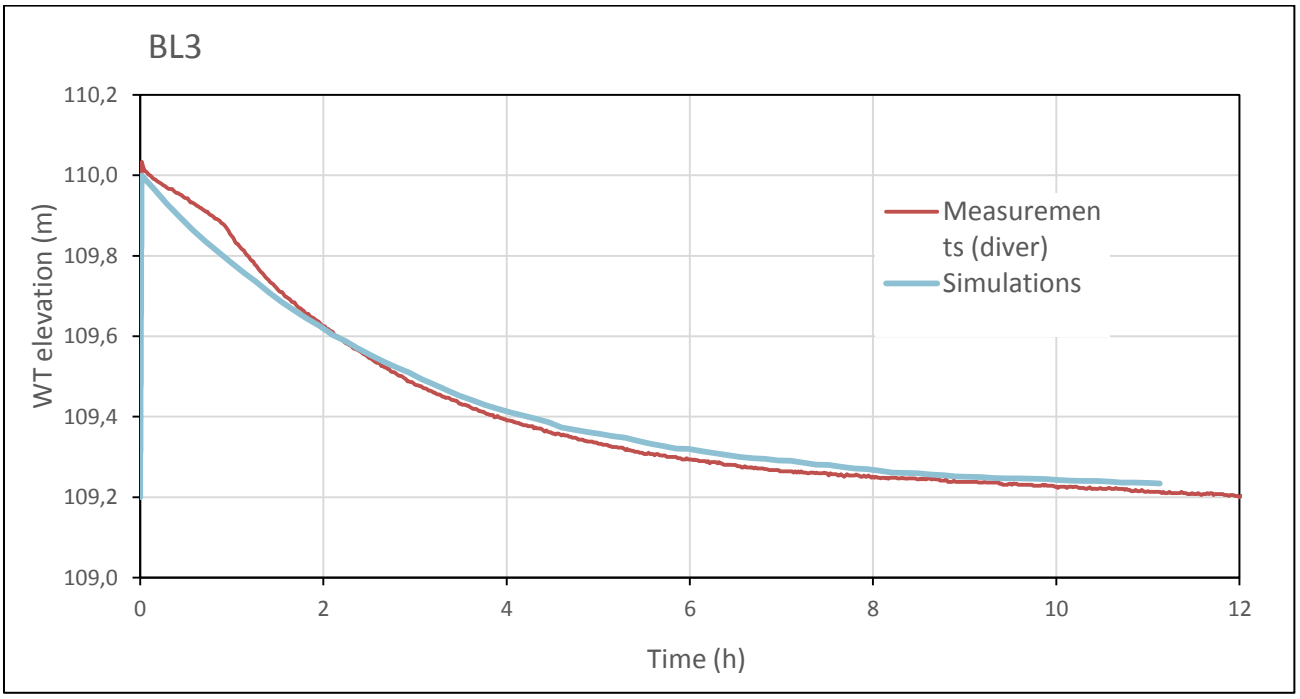

Figure 25 Modelling of pouring steps of well BL2 from the Bekkelaget site

4.3.4 Folkehelseinstituttet

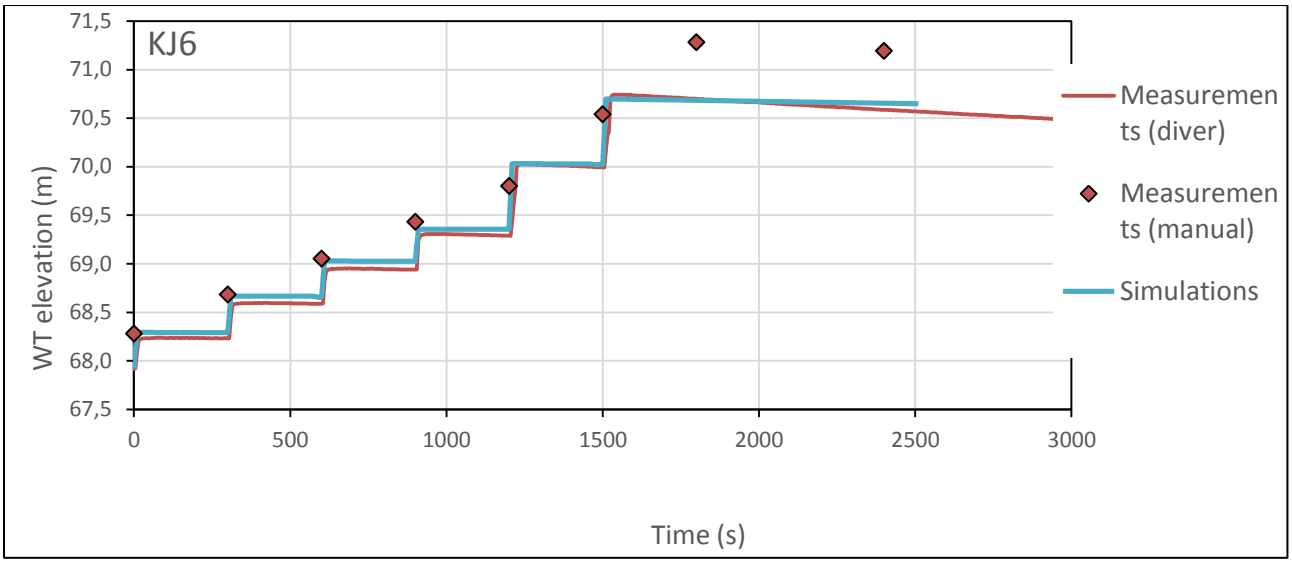

Figure 26 - Modelling of pouring steps of well KJ6 from the Folkehelseinstituttet site

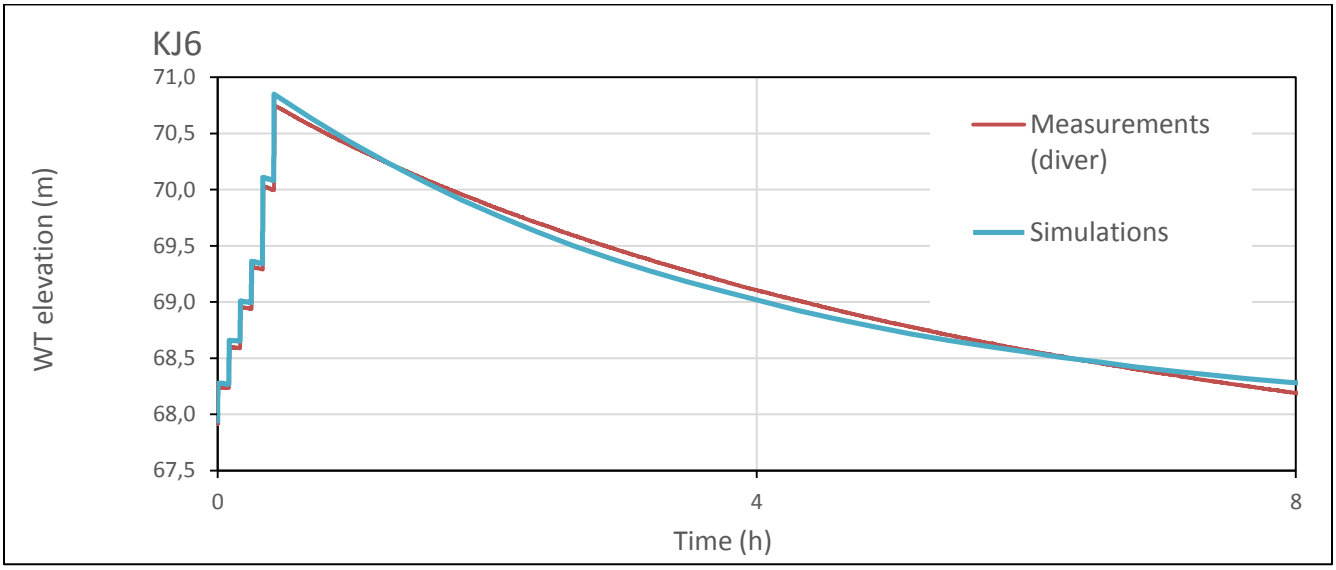

Figure 27 - Modelling of drawdown steps of well KJ6 from the Folkehelseinstituttet site

4.4 Analysis

In the following a short analysis one low and one high permeability well will be presented and discussed briefly as examples of the simulation of the slug tests.

4.4.1 Low permeability well: KJ7

The well KJ7 is from the location Folkehelseinstituttet and gives an example of a low permeability well in both the pouring and draining steps. It was injected six times with 1L the first four and 2L the last two steps.

As seen in Figure 28 there is practically no drawdown over the course of injecting water in to the well. The figure does show some slight differing from the curve during the pouring steps of the slug test. This is can stem both from weaknesses in the model or measurement errors in the diver. Another more probable explanation is irregularities in the well diameter. Given that the total simulated heave equals the measured amount the differing in the pouring steps is not regarded critical since the injected and simulated water amount is the same.

Also note that the manual measurements marked with red dots tend to not correspond exactly with the diver-measured values. This probably stems from manual measurement errors as the precision of those measurements are not very high.

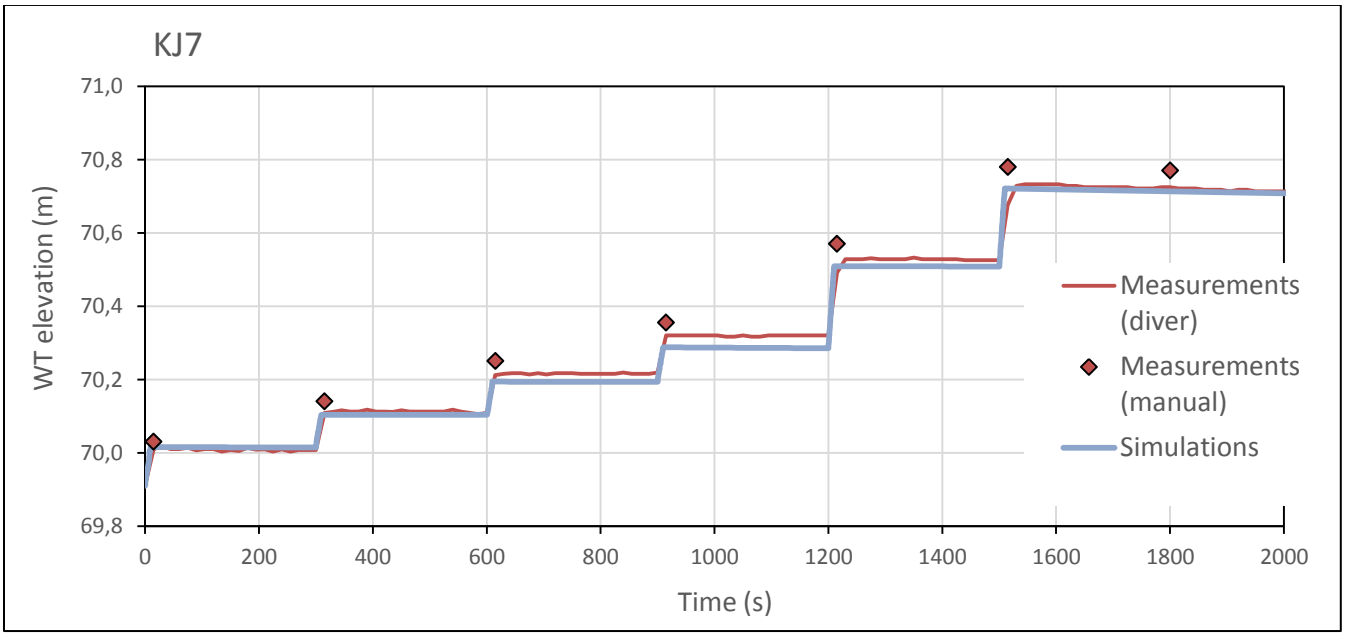

Figure 28 - Modelling of pouring steps of well KJ7

In Figure 29 the long-time draining of the well can be seen and the figure show that it takes over 24 hours before the well has recovered to the initial groundwater. The curve is matched well in this case the simulated hydraulic conductivity is $7e^{-9}$[m/s].

Considering both the matched water level heave and drawdown curve is matched the model is considered good and the results are thought to be equally trustworthy.

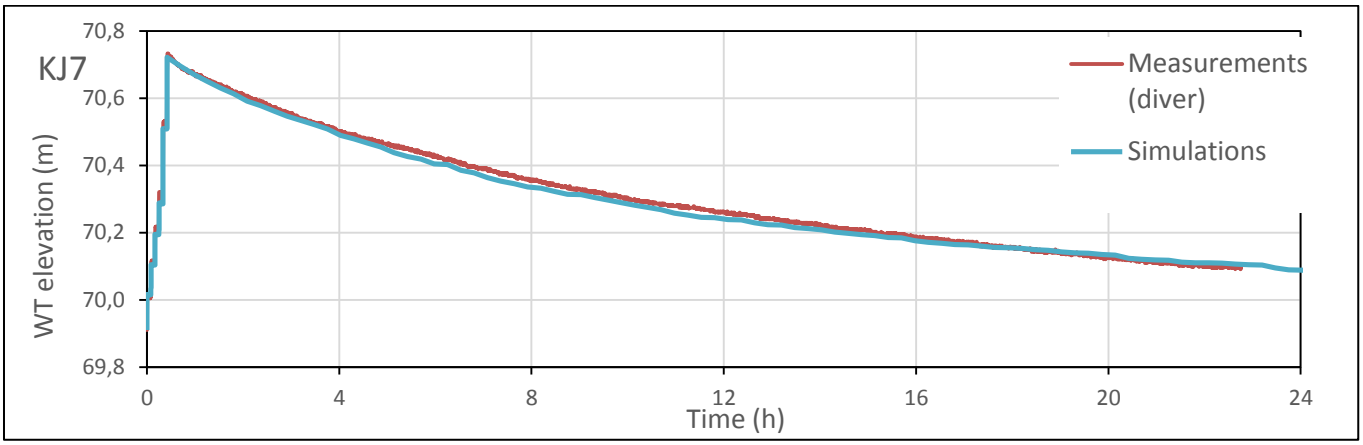

Figure 29 - Modelling of drawdown of well KJ7

4.4.2 High permeability well: BL2

The well BL2 is from the Bekkelaget location. It was injected twice with 10L water each time. This well shows an example of a high permeable well in Figure 30. The fast drawdown shows that the rock around this well has a high permeability. The initial water level is reached at approximately 2500 seconds, i.e. 42 minutes. The simulated hydraulic conductivity of this well is $1{,}5e^{-6}$[m/s]

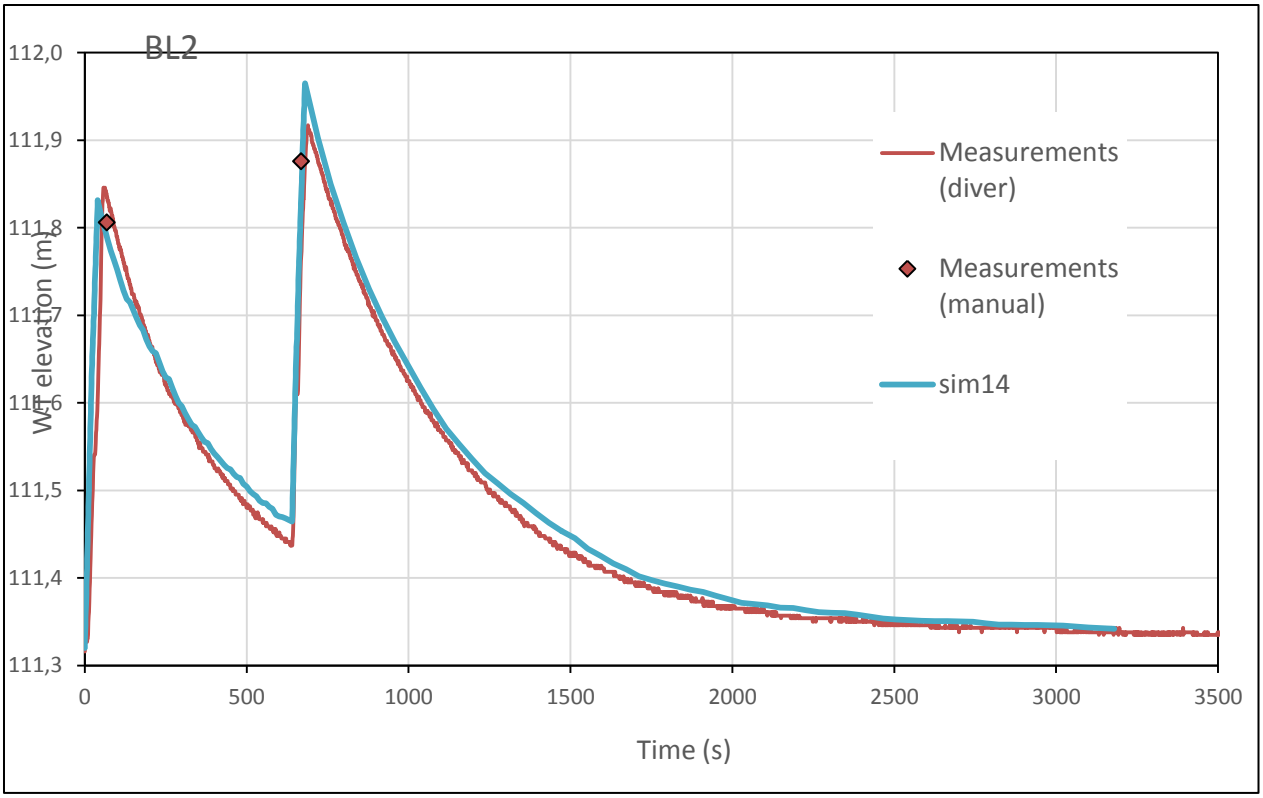

Figure 30 - Modelling of pouring and draining steps of well BL2

The fit of this simulation with the measured values is less precise than the low permeability well although it is not considered bad. Generally it has proven more difficult to fit high permeable wells than low permeable wells. The reason for this might be a more inhomogeneity's within the well which is hard to adjust for in a simplified model. This can give effects such as lower or higher rise with each injection because of irregular walls or quick losses of injected water because of high permeable zones such as fractures.

The effective diameter of this well is 15 cm. Given that the injected volume is 0,01m^3 this suggests that the sensibility of the test is somewhat high. The high volume of injected water has been carried out for most of the high permeable wells making this another factor for them being harder to fit to the simulated values than low permeable wells.

Based on the high sensibility of this well and the general good curve fit the model of this well is considered good.

4.4.3 Sensitivity analysis

The saturated and residual water contents were estimated based on RQD values and kept the same over all of the slug tests. By doing a sensitivity analysis of both the saturated and residual water contents by changing them to 0,06 [m^3/m^3] and 0,015 [m^3/m^3] respectively the graph in Figure 31 is found. It compares the two scenarios and does not show any significant differences thus supporting that the chosen parameter levels are valid.

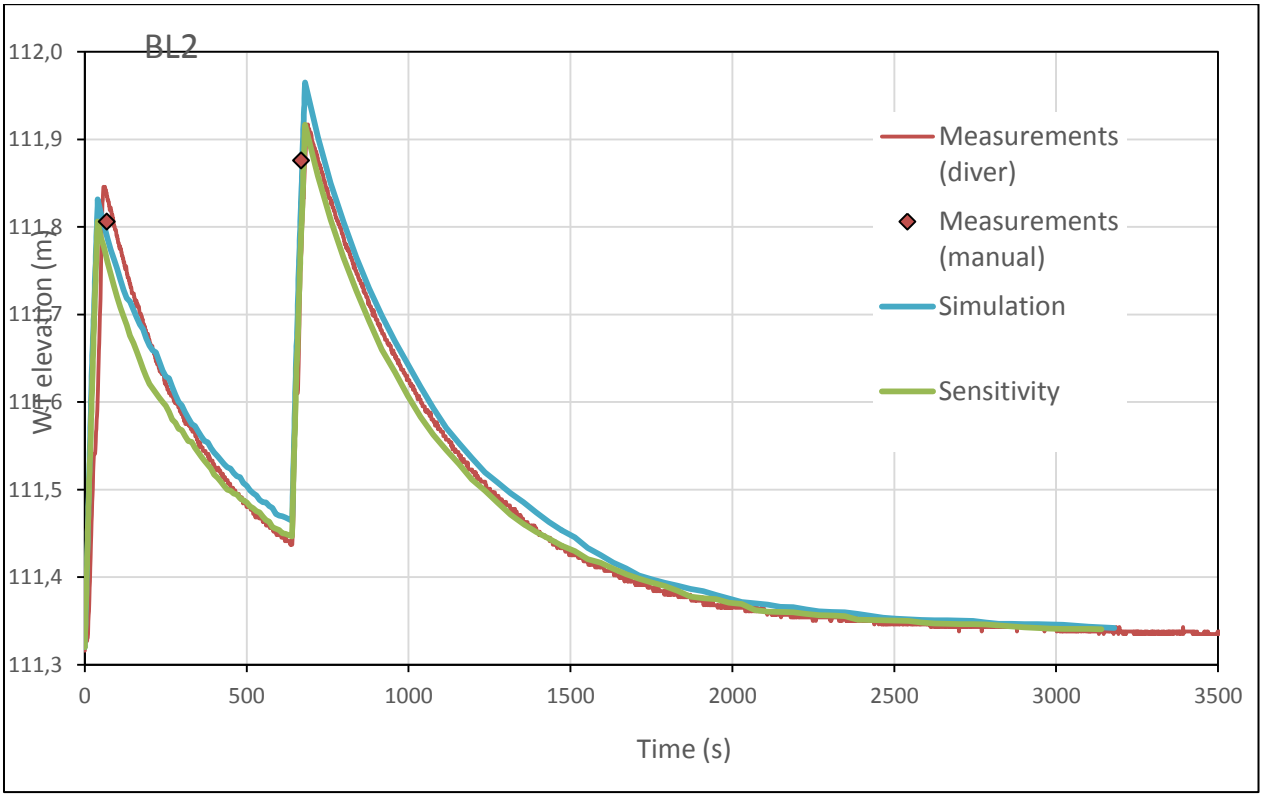

Figure 31 – sensitivity analysis of well BL2 based on different saturated(SWC) and residual water contents(RWC). The line "simulation" is the assumed water contents used for all the simulations at SWC=0,03 and RWC=0,01. The line "Sensitivity" is given a SWC=0,06 and a RWC=0,015.

5.0 Laboratory tests

The laboratory work was executed 27-29/12-2013 at Norway's Geological Institutes (NGI) laboratory in Oslo supervised by Thomas Pabst of NGI. The aim of the laboratory work was to do a 1D infiltration test between two different soil types in order to see the change of the water propagation over the interface between them. The main objective is to calibrate and validate models with special regards to water accumulation on the interface. Two tests were executed with two materials on top of each other, changing place between the two tests.

5.1 methodology

The methodology chapter contain both the description of the practical execution of the laboratory work carried and a description of the numerical code developed to simulate the recorded values.

5.1.1 Test equipment and procedures

The test procedure was suggested by Mr. Thomas Pabst of NGI and is by no means a standard test. Therefore a throughout description of the laboratory test is presented in the following in order to give a good understanding of the methods and procedures used in the test.

5.1.1.1 Material

The materials at hand were two fractions of limestone which was taken from the same source. The two materials consisted of one fine grained 0-2mm and one coarse 0-10mm. These materials stems from a contamination project carried out by NGI on behalf of NOAH (Norwegian Deposit Handling) on the island Langøya in the Oslofjord of southern Norway. The specific density of the material is

$$\rho = 2{,}7 \ {}^{g}/_{m^3}$$

Equation 55

The fine material's grain size distribution curve is presented in Figure 32. As seen from the grain distribution curve in Figure 32 the material is sandy, silty and coarse material. The uniformity coefficient C_u is 93,1 which is found from reading the graph at D_{10} =0,014 and D_{60} =1,303 . The clay content is 1,5%.

In the grain size distribution in Figure 32 the main part of the fine material can be seen to lie within the sand fraction ranging from 0,63µm-2mm. It is relatively well graded albeit there is a good sorting around the larger parts of the sand fractions. A well graded material contains relatively like amounts of each material whereas a well sorted material will have a large portion of the material within a certain fraction.

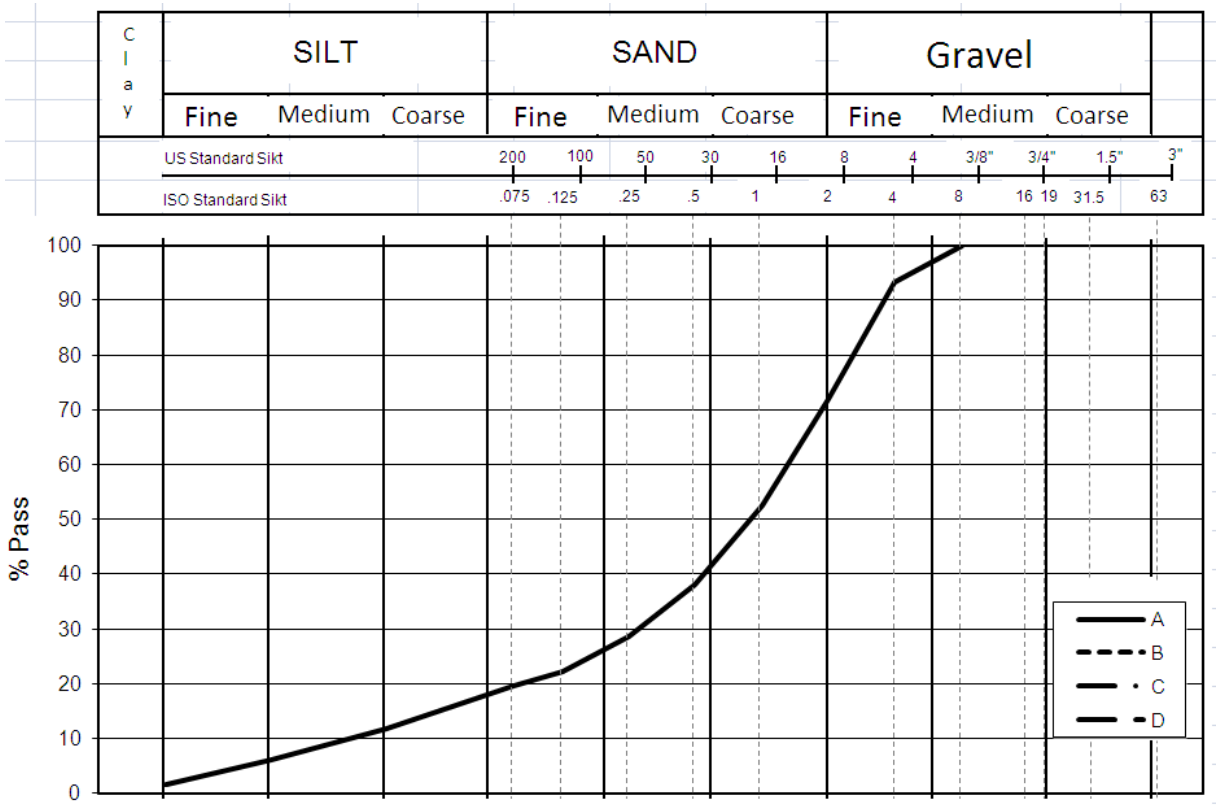

Figure 32 – Grain size distribution of the fine material from NOAH&NGIs Langøya Deposit Project.

From the Kozeny-Carman equation the hydraulic conductivity can be estimated. By using a dynamic viscosity at 20˚C which is µ=1,002 and an effective porosity of n_{eff}= 0,323 which was calculated during the tests an estimated hydraulic conductivity will be;

$$K = \left(\frac{2{,}7 * 9{,}81}{1{,}002}\right) * \left[\frac{0{,}323^3}{(1-0{,}323)^2}\right] * \left(\frac{0{,}014^2}{180}\right) = 1{,}083 * e^{-6}\ [^m/_s]$$

Equation 56

As for the coarse material the grain size ranges from 0-10 mm. There is no grain size distribution available because the material mainly lies in the upper end of the scale with fractions close to 10 mm. This makes the material not applicable for the grain size distribution.

5.1.1.2 Apparatus

The test was mostly planned out by Mr. Thomas Pabst at NGI which had an apparatus built for the purpose.

The apparatus consists of a cylindrical pipe of Perspex with holes for sensors with equal distance between them, see Figure 33. There also holes in the bottom for the purpose of draining out water which comes through the material while testing. The height of the cylinder is 41,24 cm and the inner diameter is 14 cm.

Other equipment used was:

- Volumetric moisture content measure device: *Decagon Devices EC-5*.
- Water pipes
- Weight with 0,001g accuracy
- Water
- Camera
- Computer

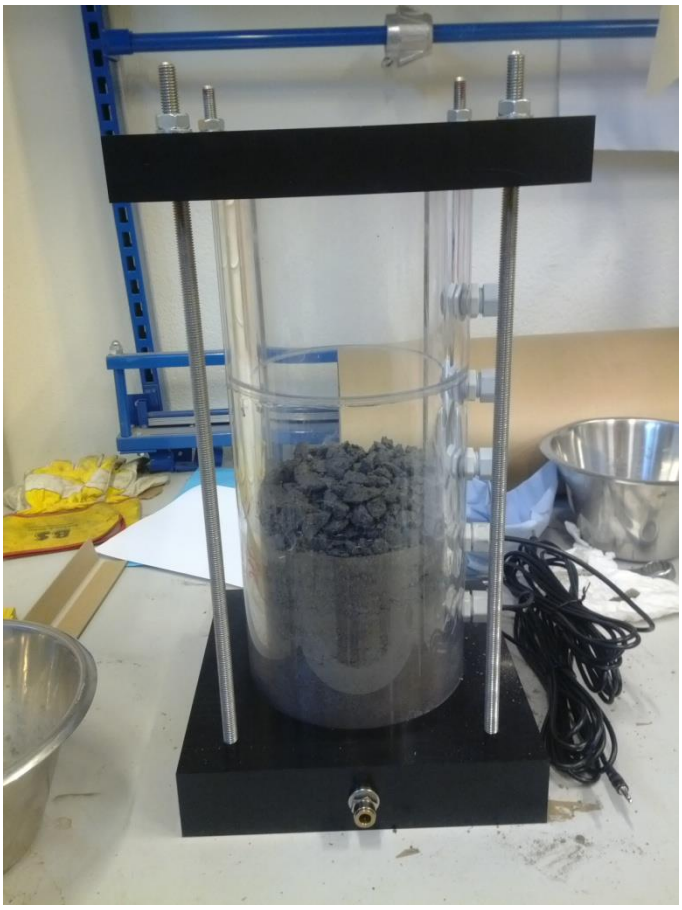

Figure 33 – The apparatus used at the laboratory testing at NGI. The apparatus is partially filled with material and has two sensors installed at this point.

The Decagon Devices EC-5 sensor for measuring the volumetric moisture content is a rather small sensor which installs easily in the soil. It has according to the manufacturer an accuracy of ± 3%.

5.1.1.3 Test 1: Coarse material over fine

The laboratory work started Wednesday 27/11-2013. The apparatus was set up and the material prepared. In the first test the fine material was placed at the bottom and the coarse on top. The apparatus needed to stay put overnight which meant there could only be one test executed per day. There was put in a sprinkling filter made of plastic with holes and a filter paper at the bottom of the cell. This was to avoid fine grains to get drained in to the pipes leading out of the cell and thus keeping all of the material within the cell as well as avoiding clogging of the draining pipe.

In order to get a relatively homogenous distribution the two materials were put in to the cylinder with 4-6 cm layers before they were stamped with a metal piece. By stamping as

often as this there will be less problems with layering within the material and the stamping of the material makes a homogenous distribution over the entire soil layer. In addition the fine material was initially partially wet which created lumps. Therefore the material was also stirred and de-lumped in to its natural state by a spoon prior to the setup of the apparatus. Each layer was also weighed and height was measured after the stamping in order to get data for the porosity, initial moisture content and saturation ratio correct. Also, there was taken a small sample of material for each layer which was dried at 110˚C±5˚C for over 24h. From this it is possible to obtain the water content in the sample.

Between each layer there was installed a sensor for measuring the moisture content in different parts of the soil. They were approximately 5 cm apart but this varied as the thickness of the layers being put in to the cell was of varying thickness as well. The two sensors in the coarse material were put inside a small amount of fine material in order to protect them from the stamping. The effect of this is probably less than one can expect due to the sensors using a frequency/domain technology which measures average values of a certain radius around the sensor.

Figure 34 - Installation of sensor

After installing two sensors in each material and with a height of the fine and coarse layers were both approximately 13,8 cm. With the sensors measuring the moisture content and knowing the specific density and volume of the schist the sample is taken from the volumetric moisture content, porosity and degree of saturation can be calculated.

The full setup can be seen in Figure 35. Note the pencil pointing at tendencies of layering within the fine material. It is hard to say how much this affects the permeability of the cell as a whole, but it has been a priority to lessen the presence of them in order to get as few sources of error as possible.

Figure 35 – The full setup after preparing both the fine and coarse material as well as the sensors within the cell.

After the cell was installed with the sensors and the layers the test was ready to be executed. The pipe leading from the two drains lead in to a plastic bucket which had a sensor for measuring the water head, which allows the volume of water which goes through the cell to be calculated.

There was decided to pour the water amount equal to 10mm water rise in to the cell every 10 minutes. This equals 154 ml which was the approximate amount poured in every time. The water was weighed rather than eye measured in order to get as accurate amount as possible.

The first pouring that the water would infiltrate through the coarse layer quickly before creating a water head at the interface between the two materials and which sunk at a steady pace. The water infiltrated slowly in the fine material and it was not before 26 minutes had passed that the water front reached the bottom of the cell. There was set up a computer so that it was possible to see the in situ moisture content of the sensors whilst the test was being executed. The test stopped at 8 rounds of pouring because it did not seem to have any further effect on the moisture content in the fine soil.

After the pouring of water in to the cell it was left overnight to drain with the water head sensor still in the bucket.

Figure 36 - The cell in the middle of the test. If watched closely it is possible to see the water front approximately halfway down in the fine material.

The second day of the laboratory work, Thursday 28/11-2013, started out with measuring the height of the top of the cell. This was to determine possible subsidence which might have happened overnight. The new height was measured to be 27,56 cm which means that there was a subsidence of 0,02 cm. This is not significant, especially considering the irregularities on the surface which makes the measurements varying.

5.1.1.4 Test 2: Fine material over coarse

The cell was then prepared for test 2 which included washing and drying it, and removing the tested materials. The next test was set up the same way as the first test albeit the coarse material went on the bottom this time. In total there were 4 sensors and 6 layers.

Figure 37 – The cell ready during the second test after the first pouring. Note the small layer of water on top of the fine material.

The test was executed the same way as test 1 with regard to pouring. There were poured in total 8 times with the same water amount as for test 1; 154 ml which equals 10mm rise in the column.

An observation that was obvious this time was that it took a while before the waterfront hit the coarse material which was at the bottom. When it did so after 36 minutes the moisture content in the sensors in the coarse material were relatively steady. Another observation while the test was going on was the fact that there was a water head on top of the fine material. This infiltrated in to the fine material with a relatively low rate and when the final pouring was done it had a head of approximately 2,2 cm above the fine soil.

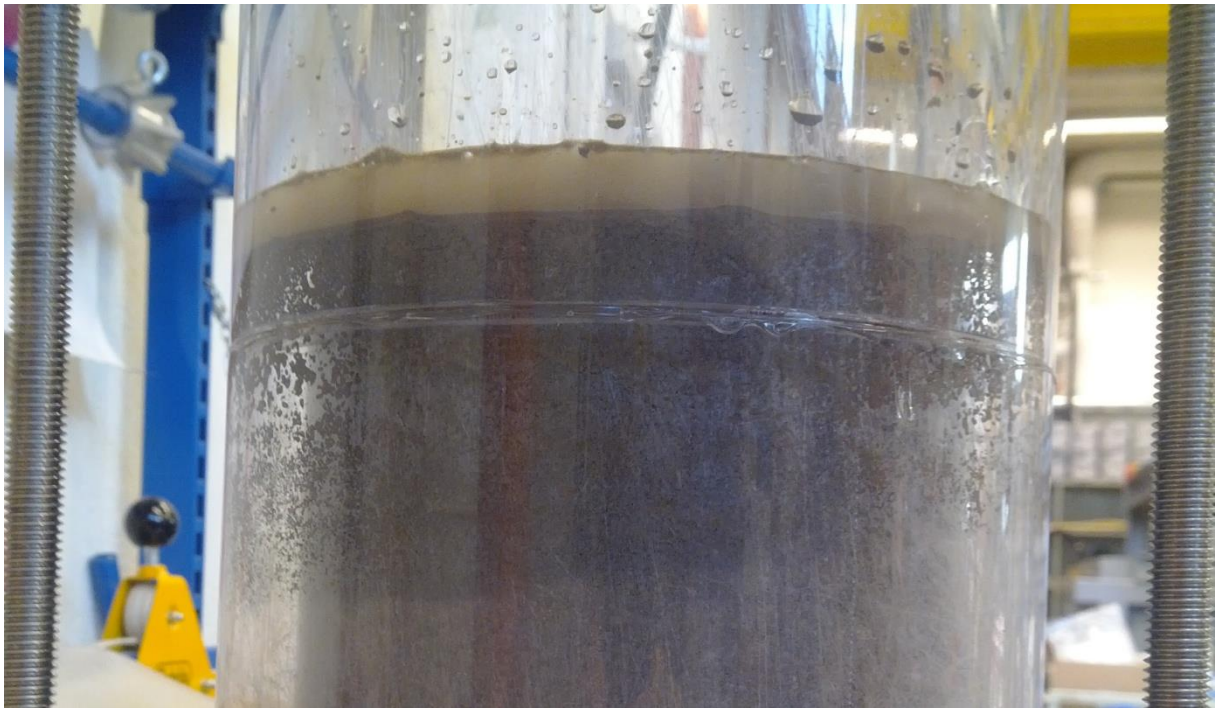

Figure 38 - Water propagation and water head above the fine material.

Another interesting observation was that the propagation through the fine material did not have an evenly distributed water front. The water front measured values between 8,2 and 10,1 cm from the top of the material at 24 minutes after the test started. The reason for this might be that the material is not homogenously distributed within the cell. Since the materials have been stamped the inhomogeneities can stem from irregular stamping of the material.

The apparatus was left overnight to drain after the final pouring.

The last day of the laboratory work, Friday 29/11-2013, consisted of finishing off test 2. This included, as for test 1, sampling from different layer, weighing dried samples from day 2 and demounting the cell. Emptying and cleaning the call was also done.

Finally, the samples gathered from the 3rd day of laboratory work which were put in the oven for drying were weighed by Mr. Thomas Pabst on Saturday 30/11-2013.

5.1.2 Simulations

The numerical software code Seep/W and the GeoStudio Suite has been largely validated during the last decades (Chapuis et al., 1993, 2001; Aubertin et al., 1996; Scanlon et al., 2002; Shuniark, 2003; Swanson et al., 2003; Weeks and Wilson, 2005; Yanful et al., 2006) and has proven to precisely and representatively simulate both saturated and unsaturated water movement, in 1D and 2D models. Furthermore the GeoStudio suite has been used to simulate the infiltration into multi-layered profiles made of significantly different materials (e.g. Pabst et al., 2011).

5.1.2.1 Objective

It was decided to carry out numerical simulations of the 1D-infiltration in a layered profile described earlier in order to test the sensitivity of the models. Practice of the software has been an integral part of this project. To check for critical parameters controlling infiltration rates and more importantly, propose a new approach to test soil-rock interface properties in the laboratory was the main objective.

5.1.2.2 General assumptions

The tests have been explained throughout in the previous chapter about the methodology of the laboratory test. The models were built with an initial conditions steady state step as well as draining and pouring steps in a transient state.

A saturated/unsaturated material mode was chosen and the code based on the Van Genuchten equations. The material properties were based on the measured porosities and grain size distribution of the materials with the use of the Kozeny-Carman equation for initial estimations. The air entry value and the Van Genuchten parameters were estimated by a trial-and-error approach. Estimating the material properties have proved tedious and difficult for the entire process of simulating the laboratory tests and has been done by changing one by one parameter for the best possible estimation.

The infiltration was simulated by using a unit flux over the course of 10 seconds which was the approximate average time measured for pouring in the lab. This gave a unit flux of q=0,001 [m/s] given the total water addition of 0,154L every time which correspond to 10mm

rise in an empty cell. A draining step of 5 minutes was included after each pouring. Finally a long time draining step of 24 hours was applied to see the long term effect.

5.1.2.3 Geometry and boundary conditions

Given that this is a 1D model the mesh has been created such that horizontal movement is not measured. The dimensions of the model were adjusted to the cell dimensions and the thicknesses of the material layers measured in the laboratory.

5.1.2.4 Test1: Coarse over fine

The case coarse material over fine was encountered first with the thought of this being the easiest case to recreate in a model. The model setup can be seen in Figure 39 together with and axis for a dimensional impression.

This model was the first case created for this project and as a result of that a lot of time was spent on the development of the model. The process was time consuming with a steep learning curve. Throughout the development of the model it proved difficult to obtain satisfying results. This process, the outcome and possible improvements are discussed further in the analysis chapter.

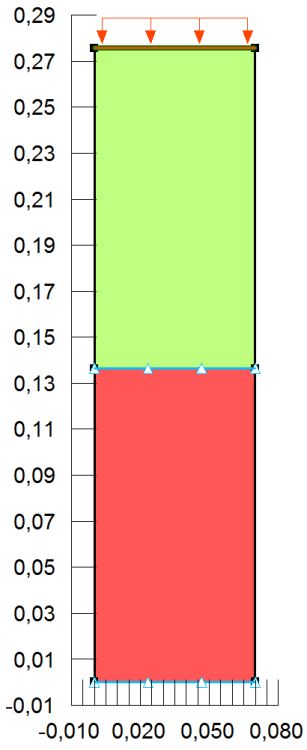

Figure 39 – the setup of the model in Seep/W, axis values in centimetres.

5.1.2.5 Test2: Fine over coarse

In the same manner as the coarse over fine case the fine over coarse case was executed except the materials obviously were in the opposite order. An example of a simulation with volumetric water contents results can be seen in Figure 40.

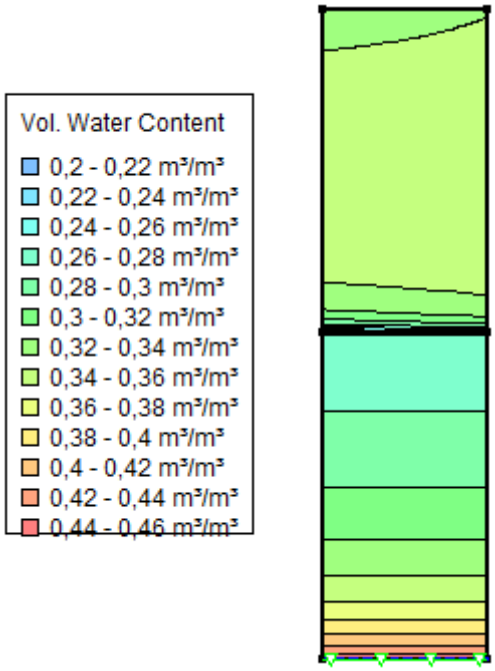

Figure 40 – Volumetric water content for a random fine over coarse case.

5.2 Results

The measured and simulated results from both lab tests are presented in the following accompanied with estimated material properties for both test scenarios.

5.2.1 Measured values

5.2.1.1 Test1: Coarse over fine

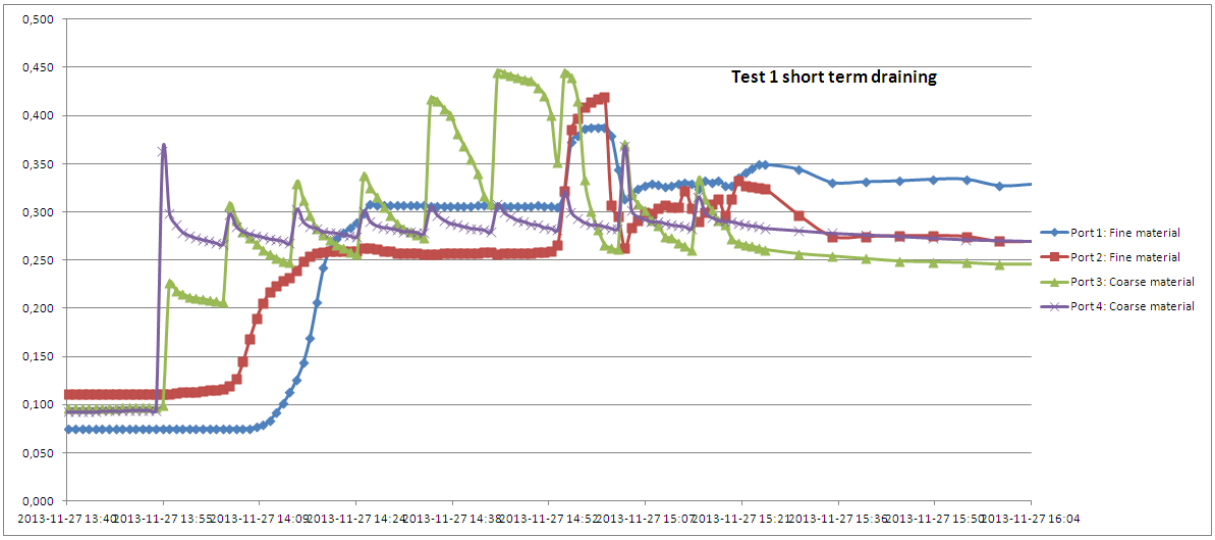

Figure 41 – The short term test phase of test 1. Water content (%) versus time.

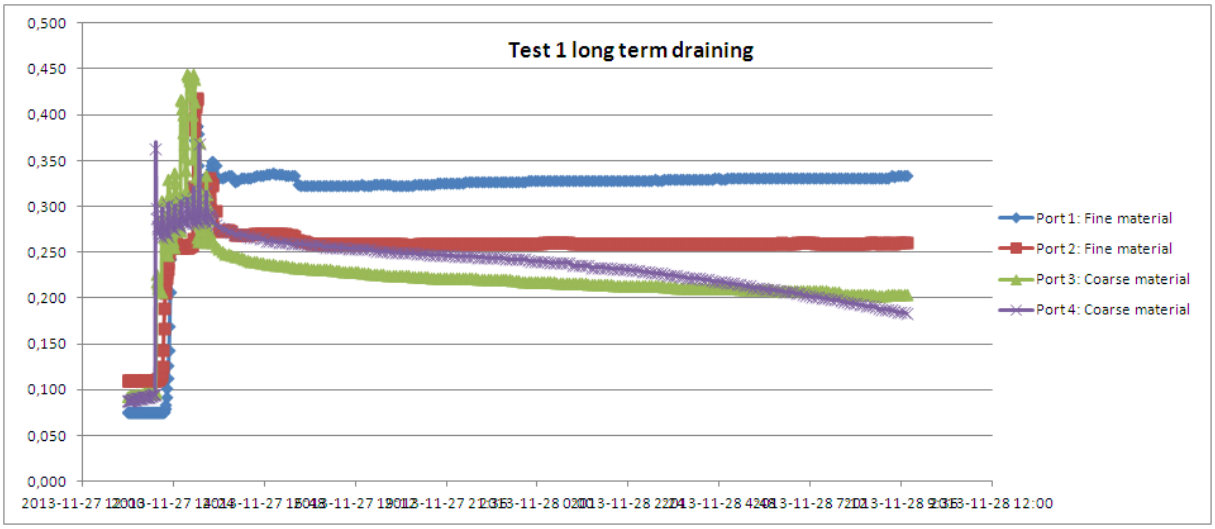

Figure 42 – The long term draining phase of test 1. Water content (%) versus time.

5.2.1.2 Test2: Fine over coarse

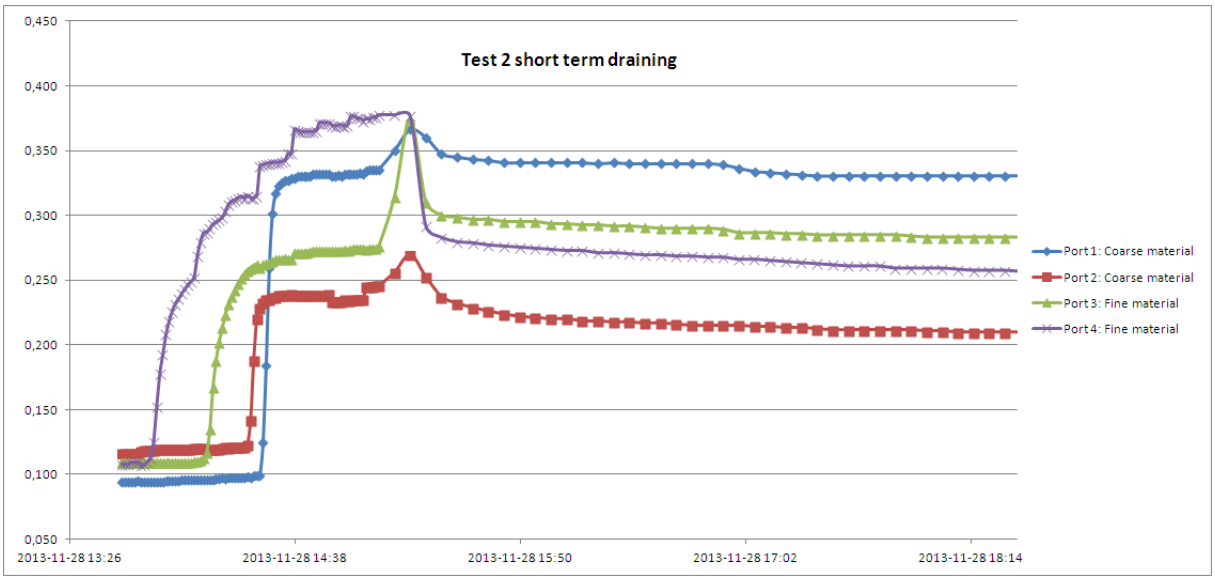

Figure 43 – The short term test phase of test 2. Water content (%) versus time.

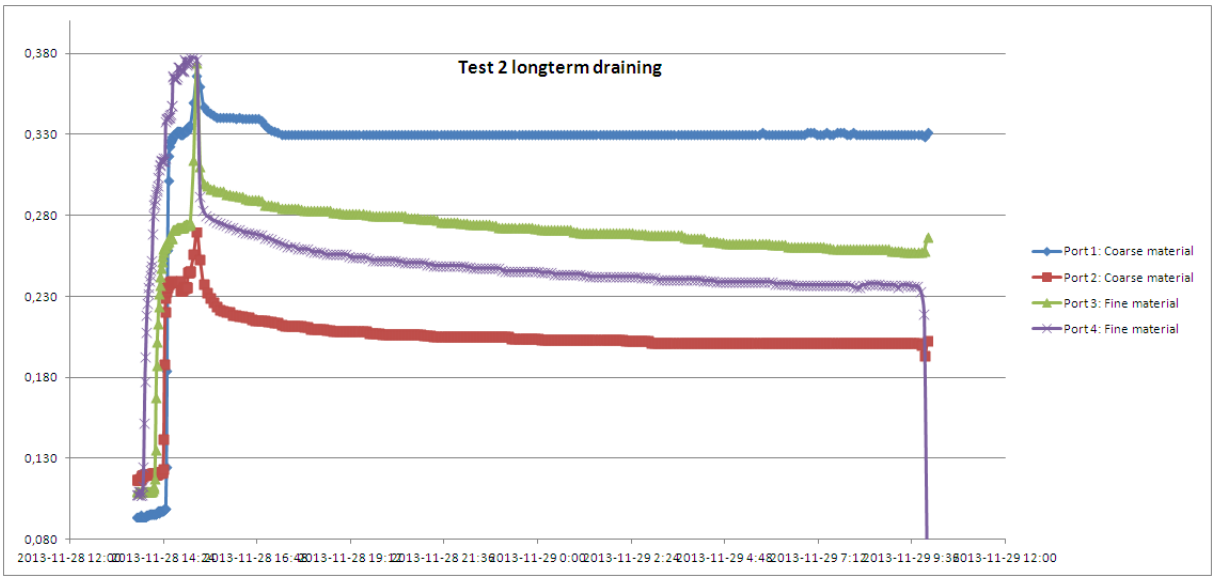

Figure 44 – The long term draining phase of test 2. Water content (%) versus time.

5.2.2 Simulated values

5.2.2.1 Test1: Coarse over fine

Table 3 – properties of simulated results of laboratory test coarse over fine. Est. means the hydraulic conductivity is estimated as a function of matric suction.

Simulation	Hydraulic conductivity [m/s]	Air entry value, a [kPa]	Van Genuchten parameter, n	Saturated water content [%]	Residual water content [%]
Sim1	$3e^{-5}$(est)	0,3	2,5	0,385	0,02
Sim2	$3e^{-5}$(est)	0,3	2,5	0,385	0,02
Sim3	$3e^{-5}$(est)	0,3	2,5	0,385	0,02
Sim4	$3e^{-5}$(est)	0,3	2,5	0,385	0,02

Table 4 – Coarse material properties

Simulation	Hydraulic conductivity [m/s]	Air entry value, a [kPa]	Van Genuchten parameter, n	Saturated water content [%]	Residual water content [%]
Sim1	0,1(est)	0,7	1,5	0,385	0,05
Sim2	0,0001	1	3	0,45	0,15
Sim3	0,001	1	3	0,38	0,15
Sim4	0,001	1	3	0,34	0,15

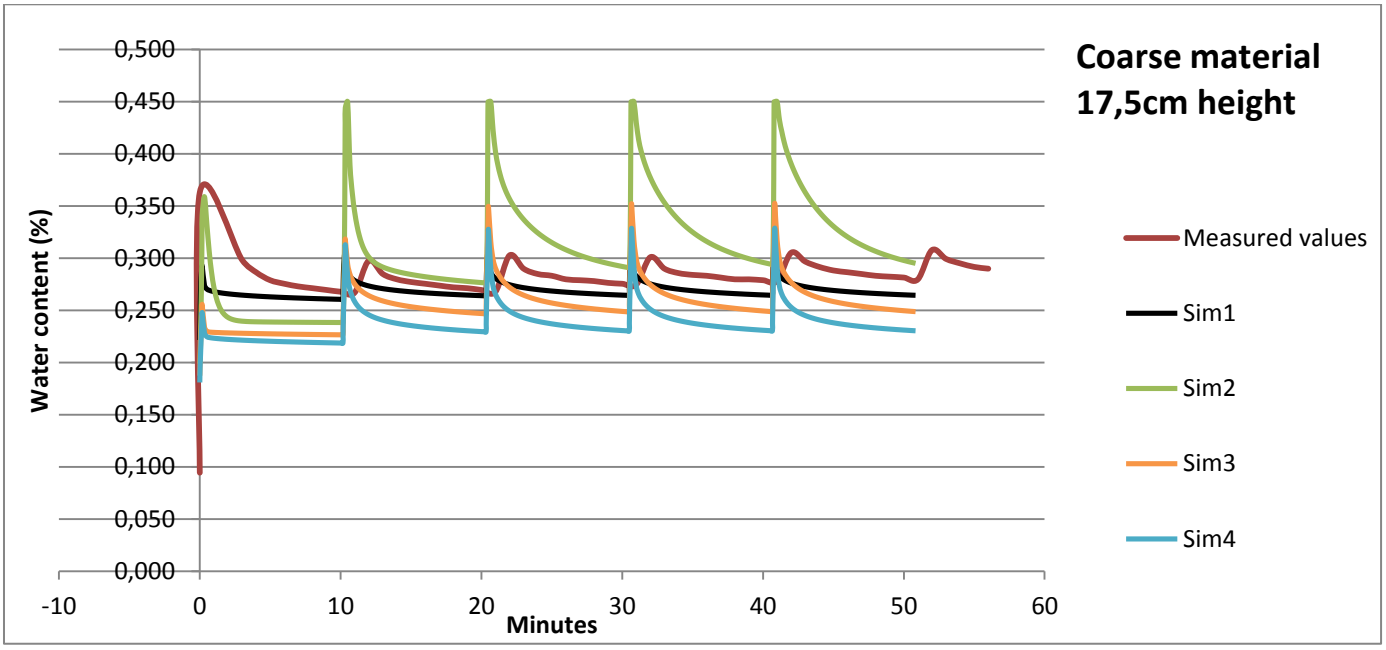

Figure 45 – Simulated and measured values of lowest port in the coarse material.

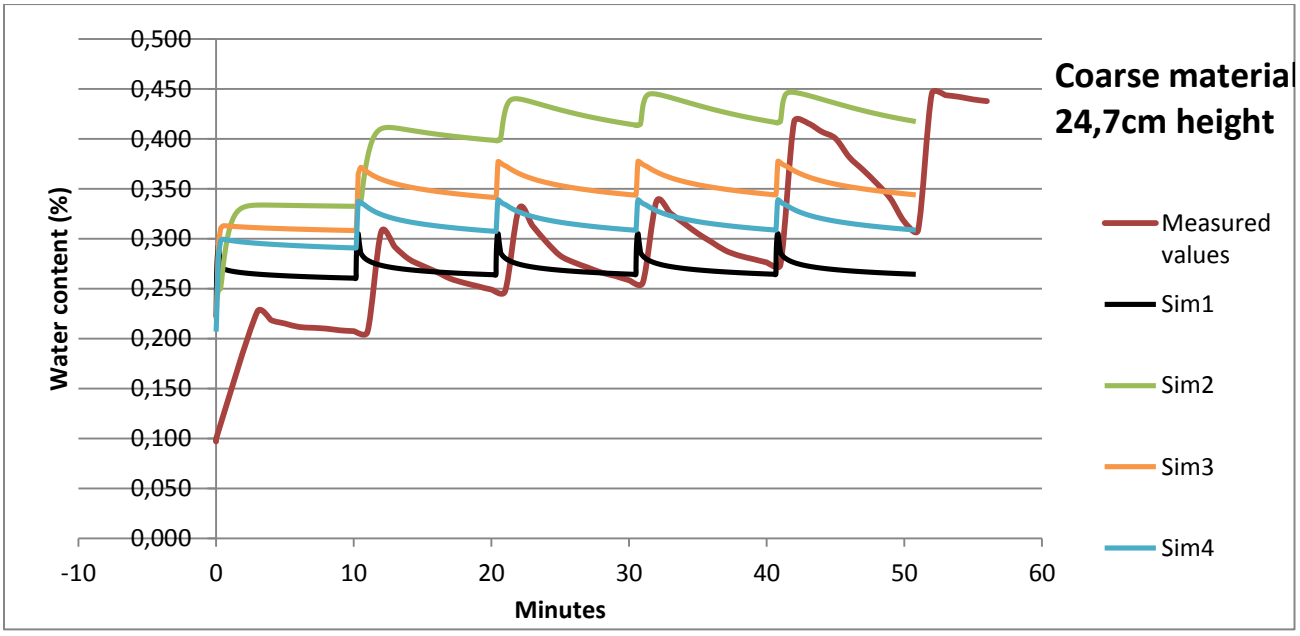

Figure 46– Simulated and measured values of highest port in the coarse material.

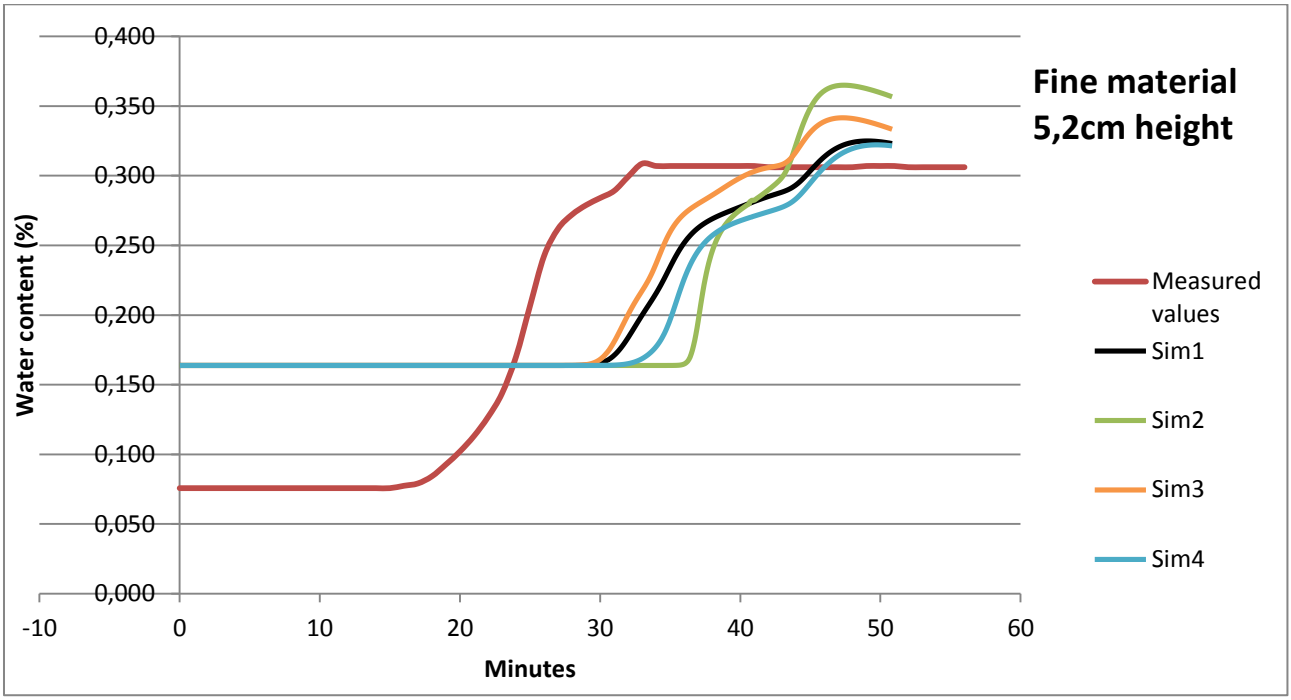

Figure 47– Simulated and measured values of lowest port in the fine material.

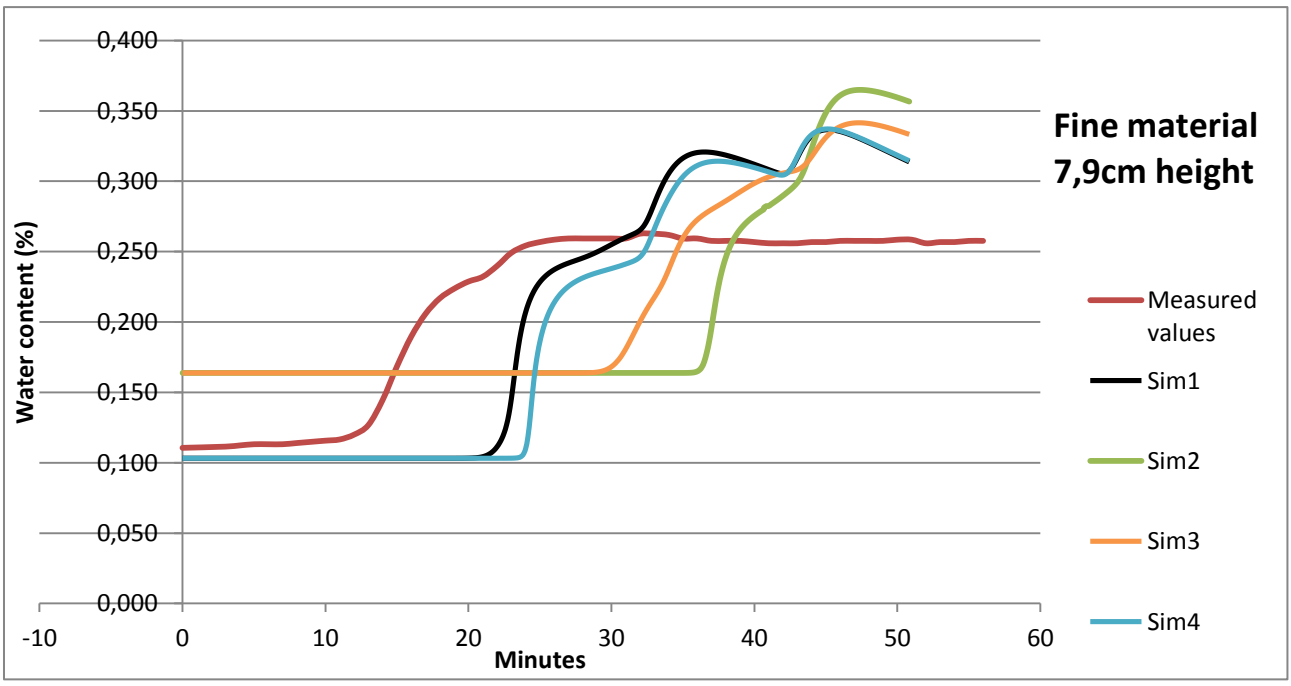

Figure 48 – Simulated and measured values of highest port in the fine material.

5.2.2.2 Test2: Fine over coarse

Table 5 – properties of simulated results of laboratory test fine over coarse. Est. means the hydraulic conductivity is estimated as a function of matric suction.

Simulation	Hydraulic conductivity [m/s]	Air entry value, a [kPa]	Van Genuchten parameter, n	Saturated water content [%]	Residual water content [%]
Coarse material	0,0001	1	3	0,45	0,1
Fine material	$5e^{-7}$(est.)	25	2,5	0,35	0

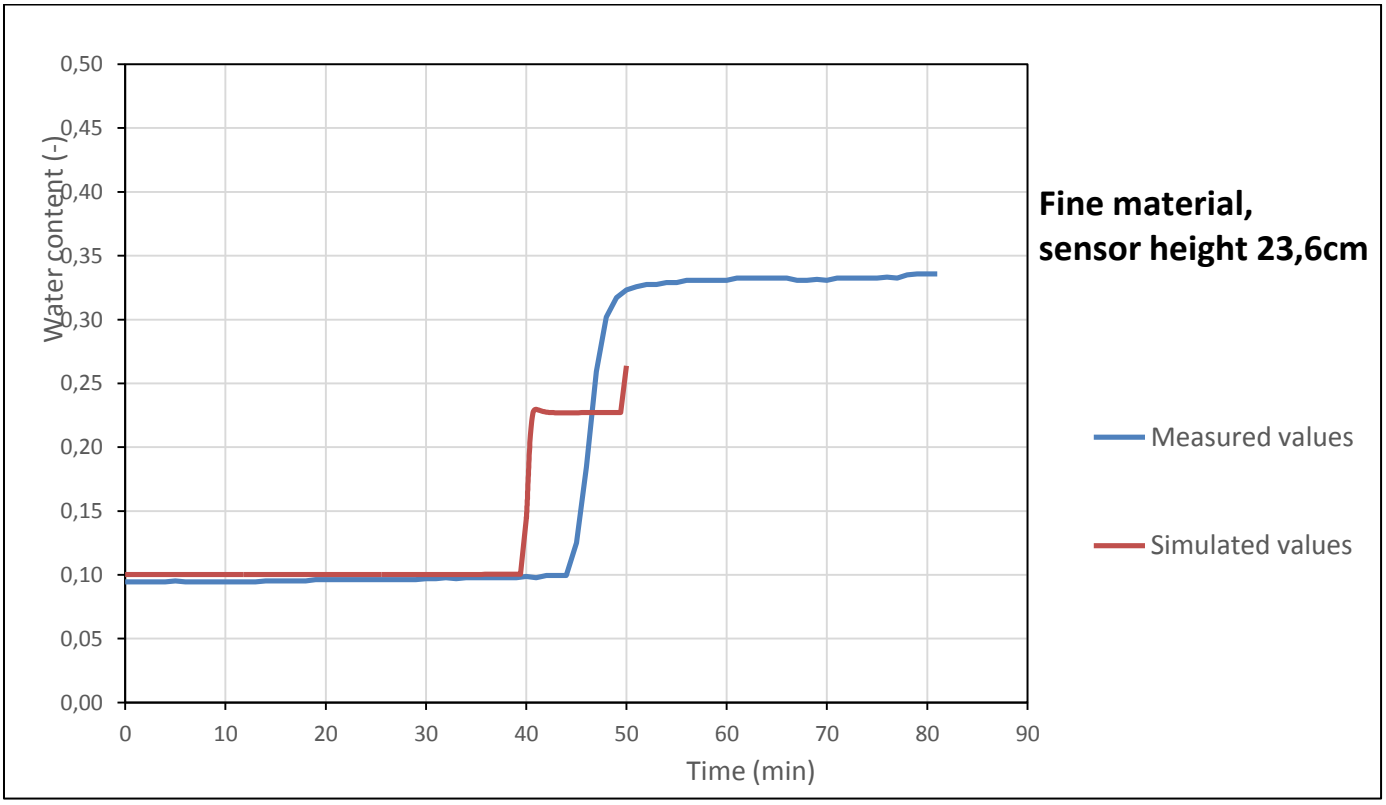

Figure 49 – Simulated and measured values of highest port in the fine material.

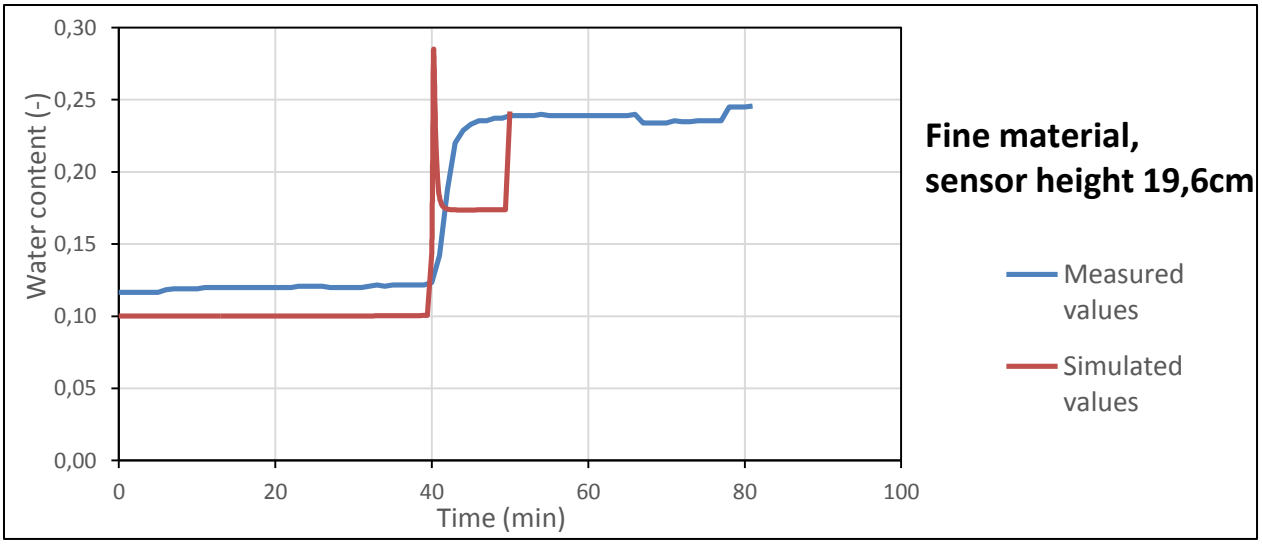

Figure 50– Simulated and measured values of lowest port in the fine material.

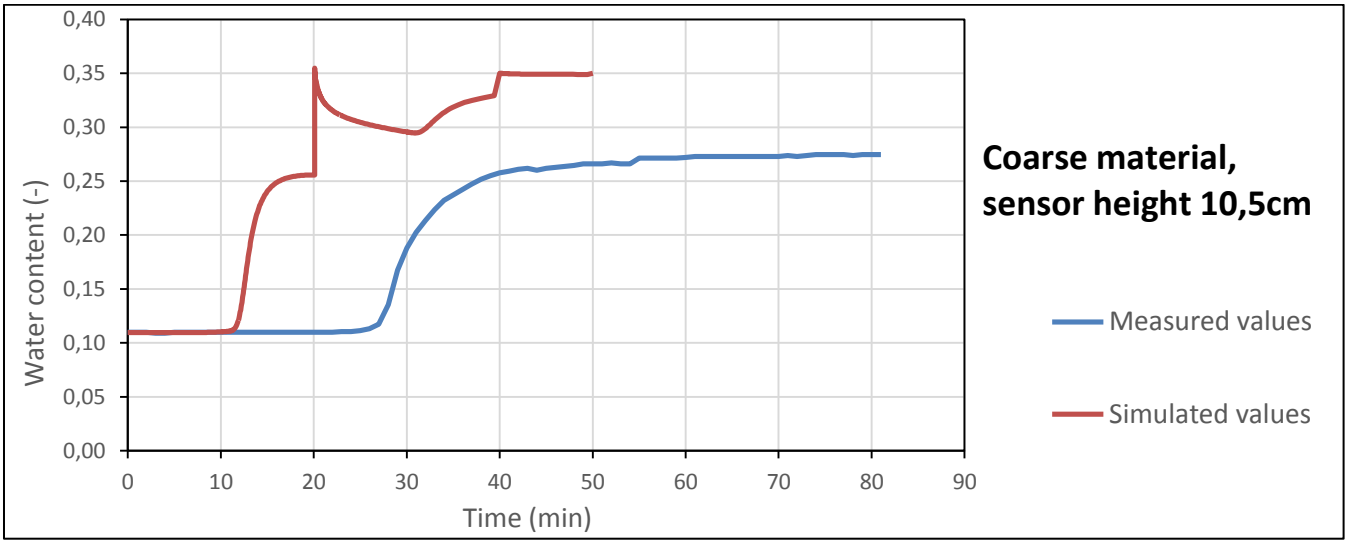

Figure 51– Simulated and measured values of highest port in the coarse material.

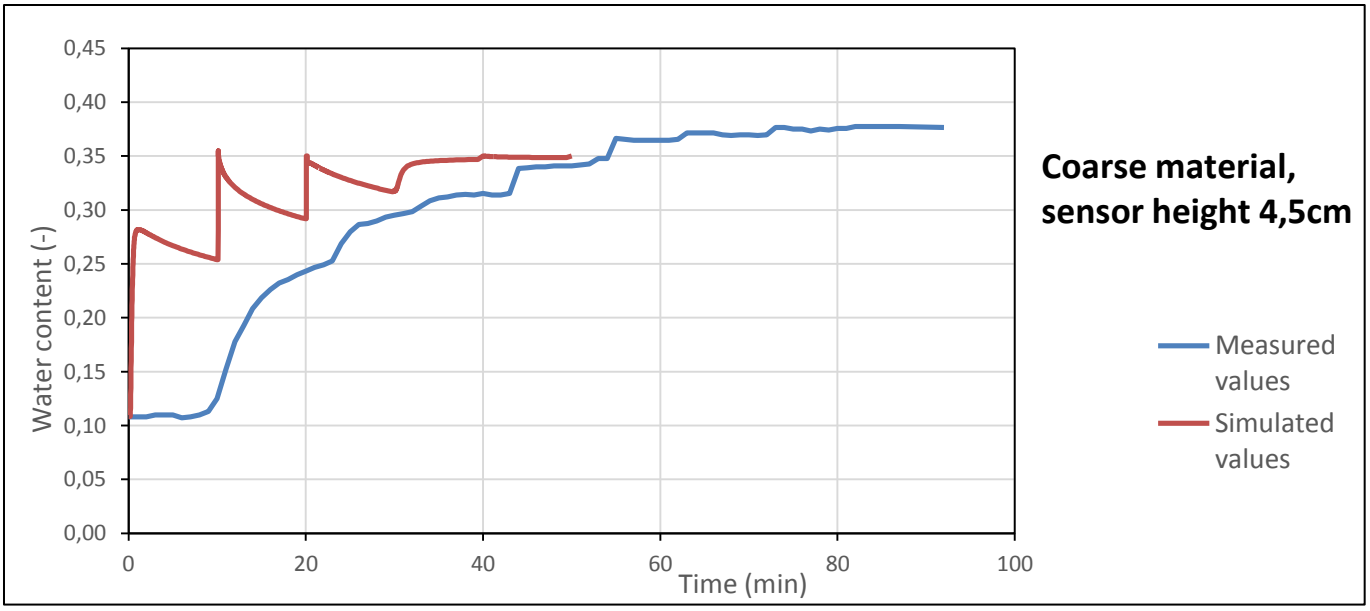

Figure 52– Simulated and measured values of lowest port in the coarse material.

5.3 Analysis

As seen from the results and briefly mentioned in the methodology chapter the results obtained do show tendencies to match the measured values albeit there are obvious differences too. In the following the obtained data will be evaluated together with general improvement suggestions.

5.3.1 Test1: Coarse over fine

Figure 45 and Figure 46 show the volumetric water content versus time for the two sensors in the coarse material. It is obvious that none of the curves fit the measured values well albeit the patterns of the graphs do follow the measured values. Because of this more than one graph that resembles the pattern of the measured values are presented with differing material properties.

The development of the model was given a significant amount of time in the process of this MSc thesis as learning the software was a large time consuming internal part of the project. The approximate patterns of the measured graphs were established. A considerable amount of time invested in the development of the models did prove exact curve fitting difficult. The models were rebuilt several times in addition to severe experimentation with material parameters without. By presenting a set of graphs with different characteristics it is thought to give an impression of the most promising material properties.

Although, what can especially be seen in Figure 45, taken from the coarse material, is the pattern of the graphs and to some extent the saturated water contents. They seem well fitted to the measured values and some even relatively well corresponding in terms of shape fit as well, especially in the case of “sim1”. What can be seen in Figure 46 for the “Sim1” case though, is the lack of rise and drawdown of the curve.

Studying the simulated values in Figure 47and Figure 48 the rise gradient seems rather appropriate albeit the residual and saturated water content does only to a certain degree add up to the measured values even though the measured values from the laboratory has been tried used together with other values.

5.3.2 Test2: Fine over coarse

As figures 41, 42, 43 and 44 show the material properties of the fine over coarse laboratory test case does also have non-satisfying fittings with the measured values. A similar approach as for the opposite case was used and some tendencies in the models indicate models with patterns resembling the measured values found. Especially Figure 51 and Figure 52 in the coarse material do have similarities with the measured values the results are not entirely convincing.

5.3.3 Evaluation and improvement suggestions

It is indeed a challenge to predict infiltration from soil to rock in projects where only limited data are available. The time constraints in this case has also not allowed deep field investigations and testing. Such setup would have been a practical way to get the relevant properties in the laboratory before using them in larger scale numerical models. As seen thereafter, the results have proven only partly convincing, but are still encouraging and it is believed that further developments may solve some of the remaining uncertainties.

Overall, and despite some discrepancies, the numerical models were able to reproduce fairly well the laboratory measurement, especially considering the limited amount of data available and the time spent on learning the software. The irregularities observed could have several explanations, amongst the assumed are:

- No calibration of the volumetric water content sensors
- Heterogeneities in the materials, including variations in compaction
- Fine grained material was used around the sensors in the coarse soil layer, in order to protect them.

An observation made during test 2 was that the water front was 2cm offset from one side of the cylinder to another. This might be a result of the aforementioned or some other sources of error.
A better control of the compaction of the materials, the calibration of the sensors, and a more detailed characterization of the soils should in the future allow a better understanding of the processes and thereby the calibration of the numerical models.

6.0 Large scale models

The large scale models are an important part of this thesis. They are created in order to see what effects different case scenarios with tunnel construction have. By the development and evaluation of the slug and laboratory tests it is shown that continuous models can simulate water infiltration to rocks and between different materials. Given that the evaluation of the laboratory tests were only partially convincing potential good and predictable results from the large scale tests will support that the models can infiltrate between different materials.

6.1 Objective

The objective of simulating large scale models is to create models of different scenarios where infiltration through the soil-rock interface and in to a tunnel is simulated. Three different cases were constructed and are evaluated later on.

6.1.1 General assumptions

All of the tests have been done with the same soil material. This is a silt based on properties of a well-graded silty material by Aubertin et al. (2003), Figure 6 in the paper A model to predict the water retention curve from basic geotechnical parameters.

Table 6 – material properties of the silt material used in all large scale tests

Hydraulic conductivity	$5e^{-7}$ [m/s]
a [kPa]	25
n	1,8
Saturated water content	0,4 %
Residual water content	0,02 %

6.1.2 Geometry and boundary conditions

The models were built 100 to 120 meters wide which proved sufficient for the side of the models not affecting the groundwater flow. The thicknesses vary a lot from case to case and are evaluated thoroughly. Soil thicknesses and tunnel depth are presented for each case. The tunnel geometry is a circular tunnel with a diameter of 6m for all cases.

Boundary conditions used are initial water tables which vary from case to case.

6.1.3 Climatic functions

There are two different climatic sites used for infiltration functions in these cases; Lillehammer and Bergen. The former is an example of a dry climate with cold winters and warm summers while the latter is from one of the wettest areas in Norway. Both data sets are from 2006.

The infiltration functions used are made from data taken from Norwegian Metrological Institute and Vadose/W has been used to estimate a boundary condition function which is a time dependent unit flux. Infiltration functions can be seen in Figure 53 and Figure 54 with daily average infiltration rates for 1 year. Cumulative infiltration data per unit length over the course of 1 year is presented in Table 7. The soil which the infiltration functions are simulated with is a silty silt with hydraulic conductivity $1e^{-6}$ and an air entry value of 1kPa. Note that the material is somewhat similar to the silt used in all the models.

Table 7 – Cumulative infiltration amount per unit length over the course of 1 year (2006).

Location	**Cumulative infiltration amount 1 year[m^3/m]**
Bergen	1,781 [m^3/m]
Lillehammer	0,0720 [m^3/m]

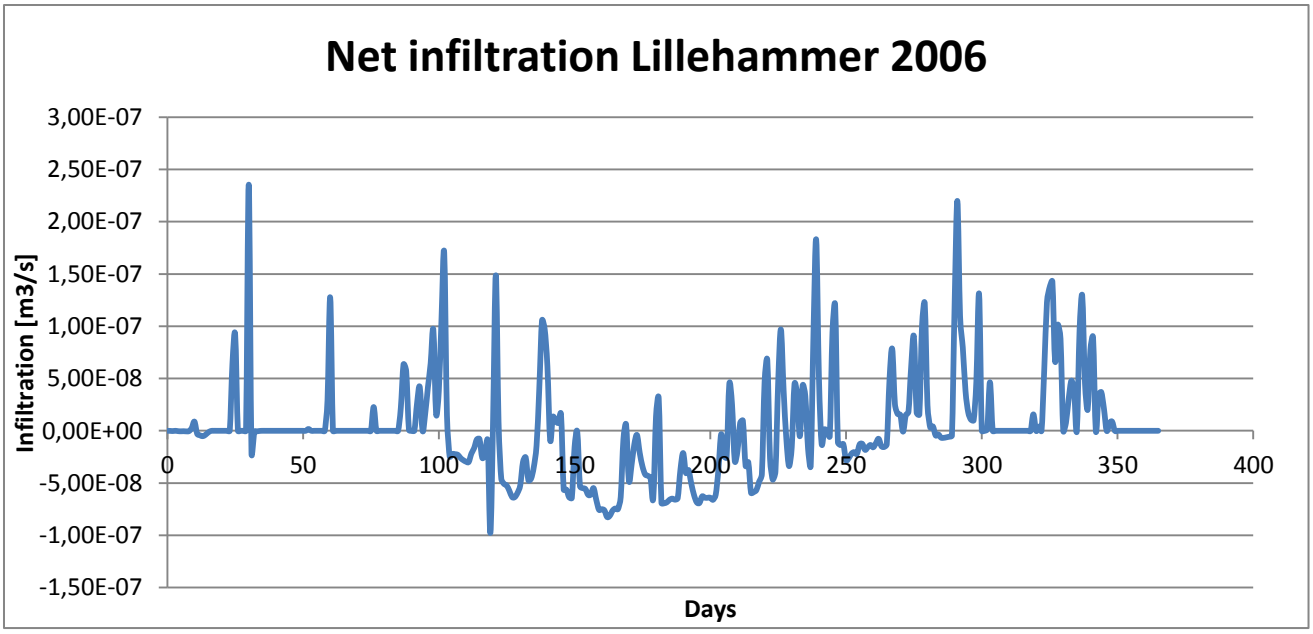

Figure 53 – Infiltration function of Lillehammer

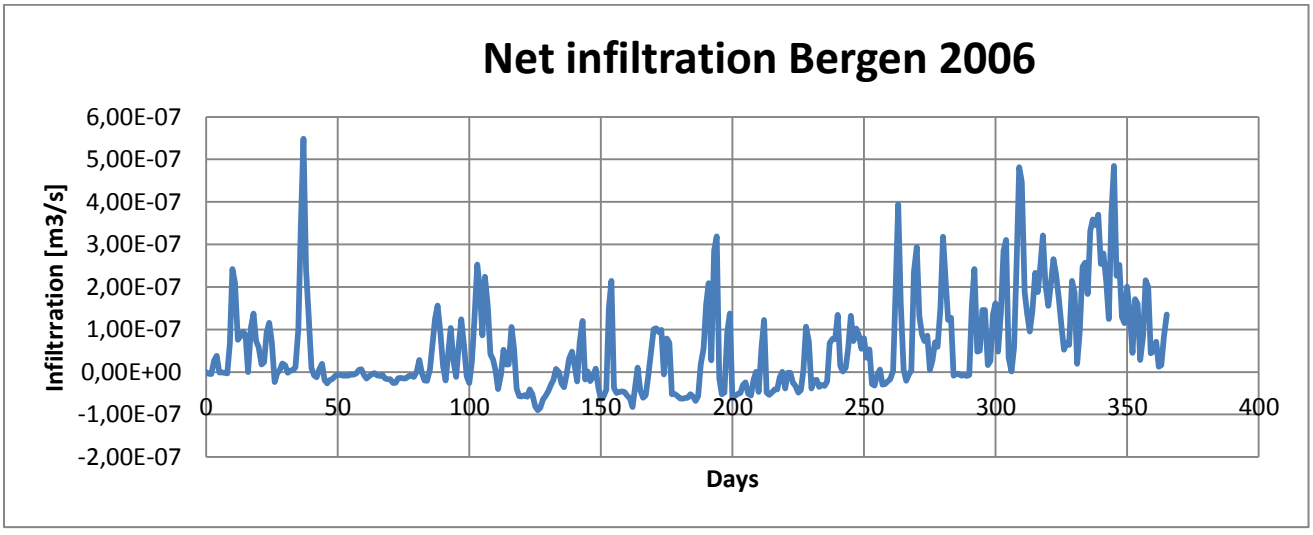

Figure 54 – Infiltration function of Bergen

6.2 Case scenarios

The cases created and later used for evaluation will be presented in the following, containing a flat case, a slope case and a lake case.

6.2.1 Flat case

The first case is a flat model with varying tunnel depths and soil thicknesses. The rock material is from well KJ3 at the Folkehelseinstituttet site and kept the same in all of the cases. The rock mass properties can be seen in Table 8 and an example of the case geometry can be seen in Figure 55. The same horizontal geometry has been used for all tests.

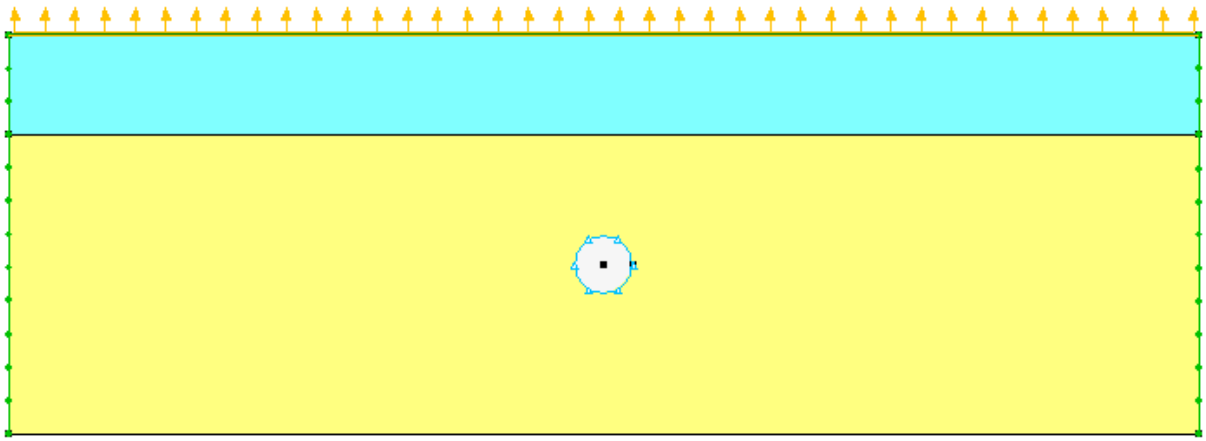

Figure 55 – Example of the flat area case. Soil thickness 10m, tunnel depth 10m beneath rock mass surface.

Table 8 – Rock mass properties of rock surrounding well KJ3 at the Folkehelseinstituttet site

	Rock mass KJ3
Hydraulic conductivity	$8{,}5e^{-7}$
a [kPa]	0,1
n	2
Saturated Water Content	0,03
Residual Water Content	0,01

In total 13 different cases were tested and the different properties can be seen in Table 9. By keeping the precipitation location and both the soil and material properties the same it is thought possible to say something about the soil thicknesses and tunnel depth's effect on

infiltration. Three cases without tunnels were also tested to see the effect of a tunnel construction on the infiltration.

Table 9 – Test case specifications.

Name	Tunnel depth below rock	Soil thickness	Rock material	Soil material	Precipitation location
Flat D2 S1	2	1	KJ3	Silt	Bergen
Flat D5 S1	5	1	KJ3	Silt	Bergen
Flat D5 S5	5	5	KJ3	Silt	Bergen
Flat D5 S10	5	10	KJ3	Silt	Bergen
Flat D10 S1	10	1	KJ3	Silt	Bergen
Flat D10 S5	10	5	KJ3	Silt	Bergen
Flat D10 S10	10	10	KJ3	Silt	Bergen
Flat D20 S1	20	1	KJ3	Silt	Bergen
Flat D20 S5	20	5	KJ3	Silt	Bergen
Flat D20 S1	20	10	KJ3	Silt	Bergen
Flat S1	No tunnel	1	KJ3	Silt	Bergen
Flat S5	No tunnel	5	KJ3	Silt	Bergen
Flat S10	No tunnel	10	KJ3	Silt	Bergen

6.2.2 Slope case

The second case is a slope case with a tunnel beneath. The idea is to see what effect a slope will have on infiltration. Both the Bergen and Lillehammer precipitation locations are used. There are also two different rock types from the Bekkelaget test site, BL2 and BL3, whose properties can be seen in Table 11. These are gneisses which to some extent is prone in Norwegian valley landscapes. Both the soil cover and slope is kept constant at 2m and 20% respectively. A soil cover of 2m is used because it is considered more realistic for a slope than a thick soil cover in a slope situation.

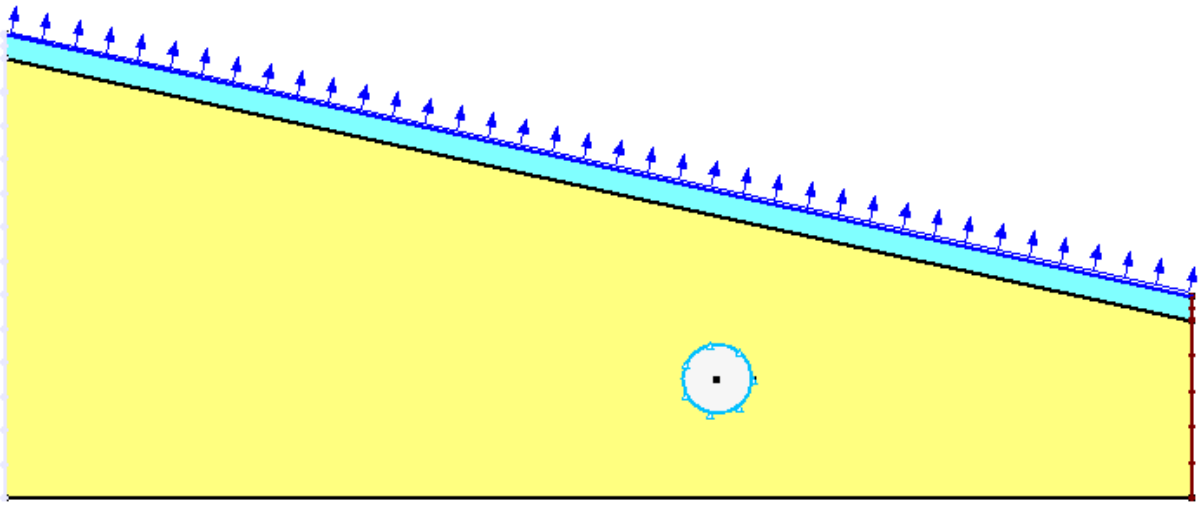

Figure 56 - Example of the slope case. Soil thickness 2m, tunnel depth 10m beneath rock mass surface.

A total of 11 cases will be evaluated for the slope case. Cases without tunnels are evaluated in this case in order to see what effect a tunnel has on infiltration in this environment. By keeping the soil cover constant the effect of infiltration as a function of depth and rock type can be evaluated. Also the change of precipitation functions makes it possible to evaluate in what grade climatic factors affects infiltration. The test properties can be seen in Table 10

.

Table 10 - test case spesifications

Name	Tunnel depth below rock	Soil thickness	Rock material	Soil material	Precipitation location
Slope Bergen BL2	No tunnel	2	BL2	Silt	Bergen
Slope Bergen BL3	No tunnel	2	BL3	Silt	Bergen
Slope Bergen D10 BL2	10	2	BL2	Silt	Bergen
Slope Bergen D20 BL2	20	2	BL2	Silt	Bergen
Slope Bergen D20 BL3	20	2	BL3	Silt	Bergen
Slope Lillehammer BL2	No tunnel	2	BL2	Silt	Lillehammer
Slope Lillehammer BL3	No tunnel	2	BL3	Silt	Lillehammer
Slope Lillehammer D10 BL2	10	2	BL2	Silt	Lillehammer
Slope Lillehammer D20 BL2	20	2	BL2	Silt	Lillehammer
Slope Lillehammer D20 BL3	20	2	BL3	Silt	Lillehammer

Table 11- Rock mass properties of rock surrounding well BL2 and BL3 at the Bekkelaget site

	Rock mass BL2	Rock mass BL3
Hydraulic conductivity	$1{,}5e^{-6}$	$8{,}5e^{-8}$
a [kPa]	0,1	0,1
n	1,1	1,000005
Saturated Water Content	0,03	0,03
Residual Water Content	0,01	0,01

6.2.3 Lake case

The last case is a case with a flat area with a tunnel below a lake. The idea is to see what effect different tunnel depths has in interaction with the lake. A comparison of a case with no tunnel will also be evaluated. Both the Bergen and Lillehammer precipitation locations are used as well as two different rock types. In Figure 57 the case is showed and there is a 12m thick soil which goes beneath the lake. The reason for this is because a lake seldom is placed directly on a rock surface but rather on a soil surface of sediments. In a real life scenario the lake could be drained by the construction of the tunnel with the drainage case at the Romeriksporten tunnel in southern Norway (Kitterød 2000, Davik&Andersson 2001). It is assumed that the water level is kept constant around the lake by other sources.

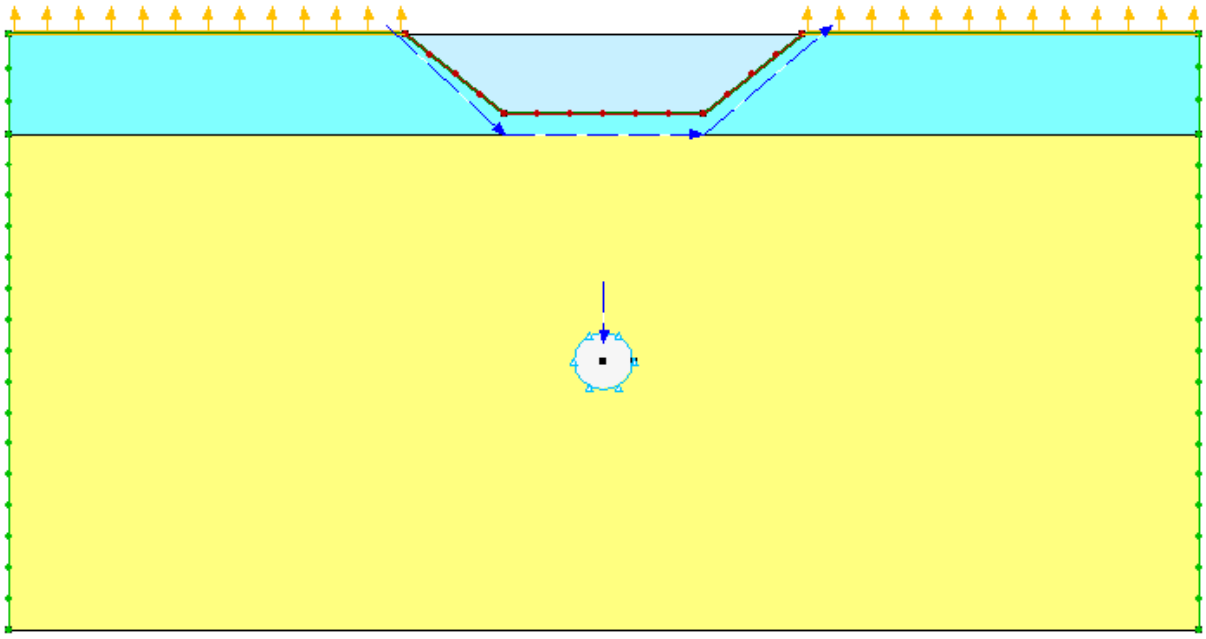

Figure 57 - Example of the lake case. Soil thickness 12m, tunnel depth 20m beneath rock mass surface.

A total of 10 cases will be evaluated for the lake case. Keeping the soil cover constant will allow the interpretations to consider the tunnel depth, precipitation function and rock type's effect on the infiltration. The two rock types used are from the Vettekollen area whose hydraulic properties can be seen in Table 12. By choosing one relatively high and one low permeability rock types the effect of this can be studied in the proximity of a lake.

Table 12 - Rock mass properties of rock surrounding well BH3 and BH4 at the Vettakollen site

	Rock mass BH3	**Rock mass BH4**
Hydraulic conductivity	$1{,}5e^{-6}$	$9{,}8e^{-8}$
a [kPa]	0,1	0,1
n	2,2	1,5
Saturated Water Content	0,03	0,03
Residual Water Content	0,01	0,01

Table 13 - test case specifications

Name	Tunnel depth below rock	Soil thickness	Rock material	Soil material	Precipitation location
Lake Bergen BH3	No tunnel	12	BH3	Silt	Bergen
Lake Bergen BH4	No tunnel	12	BH4	Silt	Bergen
Lake Bergen D10 BH3	10	12	BH3	Silt	Bergen
Lake Bergen D20 BH3	20	12	BH3	Silt	Bergen
Lake Bergen D20 BH4	20	12	BH4	Silt	Bergen
Lake Lillehammer BH3	No tunnel	12	BH3	Silt	Lillehammer
Lake Lillehammer BH4	No tunnel	12	BH4	Silt	Lillehammer
Lake Lillehammer D10 BH3	10	12	BH3	Silt	Lillehammer
Lake Lillehammer D20 BH3	20	12	BH3	Silt	Lillehammer
Lake Lillehammer D20 BH4	20	12	BH4	Silt	Lillehammer

6.3 Results and evaluation of large scale models

In this chapter there will be given a variety of water controlling properties for infiltration which will be evaluated. The scenarios are presented, results given which in its turn is followed by an analysis of the scenario. It is chosen to discuss each scenario after the results to ease interpretation of figures and tables. Finally a comparison of all of the cases is made.

6.3.1 Basic case

This is a basic case with a flat area. The thought is to see what a constructed tunnel does with the groundwater and infiltration rates. It is thought to give a basic understanding of what a tunnel does with infiltration rates and the groundwater level.

6.3.1.1 Results

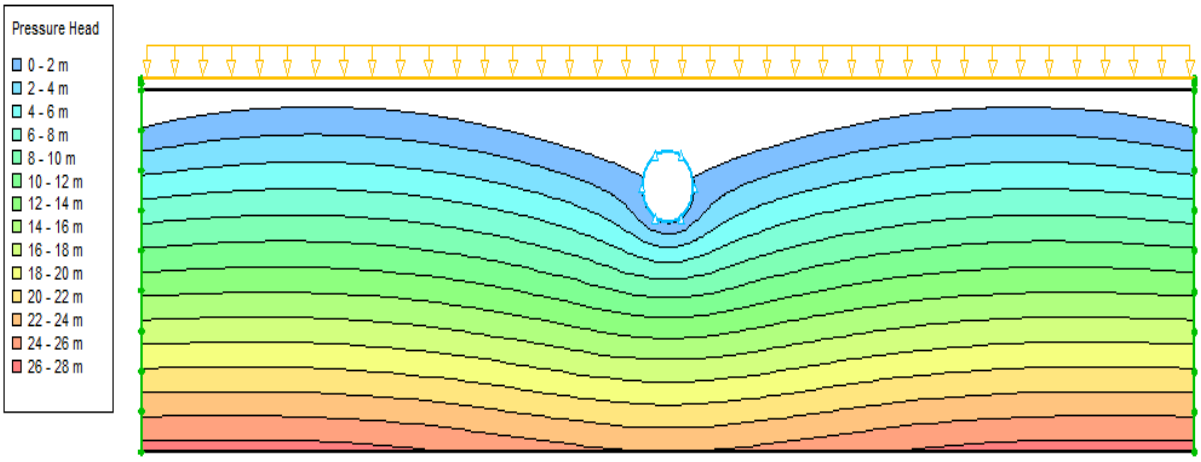

Figure 58 – Groundwater table from pressure head of the case Flat D5 S1.

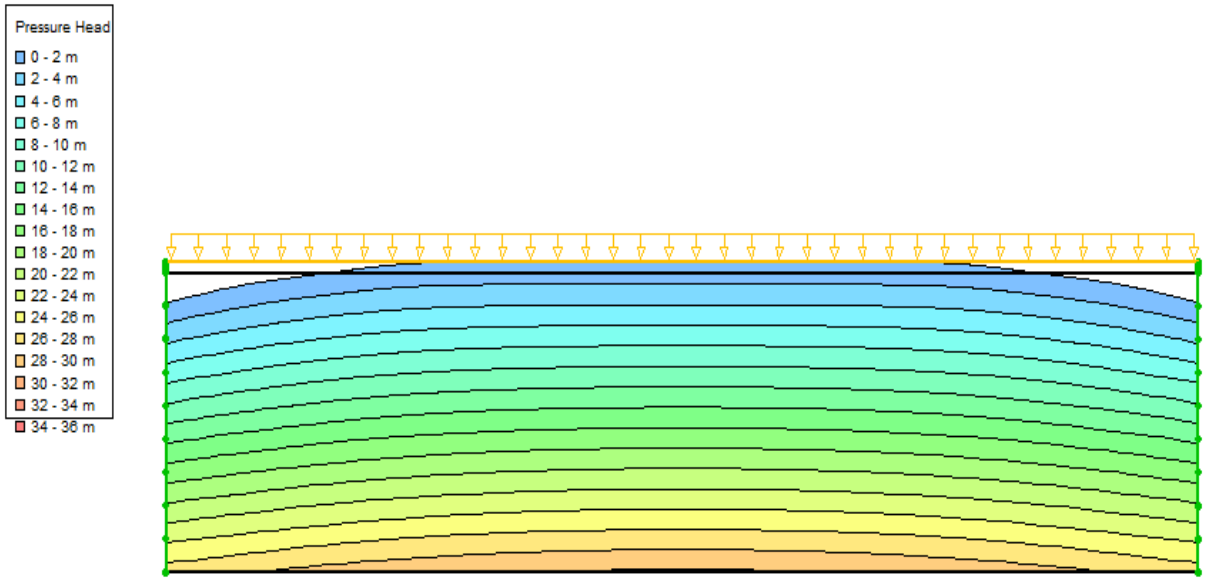

Figure 59 – Groundwater table from pressure head for the case Flat S1

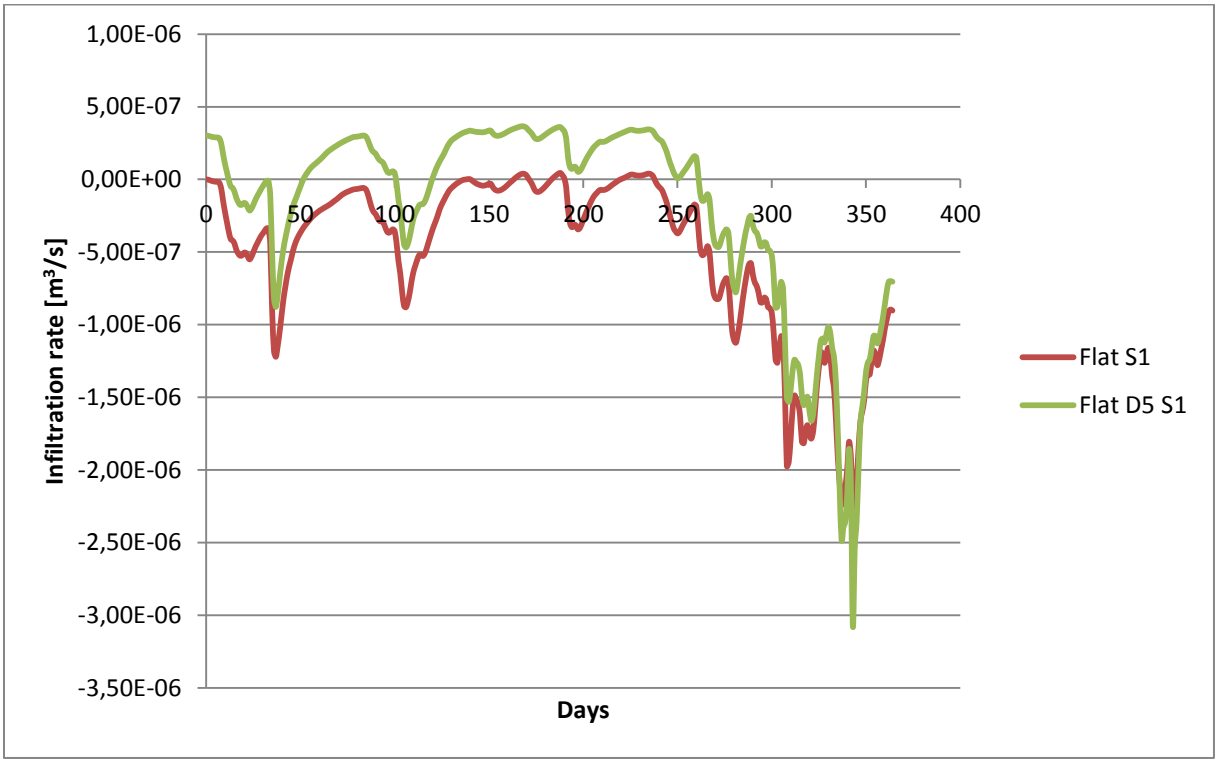

Figure 60 – Cases Flat S1 and Flat D5 S1. Effect of tunnel excavation on infiltration over soil-rock interface at soil thickness 1m with and without tunnel.

6.3.1.2 Analysis

In Figure 58 and Figure 59 the groundwater table of the cases Flat S1 D5 and Flat S1 can be seen respectively. These are two similar cases with equal climatic functions and soil depth but with and without a tunnel. From the figures it is apparent that the case Flat S1 D5 has had a drawdown effect on the groundwater. This is normally expected and not surprising.

Figure 60 show the infiltration rate over the soil-rock interface of the two aforementioned cases over the course of 1 year. Negative values indicate a downwards and positive upwards water transportation. It seems odd that a tunnel constructed affect the water infiltration in such a manner to move upwards. In the light of the groundwater tables shown in Figure 58 and Figure 59 though, it can be explained by the tunnel case having a groundwater table below the soil-rock interface whilst it being above for the non-tunnel case. The values of upwards moving water over the interface can then be explained from evaporation. Because the soil is thin the effects of this is thought to be severe which is supported by Figure 60.

6.3.2 Climatic effects

This case focuses on climatic effects and the result of this with regard to infiltration and the groundwater table. This is exemplified by cases from the lake model and comparing cumulative infiltrations as well as groundwater table and daily infiltration fluxes.

6.3.2.1 Results

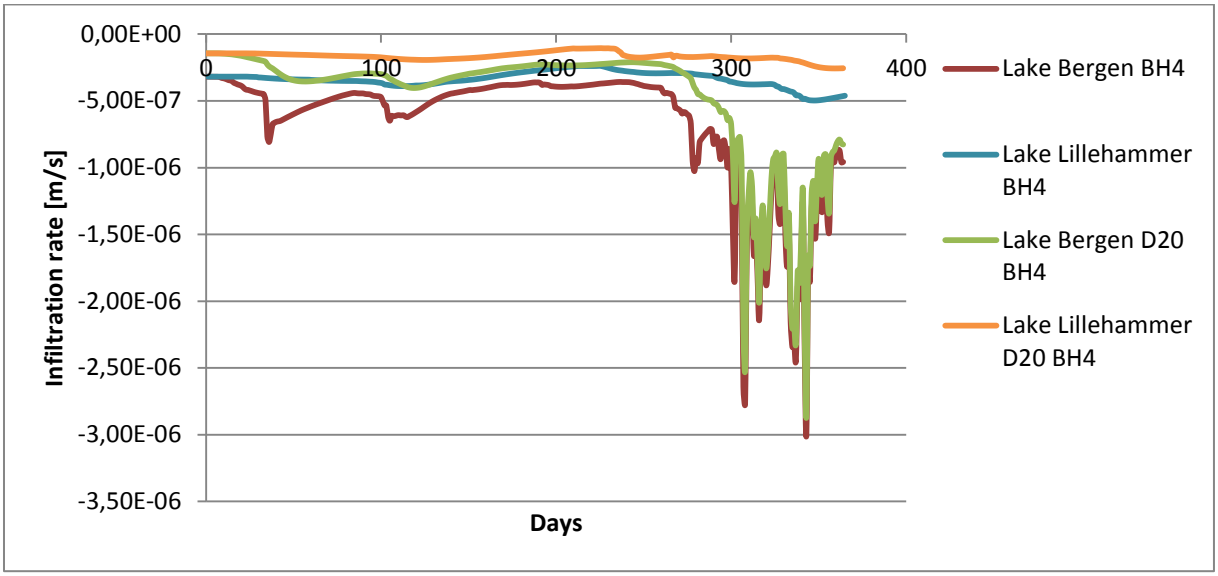

Figure 61 – Climatic effects on the lake scenario with Bergen and Lillehammer climatic conditions over the soil-rock interface. Cases with and without tunnels (20m depth). Rock mass material is the same (BH4).

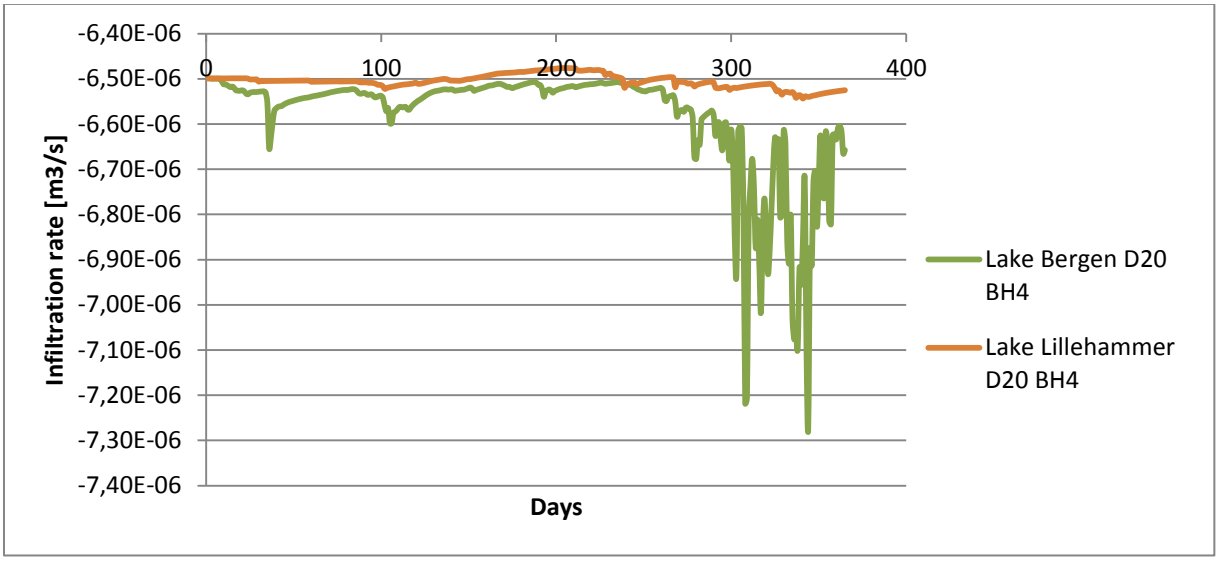

Figure 62 - Climatic effects on the lake scenario with Bergen and Lillehammer climatic conditions over the tunnel interface. Cases with tunnels of 20m depth. Rock mass material is the same (BH4).

Table 14 – Cumulative infiltration [m^3] values of cases Lake Bergen D20 BH4 and Lake Lillehammer D20 BH4 over the tunnel interface after 1 year.

	Lake Bergen D20 BH4	Lake Lillehammer D20 BH4
Cumulative water flux 1 year	207,63 m^3	205,14m^3

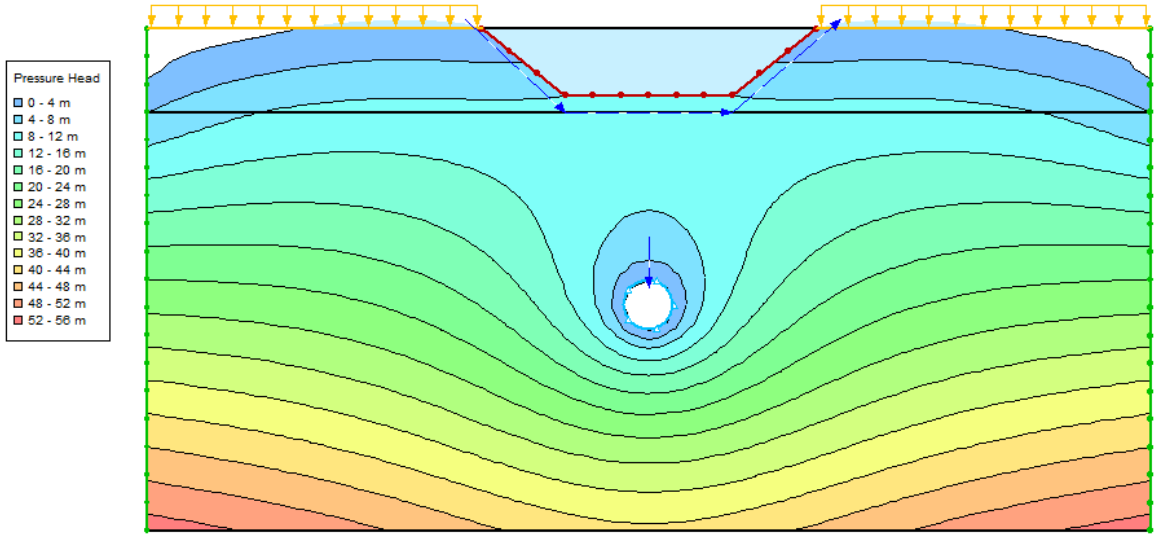

Figure 63- Case Lake Bergen D20 BH4. Groundwater level is shown as a result of tunnel construction and climatic effects of the Bergen location.

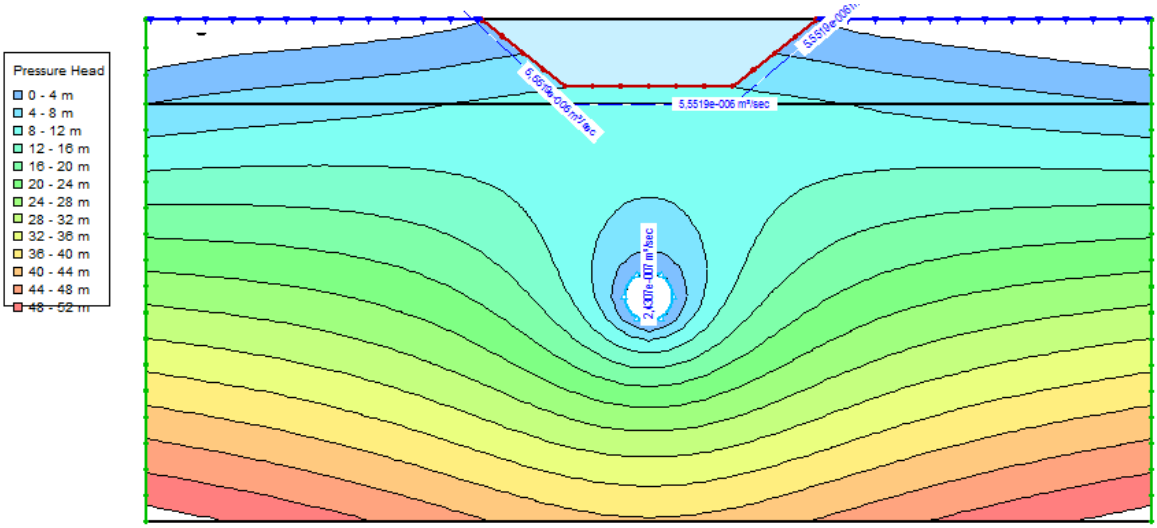

Figure 64 – Case Lillehammer D20 BH4. Groundwater level is shown as a result of tunnel construction and climatic effects of the Lillehammer location.

6.3.2.2 Analysis

In the results chapter results from two of the same cases with differing climatic conditions are presented. From Figure 62 it seems obvious that the infiltration over a tunnel interface is climatic dependent. The figure shows a link with the Bergen climatic location being more prone to infiltrating over the tunnel interface than the Lillehammer climatic location, especially at high rainfall or snow melting events. If looking at Table 1 however, the quantitative difference is rather small at 2,49m^3 over the course of 1 year. Knowing the quantitative infiltration difference it much be emphasized that the differences in the infiltration rate in Figure 62 are small and it can be said that climatic variations does not have any major influences on the infiltration in to a tunnel. This however, must been looked at in the light of the tunnel lying underneath a lake which is the main infiltration source.

In Figure 63 and Figure 64 the groundwater level as an effect of the tunnel constructed and the climatic locations Bergen and Lillehammer is shown. Figure 63 shows that the groundwater table is higher in an area with wet conditions compared with the drier climate of Lillehammer in Figure 64. The higher groundwater table is obvious connected to the wetter nature of the climatic location.

6.3.3 Soil effects

This case considers a soil's thickness' effect on the water movement. At many occasions soil is found on top of a rock mass. It works as a storage medium or a transition zone depending on the groundwater level. The soil used in these results is partially saturated above the initial groundwater table.

6.3.3.1 Results

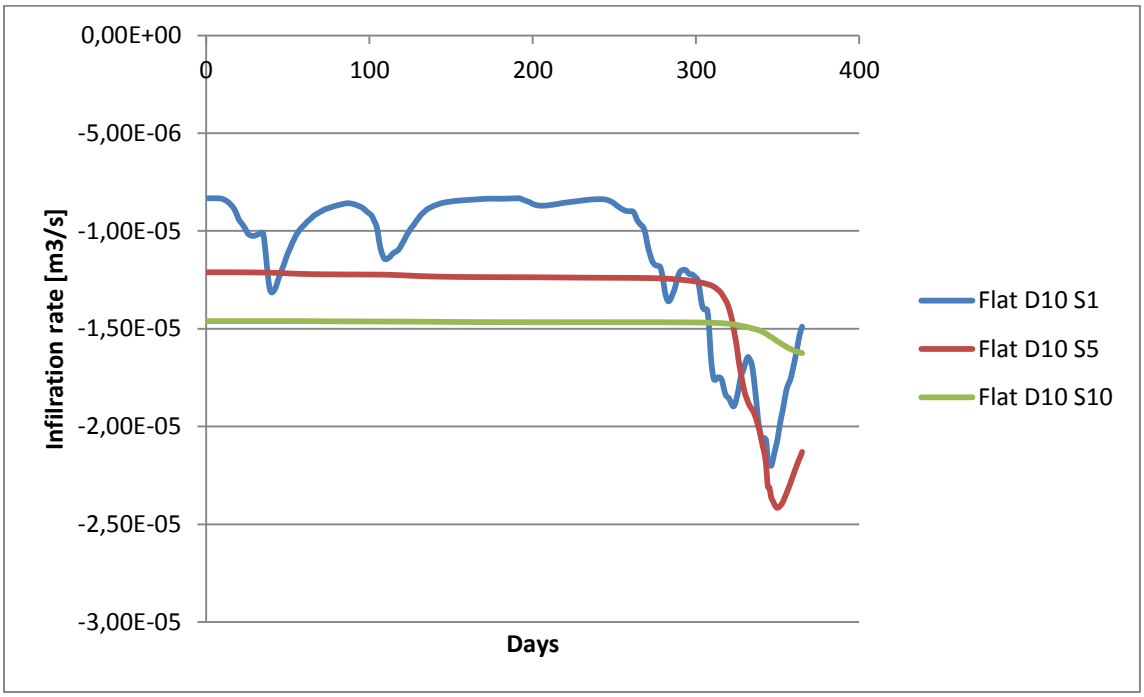

Figure 65 - Daily infiltration[m^3/s] versus time[days] of flat area cases over a tunnel interface at depth 10m and soil thicknesses 1m, 5m and 10m.

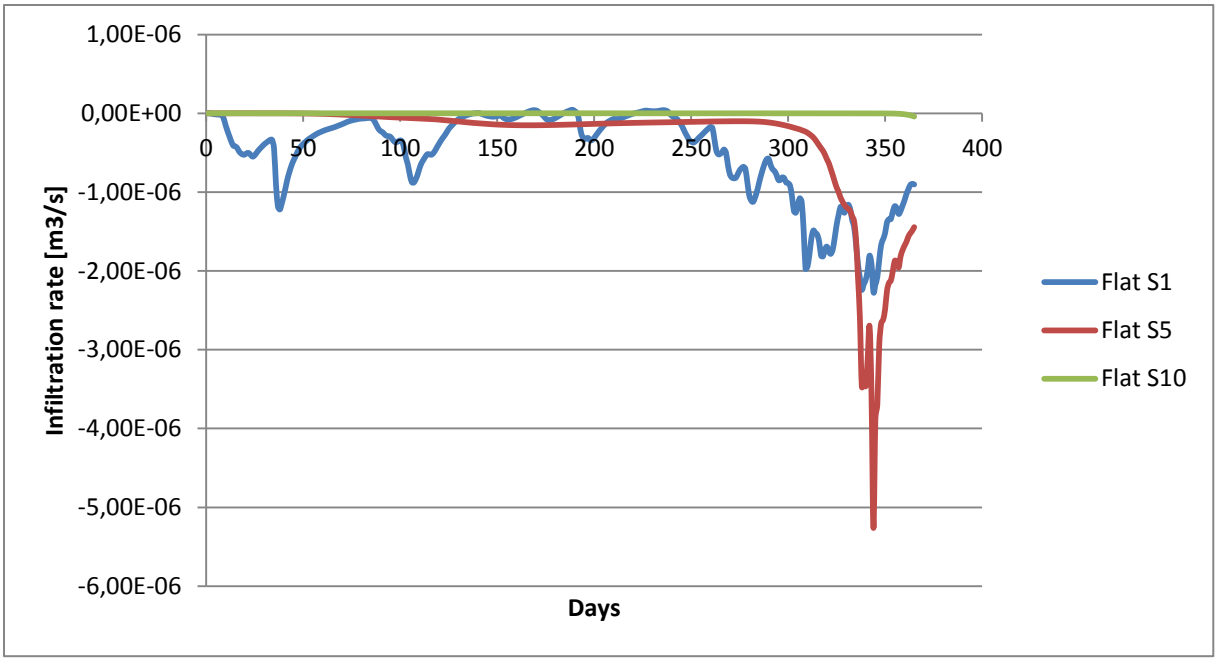

Figure 66 - Daily infiltration[m^3/s] versus time[days] of flat area cases on soil-rock interface without tunnel, soil thicknesses 1m, 5m and 10m.

Table 15 – Cumulative infiltration amounts over the tunnel interfaces

	Flat D10 S1	**Flat D10 S5**	**Flat D10 S10**
Cumulative infiltration [m^3]	346,2 [m^3]	421,5 [m^3]	464,75 [m^3]

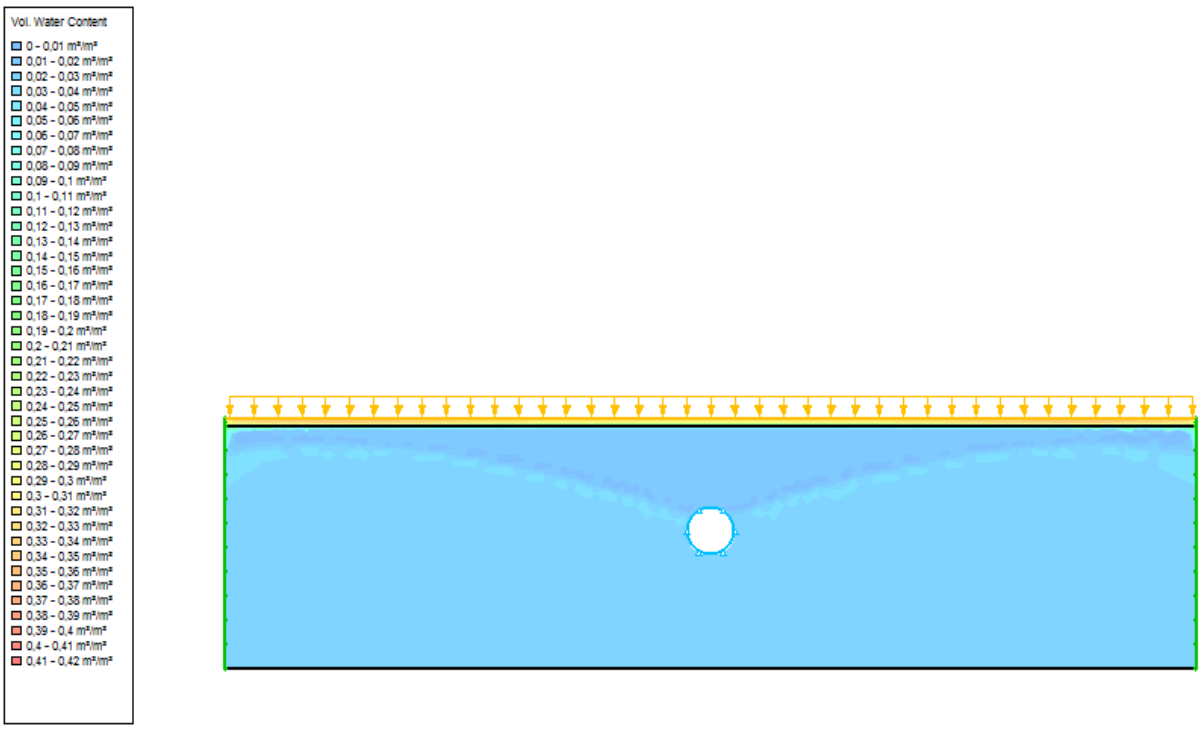

Figure 67 – Case Flat D10 S1. Volumetric Water content 1 year after tunnel construction of a 10m deep tunnel with 1m soil thickness.

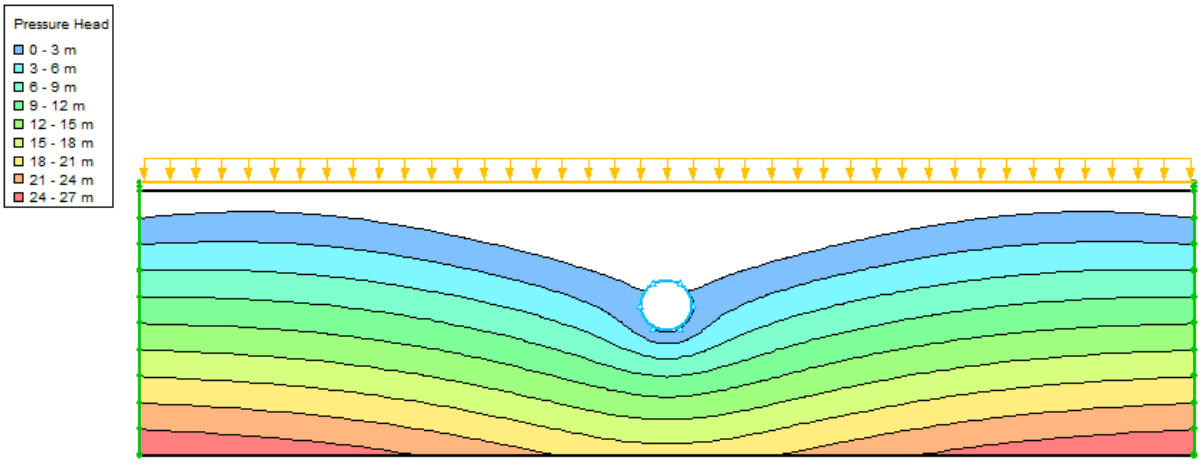

Figure 68 – Case Flat D10 S1. Groundwater table shown as pressure head 1 year after tunnel construction

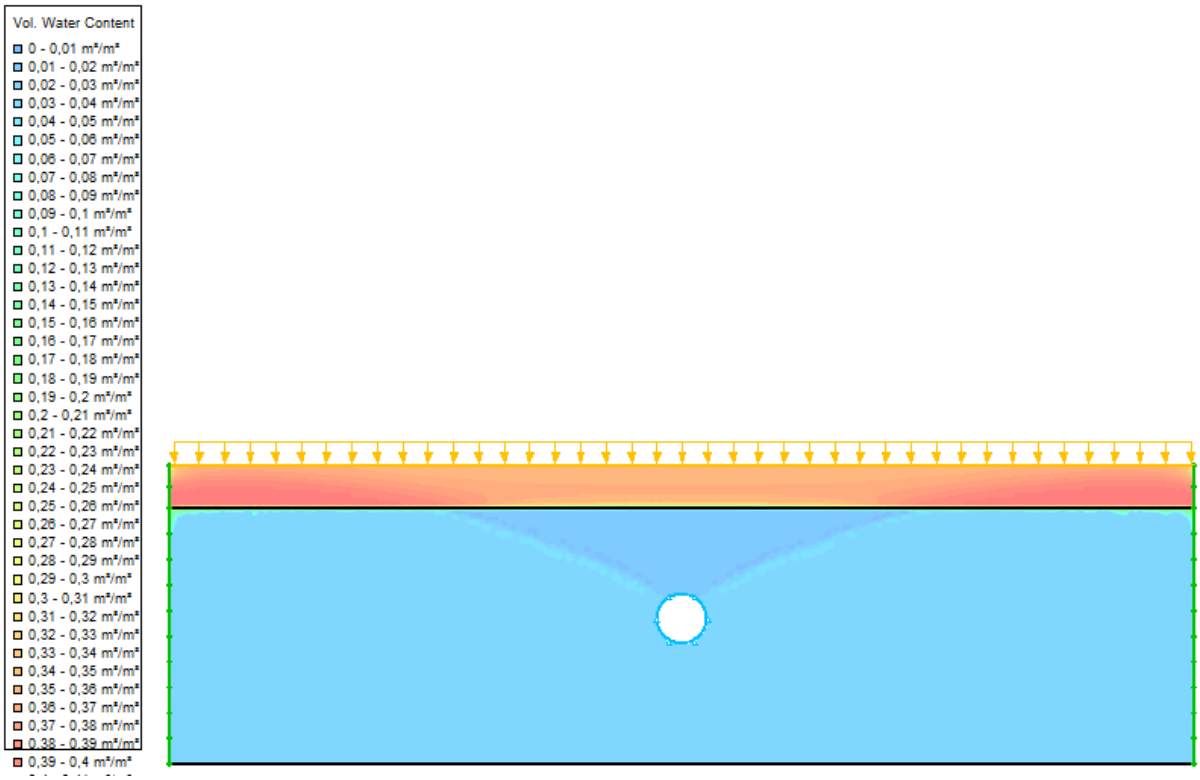

Figure 69– Case Flat D10 S5. Volumetric Water content 1 year after tunnel construction of a 10m deep tunnel with 5m soil thickness.

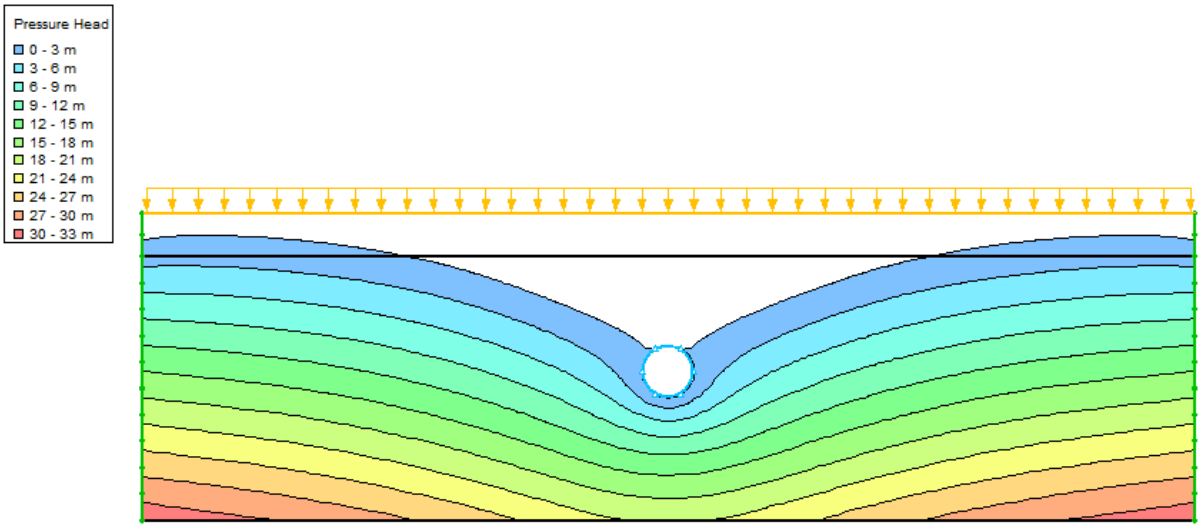

Figure 70– Case Flat D10 S5. Groundwater table shown as pressure head 1 year after tunnel construction.

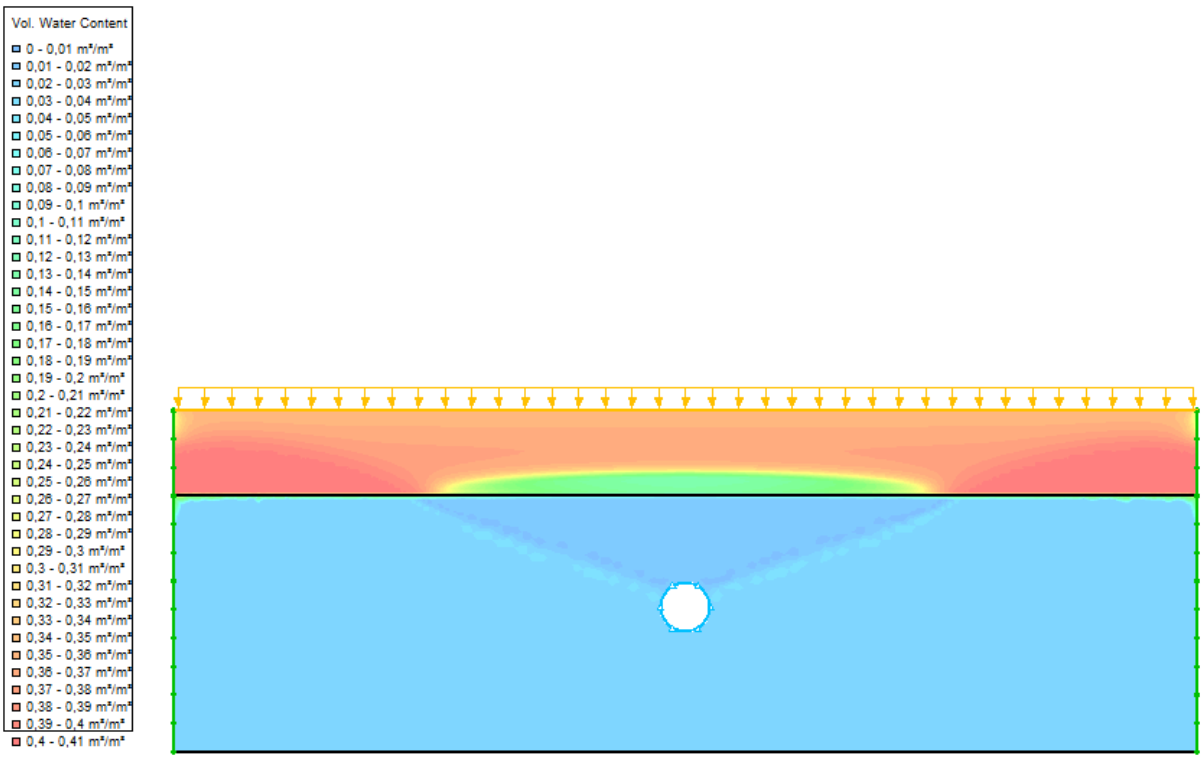

Figure 71 – Case Flat D10 S10. Volumetric Water content 1 year after tunnel construction of a 10m deep tunnel with 10m soil thickness.

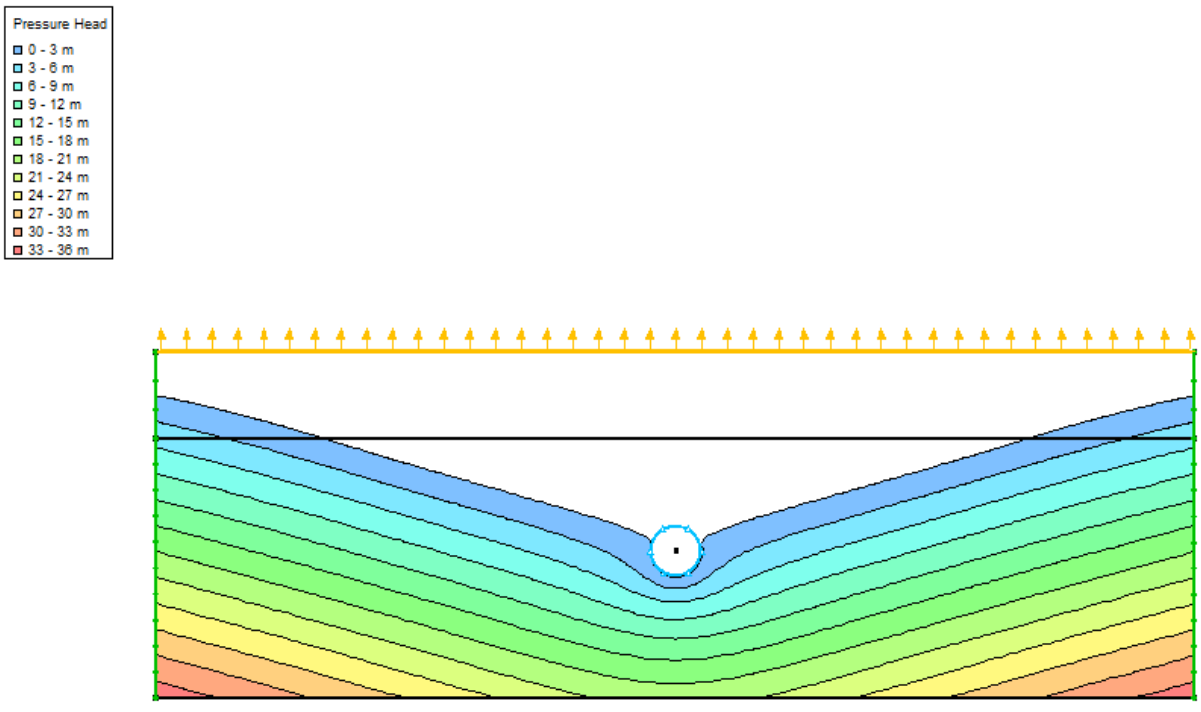

Figure 72 – Case Flat D10 S10. Groundwater table shown as pressure head 1 year after tunnel construction.

6.3.3.2 Analysis

The figures in the previous chapter are taken from a case with the same climatic conditions and a 10m deep tunnel. The soil thicknesses vary between 1m, 5m and 10m. By comparing Figure 68, Figure 70 and Figure 72 which show the groundwater table after tunnel construction it is apparent that the case with a 10m thick soil has the largest groundwater drawdown in the rock mass. This is also supported from the cumulative infiltration values over the tunnel interfaces in Table 15. In the same table the soil thickness of 5m is shown to be given a larger infiltration amount than the thinner soil of 1m.

This is also partially supported by Figure 71 where a low volumetric water content in the soil above the tunnel is present. This stems from draining of the soil above the constructed tunnel. This effect can also possibly cause settlement problems on the surface when the natural water level is lowered and the pore pressure is reduced by the reduction of water content.

Figure 66 shows the daily infiltration rate over the soil-rock interface of a flat case without a tunnel for different soil thicknesses. All of the cases had the same groundwater table which was situated in the rock mass 3m below the soil-rock interface. It seem like the thickness of the soil cover is controlling the infiltration rate over the soil-rock interface. As the case with 10m soil cover did not show any signs of infiltration a model for a 2 year period was made and it showed that there was a large infiltration after 1 year had passed. This tendency can also be seen in the figure in the case of 5m soil cover. It is thought that this delay is caused from the need of the water to infiltrate through the unsaturated soil. Therefore the variations of the graphs is being controlled by the time it takes before the water reaches the soil-rock interface which would happen faster in a thin than a thick soil.

Figure 65 show that a thick soil will infiltrate at a higher rate than a thin soil over the tunnel interface. Here the groundwater table is higher in the S10 and S5 cases and it is thought to be because of the larger amount of water available in the thicker soil that the infiltration rates are higher.

6.3.4 Rock mass effects

The rock mass is the medium the water moves through and because of this the physical properties of the rock mass are considered the single most important parameter regarding water flow. The effects of rock masses are presented in the following.

6.3.4.1 Results

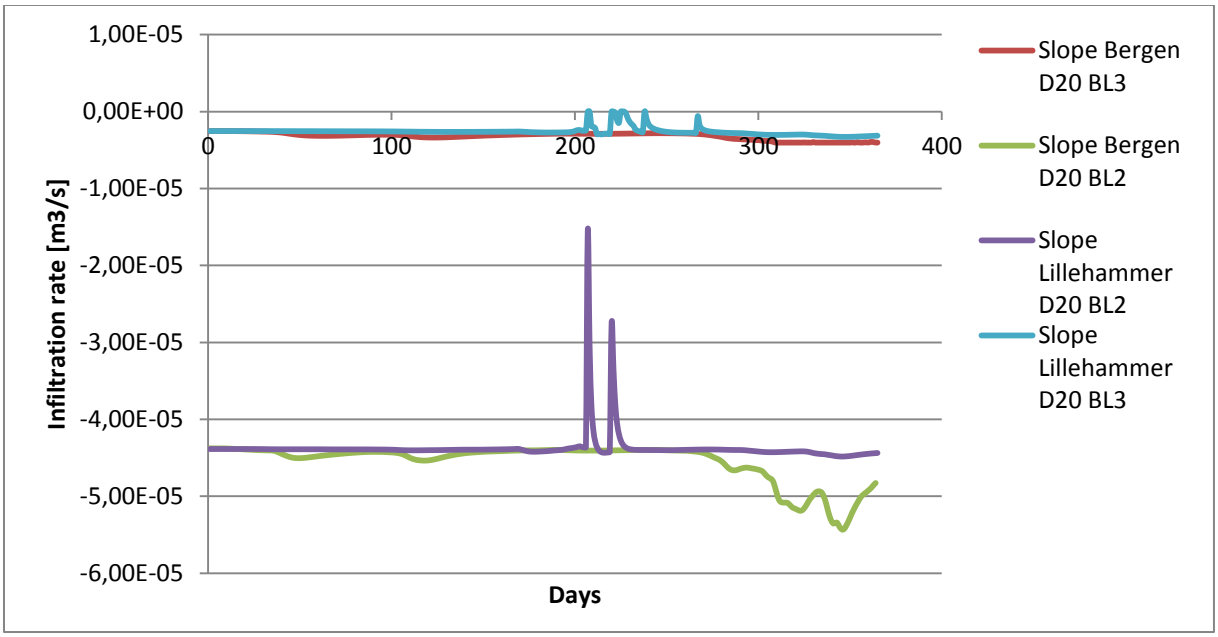

Figure 73 – Figure show daily infiltration over a tunnel interface at 20m depth in a slope case. Cases are with two different rock types, BL2 and BL3, with Lillehammer and Bergen climatic conditions.

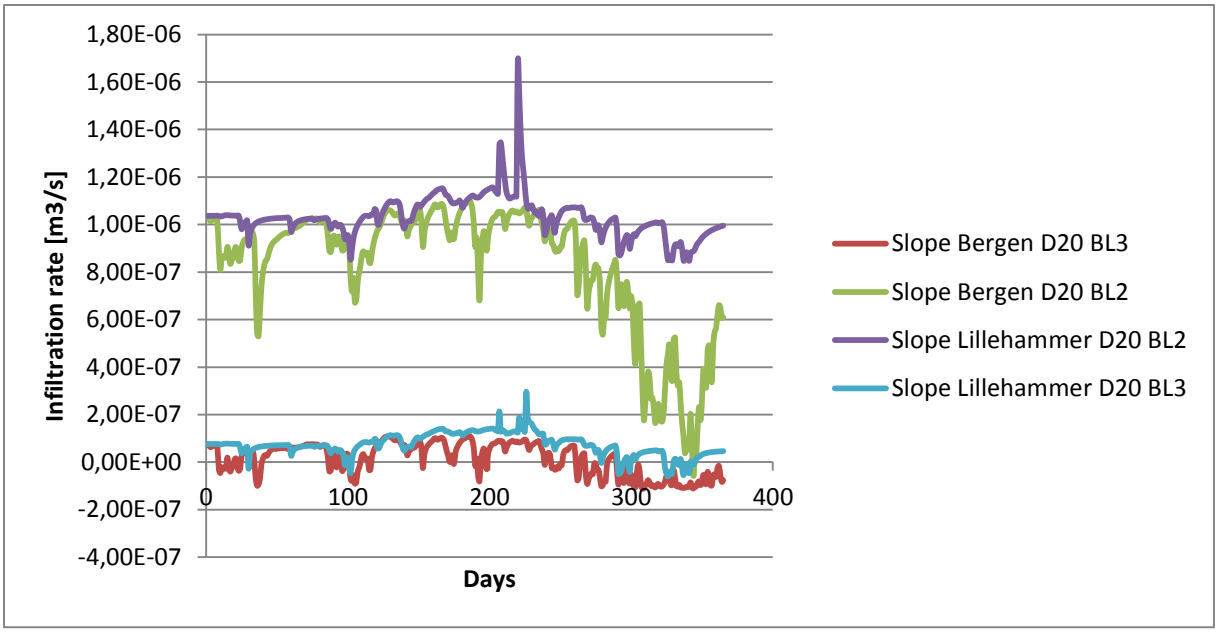

Figure 74 - Figure show daily infiltration over the soil-rock interface at 20m depth in a slope case. Cases are with two different rock types, BL2 and BL3, with Lillehammer and Bergen climatic conditions.

Table 16 – Cumulative infiltration 1 year after construction of tunnel over the tunnel interface.

	Slope Lillehammer D20 BL2	**Slope Bergen D20 BL2**	**Slope Lillehammer D20 BL3**	**Slope Bergen D20 BL2**
Cumulative infiltration	1380,5 [m^3]	1436,0 [m^3]	81,62 [m^3]	100,0 [m^3]

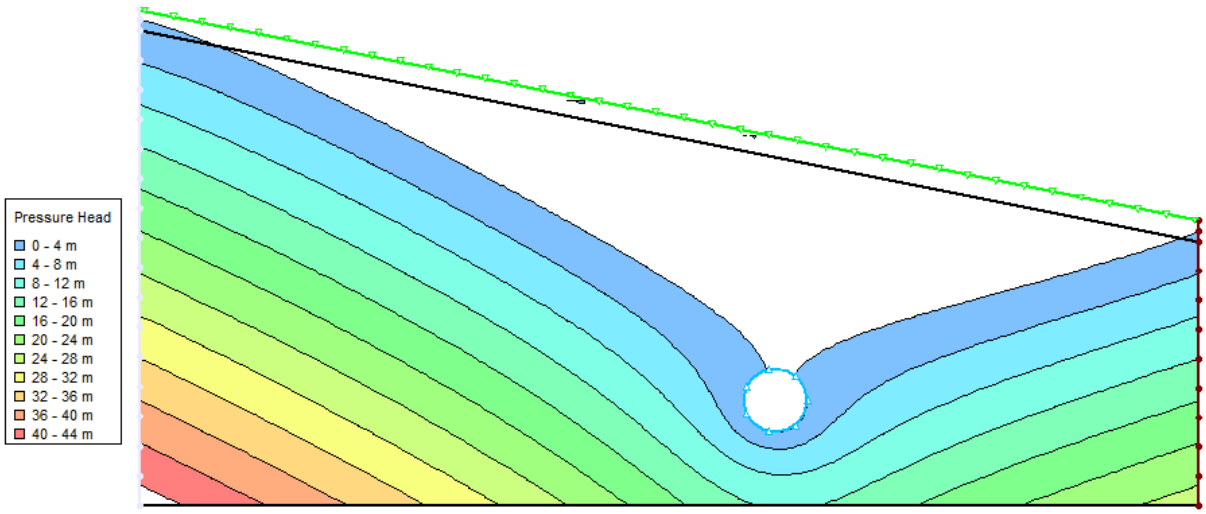

Figure 75 – case Lillehammer D20 BL2. Groundwater from pore pressure 1 year after tunnel construction.

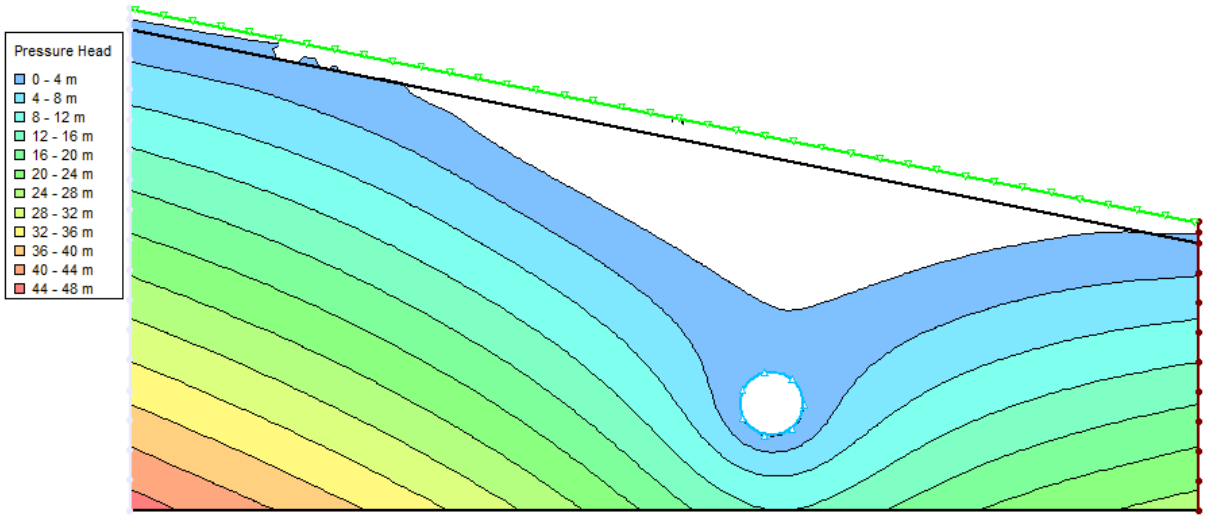

Figure 76 Case Lillehammer D20 BL3. Groundwater from pore pressure 1 year after tunnel contruction.

6.3.4.2 Analysis

In the previous results chapter the two rock masses BL2 and BL3 from the Bekkelaget location are compared in a slope case with 20m deep tunnel and 2m soil cover.

The estimated hydraulic conductivity from the slug tests for the two cases is

- BL2: HK = $1{,}5e^{-6}$ [m/s]
- BL3: HK = $8{,}5e^{-8}$ [m/s]

The difference between them is large and the effect of this is shown by Table 16 and Figure 73. The former show the large difference in total infiltrated water amount in the tunnels 1 year

after construction and the latter the major differences of daily infiltration flux over the tunnel interface. Interestingly though Figure 75 and Figure 76 show a difference in the groundwater level which is rather large but not as large as it could be expected from the magnitude differences of the rates and amounts of the hydraulic conductivity.

Studying Figure 73 it is also interesting to see that the climatic conditions do not nearly affect the infiltration rate as much as the rock mass conductivity properties do.

6.3.5 Slope effects

Slopes are encountered in many cases where tunnel construction is carried out. Because of this and the fact that water moves along a slope the effect of this is interesting to evaluate.

6.3.5.1 Results

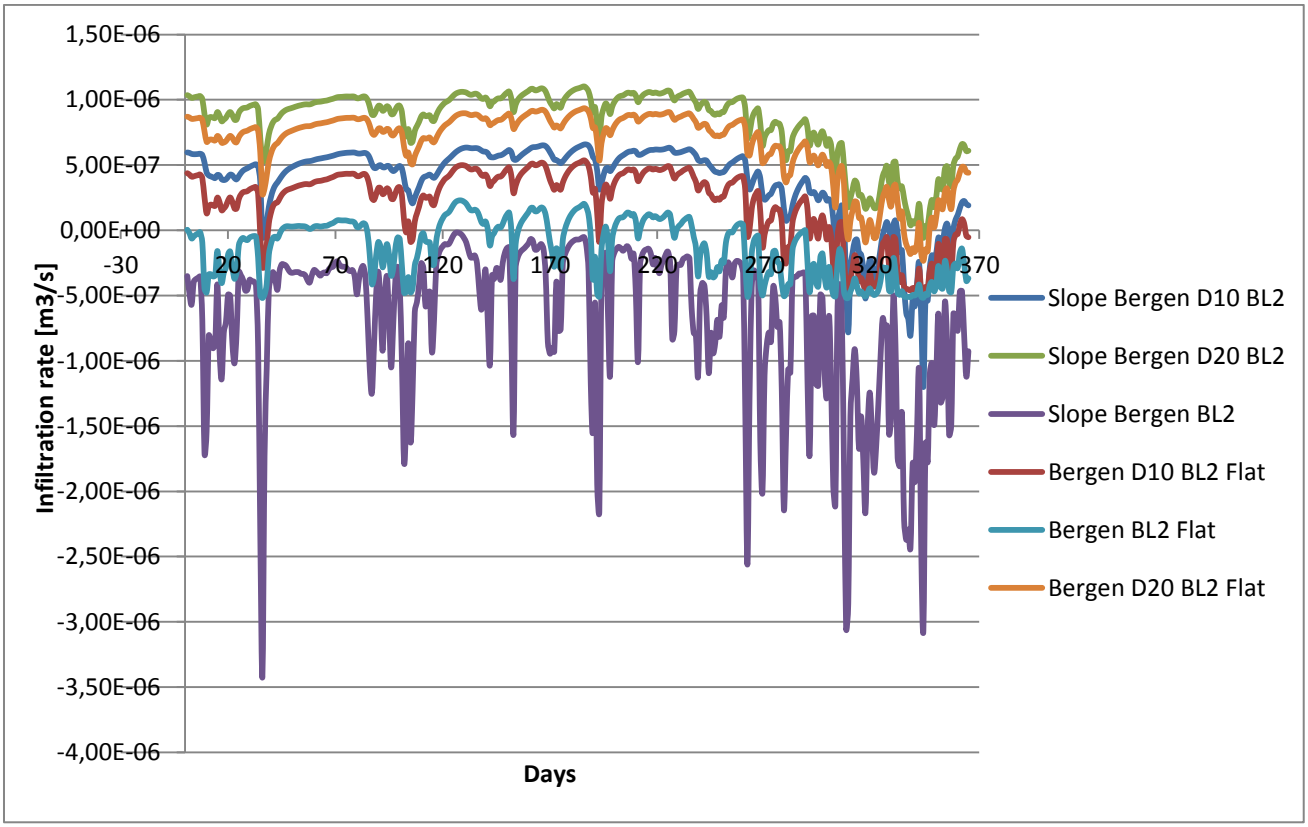

Figure 77 – Cases Slope Bergen D10 BL2, Slope Bergen D20 BL2 and Slope Bergen BL2 compared with the corresponding properties in a flat case. The graph show effect of tunnel on infiltration [m^3/s] over soil-rock interface for a tunnel compared with no tunnel.

Table 17 – Cumulative infiltration over soil-rock interface for slope and flat cases with same input parameters.

Cumulative infiltration [m^3]	Slope case	Flat case
Bergen BL2	-21,6 [m^3]	-4,25 [m^3]
Bergen D10 BL2	6,64 [m^3]	11,74 [m^3]
Bergen D20 BL2	20,77 [m^3]	26,17 [m^3]

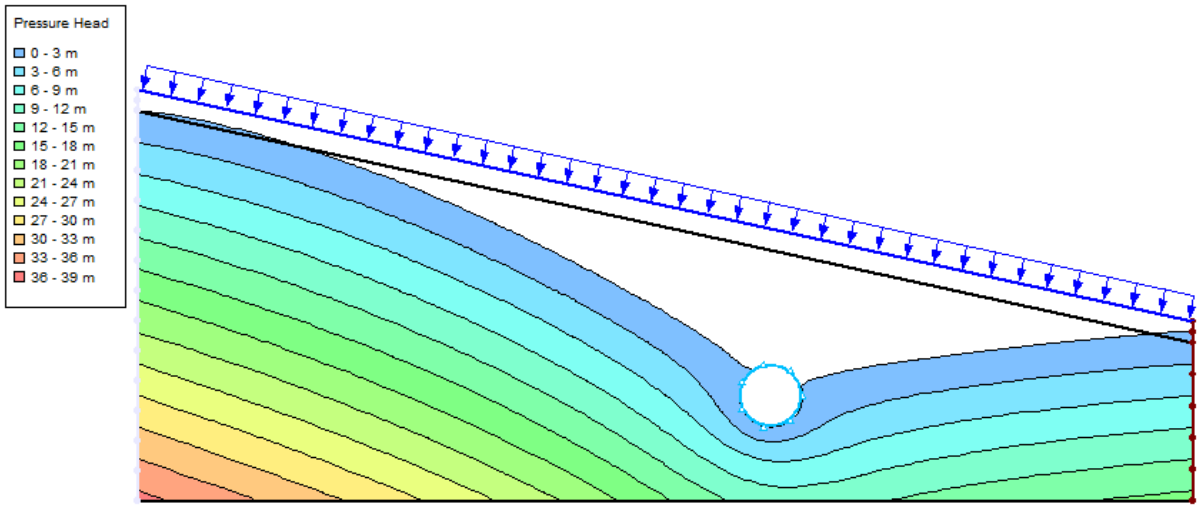

Figure 78 - Case Slope Bergen D10 BL2. Groundwater table from pressure head.

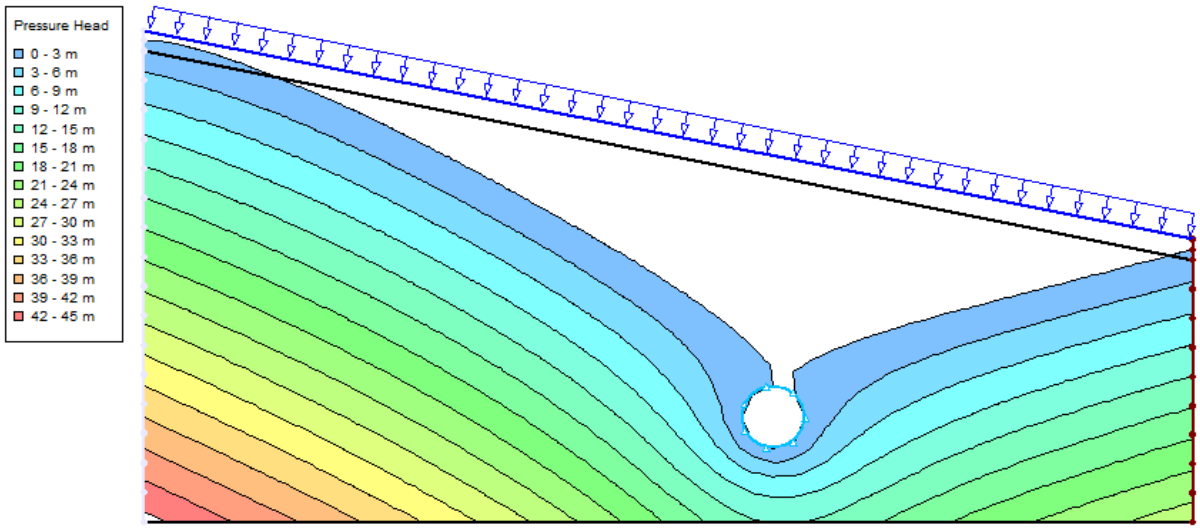

Figure 79 – Case Slope Bergen D20 BL2. Groundwater table from pressure head.

6.3.5.2 Analysis

In Figure 79 and Figure 78 the groundwater table of two slope cases from the same climatic conditions with different tunnel depths are shown. The drawdown in the deeper tunnel location is larger than the more shallow location. Seeing that there is a drawdown of the groundwater table in the light of Figure 77 which show daily infiltration over the soil-rock interface it is apparent that there will be water transport over this boundary in the event of a tunnel construction.

Figure 77 also shows the differences between a slope and flat case with the same tunnel, climatic and rock mass properties. The tendency is that there is a larger infiltration over the boundary in the event of a slope than a flat case. The reasons for this might be that there is lateral groundwater flow in a slope case which makes more water able to infiltrate than in a flat case. Also see Table 17 for total cumulative values over the soil-rock interface for the different cases. The flat case has a larger infiltration value here hence supporting the theory of lateral water movement. The negative values in the cases without a tunnel are water movement from the rock to the soil probably caused by evaporation.

6.3.6 Lake effects

Constructing underground excavations beneath lakes and ponds is a serious threat to water levels and can in a worst case scenario result in a complete drainage of a lake as exemplified by the Romeriksporten tunnel in southern Norway (Kitterød 2000).

6.3.6.1 Results

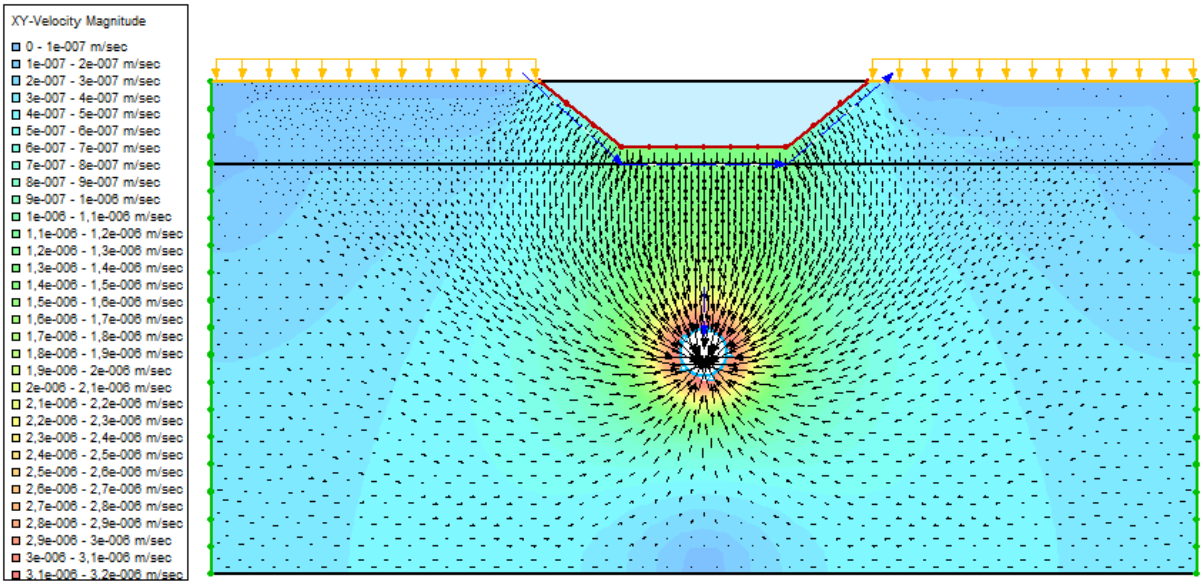

Figure 80 –Case Lake Lillehammer D20 BH3. XY velocity magnitude of lake case with a tunnel depth of 20m and rock material BH3.

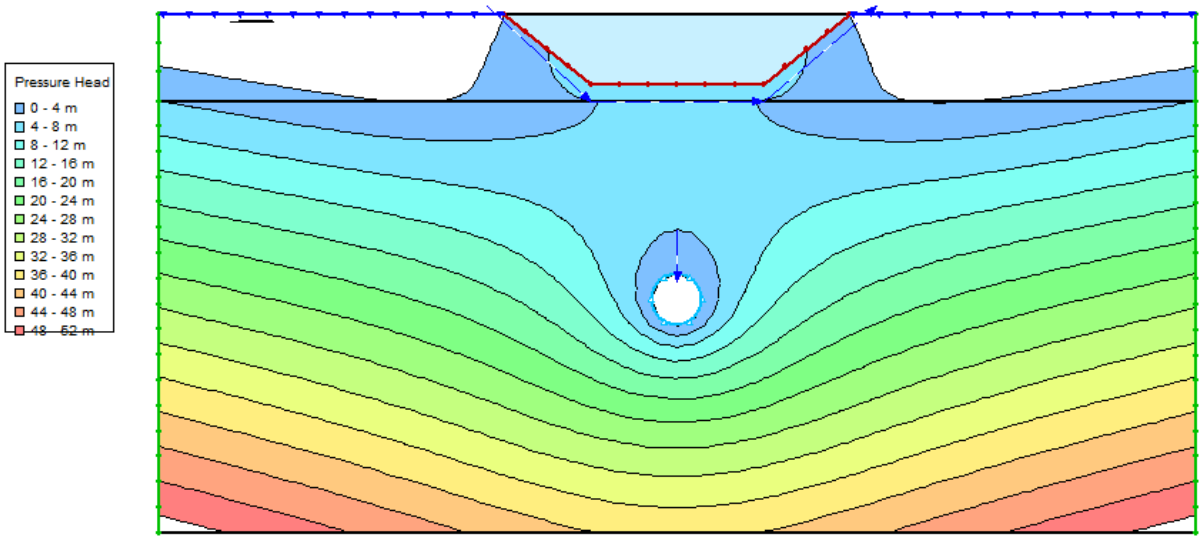

Figure 81 – Lake Lillehammer D20 BH3. Groundwater table of lake case with material BH3.

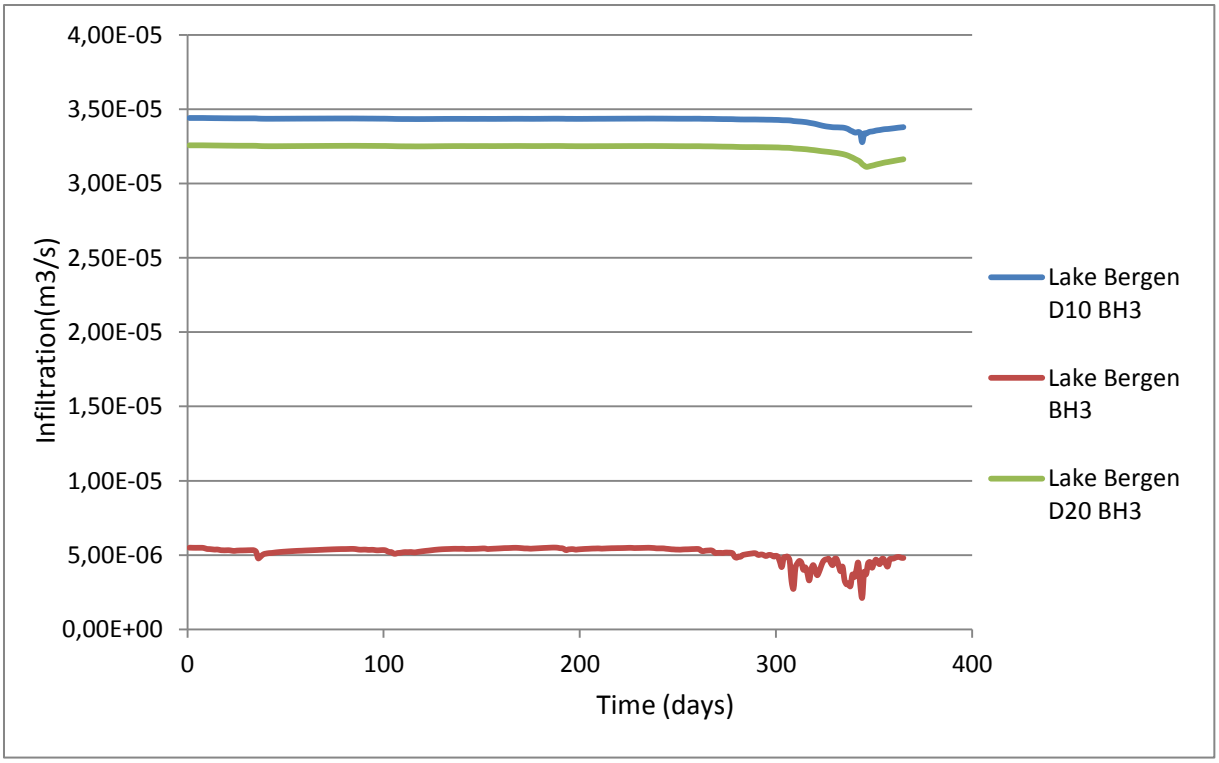

Figure 82 - Cases Lake Bergen D10 BH3 and Lake Bergen BH3. Cases with and without tunnel, infiltration rate over lake-soil interface.

Table 18 – Cumulative infiltration amounts over the tunnel interface of tunnel depth 20m with different climatic and rock mass properties

	Lake Bergen D20 BH3	**Lake Bergen D20 BH4**	**Lake Lillehammer D20 BH3**	**Lake Lillehammer D20 BH4**
Cumulative tunnel interface infiltration [m^3]	2678,46 [m^3]	207,63 [m^3]	2669,67 [m^3]	205,14 [m^3]

6.3.6.2 Analysis

The lake case was done to see what properties are the most significant with respect to water control in a tunnel beneath a lake.

The rock masses from wells BH3 and BH4 that are presented in the results have hydraulic conductivities of

- BH3: HK = $1{,}5e^{-6}$ [m/s]
- BH4: HK = $9{,}8e^{-8}$ [m/s]

If comparing Figure 81 with Figure 64 the groundwater level for the two equal cases from Lillehammer infiltration functions at 20m depth, with different rock masses can be seen. It is obvious that the groundwater level is different. Knowing that the material BH4 has a significantly lower hydraulic conductivity than BH3 the higher groundwater level seems appropriate with water infiltrating at a slower pace. This is supported by the values in Table 18 where cumulative infiltration values over the tunnel interface for a tunnel at 20m depth, rock masses BH3 and BH4, and climatic functions Lillehammer and Bergen can be seen.

Interestingly the values of the cases which are equal except for the climatic functions differ little from each other. E.g. the difference between the Lillehammer and Bergen climatic functions in the rock mass BH4 is $2{,}49m^3$. This is a good indication to the climatic functions not being the main contributor to water infiltration in a tunnel beneath a lake.

Figure 82 show the infiltration rate at the lake-soil boundary for the same rock mass and climatic function albeit with and without tunnels. An infiltration rate of approximately magnitude 5 larger is encountered in the case with a tunnel at 10m and 20m depth compared without a tunnel. When comparing the tunnel location at 10m and 20m depth the daily infiltration flux from the lake to the soil is not significantly smaller in the deeper tunnel although there are clearly some differences. Also note that the curves do not seem affected by climatic conditions which correspond well with the cumulative infiltration amounts from Table 18.

6.3.7 General trends

The six case scenarios evaluated have come across a variety of properties which affect water flow in rocks, soils and between the two mediums. The climatic effects on infiltration have some effect but when in combination of a larger water resource such as a lake the infiltration from the lake dominates the infiltration to a large degree.

Generally a thicker soil will create a larger cumulative infiltrated water amount in a tunnel than a thinner soil cover. Based on the data in this project it is difficult to tell if it is because of the soil's properties but it is thought to be because of a larger storage volume for groundwater above a tunnel which makes for a higher volume of water available for infiltration. This is based on the assumption that a tunnel is built at the same depth within the rock mass.

The rock masses do to a large degree affect the infiltration properties over both the soil-rock and tunnel interface as exemplified in Figure 73 and Figure 74. The reason for this is thought to be the difference in the hydraulic conductivity magnitude in a low conductivity rock mass and a soil. E.g. the saturated hydraulic conductivity of the silt used in these models is $5e^{-7}$ whereas the low conductivity rock BL3 mass in the figures is $8{,}5e^{-8}$. In some of the cases presented though, rock masses had higher conductivities than the soil used. In these cases the opposite result will probably be the case with the soil transporting the water slower than the rock. It is generally thought that the higher the hydraulic conductivity of the rock mass is the more prone an underground excavation is to climatic effects affecting the infiltration in to the excavation.

The special landscape cases gave to a large degree expected results with the lake case showing a high infiltration, especially in high conductivity rock masses. The slope case proved that lateral groundwater movement within the rock mass must not be neglected when working in an angled terrain.

7 Conclusion

The results of the simulations of the slug tests are considered good thus proving that the numerical code utilized can simulate water transport to a rock mass in a satisfactory fashion.

The simulation of the laboratory tests did not prove to turn out in a satisfactory fashion albeit the results do have resemblances of the patterns measured in the laboratory tests. Given that the patterns were recreated and that similar tests of the same objective (Pabst 2011) have obtained good results it is considered probable that infiltration between layers can be done thus supporting the results of the large scale models.

Finally, the large scale models give a general trend of expected outcomes for the various scenarios simulated. This in its turn support that the infiltration over layers of different material properties. The somewhat imperfect results from the laboratory tests should be seen in the light of this and it is thought that further work with these data could give satisfactory results.

8 Further work

It is suggested that further work which could improve the findings in this thesis is:

- Improve the laboratory test by; calibrate volumetric water content sensors, avoid heterogeneities in material, not include fine grained material around sensors
- Find interesting relevant cases to build large scale models and evaluate these based on the case results. E.g. (Vegvesen 2003, Vegvesen 2003), (Davik&Andersson 2001) & (Norwegian Geotechnical Institute 2001) can be used.

Reference list

ASTM (2008) “Standard Test Method for (Field Procedure) for Instanteous change in head (Slug) Test for Determining Hydraulic Properties of Aquifers.”

Aubertin, M., Bussière, B., Aachib, M., Chapuis, R.P, & Crespo, J.R. (1996). “Une modélisation numérique des écoulements non saturés dans des couvertures multicouches en sols.” Hydrogéologie, 1, 3-13.

Brattli, B. (2011). "Fysisk og Kjemisk Hydrogeologi." (3rd Issue).

Brooks&Corey (1964). "Hydraulic properties of porous media." Hydrology papers **3**.

Butler, J. J. (1998). "The Design, Performance, and Analysis of Slug Tests."

Bliss&Rushton (1984) “The reliability of packer tests for estimating the hydraulic conducivity of aquifers” Quarterly journal of Engineering Geology and Hydrogeology 1984 v.17, p81-91.

Campbell, G. S. (1974). "A simple method for determnining unsaturaded conductivity from moisture retention data." Soil Science **117**: 311-314.

Chapuis, R.P., Crespo, J.R., Chenaf, D. et Aubertin, M. (1993). "Evaluation of a groundwater F.E.M. software for steady and unsteady state conditions." In Proceedings of the 46th Canadian Geotechnical Conference, Saskatoon, SK, 61-70.

Chapuis, R.P., Chenaf, D., Bussière, B., Aubertin, M., & Crespo, R.J. (2001). "A user’s approach to assess numerical codes for saturated and unsaturated seepage conditions." Canadian Geotechnical Journal, 38(5), 1113-1126.

Davik&Andersson (2001), "Urban Road Tunnels, a Subsurface Solution to a Surface Problem".

Dellur, J. W. (1999). "The Handbook of Groundwater Engineering."

Domenico&Schwartz (1990). "Physical and Chemical Hydrogeology."

Genuchten, M. T. V. (1980). "A closed-form equation for predicting the dyraulic conducivity of unsaturated soils." Soil Science Society Am. **44**: 892-898.

Green&Ampt (1911). "Studies of Soil Physics." The Journal of Agricultural Science **4**(1): 1-24.

Gupta&Singhal (2010). "Hydrogeology of Fractured Rock."

Hillel, D. (1998). "Environmental Soil Physics."

Horton, R. E. (1933). "The role of infiltration in the hydrologic cycle." Transactions, Americal Geophysical union **14**: 446-460.

Horton, R. E. (1940). "An approach towards a physical interpretation of filtration capacity." Soil Science Society of America.
Lohman, S. W. (1972). "Ground-water Hydraulics." U.S. Geological Survey Prof.paper 708.
Mavis&Tsui (1939). "Percolation and Capillary Movements of Water Trough Sand Prisms."
Neumann, E.-R. (1991). "The Oslo Rift: a review." Tectonophysics **208**.
NGU (2013). "Norwegian Geological Survey (NGU) geological map from www.ngu.no."
Nilsen&Broch (2009). "Ingeniørgeologi-berg Grunnkurskompendium."
Norwegian Geotechnical Institute (2001). "Prediction of leakage into Lunner tunnel based on discrete fracture flow model. "
Pabst, T., Molson, J., Aubertin, M., and Bussière, B. (2011). "Column tests to assess water flow and oxygen transport in a monolayer cover placed on acid generating tailings." Proc. 2011 Mine Closure Conference, Lake Louise, AB, September 18-21, 2011.
Scesi&Gattioni (2009). "Water Circulation in Rocks."
Scanlon, B.R., Christman, M., Reedy, R.C., Poro, I., Simunek, J., & Flerchinger, G.N. (2002). "Intercode comparisons for simulating water balance of surficial sediments in semi arid regions." Water Resources Research, 38, 1323-1339.
Shuniark, R.E. (2003). "Predictive modeling of moisture movement with soil cover systems for saline/sodic overburden piles." Master Thesis, University of Saskatchewan, Saskatoon, SK.
Swanson, D.A., Barbour, S.L., Wilson, G.W., & O'Kane, M. (2003). "Soil-atmosphere modelling of an engineered soil cover for acid generating mine waste in a humid, alpine climate." Can. Geotech. J., 40, 276-292.
Todd&Mays (2005). "Groundwater Hydrology."
Vegvesen, S. (2011). "Håndbok 018 Vegbygging."
Vegvesen, S (2003a). "Miljø og samfunnstjenelige tunneler. Vanninfiltrasjon - erfaringer og anbefalinger."
Vegvesen, S (2003b). "Undersøkelser og krav for å ivareta ytre miljø. "
Weeks, B., & Wilson, G.W. (2005). "Variations in moisture content for a soil cover over a 10 year period." Can. Geotech. J., 42, 1615-1630.
Yanful, E.K., Mousavi, S.M., & De Souza, L.P. (2006). "A numerical study of soil cover performance." Journal of Environmental Management, 81, 72-92.

Apendix A: Test results laboratory test 1

Weight and densities before test 1								**Diameter**		**7**	Reference height		41,24						
Schist #	**bowl weight [g]**	**Total weight before drying [g]**	**Total weight after drying [g]**	**Difference [g]**	**Weight of schist**	**Moisture content w**	**%**	**Height from top [cm]**	**Height of material**	**Height of schist [cm]**	**Volume of schist [cm^3]**	**Volume of solids**	**Water content[cm^3]**	**Tetha**	**Porosity [%]**	**Degree of saturation**	**Sensor depth [cm]**	**Material**	**Comment**
1	2,14	70,54	68,2	2,34	1364,3	0,0343	3,43	36,42	4,82	4,8	742,0	488,5	25,5	0,034	34,2	10,04		Fine	
2	2,16	74,45	71,86	2,59	1135,32	0,0360	3,60	32,28	8,96	4,1	637,3	405,9	23,0	0,036	36,3	9,92	32	Fine	

3	2,14	71,12	68,67	2,45	1440,42	0,0357	3,57	27,48	13,76	4,8	738,9	515,1	26,4	0,036	30,3	11,78	27,7	Fine	
4	2,12	71,96	69,9	2,06	885	0,0295	2,95	24,14	17,10	3,3	514,2	318,4	15,2	0,029	38,1	7,74	23	Coarse	
5	2,12	83,24	80,9	2,34	1640,14	0,0289	2,89	18,34	22,90	5,8	892,8	590,4	25,8	0,029	33,9	8,54	17,3	Coarse	
6	2,14	71,45	68,19	3,26	1134	0,0478	4,78	13,66	27,58	4,7	720,4	400,8	34,4	0,048	44,4	10,78	13,8	Coarse	
Weight and densities after test 1										**13,82**									

Schist #	bowl weight [g]	Total weight before drying [g]	Total weight after drying [g]	Difference [g]	Weight of schist	Moisture content	%	Height from top [cm]		Height of schist [cm]	Volume of schist [cm^3]	Volume of solids	Water content[cm^3]	Tetha	Porosity [%]	Degree of saturation	Sensordepth [cm]	Material	Comment
6	2,14	68,15	66,9	1,25	1134	0,0187	1,87	13,68	27,56	4,7	720,4	412,3	13,5	0,019	42,8	4,37		coarse	Surface
6	2,14	73,67	71	2,67	1134	0,0376	3,76	16,5	24,74	4,7	720,4	404,8	27,1	0,038	43,8	8,58		coarse	at sensor 4
5	2,14	69,44	67,32	2,12	1640,14	0,0315	3,15	20,2	21,04	5,8	892,8	588,9	28,1	0,031	34,0	9,25		coarse	
5	2,14	84,29	79,8	4,49	1640,14	0,0563	5,	23,8	17,44	5,8	892,8	575,1	50,2	0,056	35,6	15,81		Fine aroun	at senso

							63											d sensor	r 3
4	2,14	73,62	70,84	2,78	885	0,0392	3,92	27,4	13,84	3,3	514,2	315,4	20,2	0,039	38,7	10,15		coarse	at interface, above
3	2,14	67,07	61,28	5,79	1440,42	0,0945	9,45	27,8	13,44	4,8	738,9	487,4	69,8	0,094	34,0	27,76		fine	at interface, below
3	2,14	111,16	100,98	10,18	1135,32	0,1008	10,08	33,3	7,94	4,8	738,9	382,0	74,5	0,101	48,3	20,87		fine	at sensor 2
2	2,14	89,08	79,3	9,78	1135,32	0,1233	12,	36,1	5,14	4,1	637,3	374,3	78,6	0,123	41,3	29,89		fine	at sensor 1

							33												
1	2,14	103,23	91,28	11,95	1364,3	0,1309	13,09	39,8	1,44	4,8	742,0	446,8	97,1	0,131	39,8	32,91		fine	bottom

Table 19 - Pouring amounts test1

Pouring #	Amount [ml]	Time [min]	Equals mm
1	153,8	0	10,00
2	154,01	10	10,01
3	154,19	20	10,02
4	153,83	30	10,00
5	153,92	40	10,00
6	153,73	50	9,99
7	153,78	60	9,99
8	153,93	70	10,00

Appendix B:

Test results from laboratory test 2

								Reference height:		41,24								
Weight and densities before test 2								Diameter		14								
Schist #	**bowl weight [g]**	**Total weight before drying [g]**	**Total weight after drying [g]**	**Difference [g]**	**Veight of schist [g]**	**Moisture content [Volumetrical]**	**%**	**Height from top [cm]**		**Height of schist[cm]**	**Volume of schist [cm^3]**	**Water content [cm^3]**	**Volume solids [cm^3]**	**Moisture content**	**Porosity**	**Degree of saturation [%]**	**Sens ordepth [cm]**	**Material**	**Comment**
1	2,14	79,53	77,12	2,41	1630,55	0,0313	3,13	36,2	5,1	5,1	782,0	24,4	603,9	0,031	22,8	13,7	35	Fine	
2	2,18	65,69	63,66	2,03	1311,25	0,0319	3,19	30,9	10,3	5,3	809,7	25,8	485,6	0,032	40,0	8,0	29,6	Fine	

3	2,16	72,11	70,12	1,99	1361,78	0,0284	2,84	26,2	15,0	4,7	720,4	20,4	504,4	0,028	30,0	9,5		Fine	Interface
4	2,13	69,11	66,95	2,16	790,01	0,0323	3,23	23,9	17,4	2,4	363,3	11,7	292,6	0,032	19,5	16,6	23,6	Coarse	
5	2,14	78,62	76,01	2,61	1537,75	0,0343	3,43	18,7	22,6	5,2	800,5	27,5	569,5	0,034	28,9	11,9	18,3	Coarse	
6	2,12	78,48	76,58	1,9	1309,81	0,0248	2,48	14,1	27,1	4,5	698,9	17,3	485,1	0,025	30,6	8,1		Coarse	Bottom
Weight and densities after test 2																			

Schist #	**bowl weight [g]**	**Total weight before drying [g]**	**Total weight after drying [g]**	**Difference [g]**	**Weight of schist [g]**	**Moisture content**	**%**	**Height from top [cm]**		**Height of schist**	**Volume of schist [cm^3]**	**Water content [cm^3]**	**Volume solids [cm^3]**	**Moisture content**	**Porosity**	**Degree of saturation [%]**	**Sensor depth [cm]**	**Material**	**Comment**
6	2,18	88,62	79,7	8,92	1309,81	0,1119	11,19	36,2	5,0	4,5	698,9	78,2	485,1	0,112	30,6	36,6		Fine	Surface
6	2,16	90,89	82,83	8,06	1309,81	0,0973	9,73	31,7	9,6	4,5	698,9	68,0	485,1	0,097	30,6	31,8		Fine	at sensor 4
5	2,15	95,78	84,66	11,12	1537,75	0,1313	13,13	26,5	14,8	5,2	800,5	105,1	569,5	0,131	28,9	45,5		Fine	at sensor 3
4	2,18	93,95	83,91	10,04	790,01	0,1197	11,9	24,1	17,1	2,4	363,3	43,5	292,6	0,120	19,5	61,5		Fine	Interf

							7											ace
3	2,16	92,42	87,59	4,83	1361,78	0,0551	5,51	19,4	21,8	4,7	720,4	39,7	504,4	0,055	30,0	18,4		Coarse	Interface
3	2,19	87,16	83,27	3,89	1361,78	0,0467	4,67	14,7	26,5	4,7	720,4	33,7	504,4	0,047	30,0	15,6		Coarse	Sensor 2
2	2,19	106,28	100,05	6,23	1311,25	0,0623	6,23	9,5	31,8	5,3	809,7	50,4	485,6	0,062	40,0	15,6		Coarse	Sensor 1
1	2,24	99,7	96,49	3,21	1630,55	0,0333	3,33	4,4	36,8	5,1	782,0	26,0	603,9	0,033	22,8	14,6		Coarse	Bottom

Table 20 - Pouring amounts test2

Pouring #	Amount [ml]	Time [min]	Equals mm
1	153,88	0	10,00
2	153,96	10	10,01
3	153,86	20	10,00
4	154	30	10,01
5	153,79	40	10,00
6	153,97	50	10,01
7	154,48	60	10,04
8	153,78	70	9,99

Appendix C

Results from simulations of slug tests

Table 21 – Slug test measurements Bekkelaget

BL-1A/B			
Time [min]	**Amount [L]**	**Initial G.W [m]**	**G.W after [m]**
0	10	2,595	2,03
10	10	2,03	1,45

BL-2A/B			
Time [min]	**Amount [L]**	**Initial G.W [m]**	**G.W after [m]**
0	10	2,2	1,71
10	10	2,09	1,64

BL-3A/B			
Time [min]	**Amount [L]**	**Initial G.W [m]**	**G.W after [m]**
0	10	7,31	6,64
18	10	6,71	6,54

Table 22 – Slug test measurements Vettakollen

	Orientation:	**N205**
BH2	**Angle:**	**45**
Time [min]	**Amount [L]**	**G.W. [m]**
GW before		5,31
0	1	5,295
5	6	5,26
10	13,8	5,18

	Orientation:	**N345**
BH4	**Angle:**	**65**
Time [min]	**Amount [L]**	**G.W. [m]**
GW before		4,48
0	1	4,43
5	2	4,34
10	6	4,07
15	6	3,82

BH3	**Orientation:**	**90**

	Orientation:	**N395**
BH5	**Angle:**	**43**

Time [min]	Amount [L]	G.W. [m]
GW before		13,57
0	1	13,54
5	1	13,52
10	2	13,46
15	2	13,43
20	6	13,23
25	6	13,15

Time [min]	Amount [L]	G.W. [m]
GW before		14,4
2	1	14,35
6	1	14,32
10	1	14,3
15	1	14,29
20	2	14,23
25	2	14,2
30	6	13,96

Simulation of wells from Folkehelseinstituttet:

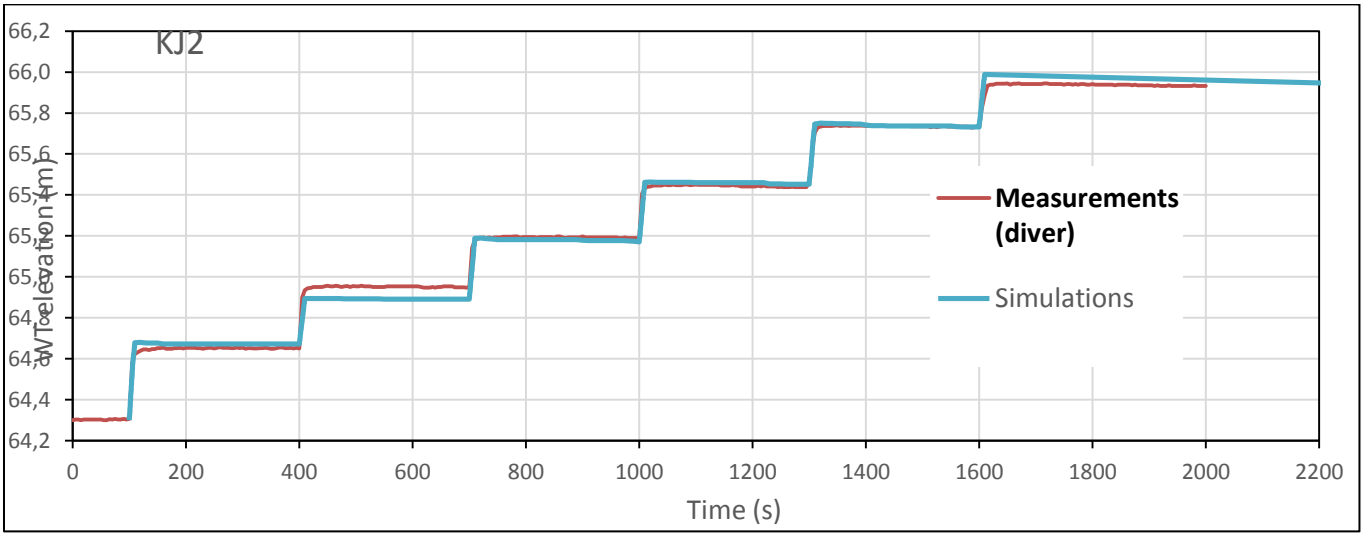

Figure 83 - Modelling of pouring steps of well KJ2

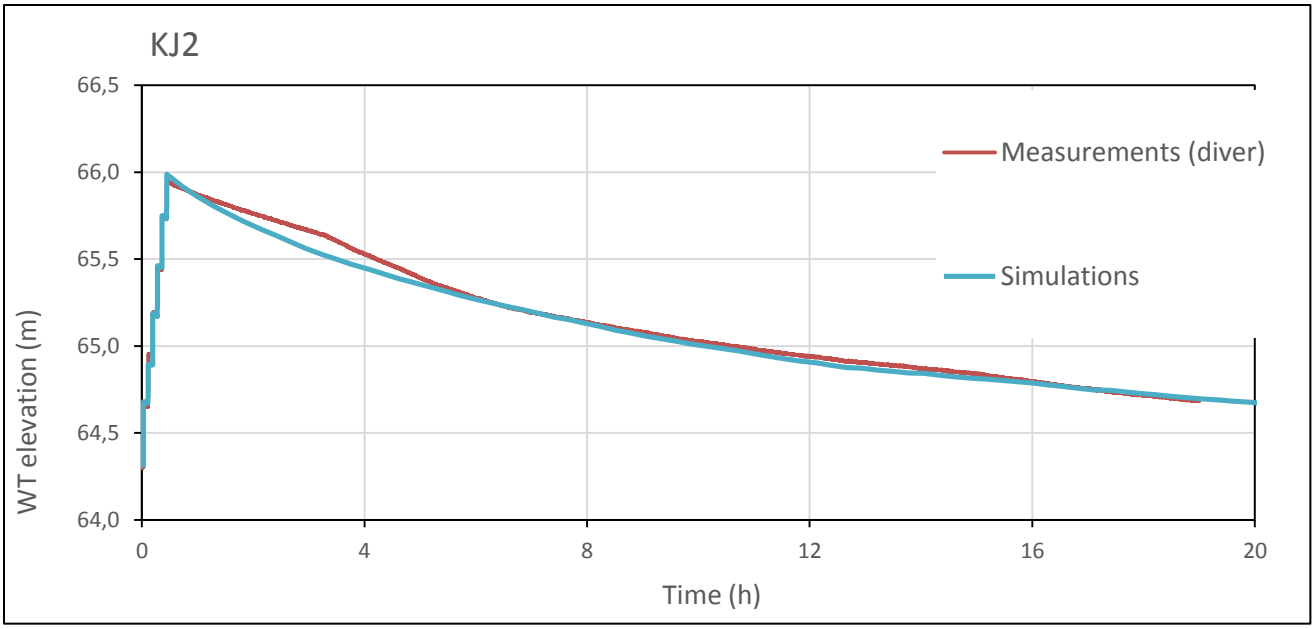

Figure 84 - Modelling of drawdown of well KJ2

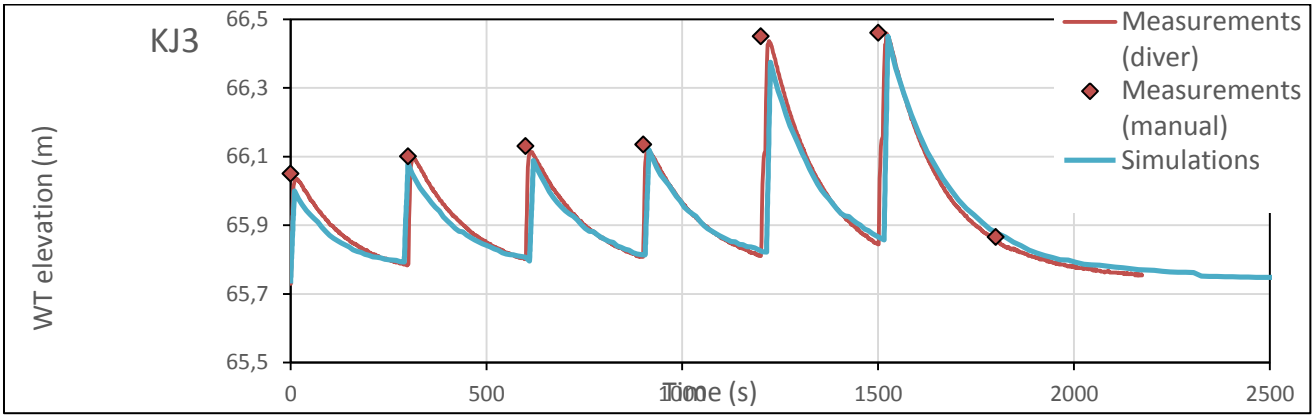

Figure 85 - Modelling of pouring and draining steps of well KJ3

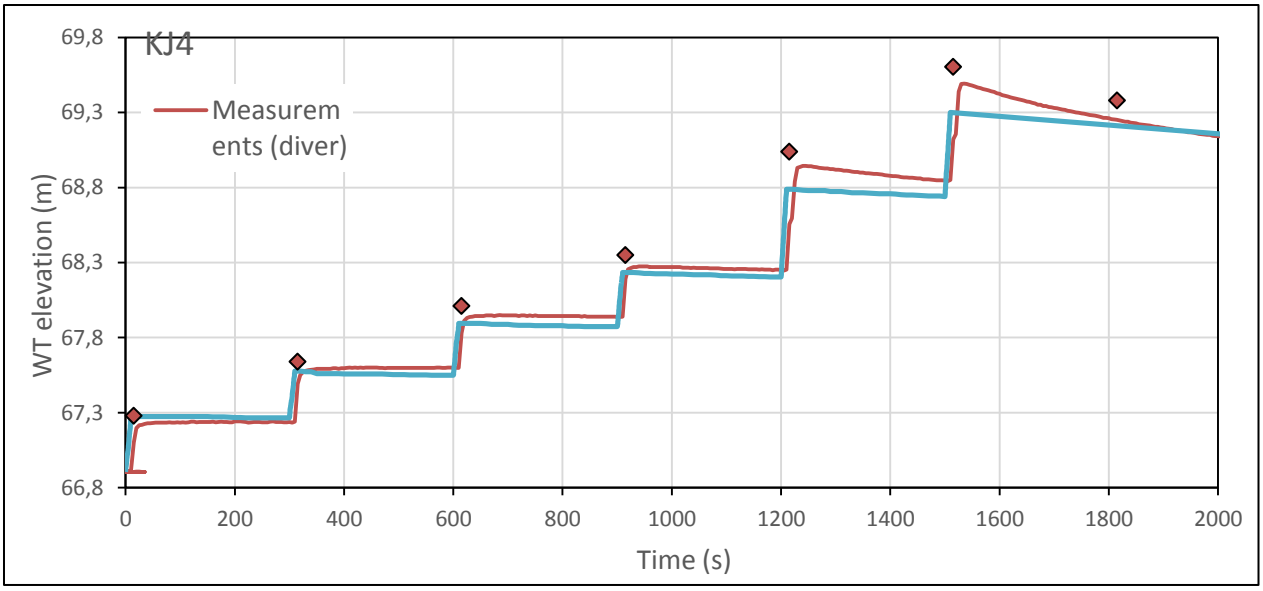

Figure 86 - Modelling of pouring steps of well KJ4

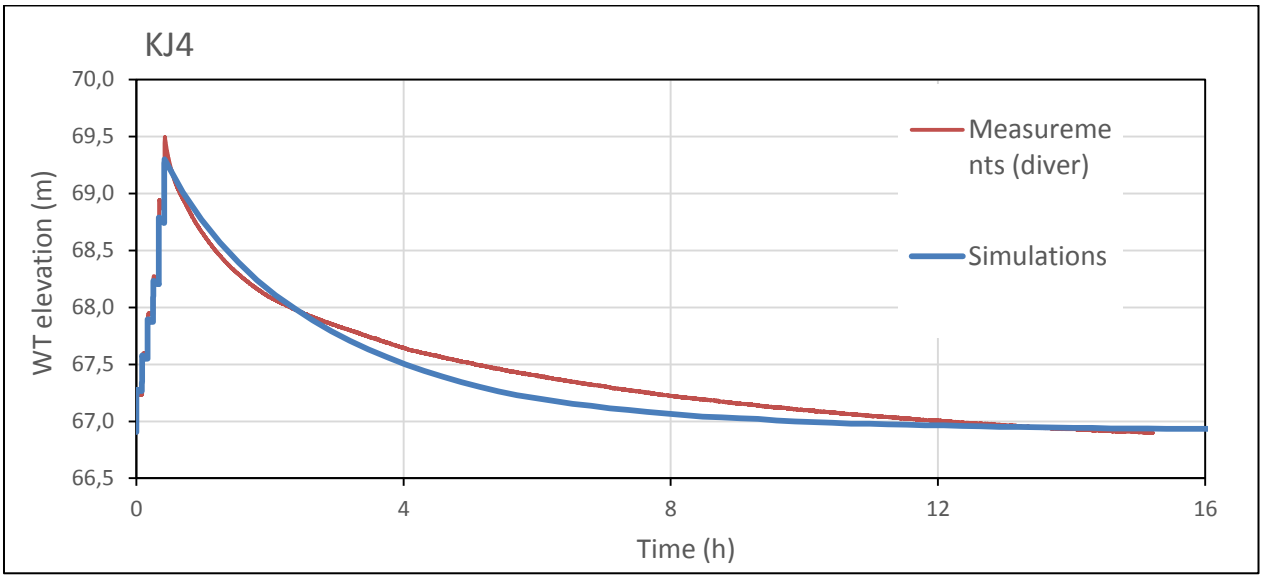

Figure 87 - Modelling of drawdown of well KJ4

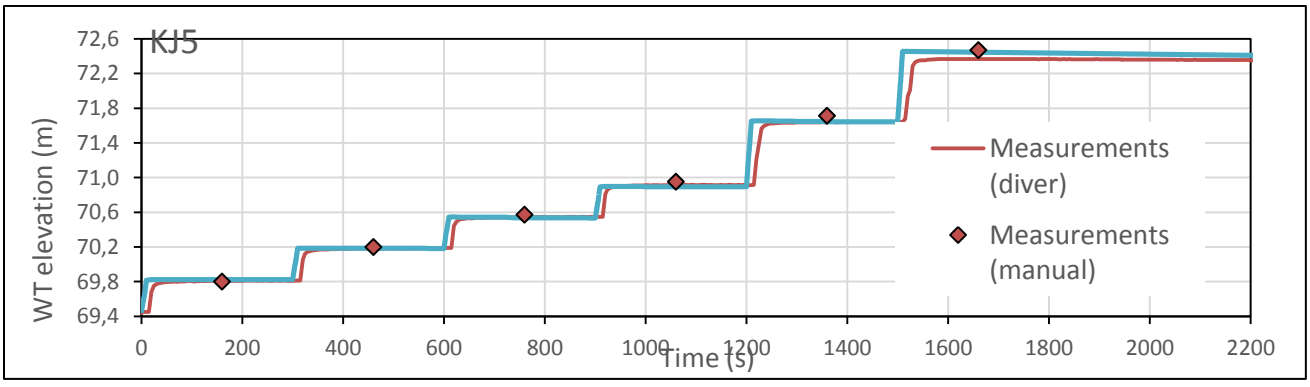

Figure 88 - Modelling of pouring steps of well KJ5

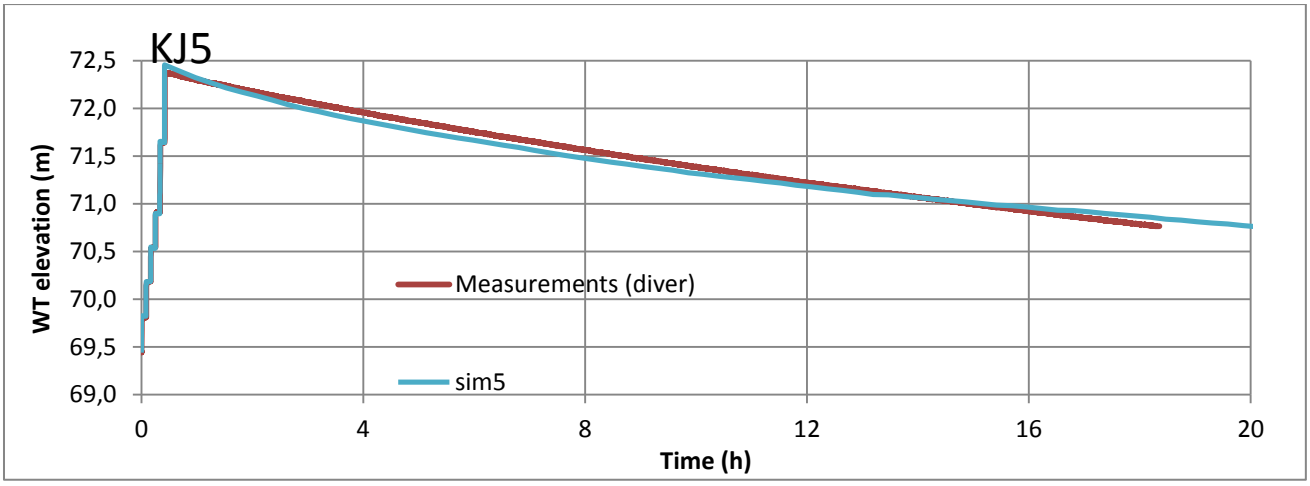

Figure 89 - Modelling of drawdown of well KJ5

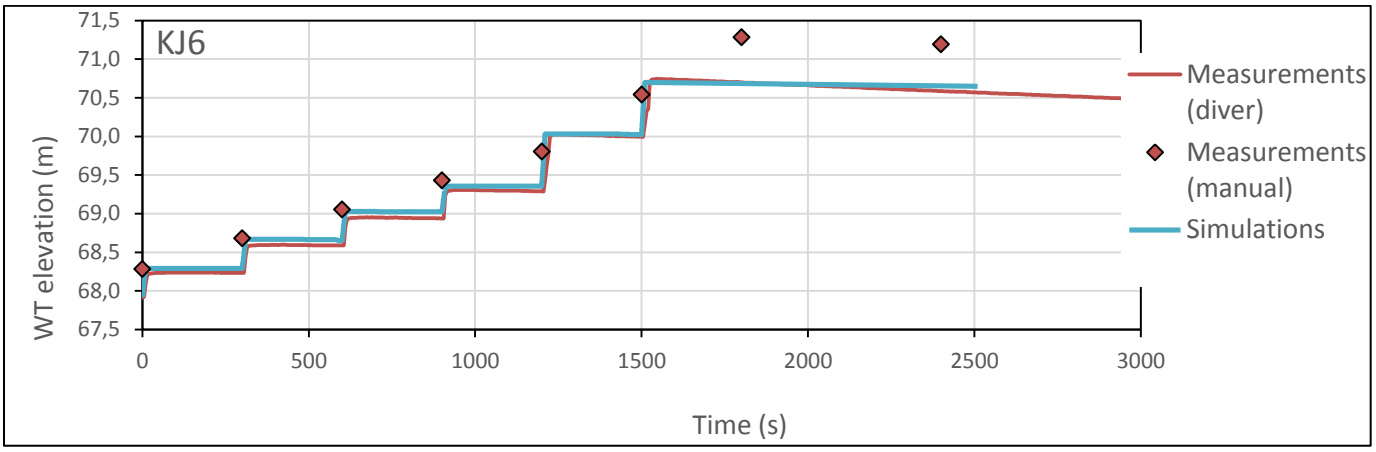

Figure 90 – modelling of pouring steps of well KJ6

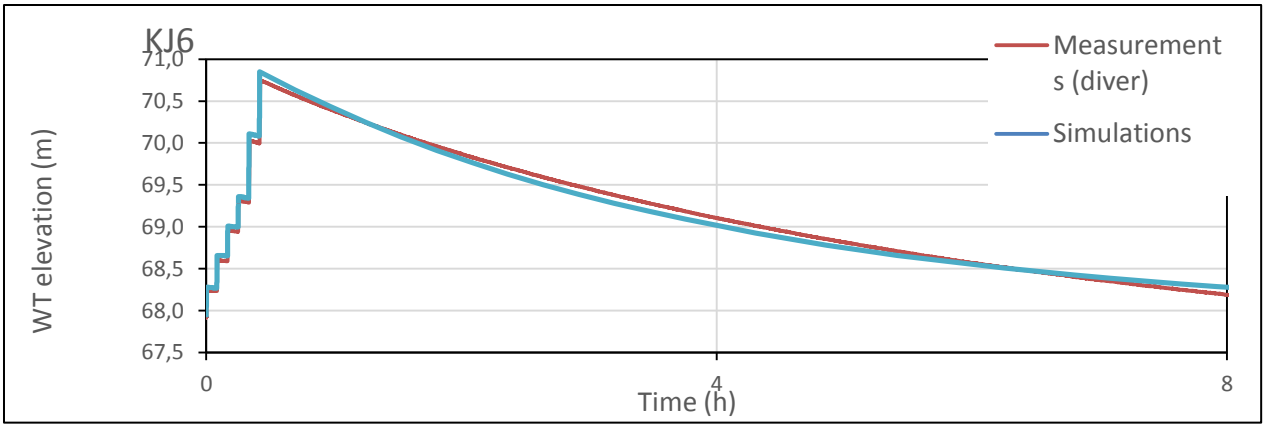

Figure 91 - Modelling of drawdown steps of well KJ6

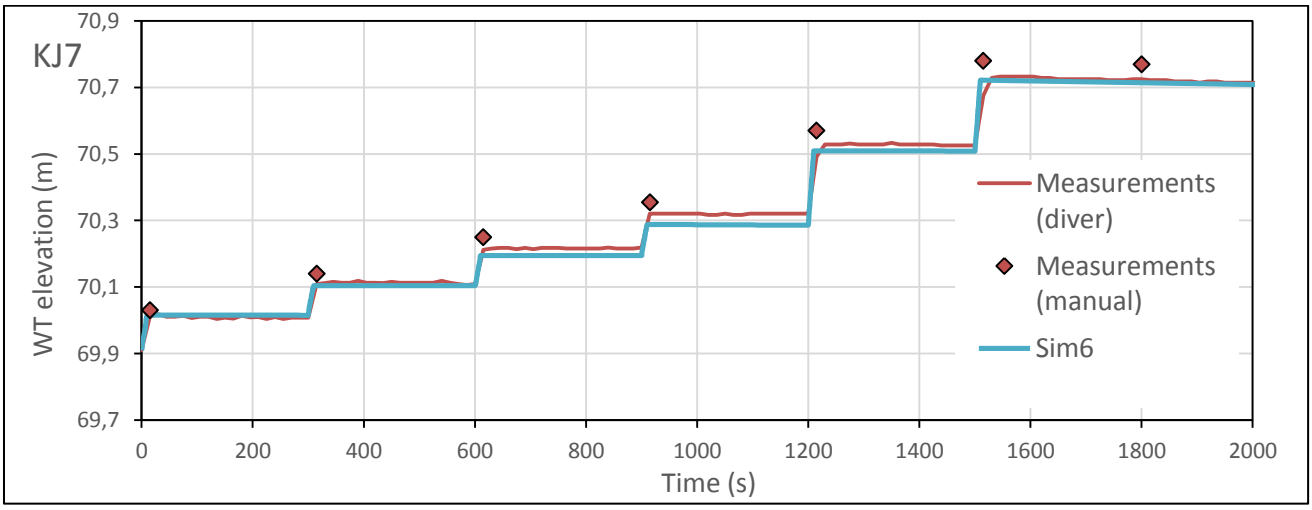

Figure 92 - Modelling of pouring steps of well KJ7

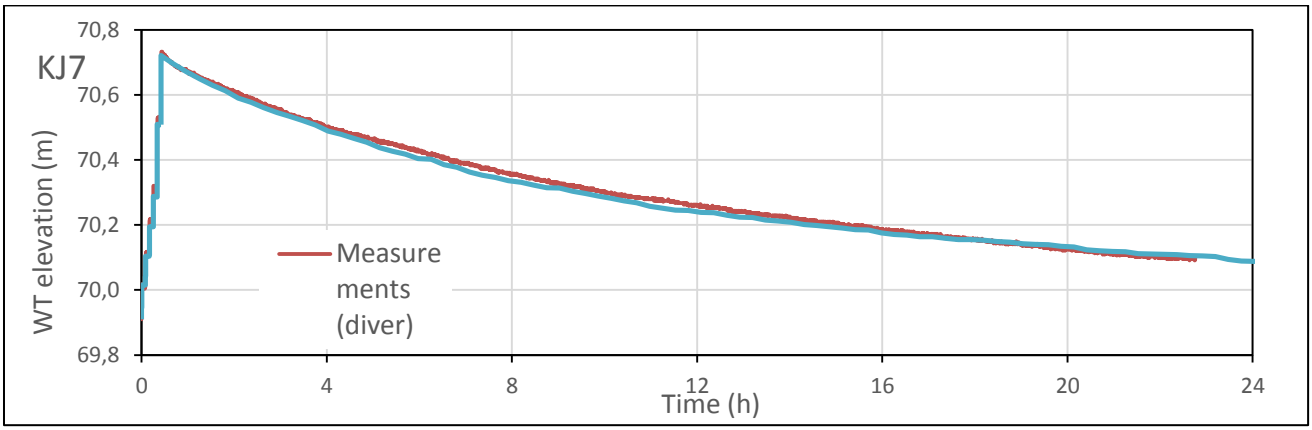

Figure 93 - Modelling of drawdown of well KJ7

Simulation of wells from Bekkelaget:

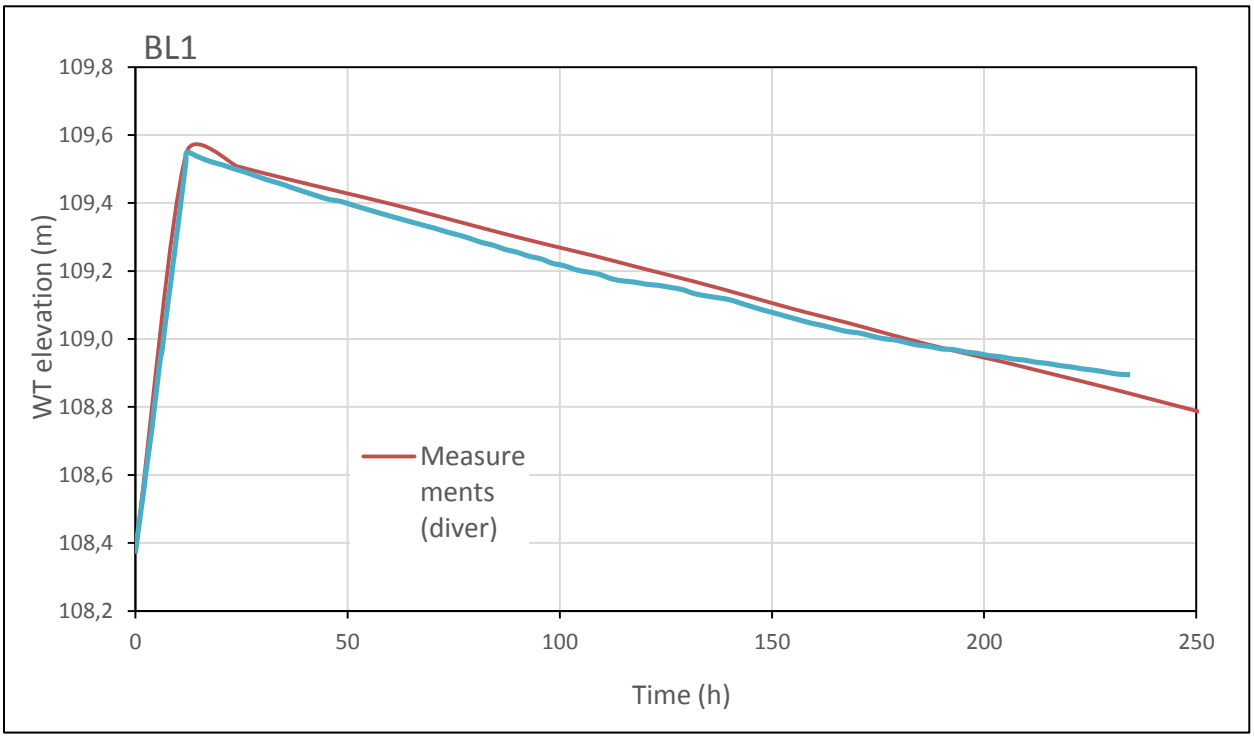

Figure 94 - Modelling of pouring and draining steps of well BL1

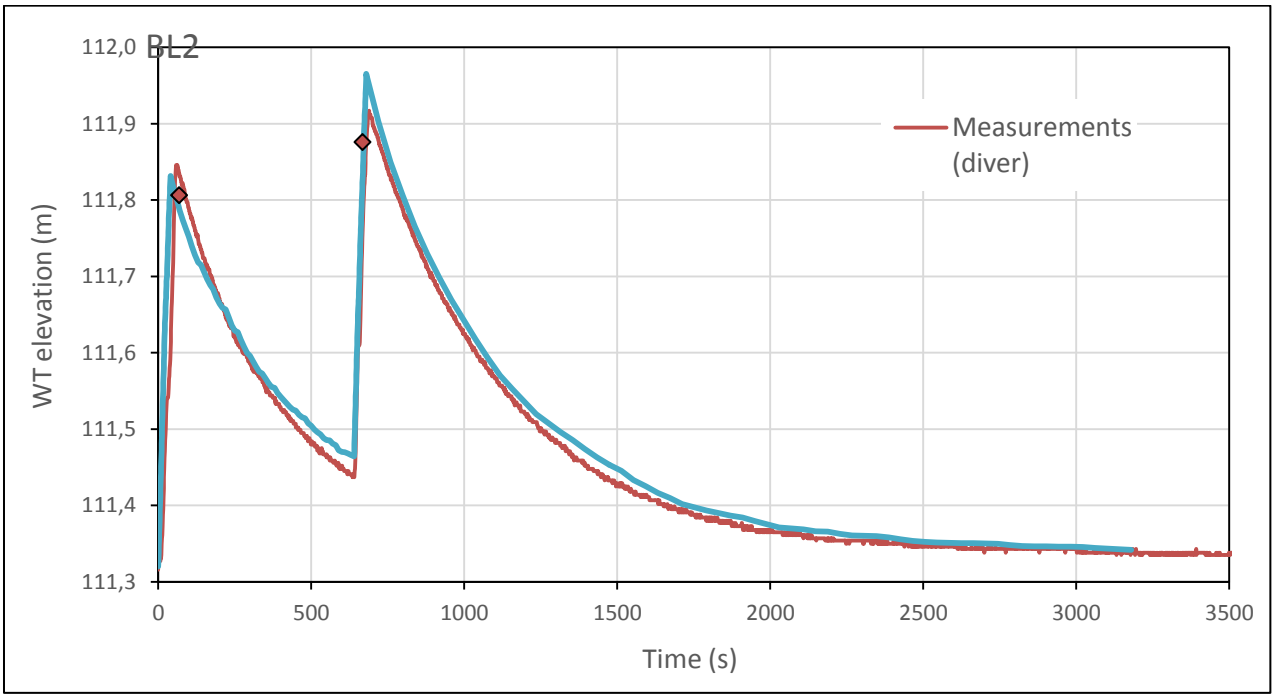

Figure 95 - Modelling of pouring and draining steps of well BL2

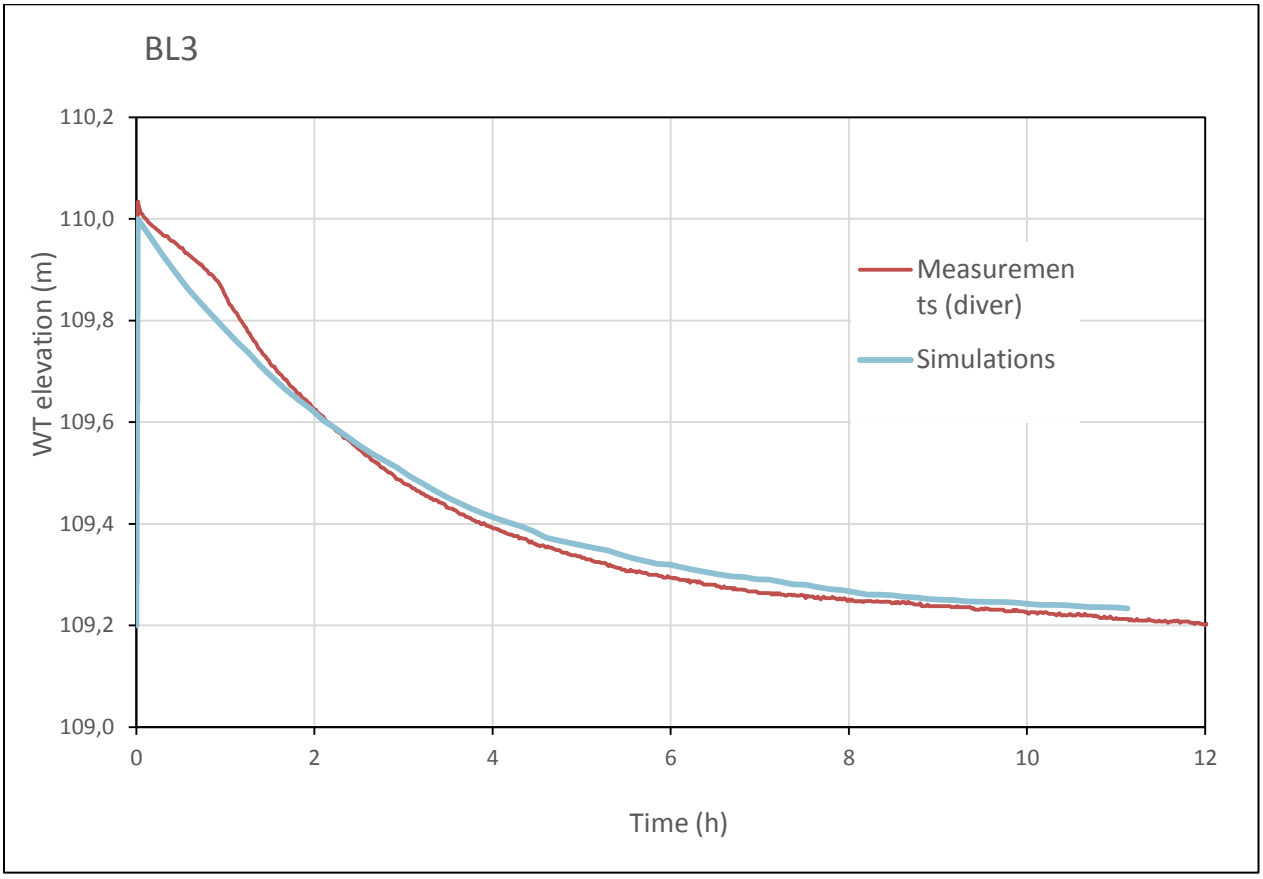

Figure 96 - Modelling of pouring and draining steps of well BL2

Simulation of the Vettakollen wells:

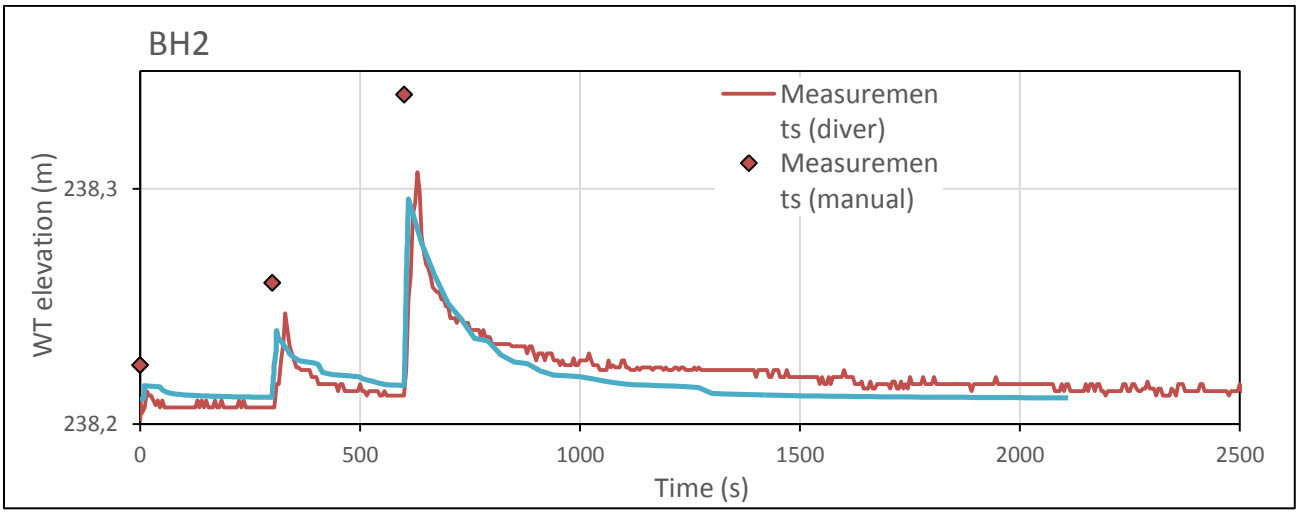

Figure 97 - Modelling of pouring and draining steps of well BH2

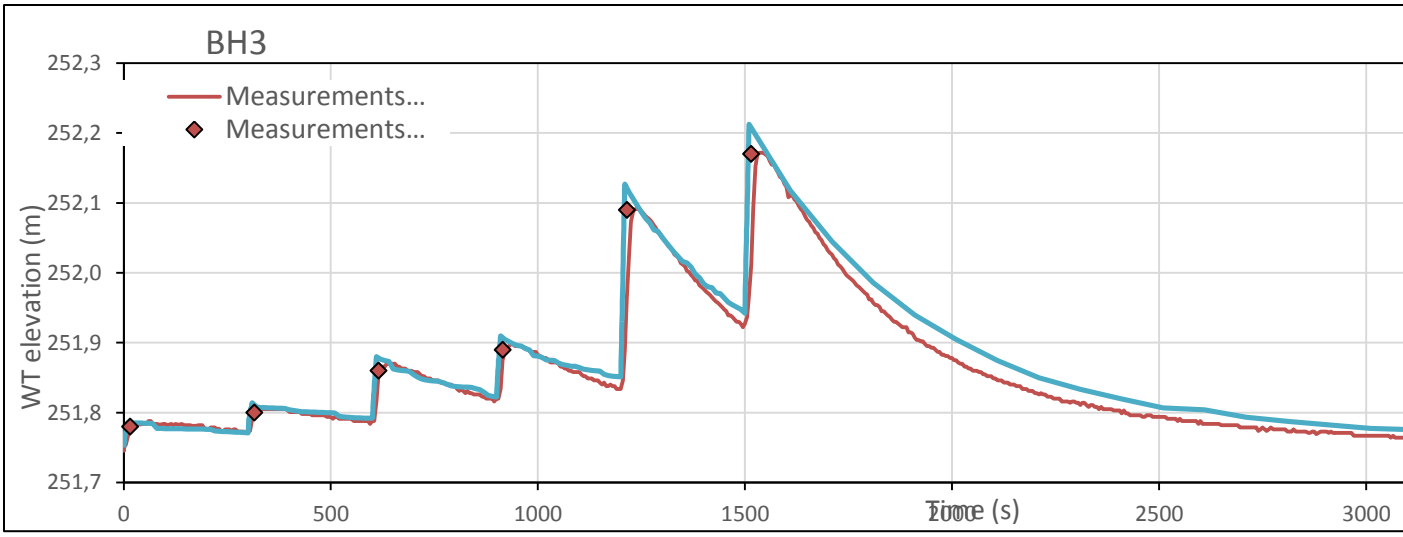

Figure 98 - Modelling of pouring and draining steps of well BH3

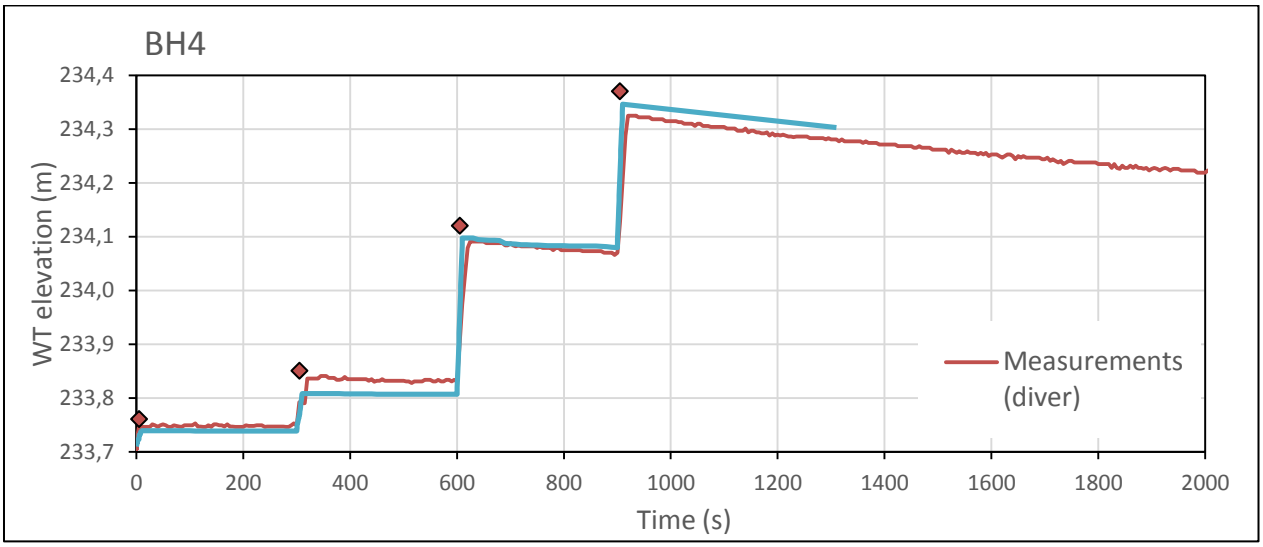

Figure 99 – Modelling of pouring steps of well BH0034

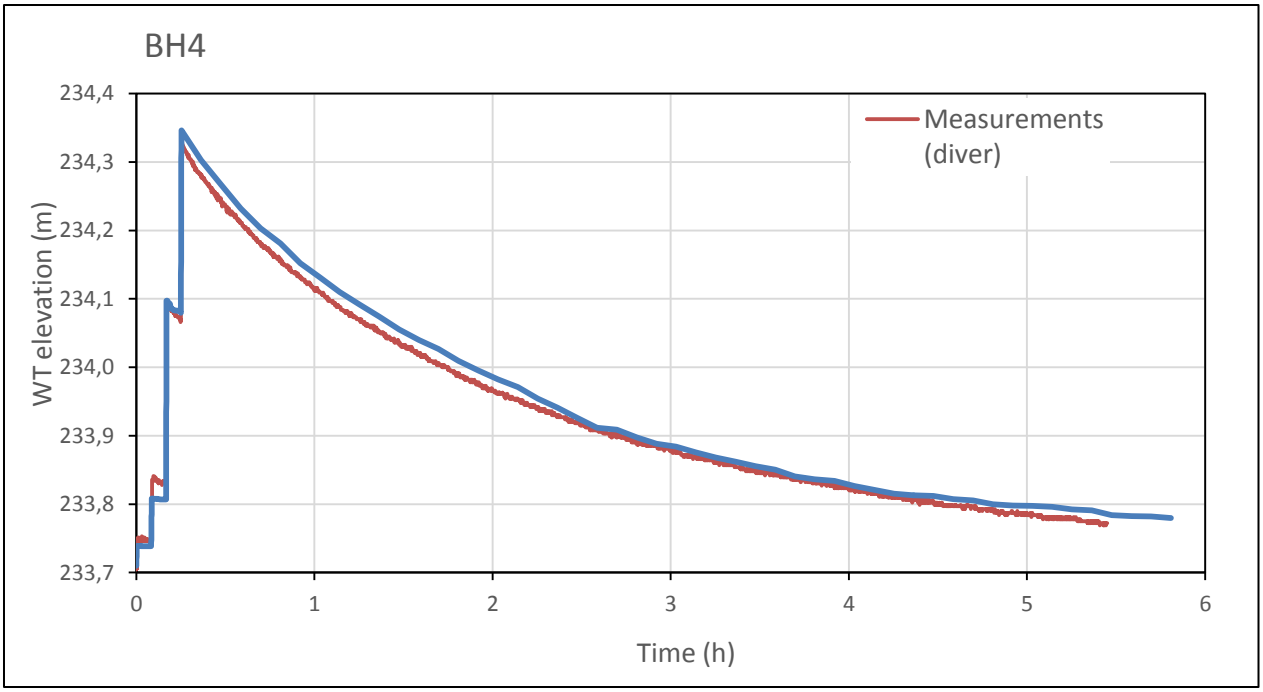

Figure 100 – Modelling of drawdown of well BH4

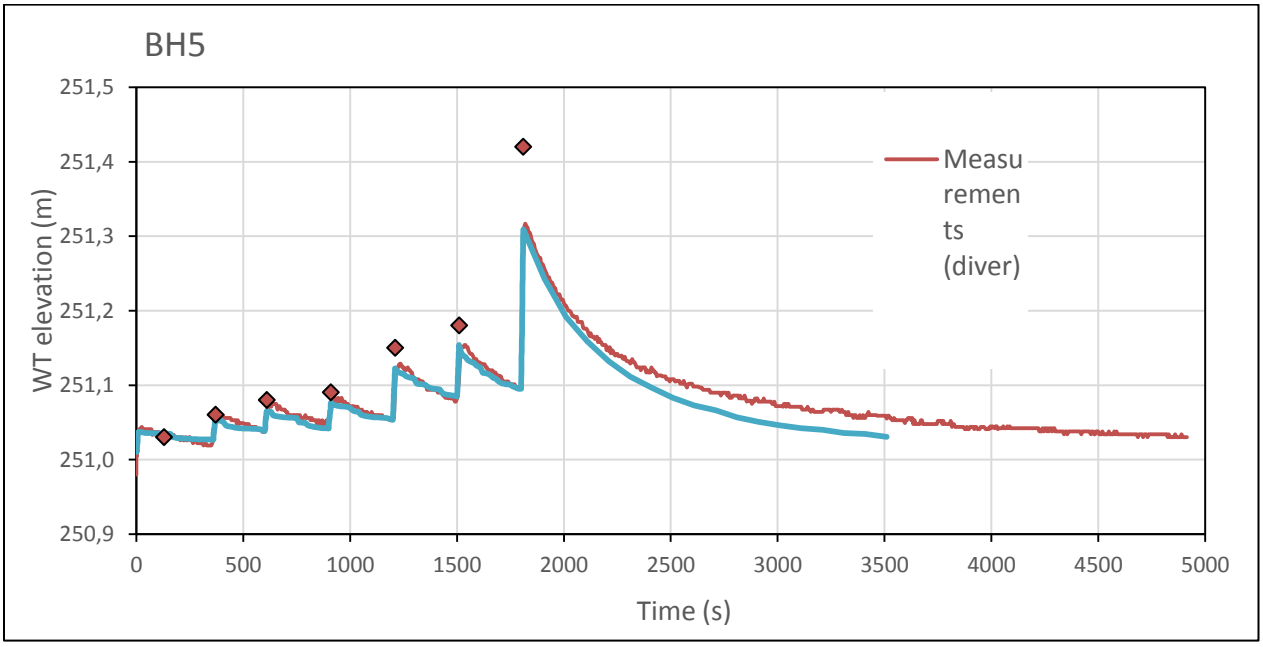

Figure 101 - Modelling of pouring and draining steps of well BH5

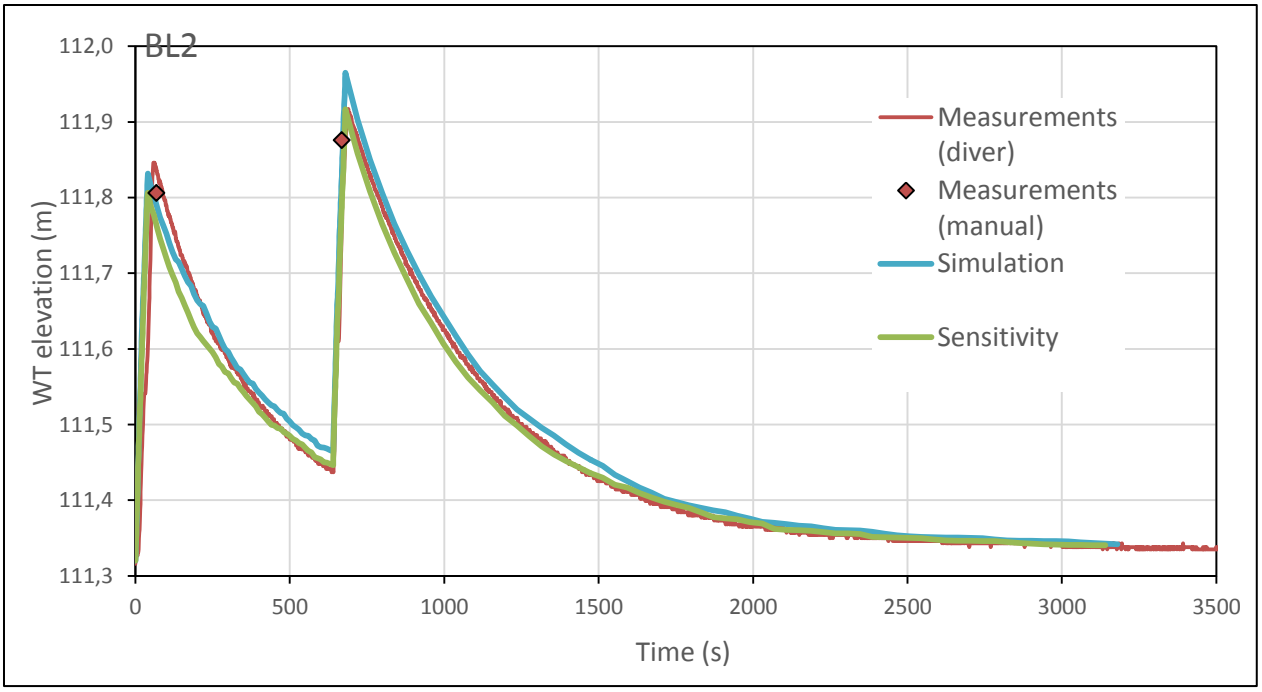

Figure 102 – sensitivity analysis of well BL2 based on different saturated (SWC) and residual water contents(RWC). The line "simulation" is the assumed water contents used for all the simulations at SWC=0,03 and RWC=0,01. The line "Sensitivity" is given a SWC=0,06 and a RWC=0,015.

Appendix D: Simulation data large scale: Flat case

Infiltration rates over tunnel interface:

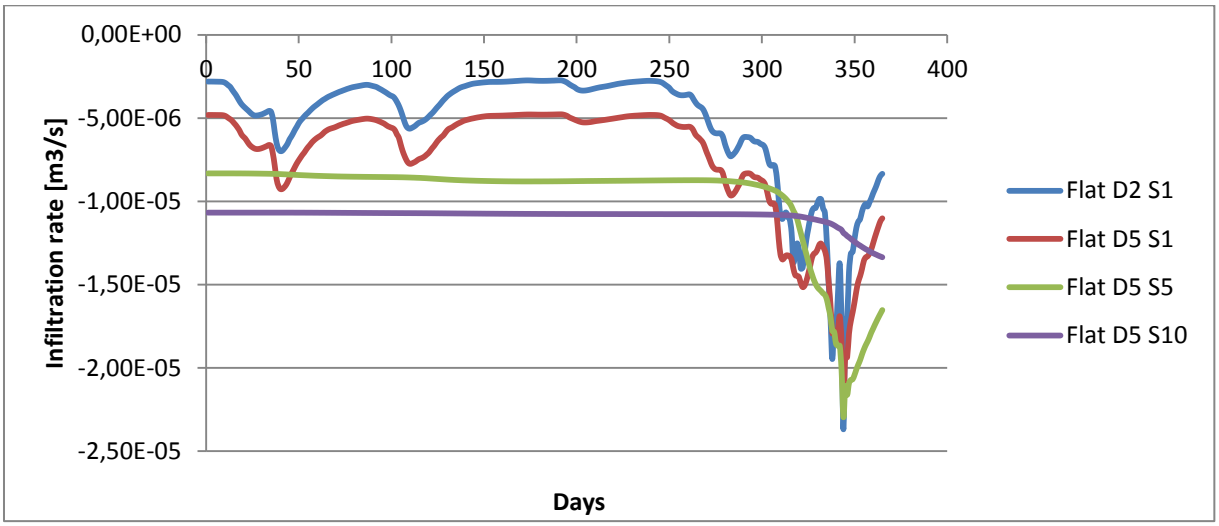

Figure 103 – Infiltration rates over tunnel interface

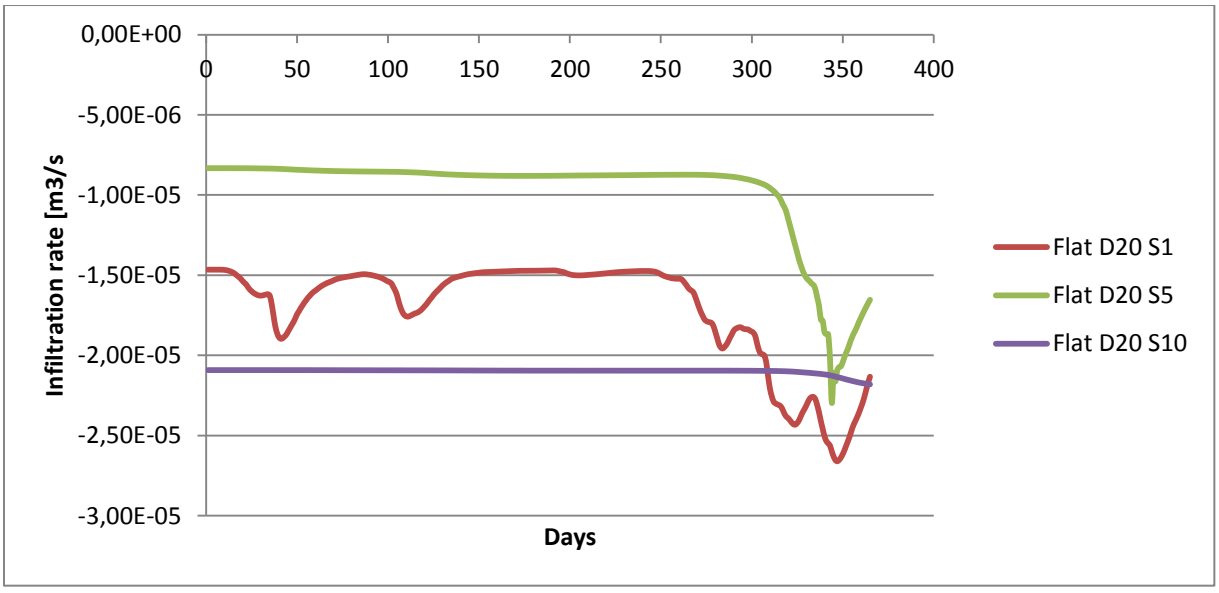

Figure 104 – Infiltration rates over tunnel interface

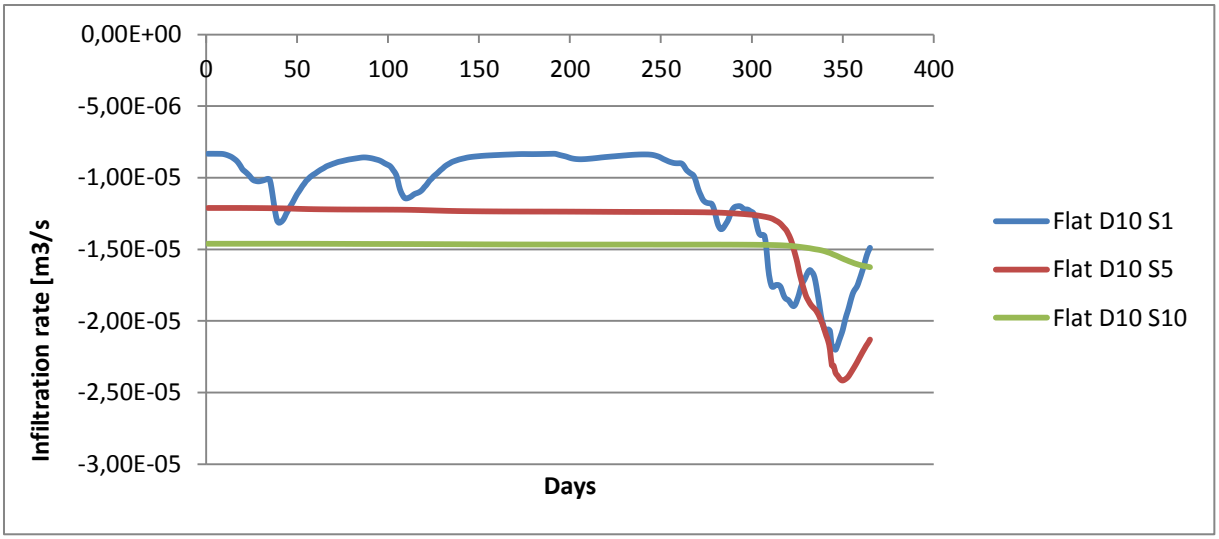

Figure 105 – Infiltration rates over tunnel interface

Infiltration rates over soil-rock interface:

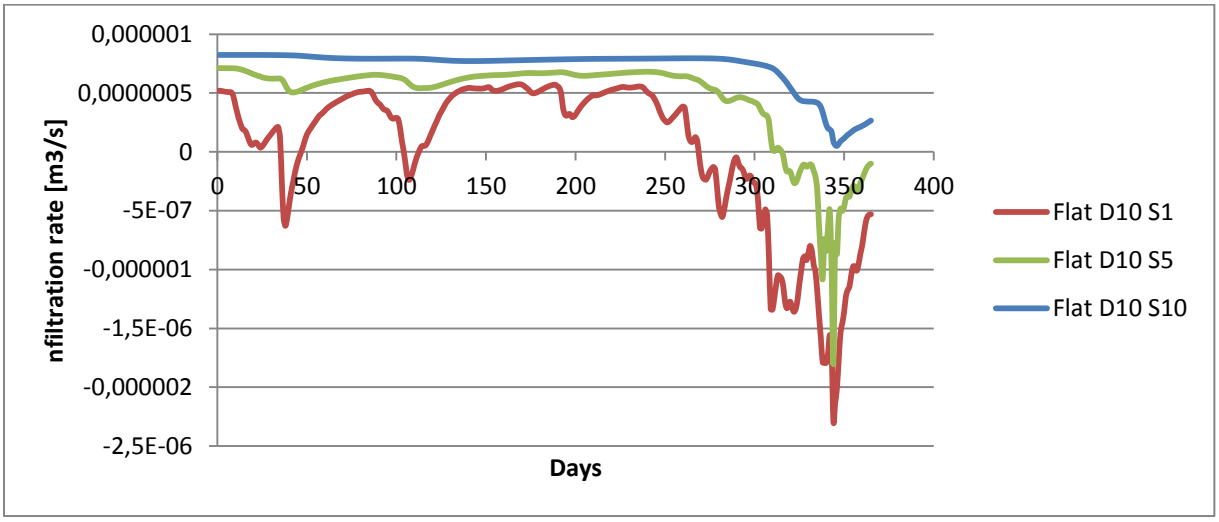

Figure 106 – Infiltration rates over soil-rock interface

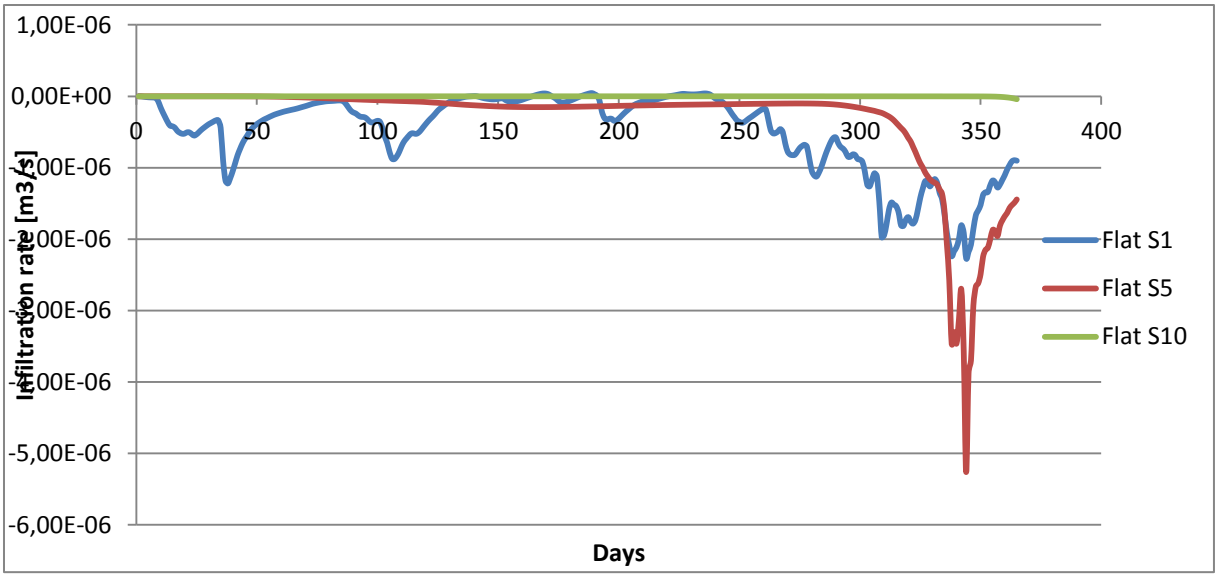

Figure 107 – Infiltration rates over soil-rock interface

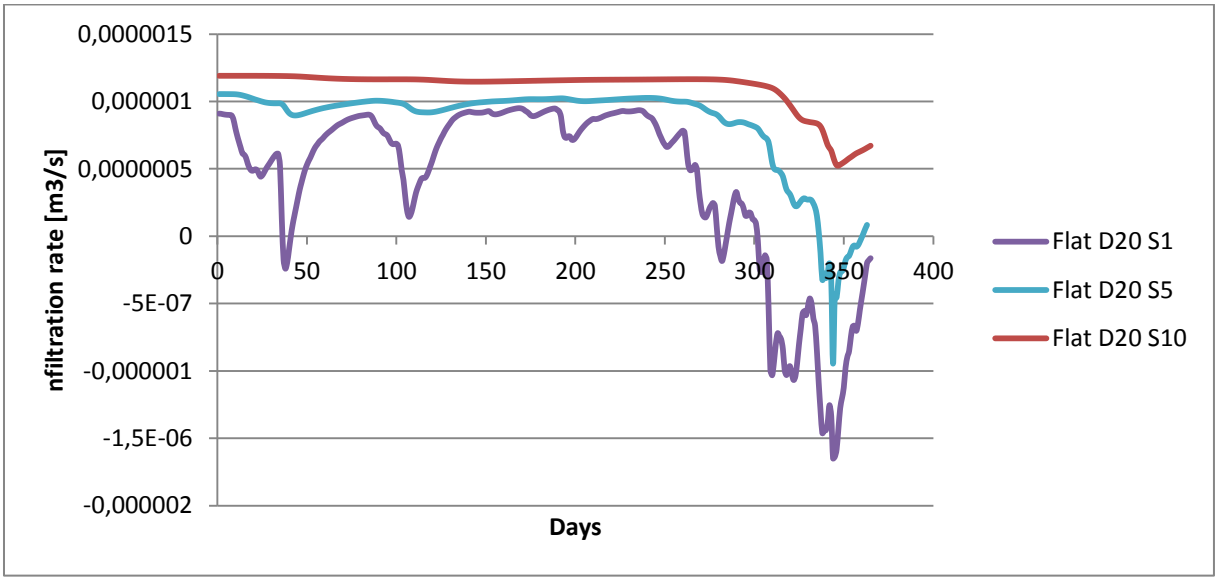

Figure 108 – Infiltration rates over soil-rock interface

Groundwater tables:

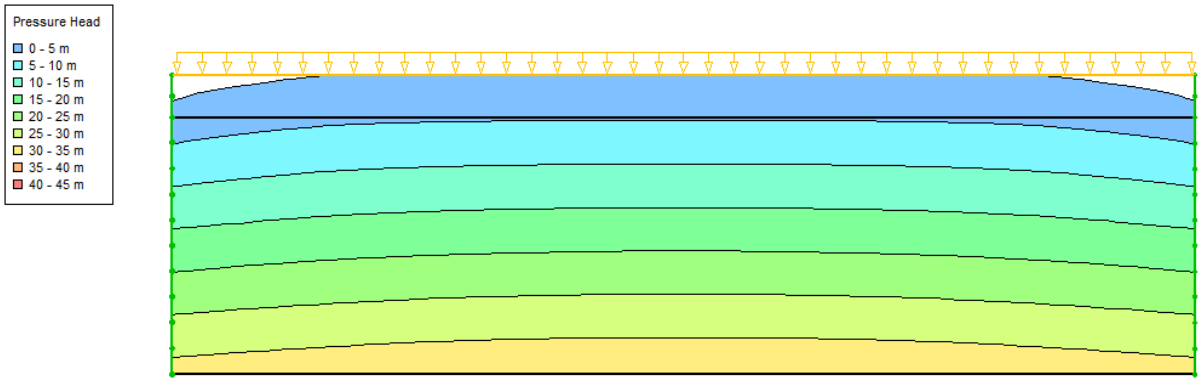

Figure 109 - Flat S10

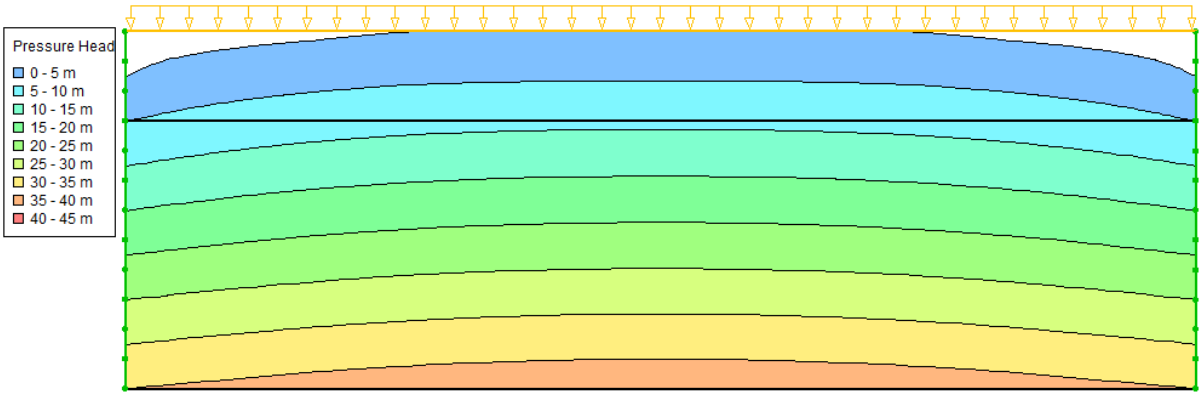

Figure 110 - Flat S1

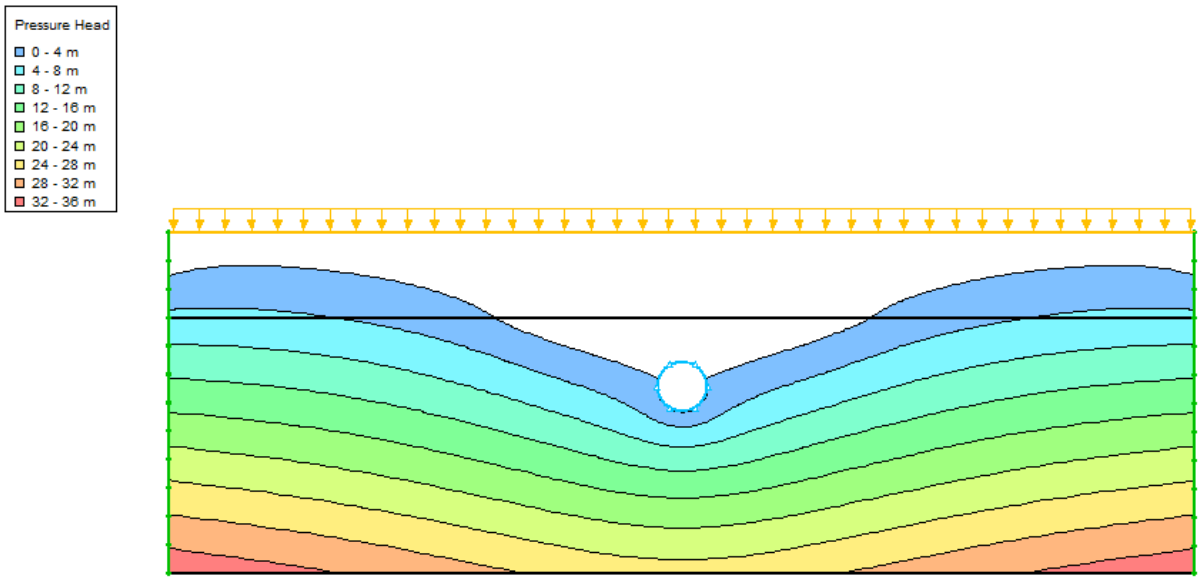

Figure 111 - Flat D5 S10

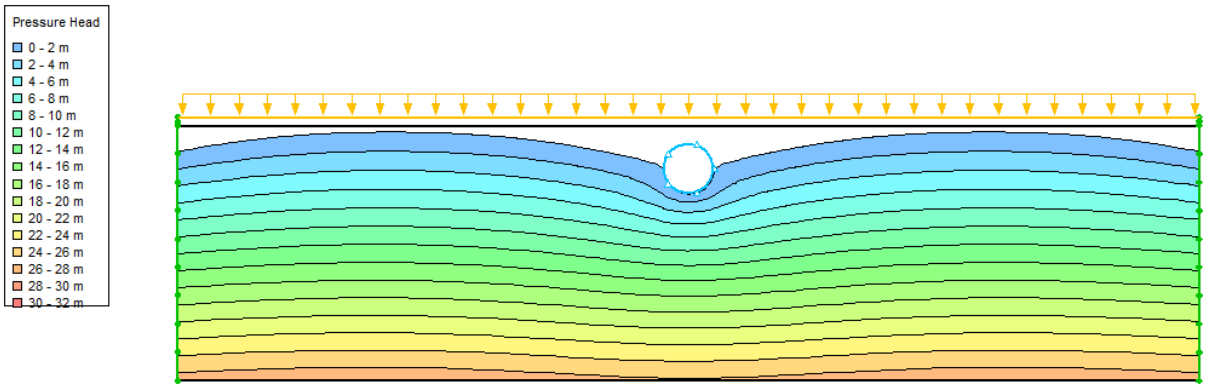

Figure 112 - Flat D2 S1

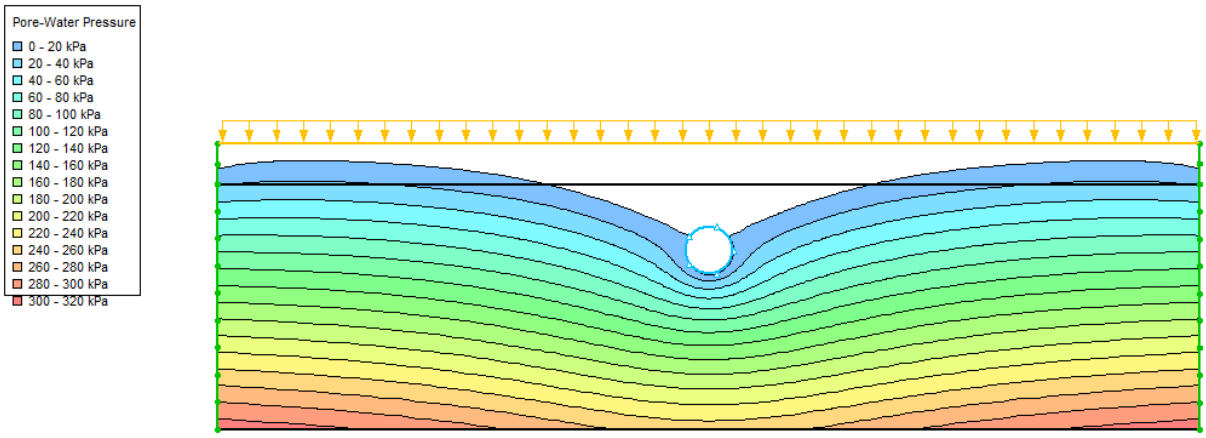

Figure 113 - D5 S5

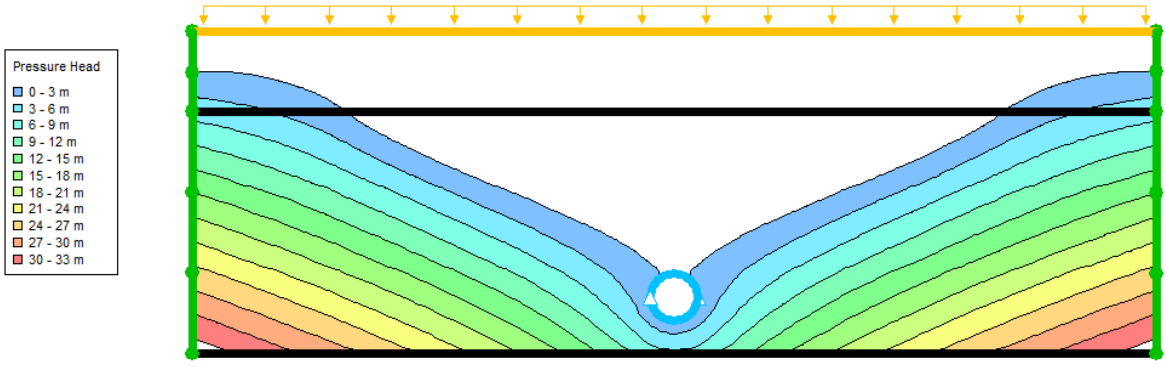

Figure 114 - Flat D20 S10

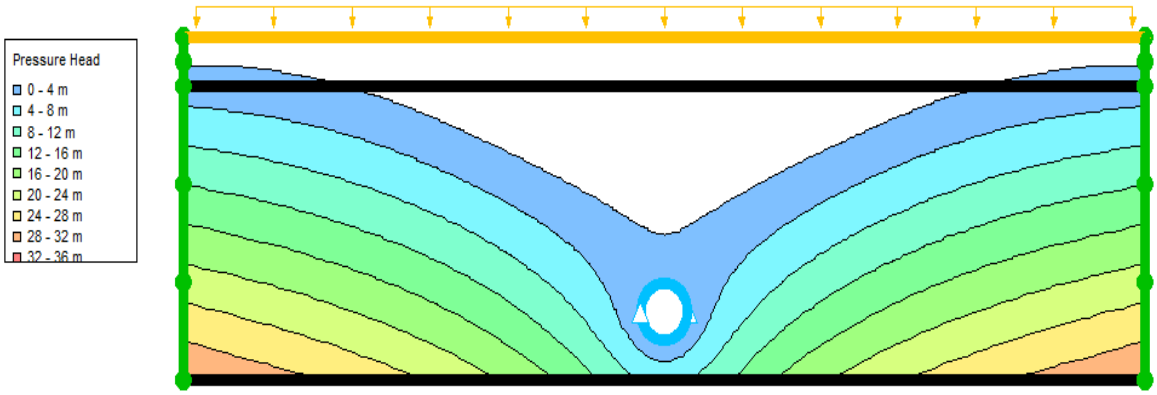

Figure 115 - Flat D20 S5

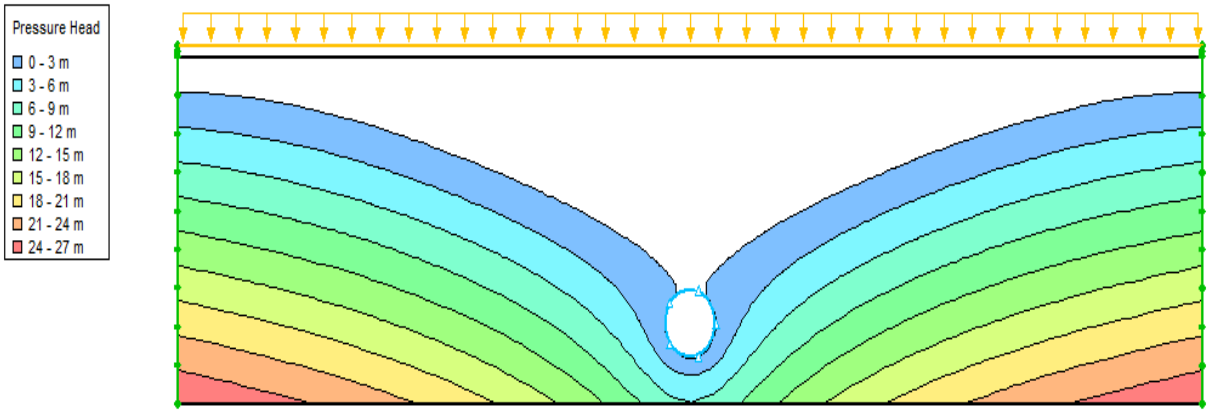

Figure 116 - Flat D20 S1

Appendix E: Simulation data large scale: Lake case

Initial rates:

Table 23 – Initial infiltration rates over tunnel interface

Case	Infiltration rate [m3/s]
Lake Bergen D10 BH3	-6,91E-05
Lake Bergen D20 BH3	-8,46E-05
Lake Bergen D20 BH4	-6,50E-06
lake Lillehammer D10 BH3	-6,91E-05
Lake Lillehammer D20 BH3	-8,46E-05
Lake Lillehammer D20 BH4	-6,50E-06

Table 24 - Initial infiltration rates over soil-rock interface

Case	Initial infiltration
Bergen BH3	-4,82E-07
Bergen BH4	-3,18E-07
Lillehammer BH3	-4,82E-07
Lillehammer BH4	-3,18E-07
Lake Bergen D10 BH3	6,16E-07
lake Bergen D20 BH3	1,06E-06
Lake bergen D20 BH4	-1,44E-07
Lake Lillehammer D10 BH3	6,16E-07
Lake Lillehammer D20 BH3	1,06E-06
Lake Lillehammer D20 BH4	-1,44E-07

Infiltration rates over tunnel interface:

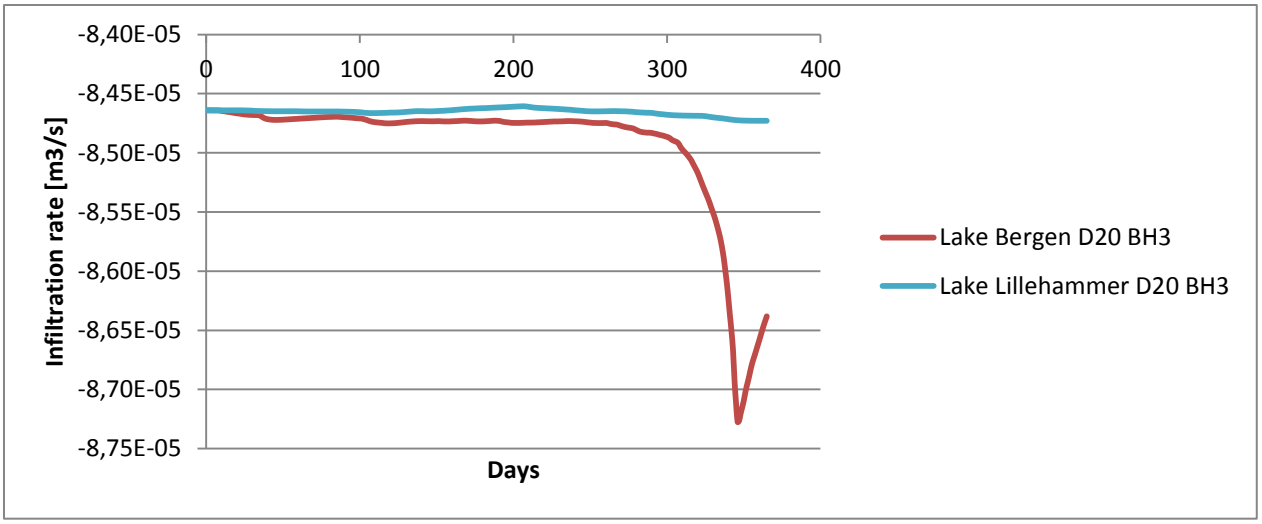

Figure 117 – Infiltration rate over tunnel interface

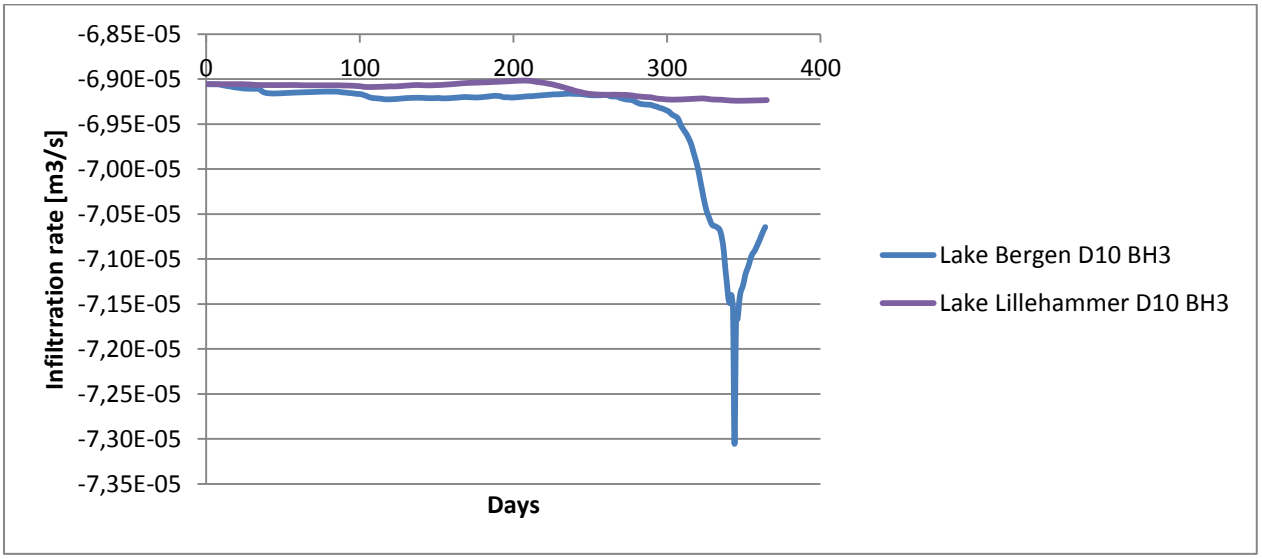

Figure 118 – Infiltration rate over tunnel interface

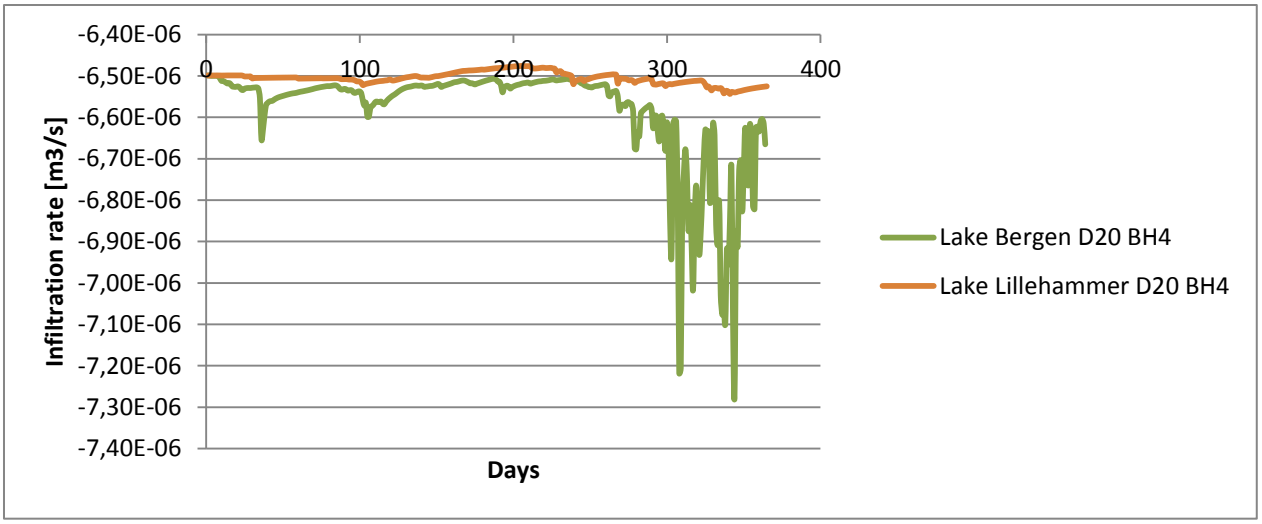

Figure 119 – Infiltration rate over tunnel interface

Infiltration rates over soil-rock interface:

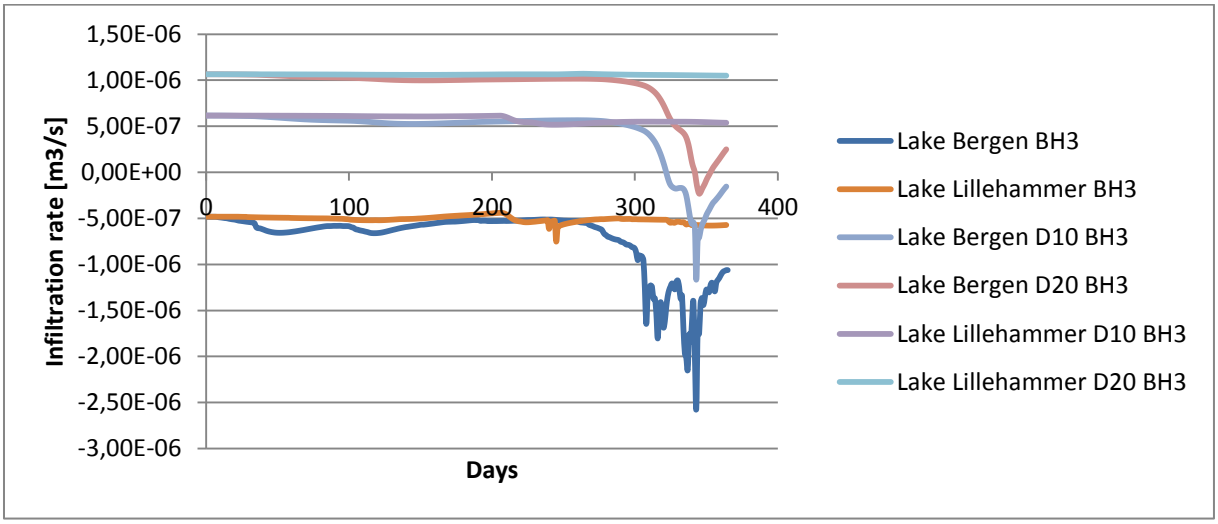

Figure 120 – Infiltration rates over soil-rock interface

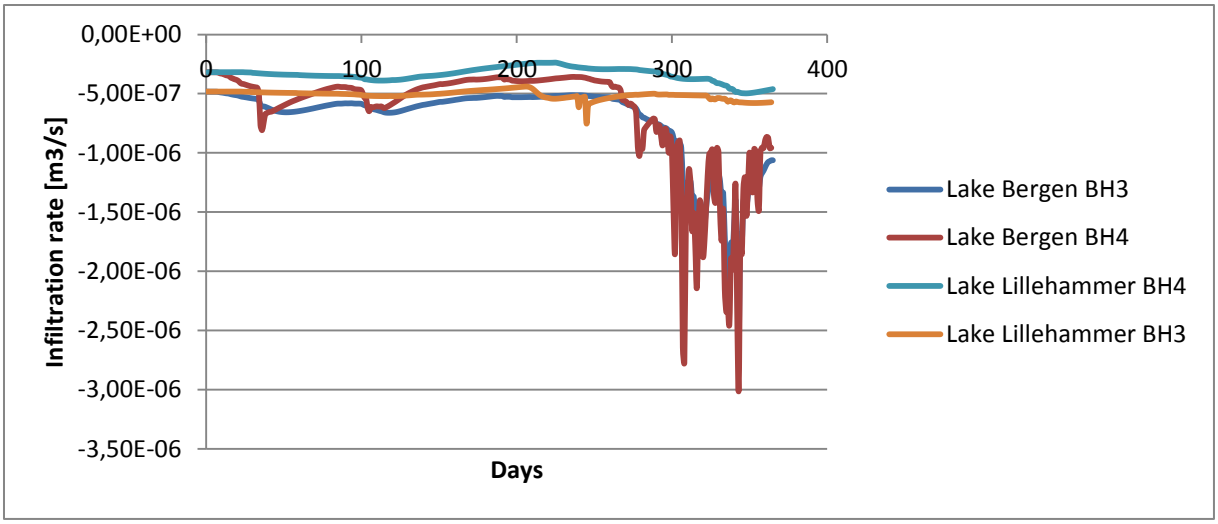

Figure 121 – Infiltration rates over soil-rock interface

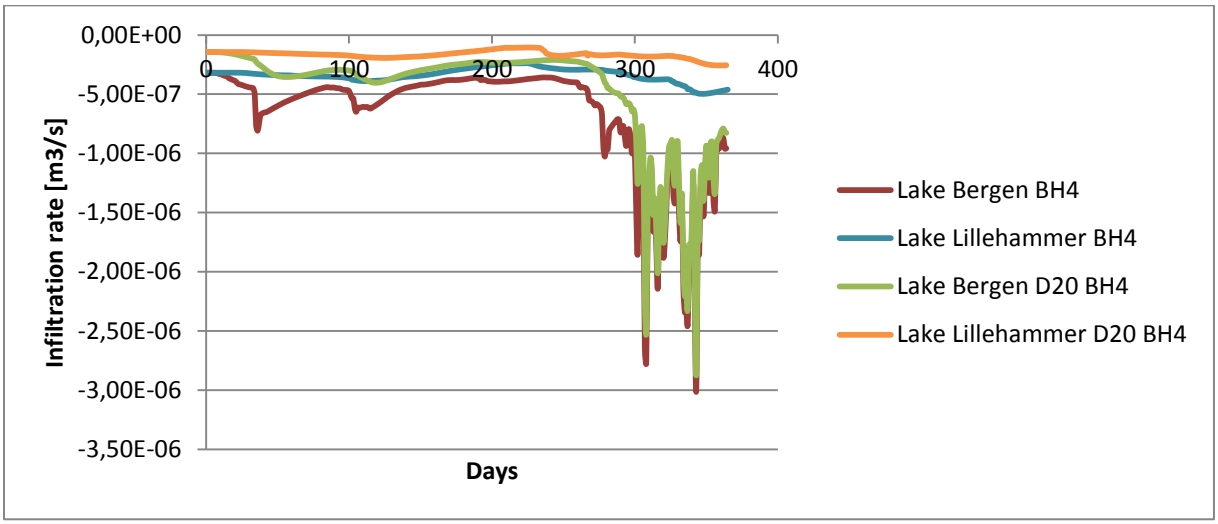

Figure 122 – Infiltration rates over soil-rock interface

Groundwater levels:

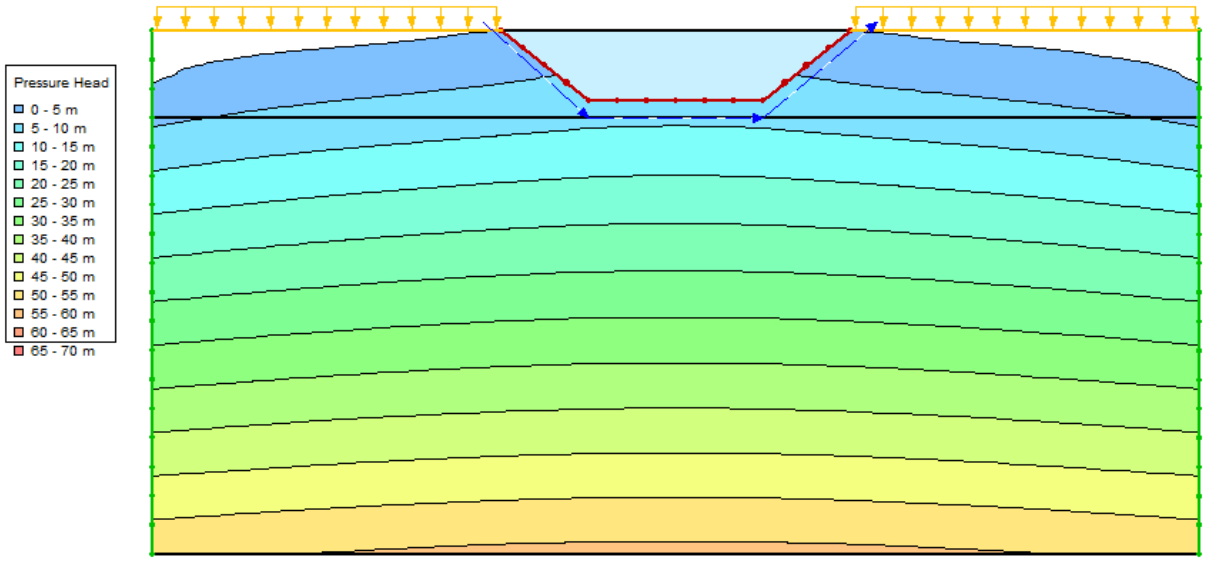

Figure 123 – Lake Bergen BH3

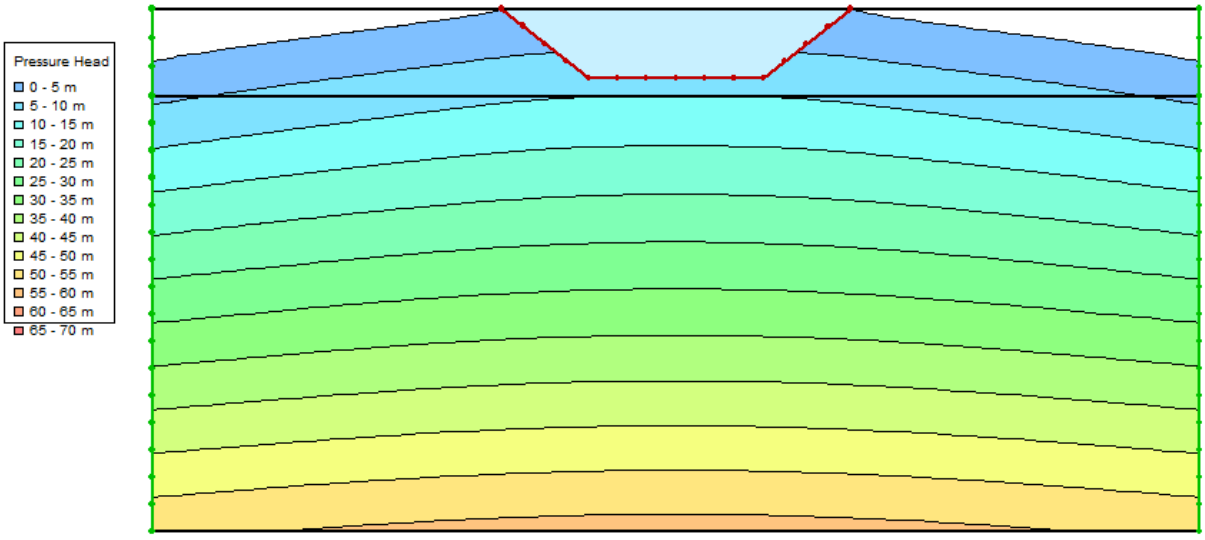

Figure 124 - Lake Bergen BH4

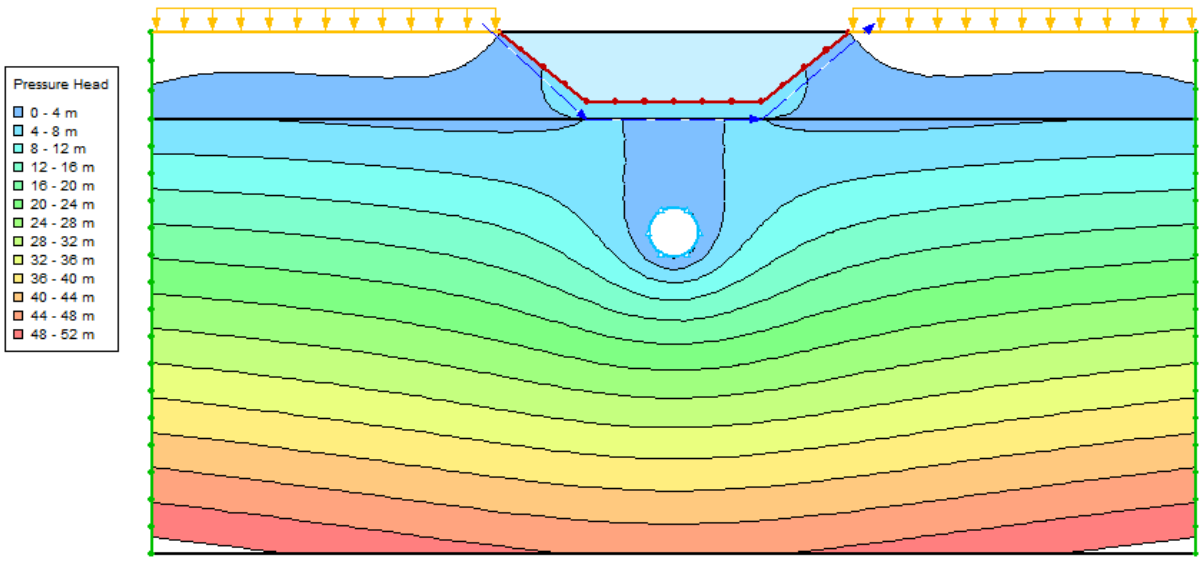

Figure 125 - Lake Bergen D10 BH3

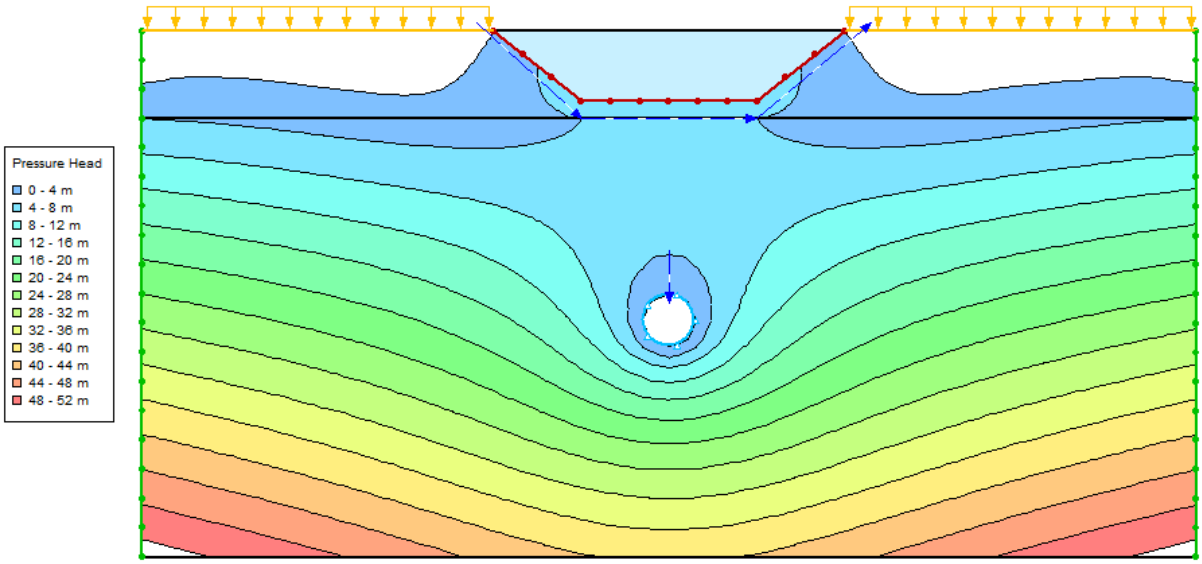

Figure 126 - Lake Bergen D20 BH3

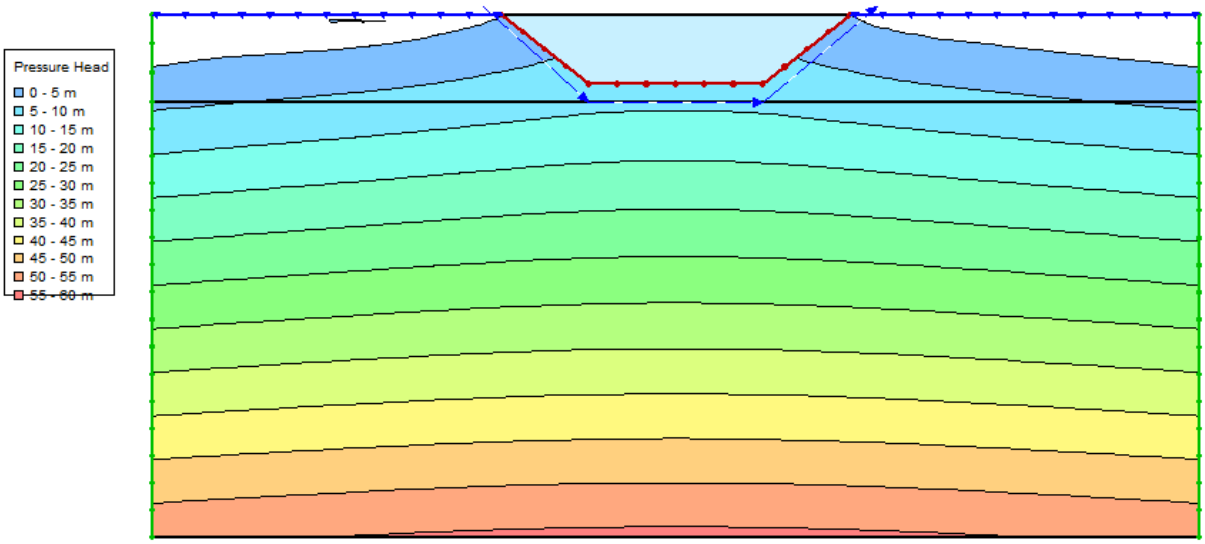

Figure 127 - Lake Lillehammer BH3

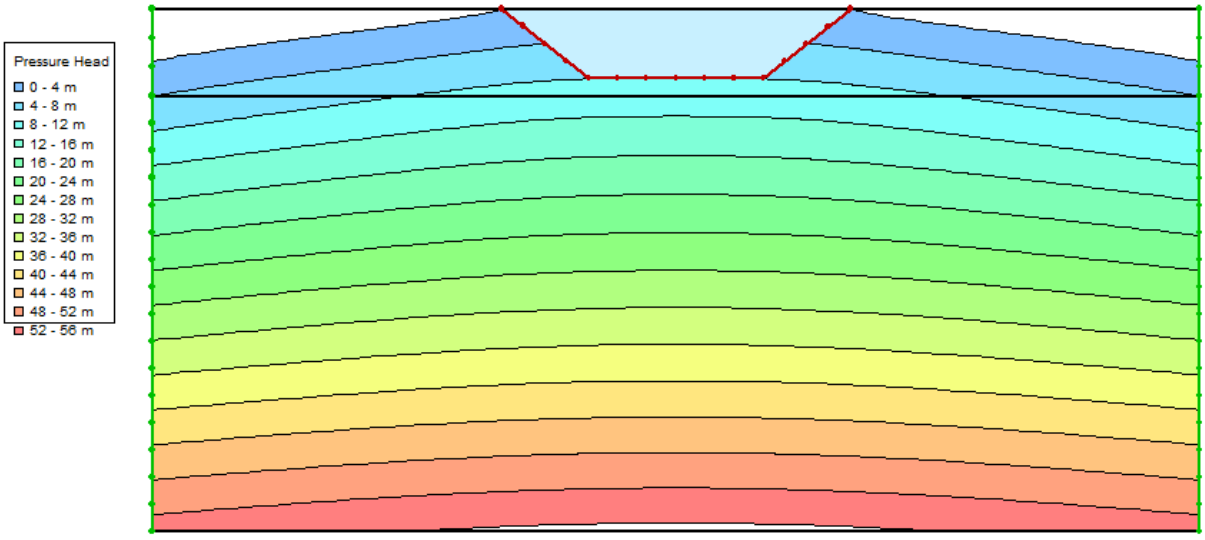

Figure 128 – Lake Lillehammer BH4

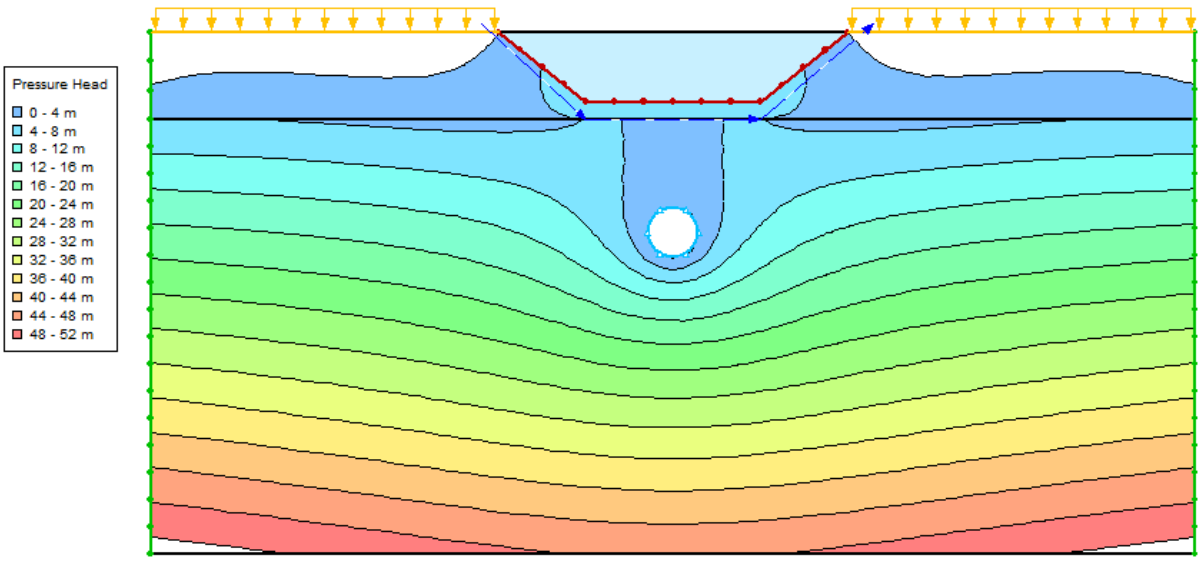

Figure 129 - Lake Lillehammer D10 BH3

Appendix F: Simulation data large scale: Slope case

Infiltration rates:

Table 25 – Initial infiltration rates over tunnel interface

Test case	Initial infiltration rate [m3/s]
Slope Bergen D10 BL2	-2,31E-05
Slope Bergen D20 BL3	-2,52E-06
Slope Bergen D20 BL2	-4,38E-05
Slope Lillehammer D10 BL2	-2,31E-05
Slope Lillehammer D20 BL2	-4,39E-05
Slope Lillehammer D20 BL3	-2,53E-06

Table 26 - Initial infiltration rates over soil-rock interface

Test case	Initial infiltration rate [m3/s]
Slope Lillehammer BL3	1,40E-08
Slope Lillehammer BL2	-4,91E-07
Slope bergen BL3	9,20E-09
Slope Bergen BL2	-3,70E-07
Slope Bergen D10 Bl2	5,96E-07
Slope Bergen D20 BL3	7,59E-08
Slope Bergen D20 BL2	1,03E-06
Slope Lillehammer D10 BL2	5,96E-07
Slope Lillehammer D20 BL2	1,04E-06
Slope Lillehammer D20 BL3	7,62E-08

Infiltration rates over soil-rock interface:

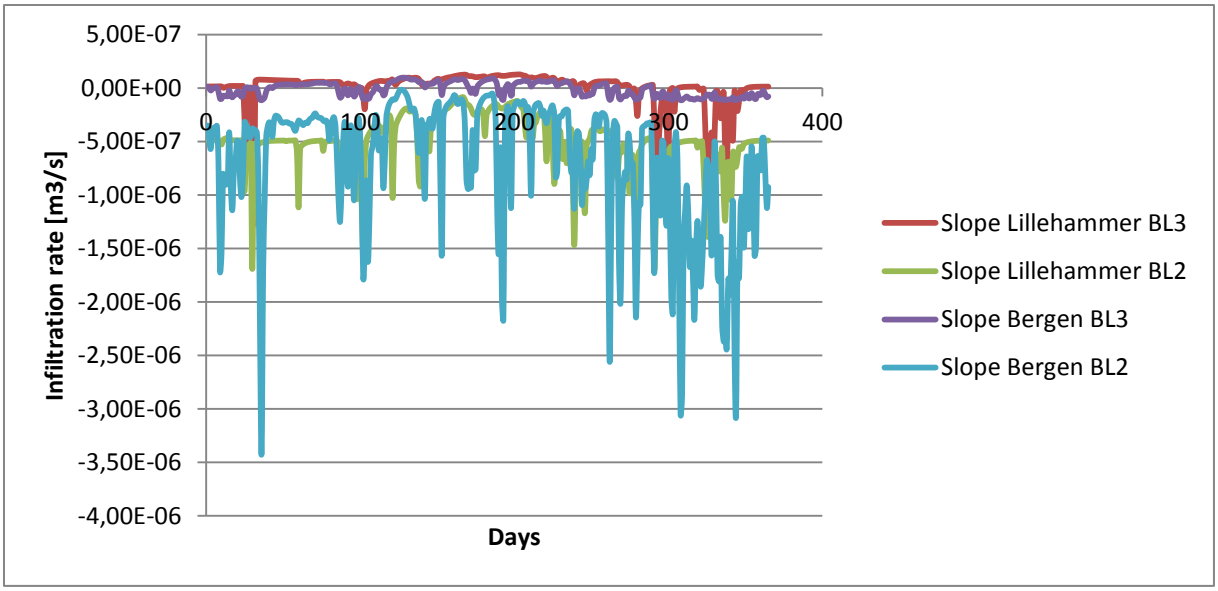

Figure 130 – Infiltration rates over soil-rock interface

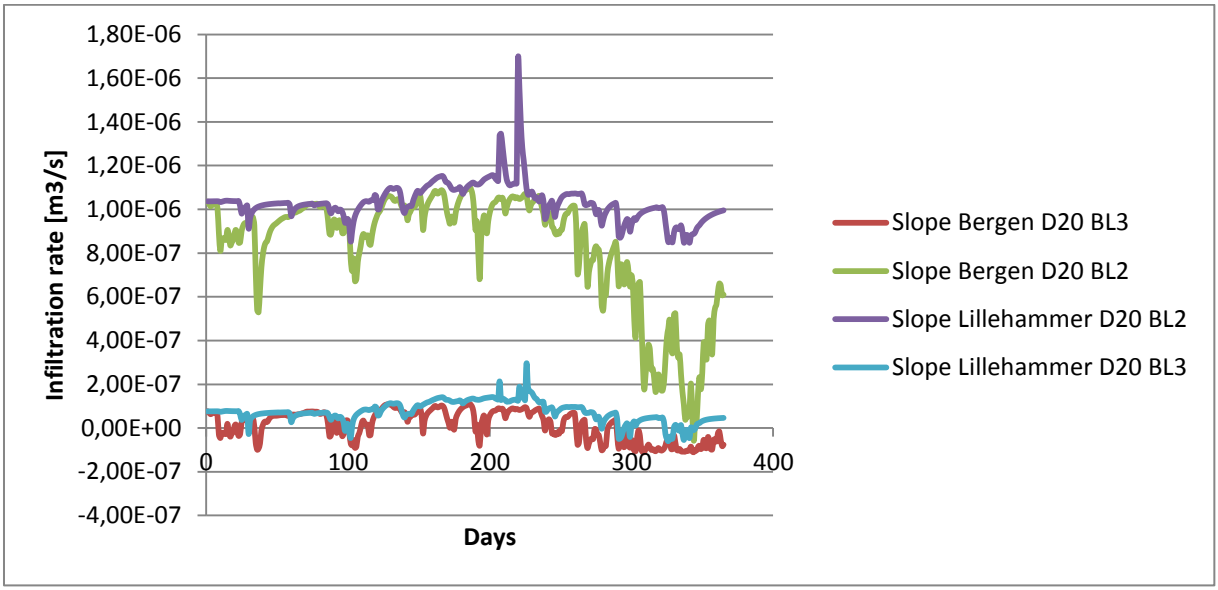

Figure 131 – Infiltration rates over soil-rock interface

Infiltration rates over tunnel interface:

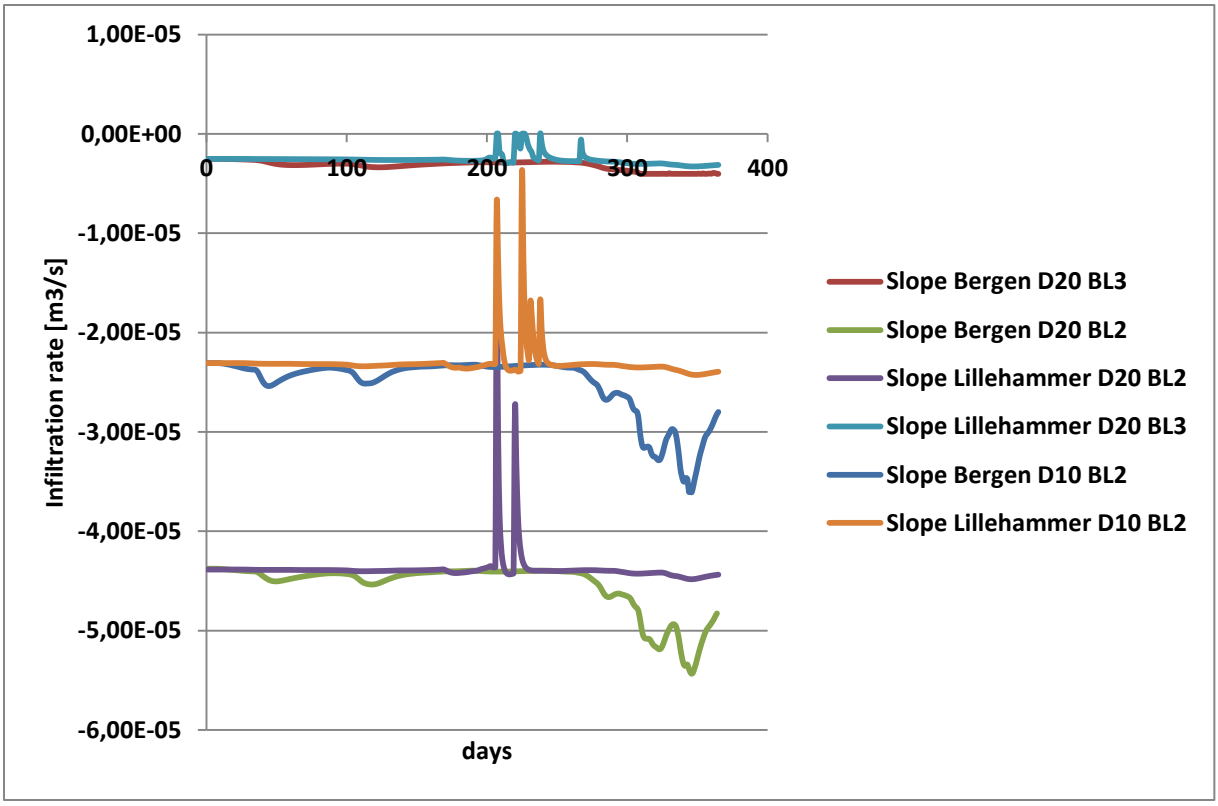

Figure 132 – Infiltration rates over tunnel interface

Groundwater tables:

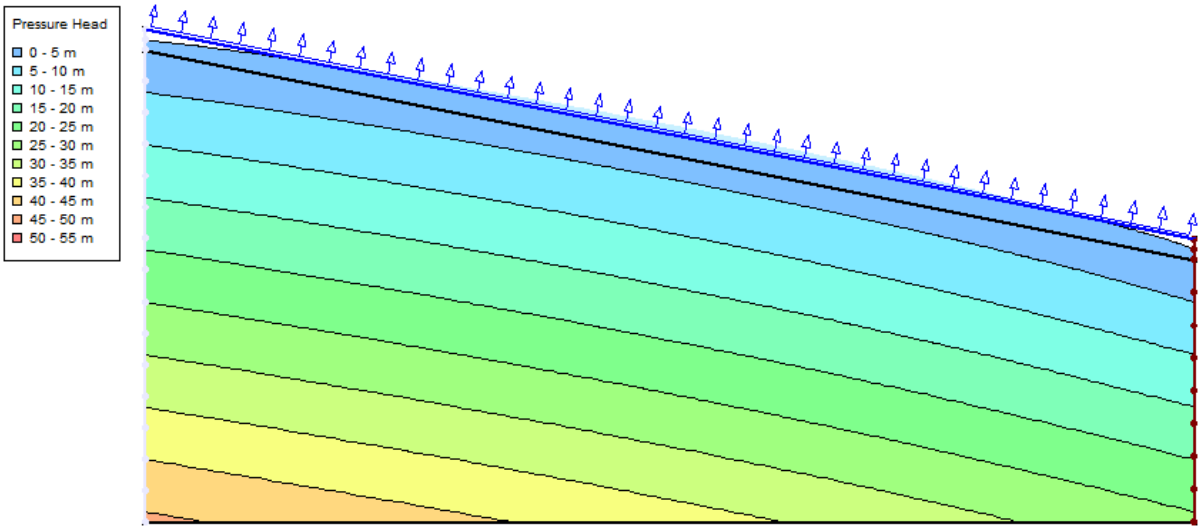

Figure 133 - Slope Bergen BL2

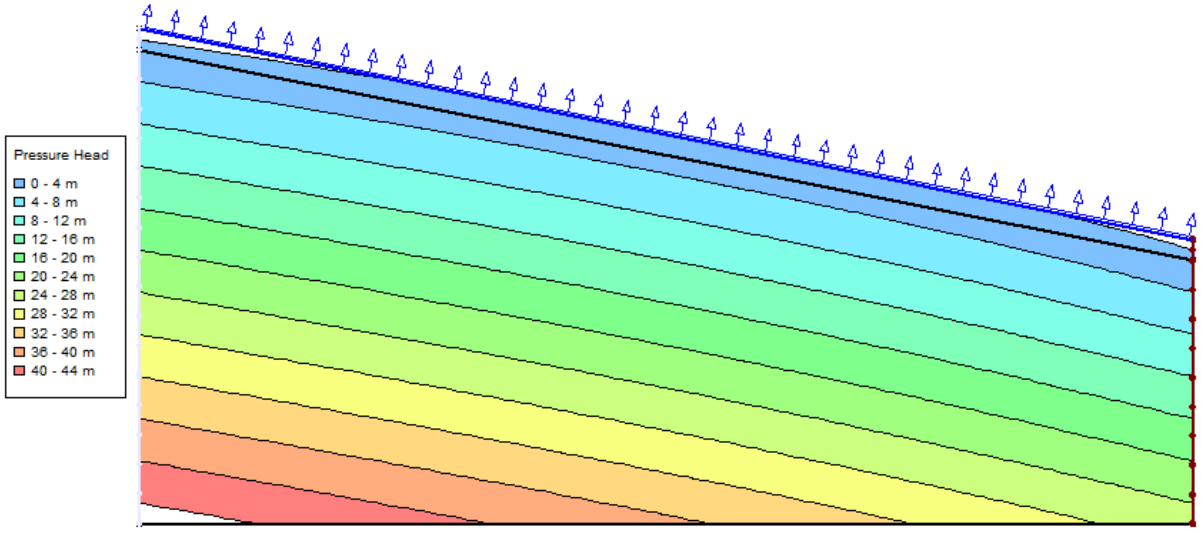

Figure 134 - Slope Bergen BL3

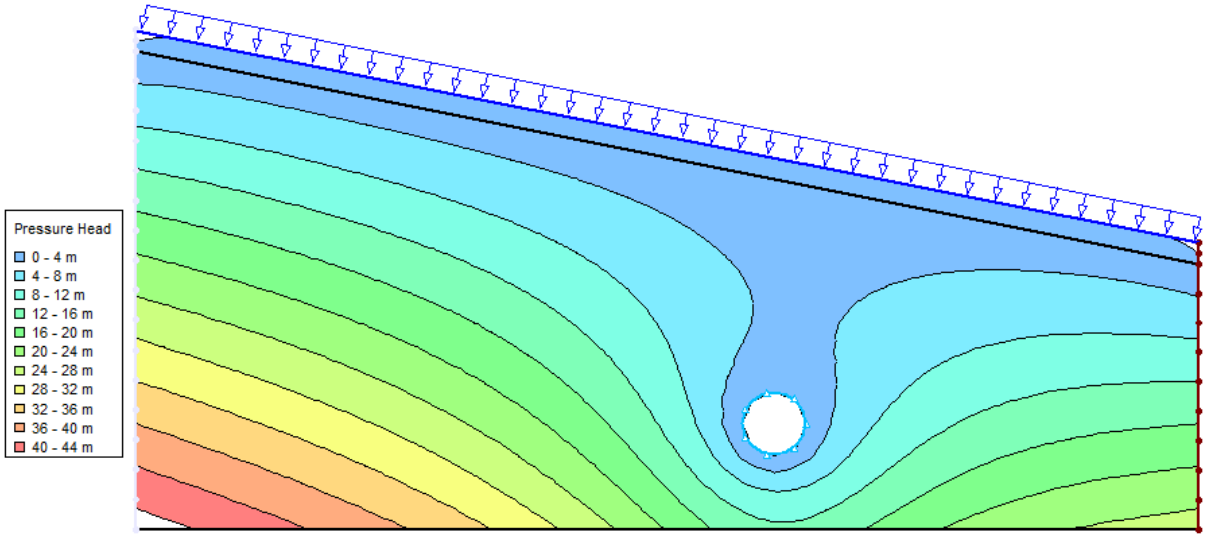

Figure 135 - Slope Bergen D20 BL3

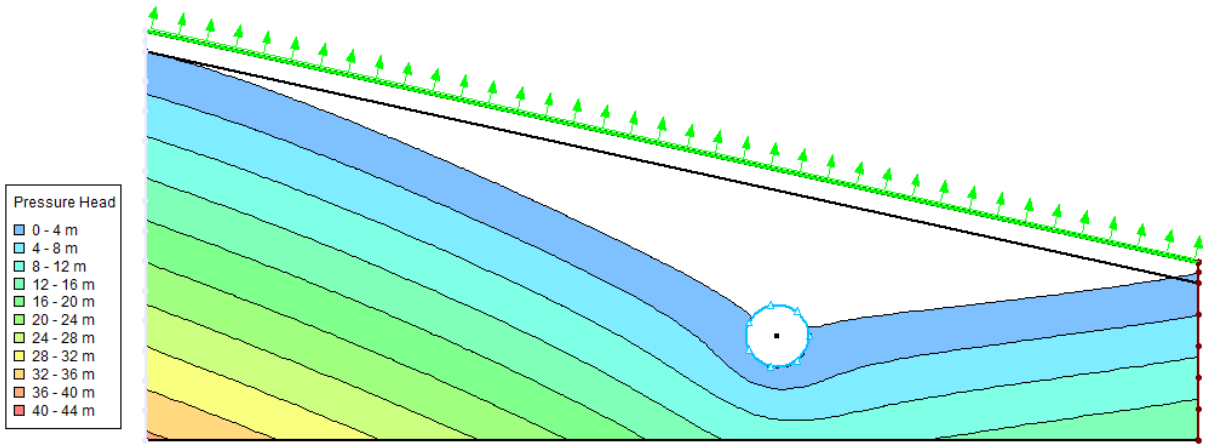

Figure 136 - Slope Bergen D10 BL2

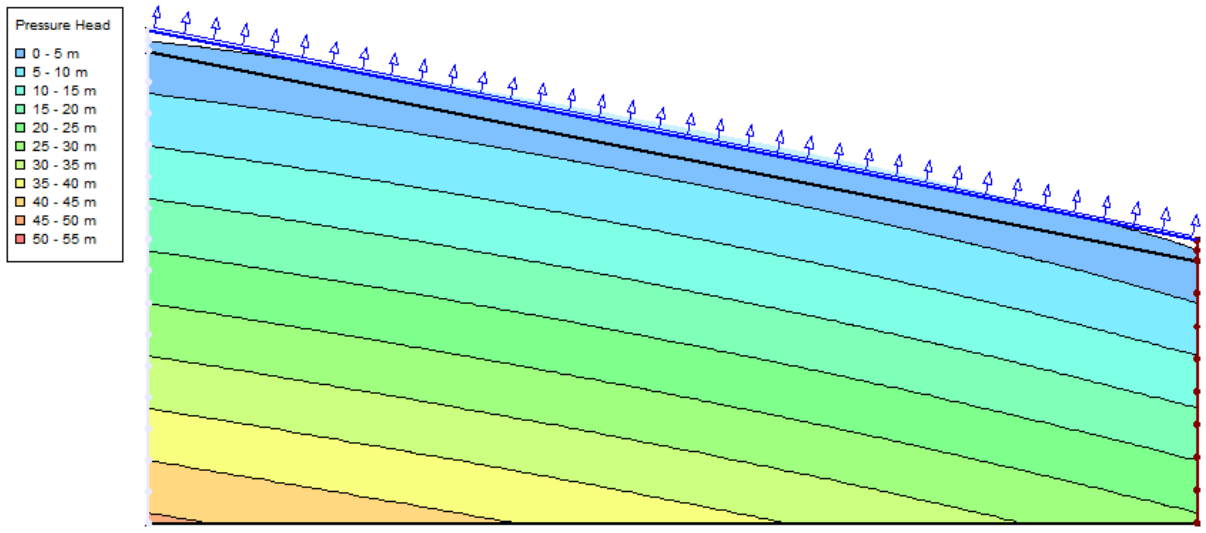

Figure 137 - Slope Lillehammer BL2

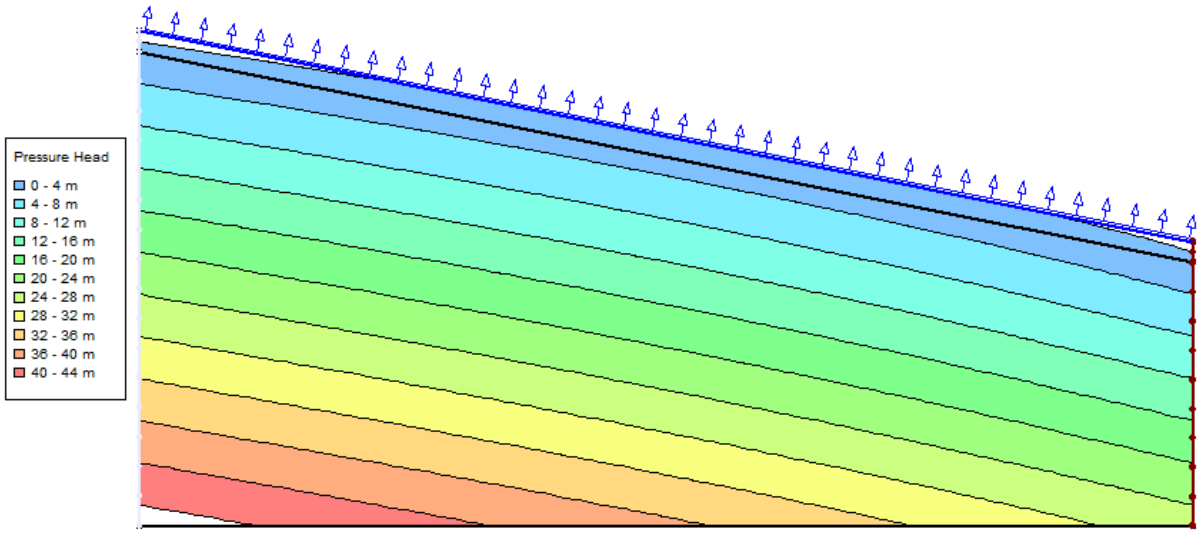

Figure 138 - Slope Lillehammer BL3